

Thèse de Doctorat

Siwar CHIBANI

*Mémoire présenté en vue de l'obtention du
grade de Docteur de l'Université de Nantes
sous le label de L'Université Nantes Angers Le Mans*

École doctorale : Matière, Molécules, Matériaux en Pays De La Loire
Discipline : Chimie
Spécialité : Chimie Théorique
Unité de recherche : CEISAM, Université de Nantes

Soutenue le 05 Novembre 2014
Thèse N° :

TD-DFT Simulation of the Properties of the Excited States

JURY

Rapporteurs : **Xavier ASSFELD** , Professeur, Université de Lorraine, Nancy
Ilaria CIOFINI , Directeur de Recherche CNRS, ENSCP, Paris

Examineurs : **Karine COSTUAS** , Directeur de Recherche CNRS, Université de Rennes
Gilles ULRICH , Directeur de Recherche CNRS, Université de Strasbourg

Directeur de Thèse : **Denis JACQUEMIN**, Professeur, Université de Nantes

CONTENTS

Acknowledgements	v
Introduction	1
1 Methods	7
1.1 Definition of the transition energies	8
1.1.1 Gas phase	8
1.1.2 Condensed phase	9
1.2 Vibronic spectra	13
1.3 Quantum chemical methods	13
1.3.1 Atomic basis sets	14
1.3.2 Exchange-correlation functionals	15
Results	17
I	18
2 Aza-Boron-Dipyrromethene Dyes: Aza-BODIPY	19
2.1 Computational Details	21
2.2 Methodological Study	21
2.2.1 Basis set effects	21
2.2.2 Solvent effects	24

2.2.3	Functional effects	26
2.3	Applications	28
2.3.1	Asymmetric dyes	28
2.3.2	Auxochrome impact on band shapes	29
2.3.3	Complexation effects	30
2.3.4	Acidochromism	31
2.4	Conclusions	34
3	Boron-Dipyrromethene Dyes: BODIPY	35
3.1	Methods	37
3.2	Adiabatic energies	37
3.2.1	Benchmarks of DFT functionals	37
3.2.2	Test cases	39
3.3	Applications	40
3.3.1	Vibrationally resolved band shapes	40
3.3.2	Dimers	42
3.3.3	pH probes	46
3.3.4	Ion sensing	49
3.3.5	NIR structures	51
3.4	Conclusions	54
4	Boranil and Related NBO Dyes	57
4.1	Computational Details	59
4.2	Methodology	59
4.3	Applications	64
4.3.1	Auxochromes' impacts	64
4.3.2	Comparing theoretical and experimental band shapes	66
4.4	Conclusions	67
5	Dioxaborine Dyes	69
5.1	Computational Details	69
5.2	Methodological investigation	70
5.3	Applications	74
5.3.1	Impact of the auxochromes	74
5.3.2	Vibronic shapes	76

5.3.3	Double BF_2 complexes	79
5.3.4	Further discussions	81
5.4	Conclusions	86
Conclusion- Part I		87
II		90
6	Excited-States Geometries with Corrected Linear-Response Model	91
6.1	Computational Details	92
6.2	Quasi-Linear Cyanines	93
6.3	Fluoroborates	96
6.4	Conclusions	99
7	Connecting TD-DFT vertical energies with SOS-CIS(D)	101
7.1	Computational Details	102
7.2	Protocol	104
7.3	Results and discussion	104
7.3.1	BODIPY dyes	104
7.3.1.1	0-0 energies	104
7.3.1.2	Impact of the Auxochromes	108
7.3.1.3	Vibronic spectra	108
7.3.2	Aza-BODIPY dyes	111
7.4	Conclusions	113
Conclusion- Part II		115
Summary and Outlook		117
List of Publications related to this PhD thesis		121
A	Aza-Boron-Dipyrromethene Dyes: Aza-BODIPY	125
B	Boron-Dipyrromethene Dyes: BODIPY	131
B.1	Experimental and theoretical data for the test and training sets.	131
B.2	Additional simulation of spectral shapes.	134

B.3	Additional density difference plots.	138
B.4	Huang-Rhys graphs.	140
B.5	List of transition energies.	140
C	Boranil and Related NBO Dyes	155
D	Dioxaborine Dyes	169
E	Connecting TD-DFT vertical energies with SOS-CIS(D)	179
E.1	Vibronic shapes	183
	Bibliography	185

ACKNOWLEDGEMENTS

I wish to express my thanks in french ...

Certaines personnes sont capables de transmettre une partie de leurs connaissances avec tant de patience, d'enthousiasme et de générosité qu'elles vous transforment et transforment votre vie, dans le bon sens. Ce qu'elles vous offrent alors n'a pas de prix, à mon sens. Je ne peux que remercier chaleureusement les personnes ayant tenu ce rôle à un moment ou un autre de ma vie, sans jamais espérer, malheureusement, réussir à leur rendre une partie de ce qu'elles m'ont donné.

Mes premières pensées se tournent envers mon directeur de thèse, JACQUEMIN Denis. Je lui suis tout d'abord infiniment reconnaissant d'avoir bien voulu m'accepter comme étudiant et me guider dans sa réalisation durant toutes ces années. Je lui exprime ma profonde gratitude. Merci pour ton amitié, ta patience, tes remarques et tes indications qui m'ont fortement aidé et motivé. J'ai été très heureuse de travailler avec vous.

Je remercie chaleureusement Azzam CHARAF EDDIN et Adèle D. LAURENT, qui m'ont apporté son aide quand je les demandais, Merci pour tout.

Madame Ilaria Ciofini et Monsieur Xavier Assfeld m'ont fait l'honneur d'accepter

d'être les rapporteurs de ma thèse.

Madame Karine Costuas et Monsieur Gilles Ulrich ont accepté d'être membres de mon jury. Je les remercie chaleureusement et je suis honorée de soutenir ma thèse devant eux.

Mes années en tant que thésarde ont été les plus belles années de mes études et beaucoup de personnes ont contribué à cela. En particulier, l'ambiance au sein du laboratoire CEISAM et à Nantes aura été très agréable et respectueuse. Je tiens également à remercier les gens du laboratoire pour la disponibilité et la gentillesse dont ils ont fait preuve durant ces années. Je tiens à m'adresser à l'ensemble des doctorants et post-doctorat avec qui j'ai partagé d'excellents moments... merci à vous tous.

J'ai enfin la joie de remercier ma famille. Merci mère, qui prie toujours pour que je réussisse, de ta confiance en moi. Merci père, tu m'as toujours encouragé au cours de toutes ces années. Merci mes frères, sœurs et cousines pour m'avoir soutenu et encouragé pendant mes études. Finalement, je remercie tout spécialement, mon mari Mohamed CHEBBI de m'avoir supporté et m'avoir soutenu durant toute la durée de la thèse.

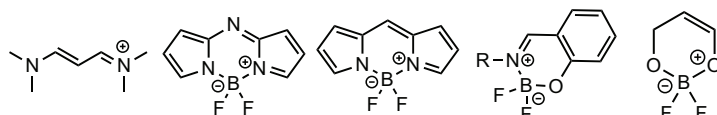
Merci à toutes celles et à tous ceux qui m'ont soutenu depuis le début et jusqu'à maintenant.

Siwar

INTRODUCTION

From several years ago, fluorescent organic dyes attracted a considerable interest. Because of their exceptional properties, these dyes become the subject of the largest number of investigations. Therefore, one of the most important properties is their near-infrared (NIR) emission. The near-infrared spectral range (700–1600 nm) includes two transparency domains where the light is less absorbed or scattered: (i) the “biological window” between 700–1100 nm corresponding to the transparency domain of living tissues giving the opportunity of non-invasive deep penetration of the biological tissues, at the origin of numerous applications in biology and medicine¹ and (ii) the “telecommunication window” at 1300 and 1550 nm corresponding to the transparency domain of silica optical fiber at the basis of the actual telecommunication network.^{2,3} These particular properties of the NIR spectral range have triggered the development of dyes featuring absorption, emission or nonlinear optical properties in this region. Among the first chromophores that have been synthesized with that goal in mind, porphyrins, fluorescein, coumarin, cyanines and squaraines dyes. Since that time, chemists, physicists and biochemists continue to develop a new molecules with red-shifted photophysical properties. Today, one of the most important organic chromophoric classes of emissive dyes is boron-dipyrromethane (BODIPY). The BODIPY can be considered as a subclass of the cyanines family (see Scheme 0.1), and are composed of a dipyrromethene bound to a central BF_2 unit, that allows to maintain the conformation of the organic large fluorescent. BODIPY and its derivatives present an excellent photophysical properties: quantum yields, high stability, photostability and near-IR (NIR) emission. However, these dyes suffer from several limitations, such

as small Stokes shifts, narrow absorption and emission bands as well as the practical difficulty of producing industrial quantities of these dyes. Therefore, the development of new fluoroborate structures presenting features correcting some of the weaknesses of BODIPY dyes while conserving the other interesting qualities of BODIPY is a highly desired goal.⁴⁻²¹ Similar compounds to the BODIPY have been investigated and this includes, aza-BODIPY, boranil and dioxaborine dyes (see below), that all can be viewed as *cis*-constrained cyanines. All these compounds have absorption and emission wavelengths spanning the 350-750 nm window. This large optical accessible optical window originates from the nature of the electronic excitations that could present a cyanine or a charge transfer (CT) character depending on the selected substituents. These chromophores present an exciting potential in numerous fields of researches as they became key tools for biological, medicinal and analytical applications. Indeed, major applications of this fluoroborates derivatives can be found in photovoltaics,²²⁻²⁹ advanced optoelectronics,³⁰⁻³³ nonlinear optics,³⁴⁻³⁷ bioimaging or sensing,³⁸⁻⁴¹ and photodynamic therapy.⁴²⁻⁴⁷



Scheme 0.1: Representation of prototypical cyanine as well as, aza-BODIPY, BODIPY, Boranil and dioxaborine cores (from left to right).

These fluoroborate fluorophores can be obviously classified into major categories depending on their atomic sequence: NBN, NBO, or OBO-bidentate ligands. In this thesis, we are interested to determine the properties of electronically excited-state of aza-BODIPY, BODIPY, boranil and dioxaborines dyes. To effectively predict these properties, theoretical chemistry can be a handy tool. In that framework, we have used *ab initio* methods, and more precisely, Density Functional Theory (DFT) and Time-Dependent Density Functional Theory (TD-DFT). In DFT, the total energy of a system is given as a functional, $E(\rho)$, of the electronic density ρ , and is minimized to find the ground state (GS) values. DFT also provides frontier orbitals (HOMO and LUMO). However, these orbitals are not suited to model absorption and fluorescence wavelengths. In order to obtain the transition energies, TD-DFT is often necessary.

TD-DFT, proposed by Runge and Gross,^{48,49} is an extension of DFT allowing to evaluate excited-states (ES) properties. Indeed TD-DFT is one of the most widely used tool in terms of balance between accuracy and computational cost to model optical spectra of organic molecules in gas-phase, solution or even in more complex environmental conditions.⁵⁰⁻⁶⁰ Using the TD-DFT approach, we can determine not only the vertical transition energies but also vibrationally resolved optical spectra and 0-0 energies. It's important to highlight that despite its popularity, TD-DFT suffers from at least a main limitation: the accuracy is related to the choice of a specific exchange-correlation functional.⁶¹

As stated above, aza-BODIPY, BODIPY, boranil and dioxaborine dyes present a significant through-space charge transfer or cyanine-like transitions. In this framework, it is important to show that TD-DFT relying on standard global hybrids is unsuccessful for both types of electronic transitions.⁶² Indeed, CT energies are often strongly underestimated by global hybrids especially when there is a large distance separating the regions gaining/losing electron density.^{63,64} To obtain a meaningful description of ES presenting CT character, it's now well-known that range-separated hybrids are the functional of the choice.^{64,65} For organic ES, the situation is more complex as both global and range-separated hybrids yield poor results.⁶⁶ Recently, Truhlar and coworkers, using the quantum Monte-Carlo results of Send *et al.*⁶⁷ as benchmarks, have nevertheless shown that the large TD-DFT errors commonly reported for cyanine derivatives can be (at least partly) ascribed to the failure of the vertical TD-DFT approximation used to obtain absorption energies, rather than to the actual weaknesses of recent DFT functionals.⁶⁸ They also demonstrate that the most modern functionals provide promising results. Therefore, there is a hope to reach accurate theoretical description of the optical properties of fluoroborate fluorophores by simulating their excited-state in a complete way including relaxation effects with a recently proposed functionals.

Let us now briefly reviewed previous theoretical investigations devoted to fluoroborates. For BODIPYs and some related derivatives, a few TD-DFT works have been achieved within the vertical approach^{13,69-79} that consists in single-point computations of the excited-state energies performed on frozen GS geometries. This approach offers relatively fast estimations of the absorption wavelengths, but hardly

helps to understand the emission signatures. While for most structures, comparing vertical TD-DFT calculations performed on GS geometries to experimental λ_{\max} is a crude but reasonable approximation, this is as stated above not the case for cyanine-like transitions. To determine fluorescence wavelengths, one needs to optimize the ES geometries, a task that was first achieved at the simple CIS level,⁸⁰⁻⁸⁴ and recently using analytical TD-DFT gradients.⁸⁵⁻⁹⁰ For instance, Zhang *et. al.* investigated the fluorescence of three aza-BODIPY dyes with side phenyl or thiophene rings,⁸⁶ whereas Chen and coworkers performed a similar analysis for eight BODIPYs, with a focus on the interplay between geometrical relaxation, charge-transfer and Stokes shifts.⁸⁸ To improve the numerous studies that relied on the vertical TD-DFT approximation, we are interested in this thesis to the calculations of both the 0-0 energies (E^{0-0}) and band shapes for all selected dyes, which allow more sound comparisons with experiment (see next Chapter for mathematical definitions).^{58,91-97} In practice, the difference between 0-0 and vertical simulations is the necessity to optimize the geometry of the excited-state, as well as to calculate the zero point vibrational energies (ZPVE) of both states. Determining these energies with theoretical tools is a major challenge but allows physically well-grounded comparisons between experimental and theoretical values:^{58,92,93} E^{0-0} data are straightforwardly comparable to the intersection of the absorption and emission spectral curves (E^{AFCP} : absorption/fluorescence crossing point).⁵⁸

The manuscript is divided into two important parts. The first part constituted of five Chapters, we first outline the methods used here and define the main parameters used, and next move to the study of optical signatures of fluoroborate fluorophores. In the last of each Chapter, we present applications aiming at gaining chemical insights and understanding the key experimental outcomes for aza-Bodipy (Chapter 2), BODIPY (Chapter 3), boranil (Chapter 4) and dioxaborine (Chapter 5) dyes. The second part of this thesis constituted of two Chapters in which we have interested to improve some weakness. In the first one, we have performed the excited-states using the corrected Linear-Response environmental model approach, not only to compute transition energies, but also to optimize the geometrical parameters in a fully consistent approach. In the second one, we have combined the (SOS)-CIS(D) to the TD-DFT (solvent and vibrational effects computed at the TD-DFT level but the transition energies were obtained with the (SOS)-CIS(D) approach) in order to de-

crease the theory/experiment correlation coefficients typical of TD-DFT level. Then, we conclude and provide an outlook of future research. Additional information about useful data are reported in appendixes.

1.1 Definition of the transition energies

1.1.1 Gas phase

Let us first define the physical properties in gas phase using Figure 1.1 as a reference. The energy difference between the ES and the GS calculated on the optimized GS geometry corresponds to the vertical absorption energy,

$$E^{\text{vert-a}} = E^{\text{ES}}(R^{\text{GS}}) - E^{\text{GS}}(R^{\text{GS}}) \quad (1.1)$$

We note that $E^{\text{vert-a}}$ cannot be rigorously compared to experimental λ_{max} of absorption, although such procedure might be effective in a homologous series of compounds.^{58,91} The vertical transition energies calculated on the optimized ES geometry are the vertical fluorescence energies,

$$E^{\text{vert-f}} = E^{\text{ES}}(R^{\text{ES}}) - E^{\text{GS}}(R^{\text{ES}}) \quad (1.2)$$

The adiabatic energies, E^{adia} , are the difference of total electronic energies calculated by considering the two states in their respective minima.

$$E^{\text{adia}} = E^{\text{ES}}(R^{\text{ES}}) - E^{\text{GS}}(R^{\text{GS}}) \quad (1.3)$$

E^{adia} can also be defined by combining the vertical absorption and fluorescence data of the ES and GS reorganization energies,

$$E^{\text{adia}} = E^{\text{ES}}(R^{\text{ES}}) - E^{\text{GS}}(R^{\text{GS}}) \quad (1.4)$$

$$E^{\text{adia}} = E^{\text{vert-f}} + E^{\text{GS}}(R^{\text{ES}}) - E^{\text{ES}}(R^{\text{GS}}) + E^{\text{vert-a}} \quad (1.5)$$

$$E^{\text{adia}} = E^{\text{vert-f}} + E^{\text{vert-a}} - E^{\text{adia}} + E^{\text{reorg-GS}} - E^{\text{reorg-ES}} \quad (1.6)$$

In that way the adiabatic energies become,

$$E^{\text{adia}} = \frac{1}{2}[E^{\text{vert-f}} + E^{\text{vert-a}}] + \frac{1}{2}[E^{\text{reorg-GS}} - E^{\text{reorg-ES}}] \quad (1.7)$$

In first approximation, the second term can be neglected so that,

$$E^{\text{adia}} \approx \frac{1}{2}[E^{\text{vert-f}} + E^{\text{vert-a}}] \quad (1.8)$$

To calculate the 0-0 energies, E^{0-0} , the differences of the zero-point vibrational energy between the ES and the GS, ΔE^{ZPVE} , should be determined and added to the adiabatic energies:

$$\Delta E^{\text{ZPVE}} = E^{\text{ZPVE}}(R^{\text{ES}}) - E^{\text{ZPVE}}(R^{\text{GS}}) \quad (1.9)$$

$$E^{0-0} = E^{\text{adia}} + \Delta E^{\text{ZPVE}} \quad (1.10)$$

Let us note that ΔE^{ZPVE} is often negative for organic molecules.^{58,93,98} E^{0-0} allows straightforward comparison with the absorption/fluorescence crossing point (AFCP) for molecules measured in gas phase.

1.1.2 Condensed phase

The experimental data are often obtained in condensed phase. For this reason, solvent effects should be included during the calculations. There are two families of solvent models: implicit and explicit. In implicit models, the solvent is considered as a continuous medium, while in the explicit approaches, the solvent molecules are treated with an atomistic method. The latter models are often more accurate but they require the determination of both the number and the positions of all solvent molecules which implies a dynamic study and therefore requires large computational efforts. In this thesis, we are interested in the determination of the structures and the properties of the excited states, a task that would be dramatically difficult with explicit methods. For this reason, we have used the most widely-known implicit continuum dielectric method, namely the Polarizable Continuum Model (PCM),⁹⁹ to model medium effects. In PCM approach, the solute is located in the center of a cavity surrounded by a continuum which has the macroscopic properties of the solvent (dielectric constant, thermal expansion coefficient...). This continuum model relies on the Self-Consistent Reaction Field (SCRF) so that the interplay between the polarizations of the solute and the solvent are self-consistently modeled. Indeed, the interaction process between the solute and the solvent is self-consistency: the charge distribution of the solute polarizes the surface of the cavity of the continuum. These charges induce a reaction which modifies the electronic density of the solute. At this stage, the continuum must adapt to this new situation... and so on until the electrostatic convergence between the distributions of the charges of the solute and of the surface of the cavity are

reached.

Considering now a solvated dye in its ground state, there is both nuclear and electronic equilibria between the solute and the solvent, so that the relevant parameter is the relative dielectric constant. This situation is standard in PCM and requires no further explanations. On the contrary, the situation is more complex for excited states. In fact, when a compound undergoes the effects of an electromagnetic field, its polarization is modified. The reaction of the solvent to this charge depends on the time former considered. In the long run, all components of the molecules of the solvent have time to align. At very short timescale, on other situation appears in which only the electron of the solvent are quick enough to adapt to the new polarization. For this reason, one should distinguish two important mechanisms of solute-solvent interactions for ES: the equilibrium (eq) and non-equilibrium (neq) limits. In the neq limit, only the electrons of the solvent do adapt to the new electronic configuration of the solute (fast process). In that case, only the "electronic" dielectric constant is taken into account and the infinite frequency dielectric constant ($\epsilon_0=n^2$, e.g., ca. 2 for water) is relevant for the new states. This is adequate for vertical transitions. On the contrary, in the eq approach, the solvent has time to fully adapt to the new electronic configuration of the solute (slow process). This latter approach is the recommended approach to calculate excited-states geometries, vibrational signatures and consequently the 0-0 energies. Indeed, in these cases the nuclei of the solute have time to move, which implies that the nuclei of the solvent do also adapt to the new electronic state of the solute, and the relevant macroscopic quantity is the dielectric constant (e.g., $\epsilon_r \sim 78$ for water).

In addition, there is the question of how the PCM cavity is polarized in the excited-state. We have used three models in this thesis: linear response (LR),^{53,100} the only available approximation for TD-DFT geometry optimization and vibrational calculations, corrected linear response (cLR)¹⁰¹ and state specific (SS)¹⁰² approaches. All the three models (LR, cLR and SS) represent the solvent polarization in terms of induced charges on the surface of the cavity embedding the dye, however the way this polarization changes with the electronic transition is differently introduced in these three schemes. Indeed, in the LR scheme the change in the PCM charges is calculated in terms of transition densities, while in cLR this change is determined perturbatively by the variation in the one-particle density matrix between the ground and the excited

state, that is by computing the actual dipole moment of the excited-states. In the SS approach a more complex iterative formulation is used to obtain a self consistent polarization of the cavity as for the ground-states.

Let us now see how we can compute the 0-0 energies in condensed phase. It was shown,⁹³ that combining two atomic basis sets, one for geometrical parameters and for transitions energies is an effective approach. Starting with E^{adia} which can be estimated in both equilibrium and non-equilibrium, [X : eq or neq], with a small atomic basis set (SBS) (see Section 1.3.1) using the LR-PCM model:

$$E_{\text{SBS}}^{\text{adia}}(\text{LR}, X) = E_{\text{SBS}}^{\text{ES}}(R^{\text{ES}}, \text{LR}, X) - E_{\text{SBS}}^{\text{GS}}(R^{\text{GS}}, \text{eq}) \quad (1.11)$$

In order to account for atomic basis set effects, we have determined the adiabatic energies with a larger basis set (LBS), through Equation 1.11 leading to $E_{\text{LBS}}^{\text{adia}}(\text{LR}, X)$.

$$E_{\text{LBS}}^{\text{adia}}(\text{LR}, X) = E_{\text{LBS}}^{\text{ES}}(R^{\text{ES}}, \text{LR}, X) - E_{\text{LBS}}^{\text{GS}}(R^{\text{GS}}, \text{eq}) \quad (1.12)$$

We have also used the SS and cLR models, [Y : SS or cLR]:

$$E_{\text{SBS}}^{\text{adia}}(Y, X) = E_{\text{SBS}}^{\text{ES}}(R^{\text{ES}}, Y, X) - E_{\text{SBS}}^{\text{GS}}(R^{\text{GS}}, \text{eq}) \quad (1.13)$$

This allows to determine a best estimate (BE) of the adiabatic energies using:

$$E_{\text{BE}}^{\text{adia}}(Y, X) = E_{\text{SBS}}^{\text{adia}}(Y, X) + [(E_{\text{LBS}}^{\text{adia}}(\text{LR}, X) - E_{\text{SBS}}^{\text{adia}}(\text{LR}, X))] \quad (1.14)$$

Where, we consider additive effects,^{93,94} a very good approximation as we demonstrate in the next Chapter. As stated above, to calculate 0-0 energies one needs to compute ΔE^{ZPVE} ,

$$\Delta E_{\text{SBS}}^{\text{ZPVE}}(\text{LR}, X) = E_{\text{SBS}}^{\text{ZPVE-ES}}(R^{\text{ES}}, \text{LR}, X) - E_{\text{SBS}}^{\text{ZPVE-GS}}(R^{\text{GS}}, \text{eq}) \quad (1.15)$$

The 0-0 energies can now be computed in the LR-PCM approach in both eq and neq limits:

$$E_{\text{BE}}^{0-0}(\text{LR}, X) = E_{\text{LBS}}^{\text{adia}}(\text{LR}, X) + \Delta E_{\text{SBS}}^{\text{ZPVE}}(\text{LR}, X) \quad (1.16)$$

and the same holds for the SS and cLR models:

$$E_{\text{BE}}^{0-0}(Y, X) = E_{\text{BE}}^{\text{adia}}(Y, X) + \Delta E_{\text{SBS}}^{\text{ZPVE}}(\text{LR}, X) \quad (1.17)$$

We underline again that cLR and SS simulations are only possible as single point calculations and cannot be used to directly optimize ES geometries. In the second part of this thesis, we show, for the first time, how to optimize ES using the cLR approach. Therefore, using Eq. 1.8, the 0-0 energies of Eq. 1.17 with SS/cLR approaches in eq limits can be approximated,

$$E_{\text{BE}}^{0-0}(Y, \text{eq}) \approx \frac{1}{2}[E^{\text{vert-f}}(Y, \text{eq}) + E^{\text{vert-a}}(Y, \text{eq})] + \Delta E_{\text{SBS}}^{\text{ZPVE}}(\text{LR}, \text{eq}) \quad (1.18)$$

Eq. 1.17 allows us to reach sound estimates of the 0-0 energies, but the results cannot be directly compared to experimental measurements. Indeed, the commonly accepted 0-0 reference is the meeting point between normalized absorption and emission curves (AFCP: absorption/fluorescence crossing point). However, this point corresponds to a non equilibrium phenomena and is strictly speaking, not the 0-0 energies. To account for neq effects, we have applied further corrections,⁹³

$$E^{\text{AFCP}}(Y, \text{neq}) = E_{\text{BE}}^{0-0}(Y, \text{eq}) + \frac{1}{2} [\Delta E_{\text{neq/eq}}^{\text{vert-a}}(Y) + \Delta E_{\text{neq/eq}}^{\text{vert-f}}(Y)] \quad (1.19)$$

The one-half factor is readily explainable from Eq. 1.18. The correction term for the neq effects is determined from the vertical absorption/fluorescence energies. In this case, we have calculated the $E^{\text{vert-a}}$ in both eq and neq limits within the SS/cLR-PCM model:

$$E_{\text{SBS}}^{\text{vert-a}}(Y, \text{neq}) = E_{\text{SBS}}^{\text{ES}}(R^{\text{GS}}, \text{neq}) - E_{\text{SBS}}^{\text{GS}}(R^{\text{GS}}, \text{eq}), \quad (1.20)$$

$$E_{\text{SBS}}^{\text{vert-a}}(Y, \text{eq}) = E_{\text{SBS}}^{\text{ES}}(R^{\text{GS}}, Y, \text{eq}) - E_{\text{SBS}}^{\text{GS}}(R^{\text{GS}}, \text{eq}), \quad (1.21)$$

So to determine the absorption correction:

$$\Delta E_{\text{neq/eq}}^{\text{vert-a}}(Y) = E_{\text{SBS}}^{\text{vert-a}}(Y, \text{neq}) - E_{\text{SBS}}^{\text{vert-a}}(Y, \text{eq}) \quad (1.22)$$

In a similar way,

$$E_{\text{SBS}}^{\text{vert-f}}(Y, \text{neq}) = E_{\text{SBS}}^{\text{ES}}(R^{\text{ES}}, Y, \text{eq}) - E_{\text{SBS}}^{\text{GS}}(R^{\text{ES}}, \text{neq}), \quad (1.23)$$

$$E_{\text{SBS}}^{\text{vert-f}}(Y, \text{eq}) = E_{\text{SBS}}^{\text{ES}}(R^{\text{ES}}, Y, \text{eq}) - E_{\text{SBS}}^{\text{GS}}(R^{\text{ES}}, \text{eq}), \quad (1.24)$$

$$\Delta E_{\text{neq/eq}}^{\text{vert-f}}(Y) = E_{\text{SBS}}^{\text{vert-f}}(Y, \text{neq}) - E_{\text{SBS}}^{\text{vert-f}}(Y, \text{eq}) \quad (1.25)$$

Finally, we underline that in the LR scheme, fluorescence calculations are rather ill-defined, as the solvent response is not adapted to the real electronic density of the excited state as is done in the cLR or SS schemes.

1.2 Vibronic spectra

The calculation of the vibrational signatures of both GS and ES allows not only to obtain the 0-0 energies, but also, to determine the shape of the optical spectra of all selected dyes.⁶¹ This is made through the calculations of the overlap between the vibrational eigenfunction of the two states considering the Franck Condon approximation. In this thesis, vibrationally resolved spectra within the harmonic approximation were computed using the FCclasses program (FC).¹⁰³⁻¹⁰⁵ The reported spectra were simulated using a convoluting Gaussian function presenting a half width at half maximum (HWHM) that was adjusted to allow direct comparisons with experiments (typical value: 0.04 eV). A maximal number of 25 overtones for each mode and 20 combination bands on each pair of modes were included in the calculation. The maximum number of integrals to be computed for each class was first set to 10^6 . In the cases where convergence of the FC factor [≥ 0.9] could not be achieved with this number of integrals, a larger value (up to 10^{12}) was used so to overcome the 0.9 limit. Note that in the thesis, the experimental fluorescence spectra measured in the wavelength scale have been transformed by applying an intensity correction proportional to ω^2 (the square frequency), in order to obtain line shapes that are directly comparable to theoretical data (the measured emission intensity physically decreasing by a factor of ω^2 which is not related to the vibronic couplings).¹⁰⁶ Indeed, this correction significantly affects the topology of the fluorescence spectra, contrary to other more negligible effects.¹⁰⁷

1.3 Quantum chemical methods

Now, that we have defined the main parameters, let us briefly go towards the quantum chemical methods used to determine those properties. As mentioned in the

Introduction, we have selected TD-DFT to model the properties of electronically excited states. However, using TD-DFT implies two major practical choices: the selection of an exchange-correlation functional and of atomic basis sets. There is no a priori "best" choice for these two parameters. For this reason, we have performed in the following benchmarks taking into account several parameters. Let us briefly summarize the different atomic basis sets and functionals used here.

1.3.1 Atomic basis sets

Atomic basis sets are an ensemble of functions used to build molecular orbitals and density. Contracted Gaussian-Type Orbitals (CGTO) are usually used to define the atomic orbitals that are combined to form molecular orbitals. Several basis sets have been developed, the most popular family was proposed by Pople. The basic Pople nomenclature is $c-v^1v^2v^3G$. Let's now explain each terms. c indicates the number of gaussian functions used to describe the core atomic orbital. v^i corresponds to the number of gaussian functions used to build the valence orbitals. For example, in 6-31G, the core orbital are composed of 6 Gaussians, and the valence electrons are described with two orbitals: one CGTO for 3 Gaussians, and one including of a single Gaussian. In order to increase the flexibility of the calculations, extended basis sets including polarization and diffuse can be used. The Pople nomenclature becomes, $c-v^1v^2v^3G++(x,y)$. y corresponds to a set of polarization functions for hydrogen atoms, and x are polarization orbitals for all other atoms. Similarly, the diffuse functions can be indicated by "+" or "++", for non-hydrogen or all atoms, respectively. Adding polarization functions adds flexibility in the basis by providing orbitals with larger angular momentum than those of valence electrons in the isolated atom (p for hydrogen, f for transition element...). Diffusion functions present the same angular momentum as valence orbitals but are much more flat. These functions are useful to describe electronic phenomena implying electron far from the nucleus like excited-states.

In the next Chapter, we have evaluated the basis set effects using a set of atomic basis set on aza-BODIPY dyes. We found that combining a small basis sets, 6-31G(d), for structural calculations and a large one, 6-311+G(2d,p) for energies yields converged results.

1.3.2 Exchange-correlation functionals

Using TD-DFT implies the choice of a specific functional that plays a key role on the accuracy of the final results. In computational chemistry, there exist several types of functionals, the two simplest being, Local Density Approximation (LDA)¹⁰⁸ and Generalized Gradient Approximation (GGA) functionals.¹⁰⁹ LDA functionals (first generation) are based on the uniform electron gas model. This method uses only the local density to define the exchange-correlation energies. It allows fast calculations but yield dramatically underestimated transition energies in molecules. In GGA (second generation), the local density as well as its gradient are used to describe the variation of the electronic density. GGA functionals give better results than the LDA one, but do not lead to a very accurate description of all the properties of the molecules.

Since the 1990s, hybrid exchange correlation functionals have emerged as "best choices" as they are able to reproduce experimental results with a much better accuracy than both LDA and GGA. Hybrid functionals include a fraction of exact exchange of Hartree-Fock (HF) form in the functional. In global hybrid this percentage is constant irrespective of the inter-electronic distance. However, in the case of charger transfer states, the conventional hybrid functionals fail accurately treat the physical phenomena. In these cases, range separated hybrids (RSH) that present a fraction of HF/DFT exchange increasing with the inter-electronic distance are much more suited.

In this thesis, we have only used hybrid functionals, e.g., B3LYP,^{110,111} the most popular DFT model, the parameter-free PBE0,^{112,113} that is known to be efficient in reproducing λ_{\max} within the vertical approximation,^{114,115} Truhlar's M06,¹¹⁶ BMK,¹¹⁷ that was demonstrated to be efficient for aza-BODIPY dyes at least for the vertical approximations (see Chapter 2),^{77,94} M06-2X¹¹⁶ that yields accurate results for BODIPY, boranil and dioxaborine dyes (see Chapters 3, 4 and 5) and is known display valuable performances for cyanines excited-states,^{68,118} as well as CAM-B3LYP,¹¹⁹ ω B97X-D and ω B97^{120,121} two range-separated hybrids providing accurate description of the adiabatic energies of organic dyes, especially for those presenting charge transfer character.^{58,65,122-124}

RESULTS

Part I

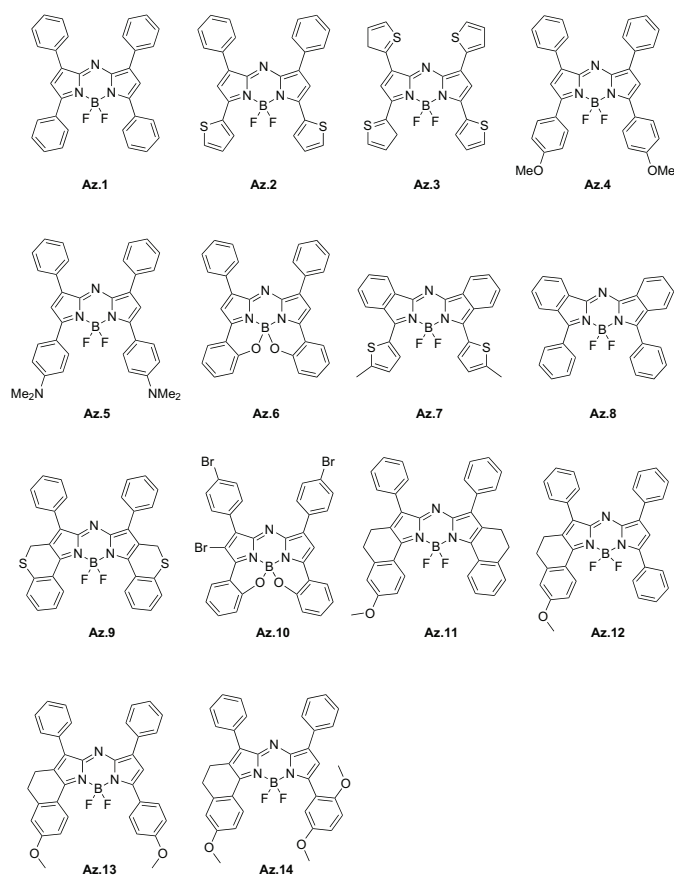
CHAPTER 2

AZA-BORON-DIPYRROMETHENE DYES: AZA-BODIPY

Aza-boron-dipyrromethene derivatives (aza-BODIPY) concentrated tremendous efforts due to their remarkable photo-physical properties.¹²⁵⁻¹²⁸ Indeed, these monomethine cyanine analogues present high photo-stability, large absorption coefficients and fluorescent quantum yields as well as tunable fluorescence wavelengths. Several studies focused on the development of new aza-BODIPY dyes with red-shifted photo-physical properties, conserving high luminescence quantum yield efficiency in the NIR range. To reach this goal, various approaches have been proposed taking benefit of the (i) peripheral functionalization with electron-donating groups,¹²⁹⁻¹³¹ (ii) rigidification of rotatable moieties,¹³²⁻¹³⁷ (iii) extension^{72, 138-140} or planarization^{86, 141-144} of the π -path.

Several (TD-)DFT works dedicated to aza-BODIPY derivatives have been published perviously.^{69, 72, 77, 142, 143, 145-147} However, at one notable exception,^{86, 148} they all relied on the crude HOMO-LUMO picture or used the vertical TD approximation to model absorption. For instance, Jiao and coworkers were used TD-DFT approximation for six aza-BODIPY dyes.¹⁴⁷ They have demonstrated that, when a strong electron-withdrawing groups placed on the *para*-positions of 1,7-phenyls, we obtain a red-shifted aza-BODIPY which emit in the long wavelength (740nm). Indeed, Gresser

et al. computed, with the B3LYP/6-31+G(d,p) approach, the positions of the optical bands that were found to be up to 100 nm off their experimental counterpart, and more importantly, at the same level of theory, the auxochromic effects were only very qualitatively reproduced.¹⁴³ Likewise, in a previous investigation by our group,⁷⁷ a computational strategy that allowed to reproduce the absorption wavelengths for aza-BODIPY characterized by a significant through-space charge-transfer (CT) was proposed but the results remained rather poor for the cyanine-like bands, that are also hallmarks of these dyes. As discussed in the previous Chapters, this failure can be partly ascribed to the vertical approximation, and we aim here to assess the more accurate adiabatic approach.



Scheme 2.1: Representation of the compounds investigated in this Chapter. The measured longest wavelength of absorption and emission wavelengths, solvents used, as well as the experimental references can be found in Table A.1 in Appendix A.

2.1 Computational Details

We considered a set of six functionals: B3LYP,^{110,111} PBE0,^{112,113} BMK,¹¹⁷ M06-2X,¹¹⁶ as well as CAM-B3LYP¹¹⁹ and ω B97X-D.¹²¹ Four split-valence atomic basis sets have been tested: 6-31G(d), 6-311+G(d), 6-311G(2d,p) and 6-311+G(2d,p), the two latter respectively lead to fully converged structural and electronic parameters in aza-BODIPY dyes.⁷⁷ The solvent effects have been accounted for with the Polarizable Continuum Model (PCM).⁹⁹ As discussed in Chapter 1, three PCM approaches have been tested (LR, cLR and SS).

2.2 Methodological Study

2.2.1 Basis set effects

Table 2.1: Basis set effects on the optical properties of **Az.1**, **Az.2** and **Az.3**, using the PCM(ACN)-TD-DFT approach with PBE0 and CAM-B3LYP exchange-correlation functionals. Values in italics have been computed with the basis set used during the geometry optimization. All values are in eV.

Dye	Basis Sets		PBE0					CAM-B3LYP							
			$E^{\text{vert-a}}$	$E^{\text{vert-f}}$	E^{adia}	ΔE^{ZPVE}	E^{0-0}	$E^{\text{vert-a}}$	$E^{\text{vert-f}}$	E^{adia}	ΔE^{ZPVE}	E^{0-0}			
Geometry	Energy	(LR,neq)	(LR,eq)	(LR,eq)	(LR,eq)	(LR,eq)	(LR,eq)	(LR,neq)	(LR,eq)	(LR,eq)	(LR,eq)	(LR,eq)	(LR,eq)		
Az.1	6-31G(d)	6-31G(d)	2.117	1.904	1.694	1.798	-0.051	1.747	2.181	1.946	1.701	1.824	<i>-0.031</i>	1.793	
		6-311+G(d)	2.071	1.852	1.645	1.765	<i>-0.051</i>	1.714	2.122	1.881	1.638	1.787	<i>-0.031</i>	1.756	
		6-311G(2d,p)	2.078	1.861	1.654	1.775	<i>-0.051</i>	1.724	2.128	1.889	1.647	1.798	<i>-0.031</i>	1.767	
		6-311+G(2d,p)	2.061	1.844	1.637	1.760	<i>-0.051</i>	1.709	2.108	1.869	1.627	1.781	<i>-0.031</i>	1.750	
		6-311+G(d)	6-311+G(d)	2.122	1.904	1.656	1.773	-0.049	1.724	2.185	1.945	1.655	1.799	-0.029	1.770
		6-311G(2d,p)	6-311G(2d,p)	2.110	1.893	1.667	1.777	-0.047	1.730	2.183	1.945	1.668	1.803	-0.025	1.778
			6-311+G(2d,p)	2.092	1.876	1.650	1.764	<i>-0.047</i>	1.717	2.162	1.924	1.650	1.764	<i>-0.025</i>	1.739
Az.2	6-31G(d)	6-31G(d)	1.954	1.717	1.575	1.645	-0.048	1.597	2.012	1.760	1.559	1.658	-0.028	1.630	
		6-311+G(d)	1.905	1.662	1.521	1.597	<i>-0.048</i>	1.549	1.950	1.692	1.492	1.597	<i>-0.028</i>	1.569	
		6-311G(2d,p)	1.914	1.674	1.534	1.614	<i>-0.048</i>	1.566	1.959	1.704	1.504	1.617	<i>-0.028</i>	1.589	
		6-311+G(2d,p)	1.895	1.651	1.514	1.592	<i>-0.048</i>	1.544	1.937	1.680	1.480	1.589	<i>-0.028</i>	1.561	
		6-311+G(d)	6-311+G(d)	1.922	1.675	1.523	1.593	-0.047	1.546	1.966	1.705	1.487	1.592	-0.025	1.567
		6-311G(2d,p)	6-311G(2d,p)	1.929	1.685	1.544	1.613	-0.044	1.569	1.986	1.728	1.513	1.616	-0.020	1.595
			6-311+G(2d,p)	1.908	1.664	1.523	1.588	<i>-0.044</i>	1.544	1.963	1.704	1.488	1.585	<i>-0.020</i>	1.565
Az.3	6-31G(d)	6-31G(d)	1.852	1.623	1.472	1.547	-0.047	1.500	1.923	1.677	1.467	1.571	-0.032	1.539	
		6-311+G(d)	1.805	1.572	1.420	1.503	<i>-0.047</i>	1.456	1.865	1.612	1.402	1.514	<i>-0.032</i>	1.482	
		6-311G(2d,p)	1.818	1.587	1.436	1.521	<i>-0.047</i>	1.474	1.876	1.626	1.417	1.536	<i>-0.032</i>	1.504	
		6-311+G(2d,p)	1.798	1.567	1.415	1.499	<i>-0.047</i>	1.452	1.854	1.602	1.393	1.507	<i>-0.032</i>	1.475	
		6-311+G(d)	6-311+G(d)	1.812	1.575	1.423	1.502	-0.048	1.454	1.874	1.618	1.400	1.508	-0.030	1.478
		6-311G(2d,p)	6-311G(2d,p)	1.833	1.598	1.445	1.521	-0.043	1.477	1.898	1.656	1.427	1.534	-0.025	1.509
			6-311+G(2d,p)	1.812	1.578	1.424	1.494	<i>-0.043</i>	1.451	1.875	1.622	1.402	1.501	<i>-0.025</i>	1.476

We have evaluated the basis set effects on the three first dyes represented in Scheme 2.1. These systems have been investigated experimentally by Gresser *et al.*¹⁴³ and Zhang *et al.*⁸⁶ Vertical B3LYP/6-31+G(d,p) absorption and B3LYP/TZVP absorption/emission results may be found in these two previous works. The PBE0 and CAM-B3LYP data for **Az.1**, **Az.2** and **Az.3** are collected in Table 2.1 and have been obtained with the LR-PCM approach. The ZPVE correction, by far the most expensive contribution in terms of computational requirements, is rather small for the tested dyes (-0.051 eV at most). Indeed, the typical values for ΔE^{ZPVE} ranges from -0.03 eV to -0.15 eV in small and medium-size molecules.^{58,93,98} More importantly, while ΔE^{ZPVE} is significantly smaller with the range-separated hybrid than with its global counterpart, the basis set effects remain trifling for this contribution. Indeed, the typical variations between the three tested atomic basis set are of the order to 0.005 eV. Therefore one could estimate the ΔE^{ZPVE} with the smallest atomic basis set, 6-31G(d), at the only price of very slight overestimations.

For the optical properties, the 6-311+G(2d,p)//6-311G(2d,p) [Energy//Geometry] combination may be used as reference, as it yields converged structures and transition energies.⁷⁷ It is obvious from Table 2.1 that the 6-31G(d) atomic basis set overestimates $E^{\text{vert-a}}$, $E^{\text{vert-f}}$, E^{adia} and E^{0-0} with errors of ca. 0.050 eV. However, vertical 6-311+G(2d,p) calculations performed on 6-31G(d) structures are sufficient to correct the largest part of the error. Such approach provides vertical transition energies within 0.020 eV of the reference, and the 0-0 energies are even more accurate due to the calculations of errors. Indeed, for the latter, the errors are rather negligible 0.008 eV, 0.000 eV and 0.001 eV, for **Az.1**, **Az.2** and **Az.3**, respectively. It is therefore reasonable to determine the geometrical parameters at the 6-31G(d) level and to compute the transition energies thanks to (vertical) calculations performed with a larger basis set. This procedure, already advocated by Grimme and coworkers,^{58,91} will be used in the following applying a 6-311+G(2d,p) as large basis set.

Figure 2.1 provides the vibronic shapes computed with three basis sets. As can be seen, both functionals foresee a significant shoulder to the main band, but the shapes are very similar for the three basis sets (PBE0), or only slightly modified by the extension of the basis set (CAM-B3LYP), confirming that 6-31G(d) provides accurate geometrical and vibrational parameters.

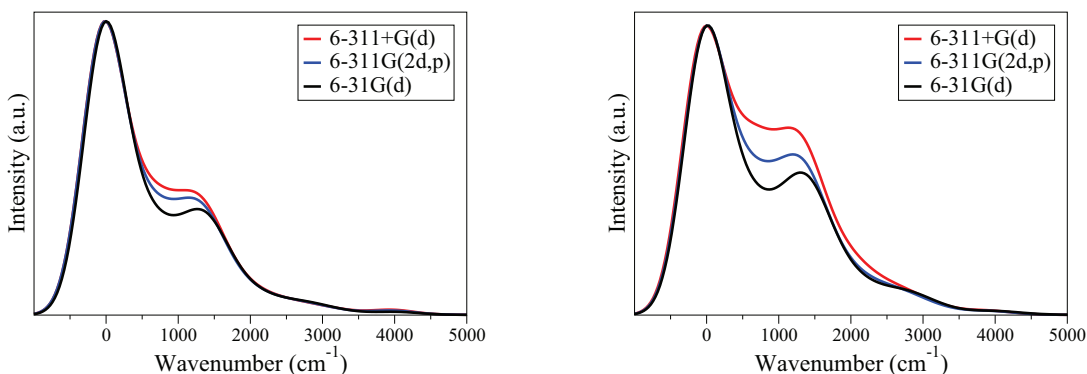


Figure 2.1: Impact of the atomic basis set on the vibronic shapes of **Az.3** with PCM-PBE0 (left) and PCM-CAM-B3LYP (right) levels. Results have been normalized for the main absorption band.

2.2.2 Solvent effects

In Table 2.2, we present PBE0/6-31G(d) transition energies obtained with a panel of solvent models and we compare them to gas phase results. The results obtained with five other functionals are available in Tables A.2 and A.3 in Appendix A and the trends are similar. We have selected the three same dyes as in Table 2.1 but have added dyes **Az.4** (in an apolar solvent) and **Az.5** (in a polar medium), that present a significant CT character in order to obtain a more representative panel. It turns out that the LR-PCM model is apparently rather unsatisfying for this class of dyes. Indeed, for E^{0-0} , the difference between the (LR,eq) and (SS,eq) results ranges from -0.361 (**Az.2**) to -0.121 eV (**Az.5**). Quite interestingly, the gas phase, cLR and SS results are alike for the aza-BODIPY with a cyanine like transition (**Az.1**, **Az.2** and **Az.3**), the solvatochromic effects estimated with LR being significantly different. This will motivate further research in the following Chapters. However, this relationship does not hold for **Az.5**, for which the (SS,eq)-gas difference attains -0.183 eV. Clearly, one should include solvent effects and go beyond the LR model, that does not capture all solvent effects. It is also noteworthy that the ΔE^{ZPVE} is significantly smaller in PCM than in gas-phase, the impact of solvation being about three times larger than the effect of the basis set. If one turns towards the absorption, one notices clearly that the perturbative cLR model, that is more computationally effective than its self-

consistent SS counterpart, is extremely efficient for the first four dyes, but that large SS-cLR differences are found for the CT dye **Az.5**: it is therefore a valid alternative for investigating cyanine-like transitions, and more studies are needed to assess the cLR/SS merits (see the following Chapters):¹⁴⁹ .

Table 2.2: Computed solvent effects for dyes **Az.1** – **Az.5**, using a panel of solvent models. All results are obtained with the PBE0/6-31G(d) approach. cLR and SS energies have been determined on the LR geometries.

Dye	$E^{\text{vert-a}}$						
	Gas	(LR,eq)	(cLR,eq)	(SS,eq)	(LR,neq)	(cLR,neq)	(SS,neq)
Az.1	2.239	1.904	2.227	2.220	2.117	2.229	2.224
Az.2	2.099	1.717	2.076	2.064	1.954	2.080	2.071
Az.3	1.994	1.623	1.972	1.959	1.852	1.974	1.963
Az.4	2.118	1.949	2.098	2.075	1.958	2.098	2.077
Az.5	1.917	1.611	1.809	1.700	1.707	1.822	1.734
Dye	$E^{\text{vert-f}}$				ΔE^{ZPVE}		
	Gas	(LR,eq)	(SS,eq)	(SS,neq)	Gas	(LR,eq)	
Az.1	2.032	1.694	2.014	2.013	-0.068	-0.051	
Az.2	1.955	1.575	1.936	1.935	-0.068	-0.048	
Az.3	1.837	1.472	1.814	1.813	-0.064	-0.047	
Az.4	1.965	1.795	1.934	1.933	-0.061	-0.051	
Az.5	1.818	1.514	1.635	1.627	-0.060	-0.039	
Dye	E^{adia}			E^{0-0}			
	Gas	(LR,eq)	(SS,eq)	Gas	(LR,eq)	(SS,eq) ^a	
Az.1	2.137	1.798	2.118	2.068	1.747	2.067	
Az.2	2.028	1.645	2.006	1.960	1.597	1.958	
Az.3	1.916	1.547	1.890	1.852	1.500	1.843	
Az.4	2.042	1.871	2.010	1.981	1.820	1.959	
Az.5	1.867	1.562	1.683	1.807	1.523	1.644	

^aDetermined using the (LR,eq) ZPVE correction and the (SS,eq) adiabatic energies.

As for the basis set effects, there is a strong parallelism between the impact of the solvent on the vertical and adiabatic results, e.g. the SS-LR difference on E^{0-0} are 0.320, 0.361, 0.343, 0.139 and 0.121 eV going down the column in Table 2.2 and the corresponding $E^{\text{vert-f}}$ ($E^{\text{vert-a}}$) variation are 0.320 (0.316), 0.361 (0.347), 0.342 (0.336), 0.139 (0.126) and 0.121 (0.089) eV, respectively. This means that the solvent effects do not significantly tune the geometrical reorganization energies of both the ground and excited states (see Chapter 1). In other words vertical transition energies capture most of the solvatochromic effects, and this justifies the approach developed in the previous Chapter. Eventually, let us note that the non-equilibrium effects are relatively small in the SS model, irrespective of the investigated phenomena. The fact that neq effects tends to be larger in LR-PCM than in other PCM models is consistent with a previous benchmark work.⁹³ For **Az.5**, we have performed the same PCM calculations but with the 6-311+G(2d,p) basis set. For $E^{\text{vert-a}}$, the neq LR, cLR and SS energies are 1.662, 1.778 and 1.695 eV, respectively. That is the cLR and SS models bring corrections of +0.116 and +0.033 eV, respectively, that are very similar to the values obtained with the 6-31G(d) basis set: +0.115 and +0.027 eV. Likewise, for the fluorescence, the (LR,eq), (SS,eq) and (SS,neq) 6-311+G(2d,p) values are 1.468, 1.594 and 1.587 eV, respectively, corresponding to successive corrections of +0.126 and -0.007 eV, once again completely in the line of the 6-31G(d) data of +0.121 and -0.008 eV. The same relationship holds for the adiabatic energies. One can therefore justify that the calculations with the largest basis set are performed only with the LR model and this procedure is systematically used in the following. Indeed, the adiabatic energies of the first seven dyes of Scheme 2.1 have been calculated, using the six functionals, to compare the results obtained with Equation 1.13 in SS, eq with both SBS and LBS (see Chapter 1). It turned out that the average absolute deviation is as small as 0.004 eV, whereas the maximal discrepancy does not exceed 0.009 eV (full list of results can be found in Table A.4 in Appendix A).

2.2.3 Functional effects

We can now provide best estimates (BE) for the 0-0 energies, using Equation 1.13 with SBS to the ZPVE correction. In fact, we have used Equation 1.19 with SS and 6-31G(d)[6-311+G(2d,p)] as SBS[LBS]. This allows to assess exchange-correlation functionals independently of basis set effects. The results obtained from Equation

1.19 for the nine symmetric dyes of Scheme 2.1 are collected in Table 2.3.

Table 2.3: Theoretical best estimates obtained for the absorption/fluorescence crossing point, Equation 1.19 with SS. All values are in eV. At the bottom of the Table, one can find the computed mean signed (MSE), absolute (MAE) and root-mean (RMS) errors compared to experiment. R is the linear correlation coefficient obtained by comparing theoretical and experimental data.

Dye	B3LYP	PBE0	BMK	M06-2X	CAM-B3LYP	ω B97X-D
Az.1	1.992	2.031	2.122	2.096	2.114	2.159
Az.2	1.873	1.908	2.005	1.923	1.953	1.937
Az.3	1.748	1.796	1.914	1.848	1.857	1.871
Az.4	1.892	1.930	2.032	2.002	2.016	2.036
Az.5	1.577	1.622	1.713	1.750	1.790	1.841
Az.6	1.852	1.883	1.923	1.946	1.937	1.927
Az.7	1.690	1.725	1.708	1.776	1.779	1.808
Az.8	1.920	1.954	1.953	1.988	1.998	2.024
Az.9	1.799	1.863	1.973	2.011	2.011	2.051
MSE	-0.129	-0.170	-0.240	-0.240	-0.252	-0.275
MAE	0.129	0.170	0.240	0.240	0.252	0.275
RMS	0.139	0.176	0.242	0.242	0.254	0.278
R	0.90	0.92	0.98	0.95	0.96	0.92

The MSE indicate that the theoretical transition energies are systematically too large, which is in the line of what has been found within the LR-PCM vertical approach for the same family of dyes,⁷⁷ and this is typical of cyanine transitions.⁶² The obtained MAE range from 0.13 to 0.28 eV, depending on the functional out this falls, within the expected TD-DFT accuracy (ca. 0.25 eV) for the E^{AFCP} of organic fluorophores.⁹³ This confirms that, by going beyond the vertical approximation, one can reasonably estimate the excited-state energies of cyanine-like transitions, thought we will see in the following Chapter that aza-BODIPY are probably a rather "easy" series.⁶⁸ The smallest average deviations are provided by B3LYP which is very close to the experimental spot (RMS of 0.14 eV). However, this quantitative success is at the price of less consistent estimates (poorer R): the variations of the optical properties

induced by chemical substitutions are satisfactorily but not accurately reproduced. BMK circumvents the problem (see Figure 2.2), with an impressive (R) and is therefore adequate for designing new aza-BODIPY. Consequently, we have applied only the B3LYP and BMK functionals in the following.

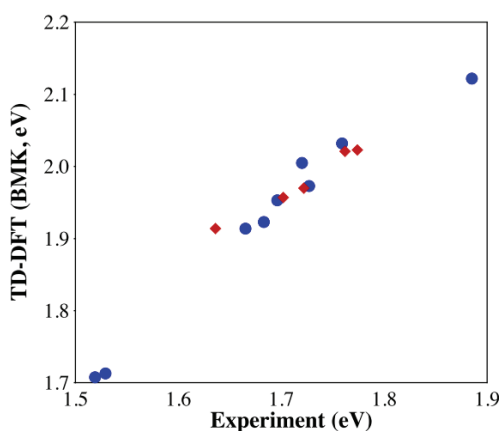


Figure 2.2: Comparison between BMK and experimental AFCP for symmetric, **Az.1**–**Az.9** (blue circles) and asymmetric, **Az.10**–**Az.14** (red diamonds), dyes. All values are in eV.

2.3 Applications

2.3.1 Asymmetric dyes

To assess the validity of our model, we have used a test set composed of dyes **Az.10**–**Az.14** (see Scheme 2.1), that present conformationally-restricted structures and large quantum yields.^{132,133} This set is not a simple extension of our training list of molecules as they are asymmetric, e.g. **Az.12**–**Az.14** are only hindered on one side, making the excited-state asymmetric. The results obtained with B3LYP and BMK functionals are collected in Table 2.4, and the BMK results are also available in Figure 2.2. As can be seen, these asymmetric structures are evaluated with a similar accuracy to their symmetric counterparts. Indeed, with BMK we obtain a MSE and a RMS of -0.258 eV and 0.258 eV for the **Az.10**–**Az.14** subset, respectively, completely in the line of the results of Table 2.3. Likewise, the R determined for the full

set (**Az.1–Az.14**) is 0.98 with BMK, that is the same as the one obtained on the symmetric structure subset. This is a further proof of the reliability of the approach.

Table 2.4: Theoretical best estimates obtained for the AFCP through Equation 1.19 with SS for dyes **Az.10–Az.14** with B3LYP and BMK. All values are in eV.

Dye	B3LYP	BMK
Az.10	1.813	1.914
Az.11	1.895	1.957
Az.12	1.946	2.023
Az.13	1.869	1.970
Az.14	150	2.021

2.3.2 Auxochrome impact on band shapes

For the three first dyes of Scheme 2.1, one can find a comparison between experimental and theoretical (PCM-TD-BMK) bands shapes in Figure 2.3. As discussed above, the SS 0-0 energies are too large with this functional and hence the computed wavelengths too small compared to experiment. However, the impact of the replacement of the phenyl rings by thiophene groups is reproduced in a very satisfying way. Indeed, not only the bathochromic shifts of both absorption and emission peaks when going from **Az.1** to **Az.2** and next from **Az.2** to **AAz.3** are well restored by TD-DFT, but in addition, the *ab initio* band shapes are accurate. Indeed, for absorption, one notes the presence of a shoulder at small wavelength in the experimental spectra⁸⁶ (see experimental spectra in Figure A.1 in Appendix A), this shoulder being higher in **Az.2** and **Az.3** than in **Az.1**. This effect is nicely reproduced by TD-DFT, though the height of the shoulder is overestimated by ca. 20% by BMK, the error being slightly mitigated by B3LYP. Likewise, the emission bands present experimentally less structure than their absorption counterparts but extend to longer wavelengths for all dyes.⁸⁶ This trend is also given by the applied model, though, the height of the shoulder is again slightly overrated. We have investigated the nature of the vibrational couplings playing a role in these shoulders. However, we found that they could not be explained by one or two isolated modes, but result from the combination of a large number of vibrational transitions, making chemically intuitive interpretations impossible.

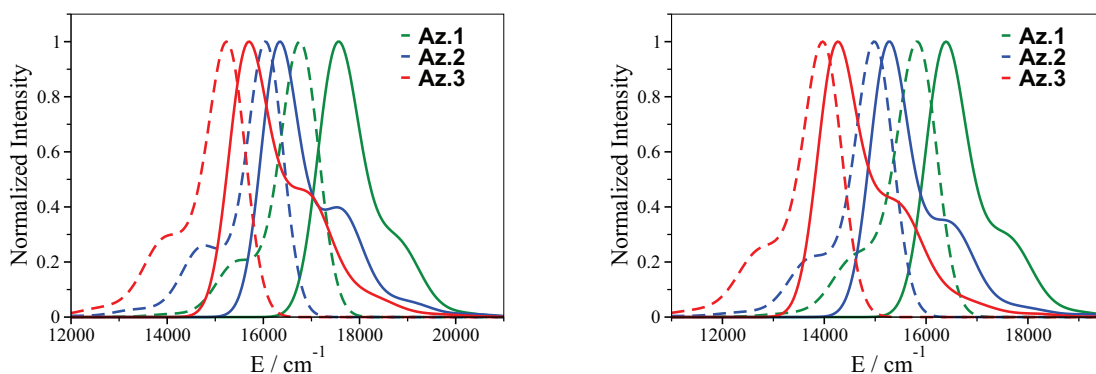
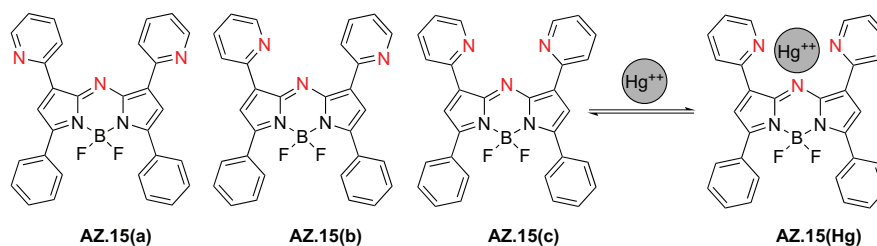


Figure 2.3: Vibronic spectra for dyes **Az.1**, **Az.2** and **Az.3** with BMK (left) and B3LYP (right). Full lines: absorption, dashed lines: fluorescence.

2.3.3 Complexation effects

One of the major applications of aza-BODIPY fluorophores is their ion sensing ability. Recently, it has been shown that the interaction between a specific aza-BODIPY dye presenting pyridine rings and mercury ions is strong enough to allow the optical detection of the latter.³⁹ The complexation clearly implies lone pairs of the three nitrogen atoms and the metallic cation (see Scheme 2.2).



Scheme 2.2: Conformers and complexation of compound **Az.15** (see Ref. 39 for experimental data).

We have simulated the optical properties of this system, using the same basis sets combination as above but applying the LanL2DZ basis set and pseudo potential for Hg^{2+} . It turns out that the most stable conformer for the free fluorophore, **Az.15(a)**, differs from the complexation isomer by the orientation of the two top pyridine rings. Nevertheless, the energetic differences between the three **Az.15** isomers of Scheme

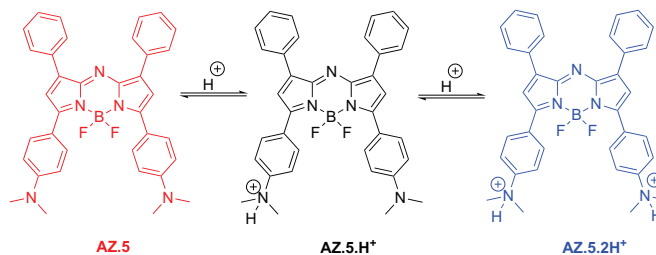
2.2 remain quite small. Indeed, PCM-BMK/6-31G(d) calculations provide relative ground-state energies of 0.00, 1.75 and 4.78 kcal.mol⁻¹ for **Az.15(a)**, **Az.15(b)** and **Az.15(c)**, respectively. These values are small compared to the estimated Hg²⁺ complexation energy of ca. 247.9 kcal.mol⁻¹,¹⁵¹ indicating that the interaction with the dication largely overcomes the cost of the rotation of the pyridine rings. Therefore, in the following, we only considered **Az.15(a)** and **Az.15(Hg²⁺)**. The charge-transfer distance, as measured by the separation between the barycenters of the electron density gain/depletion zones,^{152,153} attain 1.11 Å and 1.74 Å, for these two compounds, respectively (BMK results). This small enhancement of the charge-transfer hints for a bathochromic shift upon complexation that is observed.³⁹

The experimental AFCP point goes from 1.855 eV to 1.761 eV in acetonitrile upon Hg²⁺ binding, both the absorption and emission bands undergoing a ca. +35 nm (-0.090 eV) shift. Blindly applying our methodology provides qualitatively incorrect corrections, the estimated shifts being very far from the measurements: +0.175 eV (B3LYP) and +0.156 eV (BMK).¹⁵⁴ This is certainly a deceiving result, especially when the simpler $E^{\text{vert-a}}(\text{LR, neq})$ approximation provides an estimate of -0.090 eV (BMK), that is on the experimental spot. An analysis of the individual contributions to the theoretical $E^{\text{AFCP}}(\text{SS, neq})$ reveals that the SS correction is unrealistic for **Az.15(Hg²⁺)**, illustrating the difficulty to reach a physically-sound excited-state polarization of the PCM cavity for a dicationic derivative. Experimentally, the counter-ions are perchlorate anions and we have therefore optimized the corresponding **Az.15(Hg²⁺)**-(ClO₄⁻)₂ aggregate. As can be seen in Figure A.2 in Appendix A, the ground and excited state minima are similar, though one notices a small contraction of -0.06 Å for the Hg²⁺-N(BODIPY) distance. With this improved chemical model, our standard procedure, namely Equation 1.19 with SS, provides a variation of -0.141 eV (BMK)¹⁵⁵ between **Az.15(a)** and **Az.15(Hg²⁺)**, which reasonably fits the measurement.

2.3.4 Acidochromism

The optical signatures of **Az.5** are known to be very sensitive to the pH.¹³⁰ Indeed, while the neutral form displays an experimental AFCP point at 1.529 eV, this value attains 1.662 eV for the mono-protonated derivative and 1.892 eV for the di-protonated

form (see Scheme 2.3).¹³⁰ This corresponds to successive increase of +0.133 and +0.230 eV of the transition energies. Qualitatively, these acidochromic shifts can



Scheme 2.3: Illustration of the acidochromism effect for **Az.5** (see Ref. 130 for experimental data).

be explained by investigating the reorganization of the electronic cloud induced by the absorption (see Figure 2.4). For **Az.5**, one notes a clear charge-transfer character from the dimethylamino moieties towards the aza-BODIPY core, the top phenyl rings presenting only trifling contributions. The charge-transfer distance, computed with the above-mentioned approach,^{152,153} attains 2.55 Å for **Az.5**. Upon the first protonation, the CT character remains but is localized on one of the two arms, the protonated moiety being optically inactive. Eventually, for **Az.5.2H⁺**, the two *p*-NMe₂H⁺-Ph

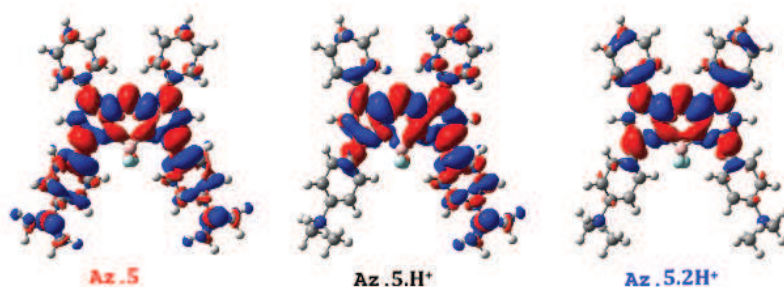


Figure 2.4: PCM-BMK/6-311+G(2d,p) electron density difference plots for neutral, cationic and di-cationic **Az.5**. The blue zones indicate electron density loss upon transition (donor) whereas the red zones correspond to increase of electron density upon transition (acceptor).

groups do not play any significant role in the optical transition, which is mainly lo-

calized on the chromogenic center. Nevertheless, one notices a small CT character from the top phenyl rings to the aza-BODIPY center (CT distance of 1.17 Å). With B3LYP (BMK), the AFCP points are estimated to be at 1.577 (1.713), 1.761 (1.937) and 2.033 (2.210) eV, for **Az.5**, **Az.5.H⁺** and **Az.5.2H⁺**, respectively. This corresponds to successive increase of the transition energies of +0.184 (+0.224) and +0.272 (+0.273) eV. The first being overestimated compared to experiment, whereas the second is accurate. In Figure 2.5, we compare experimental and theoretical absorption spectra. In the measurements, the absorption band is tighter for **Az.5.2H⁺** than for both **Az.5** and **Az.5.H⁺**, an effect that PCM-TD-BMK vibronic simulations reproduce in a very satisfying way. On the contrary, B3LYP does not give a reasonable estimate of the band shape for the **Az.5.H⁺** structure: it provides a band topology similar to **Az.5.2H⁺** rather than to **Az.5**, as in the measurements. Eventually,

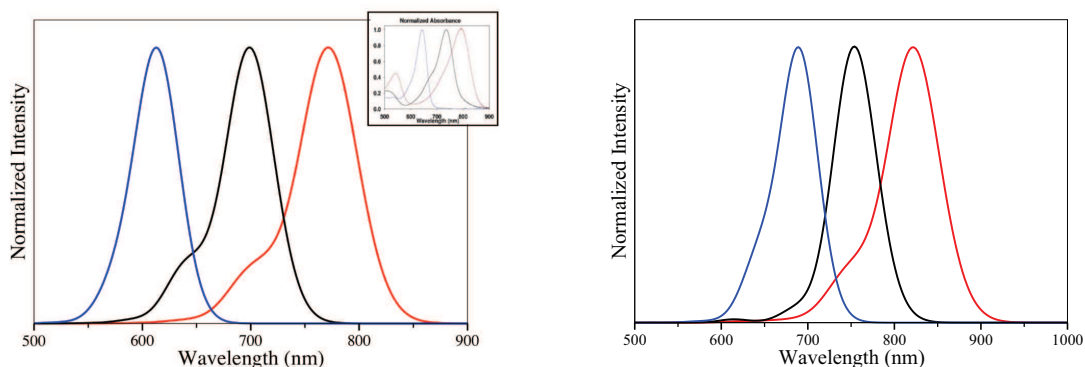


Figure 2.5: BMK (left)-B3LYP (right)-experiment comparison for the absorption bands of the three dyes of 2.4: **Az.5** (red), **Az.5.H⁺** (black) and **Az.5.2H⁺** (blue). The experimental inset on top right is reprinted with permission from *Org. Lett.* **8**, 2006 3493–3496. Copyright 2006 American Chemical Society.

though in these cases, the cationic sites are distant from the chromogenic centers (see Figure 2.4), we have also simulated the AFCP of **Az.5.H⁺** and **Az.5.2H⁺** explicitly including the counter-ions (trifluoro-carboxylate, TFA, as in the experiment).¹³⁰ The optimized structures may be found in Figure A.3 in Appendix A. With BMK, the predicted AFCP point are 1.909 and 2.150 eV for **Az.5.H⁺** and **Az.5.2H⁺**, respectively.¹⁵⁵ This corresponds to successive acidochromic shifts of +0.196 and +0.241

eV, which are closer from experiment than the corresponding simulations without TFA.

2.4 Conclusions

Using a panel of PCM-TD-DFT approaches, we have defined an efficient protocol to evaluate the spectral properties of aza-BODIPY dyes. This computationally efficient procedure relies on a systematic calculation of state-specific solvation effects as well as the determination of the vibrational signatures of both the ground and excited-states. Using the BMK functional, that was already found effective within the vertical TD-DFT approximation,⁷⁷ the evolution of the theoretical 0-0 energies are very consistent with the experimental trends but suffers from an almost constant deviation of ca. 0.25 eV. This systematic error can be reduced with B3LYP but at the price of a poorer, though still acceptable, correlation with experimental measurements. This concerns of a good trends but less accurate data (on the reverse) will also be found in the following Chapters and is related to the nature of the treated excited states. We have successfully applied our model to the investigation of asymmetrically substituted chromogens, pH-sensitive dyes as well as complexation effects. In each case, the proposed approach was both qualitatively and quantitatively consistent with experiment if the counter-ions used experimentally are explicitly included in the chemical model for charged compounds. Among the various NIR chromophores, aza-BODIPY dyes are not the most popular, boron-dipyrromethene (BODIPY) dyes have been the focus of more experimental studies. In the second Chapter 3, the methodology used to simulate the 0-0 energies and the optical properties of aza-BODIPY dyes will be discussed in the framework of simulation of the properties of BODIPY fluorophores.

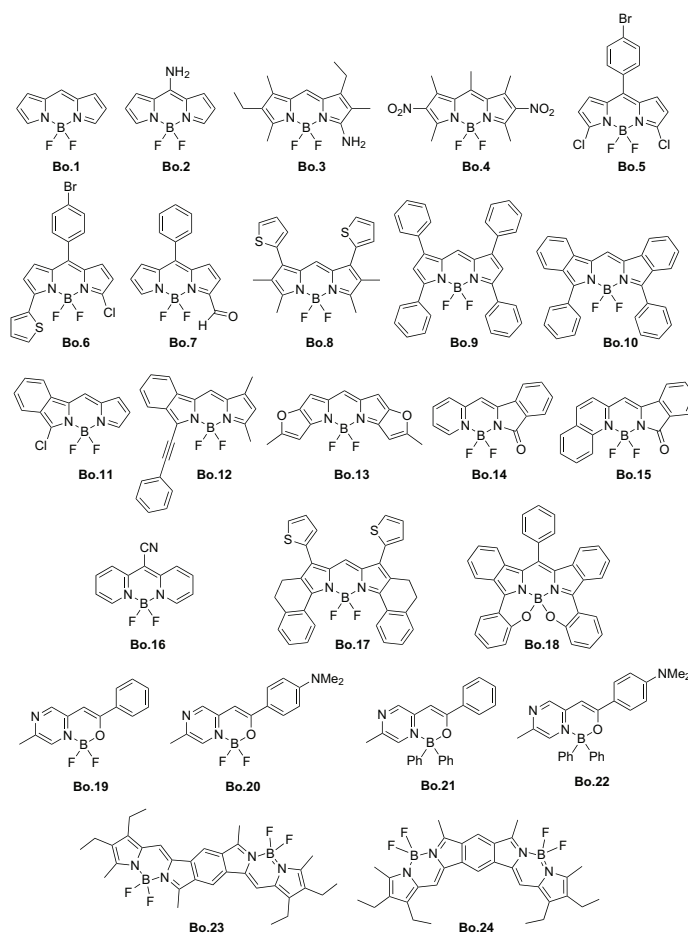
CHAPTER 3

BORON-DIPYRROMETHENE DYES: BODIPY

Boron-dipyrromethene (BODIPY) dyes have been subject to large synthetic effort due to i) their extremely rich chemistry, ii) their remarkable photo-physical properties and iii) their potential use in numerous fields of research.^{125, 156, 157} Notably, the success of this family of chromophores in *in vivo* microscopy imaging can be related to their photo-stability in biological environments whereas they also have a potential for detecting metal ions such as Cu^{2+} . The former property necessitates the specific design of water-soluble BODIPY derivatives,^{43, 158–160} whereas the latter is intimately linked to the possibility of binding metal ions at various positions of substituted BODIPYs.¹⁶¹

A set of representative BODIPY derivatives can be found in Scheme 3.1. It exemplifies the diversity of available BODIPYs for which chemical substitutions and ingenious synthetic strategies – i.e. nucleophilic substitutions at the 3- and 5- positions, electrophilic substitutions at the 2- and 6- positions, replacement of the fluorine atoms by C or O elements, insertion of donor/acceptor groups, extension of π paths, formation of dimers, structure stiffening... – have been used to tune the optical signatures of BODIPYs.^{75, 82, 125, 140, 141, 160, 162–180} Such a variety is well reflected in the experimental absorption and fluorescence wavelengths (see Table B.1 in Appendix

B) that almost cover the full range of visible spectra: from 400 nm to 750 nm. As explained before, large accessible optical window originates from the nature of the electronic excitations that could present a cyanine or a charge transfer character.



Scheme 3.1: Representation of the compounds used in the benchmark step.

BODIPY dyes have attracted significant modeling efforts during the last *lustrum*. If there exist one paper relying on CAS-SCF simulations,¹⁸¹ the vast majority of the theoretical works devoted to BODIPYs have been performed with DFT and TD-DFT. The former provides only ground-state properties allowing the representation of frontier orbitals that may offer qualitative informations and several works analyzed topologies and energies of the HOMO and LUMO orbitals.^{75, 78, 82, 88, 168, 176, 178, 182–190} Of course, a few TD-DFT works have been achieved within the vertical approach

for BODIPYs or some related derivatives.^{13,69–79} Only a few went beyond vertical absorption, Chen and coworkers performed an analysis of emission wavelength for eight BODIPYs, with a focus on the interplay between geometrical relaxation, charge-transfer and Stokes shifts.⁸⁸ Boens *et. al.*⁸⁷ (Jin *et. al.*)⁹⁰ presented an investigation of the relationship between flexibility and Stokes shift for six (four) conformationally restricted BODIPY dyes, using refined solvation models (calculations of Huang-Rhys factors). Eventually, for three iminopyrrolyl structures, Macanita’s group used the SOPRET-TD-DFT scheme to investigate the relative importances of the radiative and non-radiative ES pathways.⁸⁹ To the best of our knowledge, no TD-DFT investigation has been devoted to the simulation of the 0-0 energies of BODIPY.⁹⁵

3.1 Methods

In Chapter 2, we have performed an extensive TD-DFT assessments of basis set and solvent effects for the aza-BODIPY subclass.⁹⁴ Consequently, there is no need to further investigate these two “technical” aspects in this Chapter. The major findings were: 1) geometric and vibrational parameters can be obtained with the 6-31G(d) atomic basis set without significant loss of accuracy; 2) transition energies are much more basis set dependent and need to be determined with the 6-311+G(2d,p) atomic basis set; 3) SS and LR transition energies differ significantly; 4) the SS-LR differences are nearly basis set independent. To estimate the AFCP energies, E^{AFCP} , we have therefore applied Equation 1.19 with SS.^{93,94} The computational detail are completely similar to those of the previous Chapters and will nor be repeated here.

3.2 Adiabatic energies

3.2.1 Benchmarks of DFT functionals

In this first step, we aim to find an exchange-correlation functional providing chemically relevant information. As before, we are mainly interested in accurate simulation of auxochromic effects, the relevant criterion for dye design, and not in reproducing exactly the experimental transition energies. We have tested a series of hybrid functionals: B3LYP,^{110,111} PBE0,^{112,113} BMK,¹¹⁷ M06-2X,¹¹⁶ as well as CAM-B3LYP¹¹⁹ and ω B97X-D.¹²¹ To perform the benchmark, we have used the 24 dyes represented

in Scheme 3.1. The absorption (fluorescence) wavelengths present in this training set, range from 406 (430) nm to 758 (774) nm (see Table B.1 in Appendix B). The results obtained for the AFCP are listed in Table B.2 in Appendix B, whereas Table 3.1 provides a statistical analysis for the full set. The mean absolute errors (MAE) are quite large for TD-DFT calculations, though both B3LYP and PBE0 yield average deviations below the 0.3 eV limit. Unfortunately, this is at the price of less consistent estimates of the auxochromic effects, as seen by the quite large standard deviations and poor R^2 for these two first hybrid functionals. This behavior completely parallels the findings obtained previously. It is worth to note that the large majority of TD-DFT works performed on BODIPYs relied on B3LYP. More robust estimates are reached with the four hybrids incorporating larger shares of exact exchange. Particularly striking is the performance of M06-2X, that provides a standard deviation (SD) of 0.06 eV and a R^2 of 0.98. This is illustrated in Figure 3.1: though the theoretical values are systematically too large, the evolution is restored for the entire set with no significant outliers (see below for the test set). In fact, a simple linear correction of the M06-2X data ($-0.141 + 0.908 \times E^{\text{AFCP}}$) would allow reducing the theoretical error to less than 0.05 eV, though we will not use such statistical correction in the following.

Table 3.1: Mean signed and absolute errors (MSE and MAE, eV), standard deviation (SD, eV), maximal deviations (Max, eV), as well as the linear determination coefficient (R^2) obtained by comparing experimental and theoretical E^{AFCP} values. CAM and ω BD stands for CAM-B3LYP and ω B97X-D, respectively.

	B3LYP	PBE0	BMK	M06-2X	CAM	ω BD
MSE	0.121	0.211	0.340	0.389	0.402	0.418
MAE	0.259	0.284	0.343	0.389	0.402	0.418
SD	0.273	0.234	0.127	0.063	0.077	0.076
Max(+)	0.426	0.514	0.555	0.513	0.541	0.550
Max(-)	-0.688	-0.511	-0.034	0.295	0.269	0.268
R^2	0.576	0.678	0.883	0.980	0.966	0.968

The fact that M06-2X emerges as the most adequate functional is consistent with previous benchmarks demonstrating that this functional tends to be more efficient when full adiabatic calculations are performed, whereas B3LYP or alike approaches tend to be more effective within the vertical limit.^{58,93,118} Therefore in the rest of

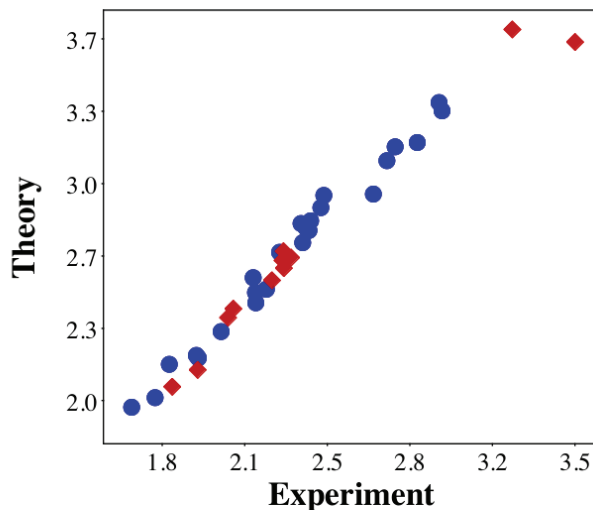


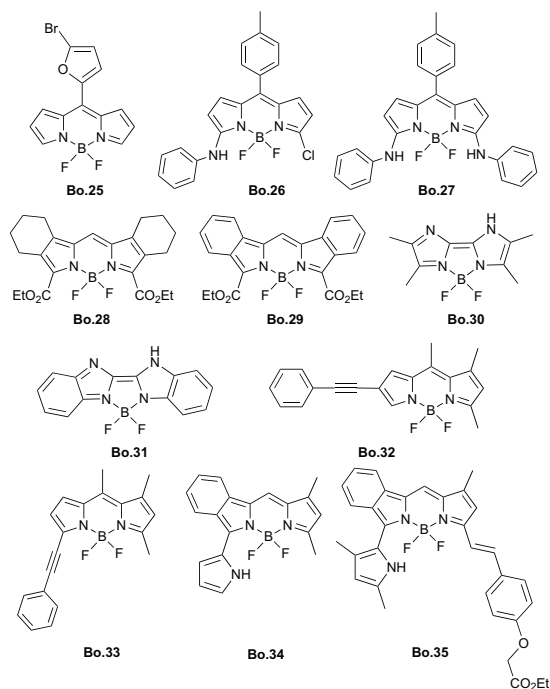
Figure 3.1: Comparison between M06-2X and experimental E^{AFCP} . Blue circles are for the training set (Scheme 3.1) whereas red diamonds correspond to the test set (see Scheme 3.2, below). All values are in eV.

this Chapter, we exclusively present and discuss M06-2X results. The fact that BMK was used for aza-BODIPY M06-2X for BODIPY can be viewed as disappointing, but we note that M06-2X results. For aza-BODIPY were also very satisfying.

3.2.2 Test cases

To ascertain the reliability of the M06-2X functional, we have used an external test set of 11 dyes (see Scheme 3.2).^{125,191–195} It contains a further diversity of structures, especially BODIPYs with strong intramolecular NH-F hydrogen bond(s) (**Bo.26**, **Bo.27**, **Bo.34** and **Bo.35**)¹⁹² and two bis-imidazole like molecules (**Bo.30** and **Bo.31**),¹²⁵ as such dyes are not present in the original training set of Scheme 3.1. The two bis-imidazole compounds (**Bo.30** and **Bo.31**), present significantly smaller fluorescence wavelengths than classical BODIPY, that is 377 and 417 nm, respectively,¹²⁵ and brings in a significant challenge. The results are listed in Table B.3 in Appendix B, and are given in Figure 3.1 as red diamonds. Though there is a significant deviation for **Bo.30** (but not for **Bo.31**), it is clear that the additional molecules do not perturb significantly the obtained trend: M06-2X is indeed an adequate functional for our purposes. This is confirmed by the statistical data obtained by considering the

full set of dyes (both Schemes 3.1 and 3.2): the MAE is 0.374 eV, the SD attains 0.076 eV whereas the R^2 is 0.971, all in the line of the results of Table 3.1.



Scheme 3.2: Panel of dyes used in our test set.

3.3 Applications

3.3.1 Vibrationally resolved band shapes

One of the most critical aspect of BODIPY dyes is their band shapes. The BODIPY core, **Bo.1** was synthesised in 2009 by two groups,^{169,196} and it appeared that the absorption and emission curves are nearly perfect mirror images of each other, with respective maxima at 503 (500) nm and 512 (516) nm in CH_2Cl_2 (THF).^{196,197} More striking is the presence of an intense (ca. one half intensity of the main band) shoulder at ca. 485 and 535 nm for absorption and fluorescence, respectively (CH_2Cl_2).¹⁹⁶ The TD-M06-2X simulation can be found in Figure 3.2 and it appears that theory reproduces the presence of this intense shoulder, displaced by ca. 15 nm compared to the main band. The only significant error of TD-DFT is to underrate the height of the emission shoulder. In terms of individual vibrational modes explaining the band

topology, the stick spectrum in Figure 3.2 clearly illustrates that there are not one or two dominating vibrational mode(s) explaining the band shape, but rather a very complex combination that does not offer chemically intuitive interpretations. As can be seen in Appendix B, the stick spectra is simplified for a conformationally restricted BODIPY (**Bo.18**), but a large combination of individual vibrational modes is still required to account for the shoulder in that case.

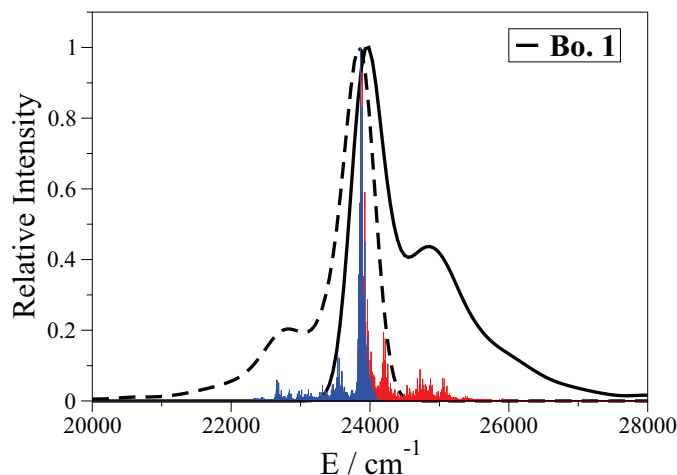


Figure 3.2: Computed stick and convoluted spectra for both absorption (full) and emission (dashed) of **Bo.1** in CH_2Cl_2 .

The two molecules possessing a keto group at position 5, synthesized by Qian and coworkers,¹⁶⁸ namely **Bo.14** and **Bo.15**, present a much more marked structure of their absorption bands than **Bo.1**. Indeed, the two main peaks present nearly the same intensity (**Bo.15**) or the longest wavelength band is the weakest (**Bo.14**). As can be seen in Figure 3.3, the proposed computational scheme restores both the shapes and relative positions of the bands with a remarkable accuracy. Computed emission bands (see Figure B.2 in Appendix B) are also in agreement with experiment.¹⁶⁸ Contrary to **Bo.1**, a few vibrational mode now dominates the total stick vibronic spectra. The most intense contributions (besides the 0-0 absorption), that can account for the second maxima of the convoluted spectra, are located at 1546 cm^{-1} and 1553 cm^{-1} for the ES of **Bo.14** and **Bo.15**, respectively. These modes mostly correspond

to in-plane wagging of the CH and distortion of the aromatic cycles but do not directly imply the BF_2 groups nor the N-B bonds.

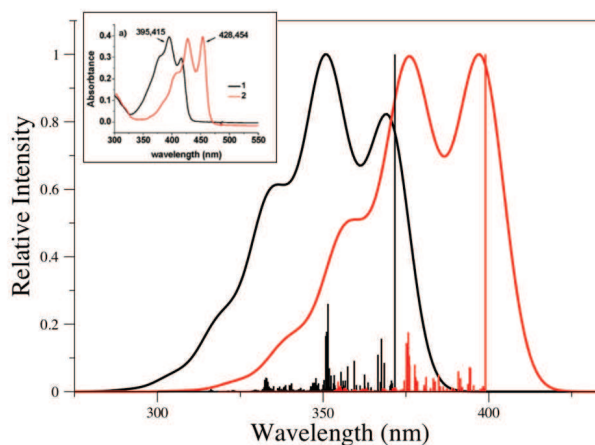


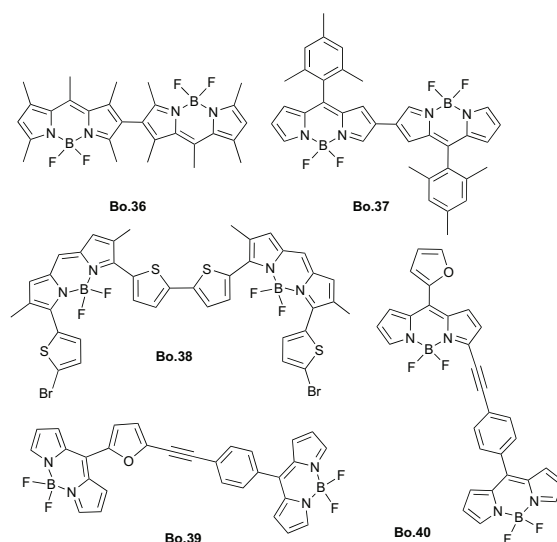
Figure 3.3: Computed stick and convoluted spectra for the absorption of **Bo.14** (black) and **Bo.15** (red) in CH_2Cl_2 . Emission spectra can be found in Figure B.2 in Appendix B. The inset is the experimental data reprinted with permission from Y. Zhou *et. al.*, *J. Org. Chem.* **2008**, *73*, 1571–1574. Copyright 2008 American Chemical Society.

A 8-cyano substitution of a modified BODIPY (leading to **Bo.16**) induces not only a hypsochromic shift (exp:+0.303 eV, theory: +0.224 eV compared to **Bo.1**, see Tables B.1 and B.2 in Appendix B), but also yields a clear multi-peak structure of both the absorption and emission spectra.¹⁷⁴ The presence of multiple maxima could also be reproduced (see Figure B.3 in Appendix B), though the agreement between theory and experiment is less impressive than in Figure 3.3. In contrast, the β -iminoketone ligands, **Bo.19–Bo.22** tend to produce broad and shapeless structures with a long decreasing tail for the emission,¹⁷⁶ and these outcomes can be qualitatively reproduced e.g., (see the spectra of **Bo.19** in Figure B.4 in Appendix B).

3.3.2 Dimers

Spectral features of multi-fluorophores are often difficult to interpret, as different phenomena may take place at the ES. Several multi-BODIPY structures have been proposed and a theoretical look on their spectra is certainly useful. Two of the

“simplest” BODIPY dimers present two structures bonded by a 6,2' link,^{198,199} but other linkages have been proposed, e.g., through thiophene rings attached at 5,3',²⁰⁰ or via a ethynylphenyl linker placed at position 3 or 8.⁷⁸ We have investigated all these possibilities (see Scheme 3.3), together with the corresponding monomers as well as the fully conjugated dimers, **Bo.23** and **Bo.24** (see Scheme 3.1),⁷⁵ so to have a representative set. Nevertheless, we underline that additional oligomeric or multi-BODIPY compounds have been synthesized.^{76, 89, 157, 181, 190, 192, 200–209}



Scheme 3.3: Representation of selected BODIPY dimers.

In **Bo.36**, going from the monomer to the dimer induces a bathochromic shift of the A_{FCP} energy by -0.186 eV,¹⁹⁸ and this effect is restored by theory that foresees a -0.200 eV displacement of the optical bands. Vibrationally resolved spectra for both the monomer and dimer may be found in Figure B.5 in Appendix B but they present no specific features: the shapes of both bands remain nearly constant when going from the monomer to the dimer. Note that in **Bo.36**, the repulsion between the methyl groups induces a significant twist between the two BODIPYs (58° in the ground-state). This contrasts with **Bo.37** for which we obtain nearly coplanar BODIPY cores, which is perfectly in the line of XRD findings.¹⁹⁹ This, in turns, implies a reorganization of the electron density spanning on the two BODIPY cores (see Figure 3.4), and hence a stronger bathochromic displacement of E^{AFCP} when going from the monomer to the dimer: -0.479 eV (experiment)¹⁹⁹ and -0.432 eV

(theory). The theoretical and experimental bands are compared in Figure 3.5, and the broadening of the bands upon dimerization is correctly provided by theory, though the topology of the absorption band of **Bo.37** could not be exactly restored.

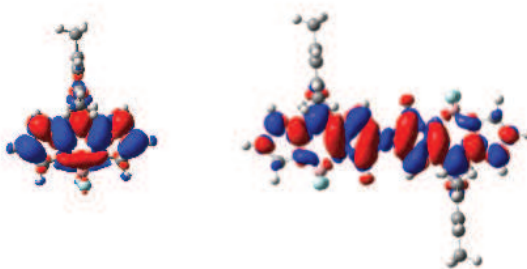


Figure 3.4: Electron density difference plots between the ES and GS for **Bo.37** (right) and its monomer (left). The red (blue) zones indicate increase (decrease) of density upon electronic transition.

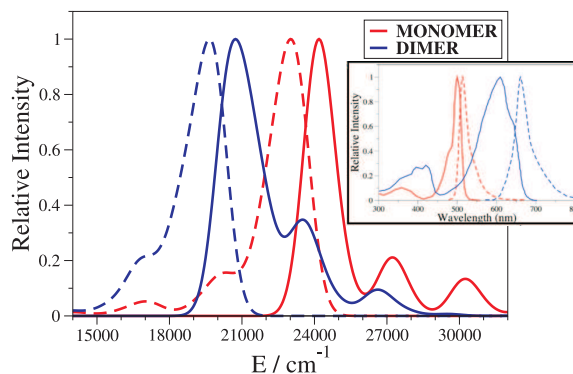


Figure 3.5: Comparison between experimental (inset) and theoretical vibrationally resolved absorption (full) and emission (dashed) spectra of **Bo.37** and its monomer. The experimental graph is adapted with permission from Y. Hayashi *et. al.*, *J. Org. Chem.* **2011**, *13*, 2992–2995. Copyright 2011 American Chemical Society.

In both **Bo.36** and **Bo.37**, increasing the oligomeric length induces variations of the position, width and intensity of the bands but no additional well defined peak could be observed experimentally: one absorption band dominates. The situation gets more complex for **Bo.38** that presents a double peak structure, with a first intense

transition at long wavelengths (ca. 700 nm), and a second slightly less intense but well separated band at ca. 600 nm.²⁰⁰ As expected from Kasha's rule, there is only one intense fluorescence band corresponding to the lowest-lying ES. We indeed found two energetically close ES presenting significant oscillator strengths in **Bo.38**. The density reorganization plots corresponding to these two ES are shown in Figure 3.6 and it is clear that the first and second bands respectively correspond to a highly delocalized phenomenon with a connection between the two fluorophores, and to a transition typical of a single BODIPY. This is consistent with measurements, as the position of the second absorption band of **Bo.38** fits the λ_{\max} of the corresponding monomer.²⁰⁰

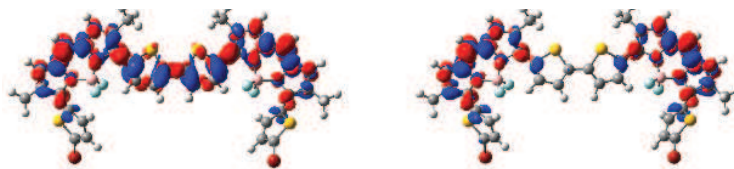


Figure 3.6: Electron density difference plots between the ES and GS for **Bo.38**. Left: first ES, right: second ES. See caption of Figure 3.4 for colour conventions.

In **Bo.40**, there are two main absorption bands, the first being significantly red shifted compared to both the monomer and to **Bo.39**, whereas the second has the same position as in the monomer.¹⁸⁴ Again, this can be qualitatively explained by Electron density difference (EDD) plots (see Figure B.8 in Appendix B): the first state is located on the BODIPY bearing the furan ring, but extends on the ethynylphenyl arm (hence is more delocalized, explaining the bathochromic shift) whereas the second state is characteristic of an isolated fluorophore and is solely centered on the second BODIPY. On the contrary in **Bo.39** none of the two first ES is significantly delocalized over the ethynylphenyl linker (see Figure B.9 in Appendix B), and one observes only a shoulder for the main absorption band.¹⁸⁴

Eventually, let us turn towards the *anti* (**Bo.23**) and the *syn* (**Bo.24**) conjugated dimers. The results are compared to experiment in Figure 3.7. As can be noticed the shift between the two systems (exp: 0.160 eV/theo: 0.198 eV)⁷⁵ is well reproduced, and the band shapes are also in qualitative agreement with, on the one hand, a

broader absorption band together with a more marked shoulder for **Bo.23** than for **Bo.24**, and, on the other hand, emission bands having less structures than their absorption counterparts. The difference between the two systems can be qualitatively understood from the density reorganization plots (top of Figure 3.7): absorption in the *syn* (*anti*) derivatives induces a reorganization mainly centered on one side of the molecule (delocalized on the full structure). Note that, according to PCM-TD-M06-2X, this principal absorption band mainly corresponds to an HOMO-LUMO transition but implies other significant molecular orbital contributions, which differs from B3LYP results.⁷⁵

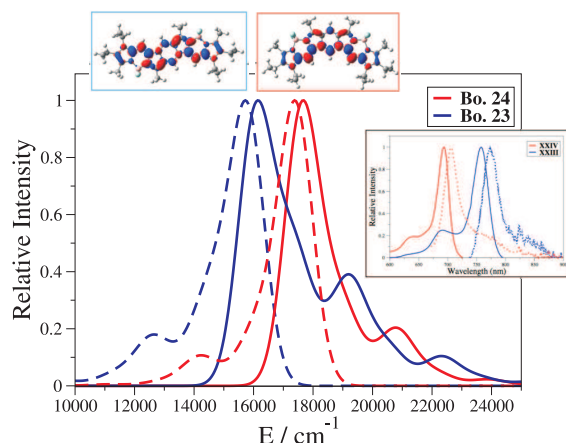
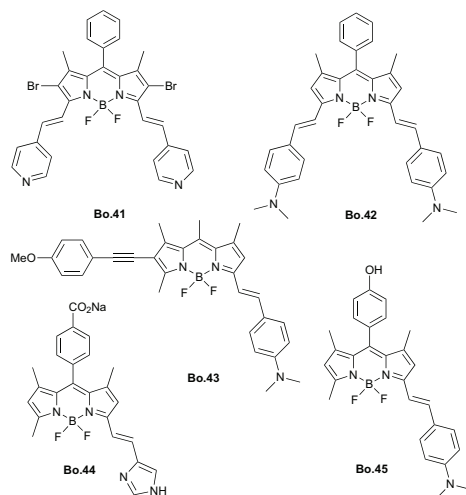


Figure 3.7: Computed absorption (full) and fluorescence (dashed) spectra of **Bo.23** and **Bo.24**. Inset: experimental data (adapted from Ref. 75, copyright RSC 2012) and density difference plots for the two dyes (top).

3.3.3 pH probes

Some BODIPYs can also be used to detect variations of the acidic/basic conditions as their absorption and/or emission properties are modified by protonation/deprotonation of side groups.^{129,139,210–216} A representative panel is depicted in Scheme 3.4.

Bo.41 and **Bo.42** designed by Akkaya and coworkers,²¹¹ are both sensitive to the pH, but undergo opposite acidochromic effects. Indeed, in chloroform, the protonation of the two pyridine rings of **Bo.41** induces a -0.113 eV bathochromic shift, whereas the full protonation of the dimethylamino groups yields a +0.275 eV hypsochromic shift in **Bo.42**.²¹¹ We have been not only able to quantitatively reproduce these effects



Scheme 3.4: Representation of selected pH probes.

with predictions of -0.095 eV and $+0.303$ eV, for **Bo.41** and **Bo.42**, respectively, but also to provide a chemically intuitive explanation. Indeed, as can be seen in Figure 3.8, the first ES of **Bo.42** presents a strong CT character, the absorption of a photon inducing a shift of the electronic density from the pushing NMe_2 groups towards the central chromogen and this effect is completely annihilated at low pH, as protonation removes the lone pairs of the two nitrogen atoms from the conjugated path. Therefore, decreasing the pH implies a change of optical features from a CT to a localized cyanine-like transition of higher energy, as for the related aza-BODIPY described in the previous Chapter. On the contrary, in **Bo.41**, protonation allows the emergence of a partial CT from the BODIPY core towards the electron deficient pyridinium rings, whereas the original pyridine rings do not play any significant role in the optical transition of the neutral **Bo.41**. The qualitative behaviours displayed in Figure 3.8 can be confirmed by computing the CT distance,^{152, 153} For **Bo.41** it increases from 0.67 Å to 1.31 Å upon diprotonation, whereas in **Bo.42**, it falls by one order of magnitude (from 2.25 Å to 0.26 Å) when decreasing the pH. The vibronic shapes of **Bo.41** and **Bo.42** are shown in Figures B.6 and B.7 in Appendix B and present a typical shoulder that is better defined in **Bo.41** than in **Bo.42**, consistently with experimental evidences.²¹¹

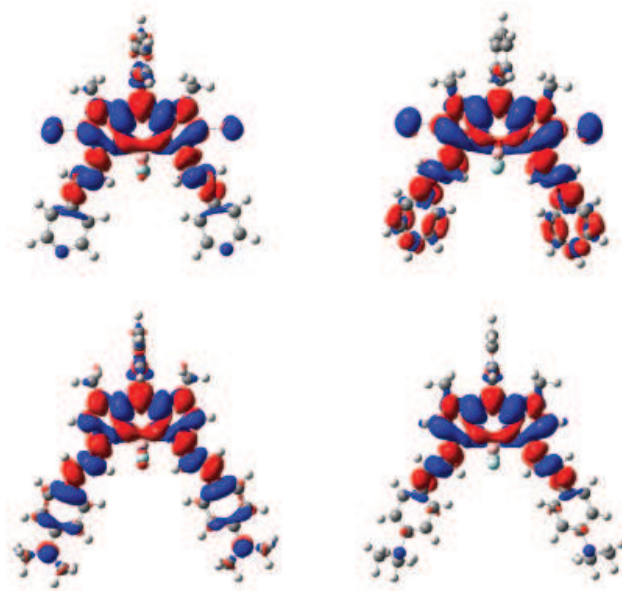


Figure 3.8: Electron density difference plots for **Bo.41** (top) and **Bo.42** (Bottom) in their neutral (left) and diprotonated (right) forms in CHCl_3 .

The asymmetric **Bo.43** behaves like **Bo.42** but the impact of protonation is less marked.²¹³ Indeed, in dioxane, going to acidic pH induces an experimental hypsochromic displacement of +0.113 eV.²¹³ In this case, the effect is only qualitatively restored by theory (+0.060 eV), part of the remaining error being probably ascribable to the lack of counter-ion in our simulation.⁹⁴ A density analysis, presented in Figure B.10 in Appendix B, clearly shows that the smaller shift can be explained by the presence of the methoxy substituent in **Bo.43**. Indeed, in the neutral form one finds a first ES characterized by a CT from NMe_2 to the BODIPY core, whereas in the presence of acid, the CT nature is conserved, but the electronic cloud now moves from OMe to the BODIPY core.

In the water-soluble **Bo.44**, the imidazole can be protonated or unprotonated and only rather small variations of the absorption and fluorescence energies have been observed.²¹² Going from a neutral to acidic environment induces a small hypsochromic shift in both experiment (+0.057 eV)²¹² and theory (+0.082 eV), whereas in basic

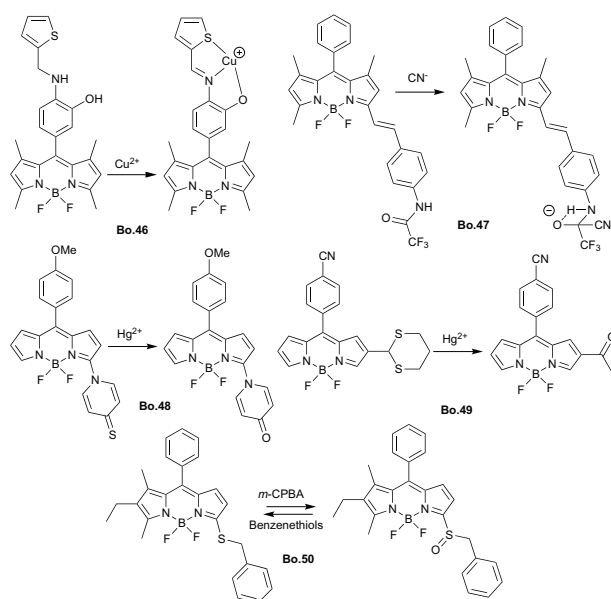
environment, experiment indicates trifling modifications of E^{AFCP} , and TD-DFT consistently foresees a very small effect (-0.025 eV).

Bo.45 is also an interesting probe allowing to detect both acid (protonation of the dimethylamino group) and basic (deprotonation of the hydroxyl group) solutions.²¹⁰ When going from neutral to protonated species, one notes a strong hypsochromic displacement of E^{AFCP} and theory perfectly matches experiment (exp: +0.248 eV,²¹⁰ theory: +0.244 eV). As previously, this effect can be explained by the annihilation of the donating character of the terminal amino group. In basic media, the situation is more complex. For the absorption, our model predicts almost unchanged signatures: the variation between the neutral and anionic forms is as small as +0.003 eV.²¹⁷ For the excited-states, the calculations indicate the presence of a first very low-lying ES (E^{AFCP} : 0.924 eV), but it presents, at the end of the geometry optimization process, a completely trifling oscillator strength (forbidden state). For the second ES, that is strongly dipole-allowed, we compute an E^{AFCP} of 2.036 eV, exactly the same as its neutral counterpart. Therefore, our calculations allow to explain the experimental observations:²¹⁰ on the one hand, the strong hypsochromic shift at low pH, and on the other hand, the unchanged absorption but negligible fluorescence at large pH, that is due to the presence of an additional forbidden low-energy ES, that implies a non-radiative deactivation path that was not present in the neutral structure.

3.3.4 Ion sensing

BODIPY and its derivatives have been widely used as ion sensors,^{73, 161, 191, 214, 215, 218–226} and a selected set of representative molecules can be found in Scheme 3.5. **Bo.46** allows to detect copper ions through a tridentate complexation.¹⁶¹ The E^{AFCP} of (free) **Bo.46** presents a hypsochromic shift of +0.319 eV (exp)/+0.362 eV (theo) compared to **Bo.6** that also presents one phenyl and one thiophene rings. Upon complexation with Cu^{2+} , theory foresees a small shift of the absorption energy (+0.047 eV),²²⁷ whereas experimentally the effect is even smaller.¹⁶¹ To detect cyanide anion, Ekmekci and coworkers proposed **Bo.47**,²¹⁹ that presents a reactive terminal amide group. This strategy was recently extended to aldehydes.²²⁵ This results in a bathochromic shift of the absorption λ_{max} (-0.123 eV) (and a quenching of the emission). Our calculations that include the counterion,²²⁸ indicate a E^{AFCP} shift of

-0.061 eV. To qualitatively reproduce this small effect of the CN^- , it is mandatory to include the counterion in the calculations, and this fits the findings of the previous Chapter.



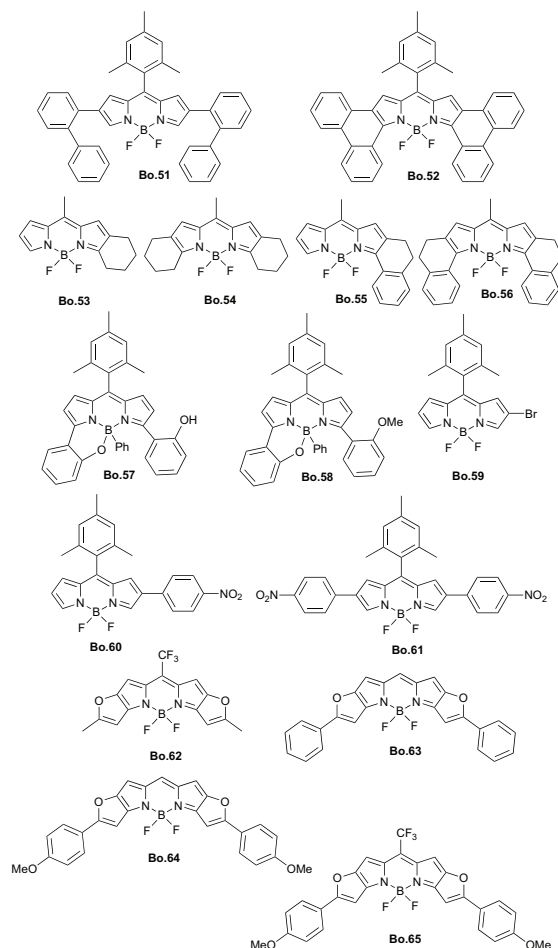
Scheme 3.5: Representation of selected ion-sensitive BODIPY.

Original ideas to obtain mercury ion sensing were proposed by, on the one hand, Khan and Ravikanth,¹⁹¹ and, on the other hand Zhang *et. al.*²²² In both cases, the presence of Hg^{2+} cations induces an irreversible reaction, from a thiocarbonyl to carbonyl group (**Bo.48**),¹⁹¹ or from dithiane to an aldehyde moiety (**Bo.49**),²²² which, in turn, influences both absorption and fluorescence signatures. For **Bo.48** the impact of the position of the 0-0 band is very limited, +0.010 eV (in CHCl_3) and our theoretical scheme qualitatively restores this effect but overshoots its magnitude (+0.041 eV). Interestingly, by considering only the (SS,neq) vertical absorption energies, one would predict a much larger effect (+0.275 eV) that is obviously off experiment. This is one clean illustration showing that the vertical TD-DFT model cannot provide a fully consistent picture for modest variations. For **Bo.49** (in THF), one notices a similar phenomenon with a hypsochromic and hypochromic displacement when going from the dithiane to the aldehyde (E^{AFCP} : +0.072 eV, ϵ : -13%),²²² and theory provides reasonable estimates (E^{AFCP} : +0.131 eV, $f(\text{SS,neq})$: -14%). Eventually, we have also investigated an equilibrated oxidation reaction that was recently proposed

to detect several thiols (**Bo.50**).²²⁴ When oxidising the sulphur into sulfoxide, the experimental E^{AFCP} undergoes an hypsochromic shift of +0.120 eV experimentally and theory predicts the correct direction for the effect but overestimates its amplitude (+0.225 eV).

3.3.5 NIR structures

Of course, it is highly interesting for practical applications to obtain BODIPY structures with fluorescence bands shifted towards longer wavelengths, that is, to obtain near-infrared (NIR) emitters. To this end, several strategies have been used: 1) improvement of the delocalizability of the ES by extending the π -conjugated path or stiffening the lateral rings;^{74, 87, 173, 177, 179, 183, 193, 195, 229–234} 2) replacement the fluorine atoms of BF_2 by oxygen atoms directly bonded to the side aromatic rings;^{178, 235, 236} 3) increase of the CT character of the BODIPYs.^{171, 199, 213, 237–240} Of course, some molecules combine two or three of these approaches to reach NIR fluorescence. One can already find several examples of these different strategies in the set of dyes treated in our training and test panels (see above), but we present additional cases in Scheme 3.6. We have first tested the biphenyl substituted **Bo.51** and corresponding aryl-fused BODIPY, **Bo.52**.¹⁸³ The oxidative cyclisation allowing to go from the former to the latter induces a bathochromic shift of the E^{AFCP} by -0.271 eV experimentally¹⁸³ and -0.266 eV with TD-DFT (both in CH_2Cl_2). The measured and simulated emission curves are in good agreement as can be seen in Figure 3.9. The density difference analysis indicates that in **Bo.52** there is a CT from the side phenyl-rings towards the BODIPY core. Next, we have tested the impact of stiffening using the series of symmetric and asymmetric BODIPY dyes proposed by Boens and coworkers.⁸⁷ Going from **Bo.1** to **Bo.53** and next to **Bo.54**, implies successive bathochromic shifts of -0.226 eV and -0.104 eV in toluene, and both are overshoot by theory: -0.329 eV and -0.151 eV. Adding one or two additional phenyl rings induces further measured (computed) bathochromic effects of -0.167 (-0.231) eV and -0.298 (-0.361) eV when going from **Bo.53** to **Bo.54** and from **Bo.54** to **Bo.56**, respectively. Therefore, though TD-DFT predicts too large bathochromic effects, their relative magnitudes are correctly restored. By comparing **Bo.10** and **Bo.18**, one notes that replacing the B-F bond by an oxygen bridge with side phenyl rings induces a strong bathochromic shift (exp: -0.184 eV, theo: -0.182 eV). In addition, we have modeled two BODIPYs



Scheme 3.6: Representation of several BODIPY dyes designed to move the absorption/emission towards longer wavelengths.

in which only one of the two fluorine atoms has been replaced, namely **Bo.57** and **Bo.58**,²³⁵ to consider asymmetric cases. By comparing **Bo.18** to **Bo.58**, we obtain a hypsochromic effect of +0.286 eV (measurements) or +0.290 eV (calculated). The situation is completely similar for **Bo.57**.

Let us now turn towards the impact of the addition of strong electroactive groups. For the dimethylamino donor, examples have already been discussed in Section 3.3.3, and we have focussed our attention on the complementary series **Bo.59**, **Bo.60** and **Bo.61** that present one or two nitro groups. The successive effects on the E^{AFCP} attain -0.099 eV and -0.157 eV experimentally,¹⁹⁹ and they are well restored by our approach: -0.103 eV and -0.144 eV. The electron density difference plots displayed

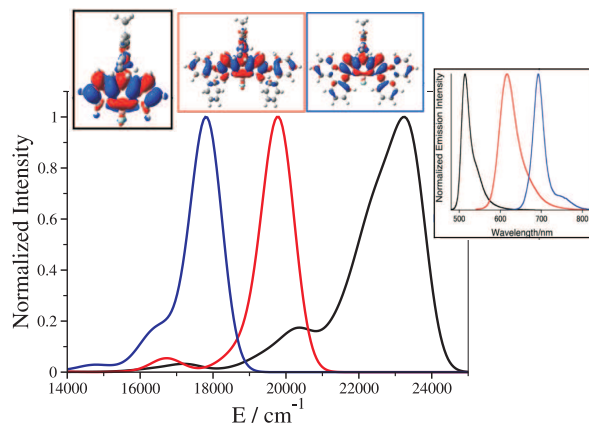


Figure 3.9: Comparison between theoretical and experimental fluorescence spectra for **Bo.51** (red) and **Bo.52** (blue), as well as the corresponding biphenyl-free structure (black). The experimental data (inset) are reproduced with permission from Y. Hayashi *et. al.*, *Org. Lett.* **2012**, *14*, 866–869. Copyright 2012 American Chemical Society. Electron density difference plots of the three dyes are provided at the top.

in Figure 3.10 explain that these relatively small displacements are more related to the extension of the conjugated path than to the CT nature: indeed, the BODIPY core is a stronger acceptor at the ES than the nitro group: there is no significant red lobes on the terminal NO_2 groups. For the records, we note that molecules similar to **Bo.61** but in which one (or two) nitro groups have been replaced by NMe_2 have been proposed.¹⁹⁹ However, they do not show emission, making comparisons of experimental and theoretical E^{AFCP} impossible. The electron density difference plots for these two additional BODIPYs are given in Appendix B. As expected, there is a strong CT character from the NMe_2 towards the central core, whereas the nitro group plays no significant role in the push-pull systems. This can explain why the asymmetric NO_2/NMe_2 structure does not present a very high λ_{max} of absorption experimentally: the BODIPY core plays the role of the acceptor once a NMe_2 group is added.

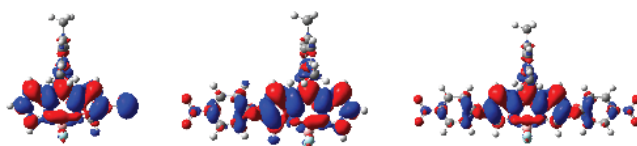


Figure 3.10: EDD plots for **Bo.59** (left), **Bo.60** (centre) and **Bo.61** (right).

Eventually, we have considered a representative series of dyes designed by Umezawa and coworkers that started from **Bo.13** and increased the accepting strength of the fluorophore (addition of a CF_3 group), improved the delocalization (side phenyl rings) as well as added donor to the extremities (methoxy groups).¹⁷¹ Besides furan rings similar fused-thiophene structures have also been developed.²³³ In the **Bo.62** to **Bo.65** series, the successive evolutions of the E^{AFCP} are -0.122, -0.060 and -0.132 eV, experimentally, whereas theory predicts similar shifts: -0.146, -0.081 and -0.168 eV, respectively.

3.4 Conclusions

We have simulated the 0-0 energies and vibrationally resolved optical signatures of a very large panel of BODIPY dyes. The proposed protocol that uses the M06-2X functional and accounts for state-specific solvation and zero-point vibrational effects, is able to reproduce the evolution of the experimental absorption-fluorescence crossing point with a good to remarkable accuracy, although the raw estimates are significantly too small compared to experimental values. This is fully consistent with the conclusion of our previous Chapter. Vibronic calculations of the BODIPY have been obtained and the results nicely reproduced the presence of shoulders and/or multiple maxima in the measured spectra. More importantly, the proposed theoretical approach delivers valuable insights to understand experimental outcomes in a diverse set of situations: building up dimers, varying the pH, extending the conjugation path, plugging electroactive groups... The only series for which our protocol was not quantitatively satisfying is the ion sensor groups. Therefore, though it is clear that the

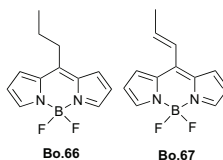


Figure 3.11: Representation of two small BODIPY dyes with similar fluorescence wavelengths but very different emission quantum yields.¹⁹⁷

proposed methodology is not flawless, one can certainly state that the obtained accuracy in the reproduction of experimental shifts of the 0-0 energies, as well as band

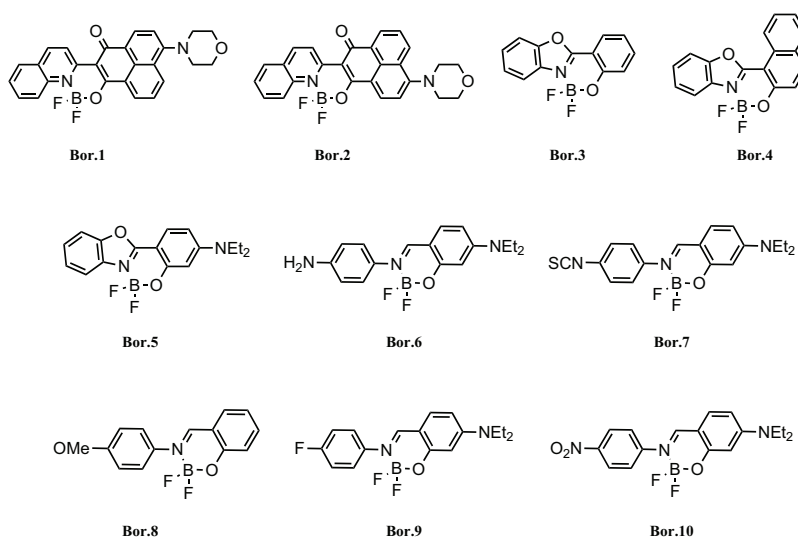
shapes is sufficient in most cases to perform effective dye design. However, a factor that was not discussed herein is the computation of quantum yields of fluorescence (Φ_F), which are obviously crucial for practical applications. We have simulated the properties of the two dyes shown in Figure 3.11. These compact BODIPYs have been recently synthesized by Arroyo *et. al.*,¹⁹⁷ and it was found that the Φ_F of the 8-propyl substituted dye is close to unity (91%), whereas its unsaturated counterpart provides a much poorer emission ($\Phi_F=5\%$).¹⁹⁷ The bathochromic shift when going from **Bo.66** to **Bo.67** is rather small (-0.097 eV) experimentally.¹⁹⁷ As expected, our approach is able to restore this shift (-0.121 eV) but it can also explain the degraded Φ_F , thanks to the computation of Huang-Rhys (HR) factors.^{90,241-243} The larger the HR factors, the more important the non-radiative relaxation pathways, the smaller the emission quantum yield. We obtain HR factors of 2.99 for **Bo.66** and 18.99 for **Bo.67**, respectively, clearly indicating that the non-radiative path is much more efficient in the latter BODIPY, consistently with experimental evidences. The HR plots, shown in Appendix B indicate that the most important vibrational mode explaining the low Φ_F of the alkene derivative presents a low frequency at 37.5 cm^{-1} on the ES. It corresponds to an out-of-plane deformation of both the BF_2 and side groups. As stated in the Introduction, fluoroborate chromophores attracted a widespread interest. These dyes can be classified into major categories depending on their atomique sequence: NBN (aza-BODIPY and BODIPY), NBO or OBO-bidentate ligands. In the two next Chapters, the optical signature of NBO and OBO dyes will be simulated to complement our study.

CHAPTER 4

BORANIL AND RELATED NBO DYES

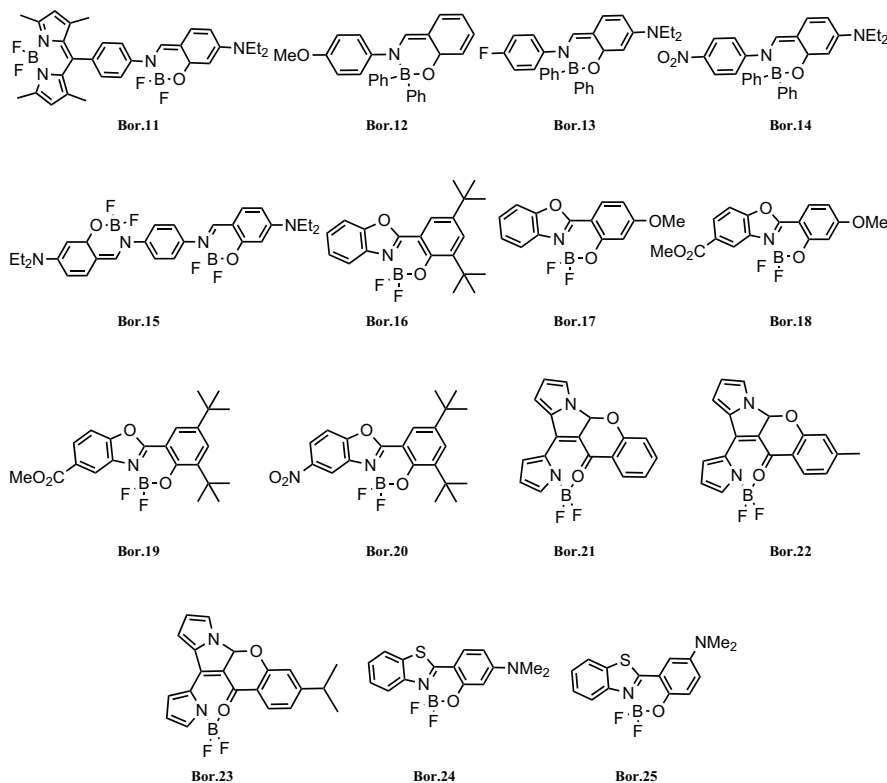
Among the most important chromophoric classes, boron-dipyrromethene (BODIPY) and aza-boron-dipyrromethene (aza-BODIPY) families, which have been discussed in the two previous Chapters, have been the subject of the largest number of investigations due to their exceptional properties. However, BODIPY derivatives often suffer from small Stokes shifts and practical difficulty of producing industrial quantities of dyes. Therefore, a highly desired goal is to increase the Stokes shifts while conserving the other interesting qualities of BODIPY.²⁴⁴ For this reason, recent efforts have been made to develop new fluoroborate structures presenting features correcting some of the weaknesses of BODIPY dyes.⁴⁻²¹ For instance, Ziessel and co-workers have synthesized new boron complexes, named boranil.^{16,20} These compounds, based on the NBO atomic sequence, can be synthesized in two steps. The first implies the reaction between aldehydes and anilines in refluxing ethanol so to reach the *anil*, whereas the second step forms the boranil dyes through the reaction of these *anil* with $\text{BF}_3 \cdot \text{Et}_2\text{O}$ in the presence of diisopropylethylamine.^{16,20} Besides boranil derivatives, other dyes with the NBO pattern have been proposed, e.g. the 2-(2'-hydroxyphenyl) benzoxazole (HBO) borate complexes.^{19,245,246} Ziessel *et al.* and Qian *et al.* independently investigated several NBO fluorophores of this latter class that present large Stokes shifts as a result of the significant charger-transfer character of the main electronic transitions.^{12,19} Members of the NBO family typically absorb (emit) from 342 (395) nm to 456 (597) nm (see Table C.1 in Appendix C).

To the best of our knowledge, only one previous theoretical work from another group has appeared for NBO structures,¹³ and it relied on TD-DFT.⁴⁸ In this study,¹³ Bakalova and co-workers used the vertical TD-DFT approximation for four NBO dyes,²⁴⁷ Nevertheless let us note that for NBO dyes were included in our BODIPY set (see Scheme 3.1) Therefore, our work is the first investigation of boranil derivatives and the first methodological assessment, performed for an extended series of NBO dyes.



Scheme 4.1: Representation of the systems used in the benchmark step. The measured longest wavelength of absorption (λ_{abs}), emission wavelength (λ_{fluor}), solvents used, as well as the experimental references can be found in Table C.1 in Appendix C.

In this Chapter, a large panel of boranil as well as other NBO dyes (see Schemes 4.1 and 4.2)^{12, 16, 19, 20, 248, 249} presenting charge transfer or cyanine-like transitions are investigated. Assessing the importance of the environment is crucial: we have demonstrated in the two previous Chapters that the SS-PCM corrections¹⁰² significantly affects the computed transition energies of both BODIPY and aza-BODIPY dyes,^{94, 250} and we focus specially on the coupling between the selected functional and the model used for solvent effects herein.



Scheme 4.2: Representation of the second series of NBO systems investigated

4.1 Computational Details

As in previous Chapters, a wide panel of hybrid exchange-correlation functionals have been used, namely B3LYP,^{110,251} PBE0,^{112,113} M06,¹¹⁶ BMK,¹¹⁷ M06-2X,¹¹⁶ CAM-B3LYP,¹¹⁹ ω B97X-D¹²¹ and ω B97¹²⁰ and the results of these benchmarks are presented below. In Chapter 2, we have performed an extensive assessment of basis set effects and we applied 6-311+G(2d,p)//6-31G(d) combination as well.⁹⁴ To quantify solvent effects, several PCM approaches⁹⁹ have been applied. As stated above, we have used both PCM approaches implemented in Gaussian 09, namely LR^{53,100} and SS¹⁰² models, applied in both their equilibrium (eq) and non-equilibrium (neq) limits.⁹⁹

4.2 Methodology

In order to determine an efficient TD-DFT scheme, we have combined a series of hybrid functionals to the five "solvent" protocols detailed above, that is Equations

1.16 and 1.17($Y=SS$) using eq and neq limits, as well as Equation 1.19($X=SS$). To this end, we have used the ten dyes shown in Scheme 4.1. Results of the statistical analysis are presented in Table 4.1: mean signed errors (MSE), mean absolute errors (MAE), standard deviations (SD), as well as the theory/experiment linear correlation coefficients (R^2). The computed individual energies are listed in Tables C.2–C.6 in Appendix C.

The results in Table 4.1 show a marked difference between the LR and SS PCM approaches. For all selected functionals, we have found that the LR-PCM model, irrespective of the selection of the eq and neq limits, is surprisingly more accurate than the SS-PCM one. Indeed, with the LR-PCM approach, the R^2 present larger values: it ranges from 0.90 (B3LYP) to 0.97 (M06-2X) whereas with the SS model a much smaller R^2 (several below 0.70) are often found, especially with the three functionals presenting low exact exchange percentages (that is B3LYP, PBE0 and M06). In the same time, both MSE and MAE systematically increase when going from LR to SS, irrespective of the functional. On the contrary, in the previous Chapters, we have shown that the SS-PCM model is the very efficient tool to simulate the optical properties of both BODIPY and aza-BODIPY dyes. To rationalize this unexpected outcome for NBO structures, we have computed the dipole moments of the ground and excited-states, as the SS correction is closely related to the magnitude of the dipole moments. For **Bor.10**, the most polar molecule of this series, the dipole moment of S_0 is 13.4 (13.7) D, while in the S_1 it increases to reach 20.2 (32.4) D with M06-2X (B3LYP). Dipoles obtained for other functionals can be found in Table C.7 in Appendix C, and it is clear that while the dipole computed for S_0 are similar for all functionals, the magnitude of the ES dipole moment is roughly proportional to the inverse of the exact exchange ratio included in the functional. For the records, the dipoles have also been determined in acetonitrile (see Table C.7 in Appendix C), a more polar solvent to assess interplay between the dielectric constant and the exact exchange ratio, and it turns out, as could be expected, that the ES-GS dipole difference seems to be problematic for functionals like BMK that were reasonable in a toluene environment. Therefore, for **Bor.10**, the combination of B3LYP, PBE0 or M06 with the SS approach yields to an unphysical (over) polarization of the cavity during the SS self-consistent calculations. This leads to unphysically small 0-0 energies, e.g., 0.806 eV with (SS,neq) and the B3LYP functional in toluene. In a similar way, the difference between the eq and neq SS excited-state energies of **Bor.10** at-

Table 4.1: Statistical analysis for the dyes shown in Scheme 4.1 obtained from comparison between experimental and theoretical 0-0 energies. MSE, MAE and SD are in eV.

Functional	Method	MSE	MAE	SD	R^2
B3LYP	Eq.1.16 ($X=eq$)	-0.104	0.153	0.116	0.937
	Eq.1.16 ($X=neq$)	-0.120	0.140	0.154	0.900
	Eq.1.17 ($Y=SS, X=eq$)	-0.364	0.420	0.682	0.533
	Eq.1.17 ($Y=SS, X=neq$)	-0.555	0.610	0.872	0.713
	Eq.1.19 ($Y=SS, X=neq$)	-0.228	0.394	0.649	0.372
PBE0	Eq.1.16 ($X=eq$)	-0.013	0.080	0.090	0.972
	Eq.1.16 ($X=neq$)	0.035	0.072	0.084	0.951
	Eq.1.17 ($Y=SS, X=eq$)	-0.157	0.317	0.510	0.649
	Eq.1.17 ($Y=SS, X=neq$)	-0.170	0.327	0.523	0.660
	Eq.1.19 ($Y=SS, X=neq$)	-0.027	0.337	0.462	0.457
M06	Eq.1.16 ($X=eq$)	-0.040	0.073	0.068	0.966
	Eq.1.16 ($X=neq$)	0.027	0.061	0.074	0.941
	Eq.1.17 ($Y=SS, X=eq$)	-0.272	0.353	0.506	0.513
	Eq.1.17 ($Y=SS, X=neq$)	-0.158	0.266	0.456	0.645
	Eq.1.19 ($Y=SS, X=neq$)	-0.173	0.351	0.483	0.319
BMK	Eq.1.16 ($X=eq$)	0.201	0.201	0.087	0.962
	Eq.1.16 ($X=neq$)	0.254	0.254	0.086	0.929
	Eq.1.17 ($Y=SS, X=eq$)	0.242	0.297	0.214	0.878
	Eq.1.17 ($Y=SS, X=neq$)	0.241	0.301	0.221	0.865
	Eq.1.19 ($Y=SS, X=neq$)	0.287	0.308	0.166	0.877
M06-2X	Eq.1.16 ($X=eq$)	0.228	0.228	0.073	0.972
	Eq.1.16 ($X=neq$)	0.282	0.282	0.055	0.966
	Eq.1.17 ($Y=SS, X=eq$)	0.310	0.310	0.137	0.939
	Eq.1.17 ($Y=SS, X=neq$)	0.310	0.314	0.138	0.939
	Eq.1.19 ($Y=SS, X=neq$)	0.335	0.335	0.104	0.949
CAM-B3LYP	Eq.1.16 ($X=eq$)	0.263	0.263	0.062	0.965
	Eq.1.16 ($X=neq$)	0.311	0.311	0.053	0.965
	Eq.1.17 ($Y=SS, X=eq$)	0.348	0.348	0.131	0.907
	Eq.1.17 ($Y=SS, X=neq$)	0.342	0.342	0.137	0.905
	Eq.1.19 ($Y=SS, X=neq$)	0.376	0.376	0.106	0.907
ω B97X-D	Eq.1.16 ($X=eq$)	0.293	0.293	0.064	0.957
	Eq.1.16 ($X=neq$)	0.343	0.343	0.064	0.950
	Eq.1.17 ($Y=SS, X=eq$)	0.383	0.383	0.126	0.899
	Eq.1.17 ($Y=SS, X=neq$)	0.380	0.380	0.130	0.898
	Eq.1.19 ($Y=SS, X=neq$)	0.401	0.401	0.104	0.905
ω B97	Eq.1.16 ($X=eq$)	0.468	0.468	0.054	0.964
	Eq.1.16 ($X=neq$)	0.519	0.519	0.062	0.958
	Eq.1.17 ($Y=SS, X=eq$)	0.581	0.581	0.085	0.933
	Eq.1.17 ($Y=SS, X=neq$)	0.580	0.580	0.088	0.930
	Eq.1.19 ($Y=SS, X=neq$)	0.589	0.589	0.075	0.935

tains 1.11 eV in acetonitrile with BMK, which is clearly a problematic correction. We have therefore performed a statistical analysis removing **Bor.10** from our set (see Table C.8 in Appendix C), and the SS R^2 significantly improve for the three low-exact exchange functionals. Therefore, though the SS scheme has been shown very efficient for coumarins that also present a sizable increase of dipole moments upon photon absorption,¹⁰² one should be cautious when performing SS calculations on such kind of molecules, especially with "conventional" exchange hybrid functionals. This also raises the question of the pertinence of SS//LR calculations, a topic treated latter in this thesis.

In fact, the differences between the results obtained in the equilibrium and non-equilibrium limits are relatively small in the LR-PCM model, and this is especially true with the bottom four functionals of Table 4.1. Indeed, the LR,eq-LR,neq R^2 discrepancies are 0.037, 0.021, 0.024, 0.033, 0.006, 0.000, 0.007 and 0.006 for B3LYP, PBE0, M06, BMK, M06-2X, CAM-B3LYP, ω B97X-D and ω B97, respectively. Of course, the good behavior of the LR approach could also be partly ascribed to error cancellation. We have therefore performed benchmark in gas phase for the ten molecules using both B3LYP and M06-2X. The obtained R^2 of 0.863 and 0.938, respectively, indicate, on the one hand, that the use of an adequate solvent model improves the consistency of the simulations, and on the other hand, that applying SS model in conjunction with the B3LYP functional is detrimental.

Let us now turn to the impact of the functionals. First, the MSE are negative with B3LYP, PBE0 and M06 hybrid functionals and are positive for the other five functionals, indicating that the theoretical results are underestimated (overestimated) for the former (latter) which is a usual trend for valence excited-states modeled with TD-DFT.²⁵² The MAE is small for the three first functionals: it ranges from 0.061 eV (M06) to 0.140 eV (B3LYP) using LR-PCM model in its neq limit and such deviations are small for 0-0 simulations.^{58,93} However, this success is at the price of a large SD and a relatively poor R^2 , at least for B3LYP. At first sight, the M06 (LR,eq) approach could be a very good compromise method: it yields a MAE of 0.073 eV, a SD of 0.068 eV and a R^2 of 0.966. However, as stated above the M06 values are very sensitive to the solvent model and strongly degrade if the SS model is applied [R^2 of 0.319 with AFCP(SS,neq)], which is clearly not an indication of a robust behavior. The five functionals that include large shares of exact exchange (BMK, M06-2X, CAM-B3LYP, ω B97X-D and ω B97), are less affected by the solvent model: they pro-

vide not only large R^2 (0.865-0.972) but also relatively small SD (0.221-0.053 eV), irrespective of the selected PCM approach. From that point of view, one notices that the three top functionals are less satisfying than the bottom five in Table 4.1. As stated above, the LR-PCM approach nicely fits experimental trends, we therefore focus on the results obtained with this approach at this stage. The range-separated hybrid ω B97X-D yields the minimal values of R^2 : 0.957 (LR,eq), 0.950 (LR,neq) whereas the largest SD are obtained with BMK [0.087 (LR,eq), 0.086 (LR,neq)]. Overall, M06-2X, CAM-B3LYP and ω B97 provide relatively similar statistical data. For the SD (R^2), we obtain 0.055 (0.966), 0.053 (0.965) and 0.062 (0.958), for these three functionals with the (LR,neq) model, respectively and these three functionals could have been chosen. In particular, the results in Table 4.1 indicate that M06-2X could supply a very good accuracy. It yields the most consistent estimations of all PCM models [R^2 reaches 0.972 (LR,eq)] and it allows us to keep consistency with our BODIPY study. We go for this functional in the following.

Table 4.2: Statistical analysis for dyes in Schemes 4.1 and 4.2 obtained from comparison between experimental and theoretical 0-0 energies. MSE, MAE and SD are in eV.

Method	MSE	MAE	SD	R^2
Eq.1.16 ($X=eq$)	0.249	0.249	0.122	0.908
Eq.1.16 ($X=neq$)	0.302	0.302	0.104	0.911
Eq.1.17 ($Y=SS,X=eq$)	0.296	0.313	0.156	0.889
Eq.1.17 ($Y=SS,X=neq$)	0.295	0.314	0.157	0.888
Eq.1.19 ($Y=SS,X=neq$)	0.315	0.322	0.135	0.903

We have just shown that the LR-PCM model in both eq and neq limits provides an interesting consistency with the experiment. To check this conclusion, obtained for a limited number of dyes, we have increased the number of NBO compounds using all boranils and NBO dyes represented in both Schemes 4.1 and 4.2. All calculations have been performed with the M06-2X hybrid functional and the statistical results are presented in Table 4.2 (raw data can be found in Appendix C). We note that the LR-PCM model in the eq limit ensures the minimal error of calculations: its MSE and MAE are 0.249 eV, as shown in Table 4.2. In Appendix C, the adiabatic energies

and the ΔE^{ZPVE} obtained from LR,eq simulations are listed: the ZPVE correction is in the line of the expected values (-0.06 to -0.12 eV).^{58,62,93} One can see from Table 4.2 that the two SS models in both eq and neq limits also provide consistent estimates but nevertheless yields the largest SD and the smallest R^2 of the five PCM model tested (around 0.156 and 0.888, respectively). Clearly, the 0-0 (SS) protocols are not the most effective for NBO dyes. The purpose designed AFCP (SS,neq) scheme improves the R^2 and SD but still does not outperform the simplest LR approach. The LR-PCM model in neq limit yields the best correlation coefficient with 0.911 but the difference with the LR,eq and AFCP schemes is negligible: it does not exceed 0.008. In short, we have selected the LR approach in the equilibrium limit to determine the optical spectra in the following.

4.3 Applications

4.3.1 Auxochromes' impacts

Figure 4.1 gives the M06-2X density difference plots computed for three NBO dyes presenting closely related structures. For **Bor.5**, the replacement of the oxygen atom located in position 1 by a sulfur atom to give **Bor.24** has a rather small impact.

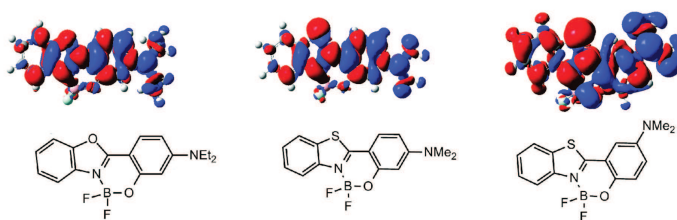


Figure 4.1: PCM-M06-2X/6-31G(d) density difference plots for (from left to right) **Bor.5**, **Bor.24** and **Bor.25** (top) and their structures (bottom). The blue (red) zones indicate density decrease (increase) upon electronic transition.

In fact, when going from **Bor.5** to **Bor.24**, we computed modest bathochromic shifts for both absorption and emission bands: +37 nm and +42 nm, respectively, which is rather close to the experimental values of +28 nm and +35 nm. These

limited variations are consistent with the similar topologies of the density difference plots in Figure 4.1. Using a recently developed approach,^{152,153} we have quantified the CT parameters for these dyes. For **Bor.5** (**Bor.24**), we obtain similar amount of CT charge, $0.49 e$ ($0.48 e$), and alike CT distances of 1.83 (1.99) Å. On the contrary, the last dye, namely **Bor.25**, presents optical signatures displaced to longer wavelengths compared to both **Bor.5** and **Bor.24**. Indeed, we found that moving the dimethylamino group from position 9 (**Bor.24**) to 10 (**Bor.25**) induces a sizable bathochromic shift ($+42$ nm) of the absorption band, and an even larger effect for the emission maximum ($+107$ nm). This outcome can be rationalized in terms of an enhanced CT character: $0.66 e$ being transferred over 2.94 Å (see Figure 4.1). Concomitantly, the (LR,eq) 0-0 energy of **Bor.25** is smaller (2.60 eV) than its **Bor.5** (3.50 eV) and **Bor.24** (3.17 eV) counterparts (see Table C.9 in Appendix C). We have carried out a similar analysis for **Bor.6** and **Bor.10**. Comparing **Bor.6** ($\mu^{\text{GS}} = 9.3$ D, $\mu^{\text{ES}} = 8.5$ D) to **Bor.10** ($\mu^{\text{GS}} = 13.3$ D, $\mu^{\text{ES}} = 20.1$ D), the impact of the replacement of a NH_2 group by NO_2 is shown to significantly reduce the Stokes shift. Impressively, using the computed vertical values at the M06-2X level, **Bor.10** presents a small computed Stokes shift of 46 nm, in line with experiment (47 nm). The much larger Stokes shift predicted for **Bor.6**, (112 nm with M06-2X) also fits experiment (123 nm). This is a valuable success, as the variations of the CT parameters are in the opposite direction, as apparent from the delta density plots of Figure 4.2. Indeed, the CT distance increases from 0.79 Å to 2.94 Å when going from **Bor.6** to **Bor.10**, and this is often viewed as inducing larger Stokes shifts. To unravel the origin of this counter intuitive phenomenon, we have investigated the geometries of the GS and ES of both structures. The most notable variation appears for the central C=N double bond that increases by 0.08 Å (0.04 Å) in **Bor.6** (**Bor.10**), which is consistent with the Stokes shift ranking: the larger geometrical relaxation at the ES, the larger Stokes Shift. For the records, the computed variation of the position of the emission band when going from **Bor.6** to **Bor.10** is -70 nm, which is rather consistent with the measured data of -54 nm.

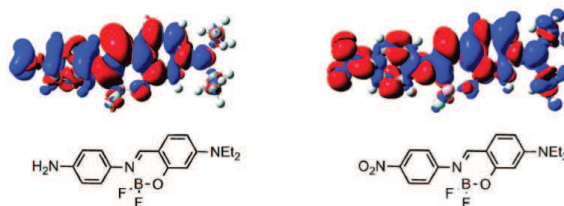


Figure 4.2: PCM-M06-2X/6-31G(d) density difference plots for **Bor.6** (left) and **Bor.10** (right).

4.3.2 Comparing theoretical and experimental band shapes

In Figure 4.3, we compare the experimental and theoretical bands of both absorption and emission of **Bor.4** and **Bor.17**, two of the dyes presenting the most notable vibrational structure. Other vibrationally resolved spectra (**Bor.2**, **Bor.3**, **Bor.5**, **Bor.16** and **Bor.19**) are available in Appendix C.

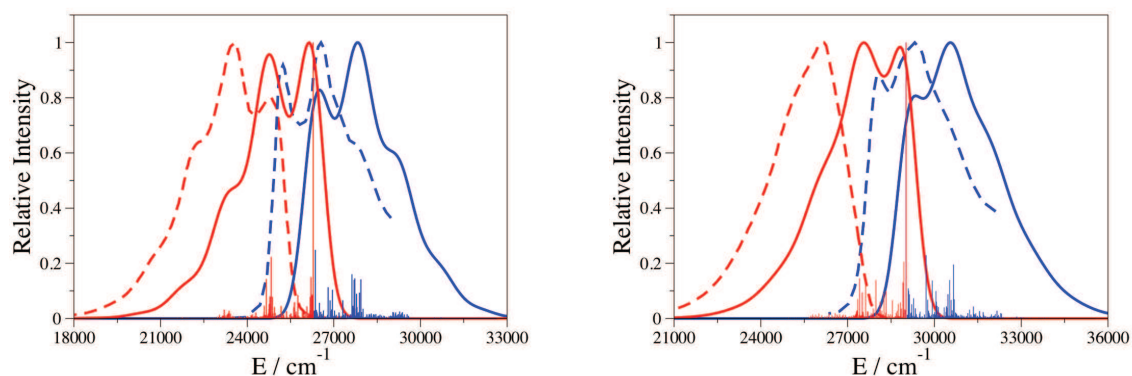


Figure 4.3: Comparison between theoretical (full lines) and experimental (dashed lines) spectra for dyes: (left) **Bor.4** and (right) **Bor.17**. Absorption and emission spectra are in green and blue, respectively. The experimental spectra are adapted with permission from Org. Lett., 14(2012)230. Copyright 2012 American Chemical Society.

Thanks to the TD-PCM-M06-2X calculations, both the positions and the shapes of all absorption and emission peaks are accurately reproduced (see Figure 4.3). Indeed, for both **Bor.4** and **Bor.17**, the crossing point of absorption and fluorescence bands, are in agreement with the experiment: 400 (375) and 360 (340) nm for experimental (theoretical), respectively. For **Bor.17**, the theoretical absorption spectrum presents two important peaks at 1633 cm^{-1} and 686 cm^{-1} . These two peaks respectively correspond to the stretching mode of CH and does not involve O-C bonds nor the BF_2 template and to the breathing of CH. For the theoretical emission band of **Bor.4**, the two main vibrational modes explaining the band shape are located at 1455 cm^{-1} and 1623 cm^{-1} . These two modes correspond to a CC stretching mode and the deformation of the aromatic cycles. In addition, for **Bor.4**, the experimental absorption band presents a smaller shoulder at ca. 345 nm. We underline that the height of the shoulder is well reproduced by our computation protocol. The same holds for the emission band, both experimental and theoretical spectra present a shoulder at longer wavelengths (ca. 440 nm).

4.4 Conclusions

In this Chapter, we have investigated a large panel of members of the NBO fluorophore family. We have performed a large list of methodological evaluations and it turned out that there is a significant interplay between the selected solvation model and hybrid functional. On the one hand, we have found that for structures possessing a strongly increasing dipole moment upon absorption, the SS model leads unphysical values when combined to global hybrids incorporating a low amount of exact exchange. In first approximation, it seems possible to detect the problematic cases either by very large LR-SS deviations of the absorption energies, or by very larger (SS,neq)-(SS,eq) differences for the transition energies. Consequently, for this specific NBO family, the LR PCM model surprisingly outperformed its SS counterpart. On the other hand, we found that global hybrids including a large share of exact exchange, or range-separated hybrids provide accurate estimates of auxochromic effects. Using the M06-2X functional, we have simulated several key optical features. It turned out that the proposed method allowed to restore and rationalize: 1) the evolution of the positions of the absorption and emission bands upon substitution; 2) the variation of the Stokes shift in counter-intuitive cases; and 3) the band shapes of compounds

possessing significant vibronic couplings. Clearly this Chapter has underlined the difficulty of having a valid model for solvent effects: SS corrections are large but might lead to unphysically values. In the next Chapter, an investigation cLR responses. cLR being a perturbative approach (not changing ground states), it is hoped that it can capture the solvent effects beyond the LR without undergoing the problems of SS for molecules possessing large charge or dipole moment upon photon absorption.

CHAPTER 5

DIOXABORINE DYES

The last series, OBO dyes are the focus of this Chapter, and can present several molecular architectures (see Scheme 5.1).²⁵³⁻²⁸⁶ The OBO compounds have absorption and emission wavelengths spanning the 350-550 nm window (see Table D.1 in Appendix D). To the best of our knowledge, no previous TD-DFT calculations have been performed to simulate the 0-0 energies nor to determine the shape of the optical spectra of OBO dyes. In fact, only three theoretical works devoted to OBO could be found.^{256,266,267} The first study²⁵⁶ aimed to determine the vertical electron affinities and intramolecular reorganization energies²⁸⁷ of bis-aryl substituted dioxaborine, whereas the second and third works^{266,267} were performed to estimate the energies of π -electronic states of three OBO dyes.²⁸⁸

5.1 Computational Details

The benchmarks performed for BODIPY and NBO dyes (see Chapters 3 and 4) have shown that the M06-2X hybrid functional¹¹⁶ stands as one of the best compromise for both vertical and 0-0 calculations of fluoroborate complexes.⁹⁴⁻⁹⁶ For this reason, we have mainly chosen M06-2X and focused our methodological study on the three PCM models described in Chapter 1, though we have also used B3LYP as test calculations. As before we have selected 6-31G(d) for determining the geometrical and vibrational parameters, whereas a much more extended basis set, namely 6-

311+G(2d,p), has been used to determine the basis set corrections through vertical TD-DFT calculations.

5.2 Methodological investigation

All experimental data have been obtained in dichloromethane with the exception of system **Obo.15** (in chloroform) and **Obo.16** (in tetrahydrofuran). We have used five solvent approximations: LR,eq [0-0, Equation 1.16], SS/cLR,eq [0-0, Equation 1.17] and SS/cLR,neq [AFCP, Equation 1.19]. Table 5.1 provides a statistical analysis for the OBO dyes displayed in Scheme 5.1: mean signed error (MSE), mean absolute error (MAE), standard deviation (SD), linear correlation coefficient (R^2) as well as the maximal positive and negative deviations Max(+) and Max(-) are reported. The 0-0 energies obtained for all dyes are given in Tables D.2 and D.3 in Appendix D. The MSE is negative for B3LYP and becomes positive for M06-2X indicating that the experimental values are underestimated (overestimated) with the former (latter) functional, which is a rather common trend with the results obtained for NBO dyes (see Chapter 4). Though B3LYP(LR,eq) provides the smallest MAE (0.170 eV) and B3LYP(cLR,eq) the smallest MSE (-0.053 eV), respectively, this apparent accuracy comes with large SD and small R^2 . In fact, M06-2X appears as a good compromise for OBO dyes corroborating previous results. Indeed, one can find from Table 5.1 that M06-2X yields the largest correlation coefficient with 0.952 and the smallest SD (0.073 eV). In the following, we comment only the results obtained with M06-2X. For the records, note that the R^2 obtained for the same set of dyes is 0.897 with PBE0,¹¹³ 0.943 with CAM-B3LYP¹¹⁹ and 0.915 with ω B97X¹²⁰ [all in the (LR,eq) model], further justifying the choice of M06-2X.

Let us now discuss the impact of the solvent. Table 5.1 clearly highlights that marked differences between the three PCM models. We start by comparing LR and SS results. The LR model, in the equilibrium limit, obviously provides more consistent results than its SS counterpart. This is illustrated by the (LR,eq) R^2 of 0.952 that is much larger than the corresponding SS values of 0.784 (eq) and 0.828 (neq). Of course, this is reflected in the SD that exceeds 0.1 eV with a SS-M06-2X combination. Clearly, the SS-PCM model cannot reproduce the experimental trends for OBO dyes in a very satisfying way. This phenomenon was already noticed in Chapter 4. With

the cLR approach, we found that equilibrium and non-equilibrium limits provide relatively similar statistical data. Indeed, for SD (R^2), we obtain 0.086 eV (0.927) in the eq limit and 0.087 eV (0.926) in the neq limit: cLR provides a consistency with experiment that is similar to the LR one (the difference of R^2 between the two models being as small as 0.025). One therefore faces a dilemma: as discussed above the LR model should be insufficient to correctly describe the ES polarization (cLR and SS corrections are large) but nevertheless yields the smallest MAE. Whilst this is not a result that can be easily explained, a general comment can help in finding a possible rationalization. All the experimental data refers to low polar solvents and we therefore should expect that a purely electrostatic model as PCM, in all its different LR, cLR and SS versions, recovers only a part of the whole solvent effect as it neglects possible important solute-solvent non-electrostatic interactions. It is true that here the focus is on 0-0 energies, i.e. differences of energies for which error cancellations should apply, however, this is not always the case: for example solvent dispersion effects are expected to significantly differ for ground and excited states, the latter being generally larger. As a result, the neglect of these non-electrostatic effects should lead to systematic errors.^{289,290} The fact that LR gives the smallest MAE could be justified by indicating that this scheme in which the solvent electrostatic response to the solute excitation is determined by a transition density and not by the real change in the state density fortuitously recovers part of the missing term. This analysis seems to be supported also by the fact that for all investigated dyes cLR gives too large 0-0 energies. This is coherent with a neglect of a dispersion effects which should stabilize more the excited than the ground state and consequently reduce the 0-0 energies. In addition LR always yields an overestimation but the error is reduced from ca. 0.4 to ca. 0.2 eV (we note that for SS both positive and negative errors are found). At this stage, we have decided to mainly go on with cLR that emerged as the best compromise between physical robustness of the model and consistency of the results, but we also present LR values in the following.

Finally, we have performed calculations with M06-2X using the Tamm-Dancoff approximation (TDA). The TDA energies obtained with different solvent models and the related statistical analysis are collected in Tables D.4 and D.5 in Appendix D. The linear correlation coefficient (R^2) obtained with TDA are smaller than with TD-DFT: it ranges from 0.725 (AFCP) to 0.896 (LR,eq). We note that when moving from TD-DFT to TDA, irrespective of the selected PCM-approach, not only R^2 decreases but

Table 5.1: Statistical analysis for dyes shown in Scheme 5.1 obtained with PCM-TD-M06-2X and PCM-TD-B3LYP approaches. All values are given in eV but R^2 .

Functional	Method	MSE	MAE	SD	R^2	Max(+)	Max(-)
B3LYP	Eq.1.16 ($X=eq$)	-0.149	0.170	0.133	0.826	0.121	-0.556
	Eq.1.17 ($Y=cLR, X=eq$)	-0.053	0.234	0.290	0.601	0.452	-0.618
	Eq.1.19 ($Y=cLR, X=neq$)	-0.090	0.274	0.358	0.501	0.450	-0.988
	Eq.1.17 ($Y=SS, X=eq$)	-0.294	0.424	0.516	0.387	0.375	-1.359
	Eq.1.19 ($Y=SS, X=neq$)	-0.224	0.366	0.449	0.433	0.379	-1.162
M06-2X	Eq.1.16 ($X=eq$)	0.189	0.189	0.073	0.952	0.332	0.085
	Eq.1.17 ($Y=cLR, X=eq$)	0.411	0.411	0.086	0.927	0.585	0.193
	Eq.1.19 ($Y=cLR, X=neq$)	0.414	0.414	0.087	0.926	0.587	0.193
	Eq.1.17 ($Y=SS, X=eq$)	0.298	0.316	0.162	0.784	0.565	-0.125
	Eq.1.19 ($Y=SS, X=neq$)	0.367	0.367	0.137	0.828	0.596	0.049

also both MSE and MAE increase. This confirms that TDA is inadequate for cyanine dyes. TDA was therefore not used further. In short, for 0-0 energies of OBO dyes, TD-DFT calculations combining the M06-2X functional to the LR-PCM/cLR-PCM models could be viewed as a reasonable choice.

5.3 Applications

5.3.1 Impact of the auxochromes

Figures 5.1 and 5.2 illustrate the density difference plots for selected OBO dyes. In all cases, the two oxygen atoms participate in the excited-state, whereas the BF_2 contribution is rather small. A comparison between **Obo.2** and **Obo.18** (see Figure 5.1) indicates that the replacement of the phenyl rings by pyrrole rings induces a modest bathochromic shift due to the emergence of intramolecular H-bonds with the oxygen atoms, allowing the stabilization of the extra charge gained by these atoms in the excited-states. We computed a shift of +33 (+49) nm for the absorption and +17 (+32) nm for the emission with cLR (*LR*). The corresponding experimental values are +52 nm and +55 nm: our approach reasonably reproduces this measured effect. Both **Obo.2** and **Obo.18** present rather small Stokes shift, that respectively amounts to 16 (37) nm and 19 (21) nm in experiment (theory). These small variations are consistent with the similar topologies of the density difference plots shown in Figure 5.1. **Obo.2** and **Obo.18** present similar q^{CT} of 0.42, 0.45 e and d^{CT} of 0.60, 0.69 Å, respectively (see Table 5.2). In other words, the CT distances, in this dipolar approximation, are small and the states can be regarded as $\pi \rightarrow \pi^*$ transitions. Indeed, in states having a large CT character, d^{CT} is larger than ca. 2.0 Å.^{152,153}

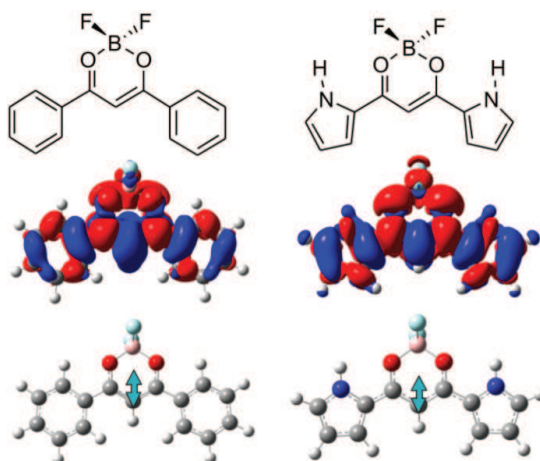


Figure 5.1: PCM-TD-M06-2X/6-31G(d) density difference plots for **Obo.2** (left) and **Obo.18** (right). The blue (red) zones indicate density decrease (increase) upon transition. At the bottom, the small dipolar CT vectors are displayed. The selected contour threshold is 0.0004 a.u.

In Figure 5.2, the density difference plots of three OBO dyes having the same skeleton including a carbazole unit are given, while the CT parameters can be found in Table 5.2. When going from **Obo.12** to **Obo.13**, a very small hypsochromic shift is calculated for both absorption and emission bands of -2 (-2) nm and -4 (-7) nm at cLR (*LR*) level, in line with the experimental values of -4 nm and -11 nm, respectively. The carbazole acts as an electron donor (see Figure 5.2), so adding a methoxy donor on the opposite site is detrimental for CT, and this reflects in the decrease of the ES dipole moment from **Obo.12** (18.45 D) to **Obo.13** (15.90 D). On the contrary, going from **Obo.12** ($\mu^{\text{GS}}=11.73$ D, $\mu^{\text{ES}}=18.45$ D) to **Obo.14** ($\mu^{\text{GS}}=10.90$ D, $\mu^{\text{ES}}=20.00$ D), provokes a bathochromic displacement of +21 (+21) nm for absorption and +22 (+19) nm for emission (in the line of the measurements of +24 nm and +37 nm, respectively) and this is related to the accepting character of the two chlorine atoms placed in meta position (mostly in red on Figure 5.2).

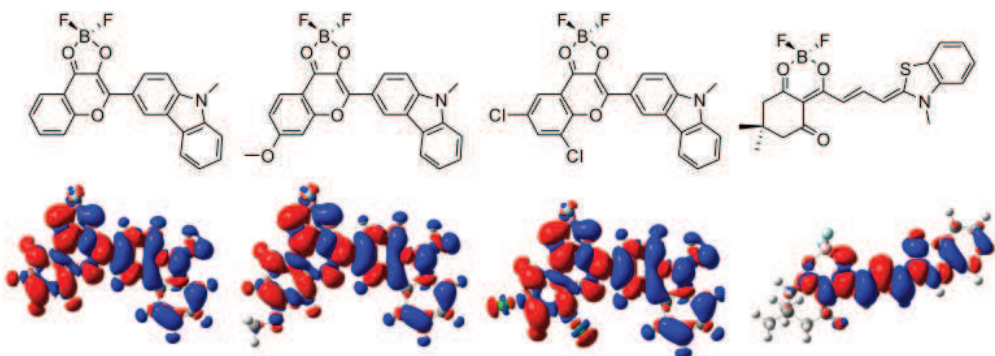


Figure 5.2: PCM-TD-M06-2X/6-31G(d) density difference plots for (from left to right) **Obo.12**, **Obo.13**, **Obo.14** and **Obo.19**. The selected contour threshold is 0.0004 a.u.

Finally, we have characterized one of the largest molecule of Scheme 5.1, namely **Obo.19**, that absorbs and emits at rather long wavelengths and is a good candidate for organic solar cell applications.²⁷⁹ The density difference plots indicate a limited CT character (see the CT distance in Table 5.2) but a significant cyanine character with an alternating pattern on the polyene segment. The estimated Stokes shift of **Obo.19** is small: 20 nm, which is consistent with the experiment (14 nm). This Section therefore illustrates that OBO structures can develop both CT and cyanine characters depending on their substitution pattern.

Table 5.2: The CT distance (d^{CT} in Å), transferred charge (q^{CT} in e), CT dipole and ground/excited state dipole moments (in Debye) for selected dyes.

Dye	d^{CT}	q^{CT}	μ^{CT}	μ^{GS}	μ^{ES}
Obo.2	0.60	0.42	1.20	9.30	10.50
Obo.18	0.69	0.45	1.40	6.00	7.40
Obo.12	3.40	0.63	6.72	11.73	18.45
Obo.13	3.10	0.60	4.40	11.50	15.90
Obo.14	3.60	0.66	9.10	10.90	20.00
Obo.19	1.11	0.40	2.04	13.05	15.09

5.3.2 Vibronic shapes

In this Section, we compare the experimental and theoretical band shapes of selected dyes, with several OBO spectra presenting notable vibronic structures. Vibrationally resolved absorption and emission bands for dyes **Obo.9**, **Obo.10**, **Obo.11**, **Obo.12**, **Obo.13** and **Obo.14** obtained in dichloromethane are displayed in Figure 5.3. Vibronic spectra for other OBO dyes are available in Appendix D. One can see that when going from **Obo.9** (black) to **Obo.14** (cyan), absorption and emission band shapes are red shifted which is in agreement with experiment (see Ref. 285). It was observed that both **Obo.9** and **Obo.11** present significant structures in both their absorption and emission bands. For this reason, we have extracted these two latter dyes and displayed stick vibronic spectra in Figure 5.4. For **Obo.9**, the agreement between experimental and theoretical band shapes is satisfactory. For this molecule, the theoretical stick absorption spectrum is composed of several characteristic peaks, two intense being located at 814 and 1679 cm^{-1} relative to the 0-0 reference. These two peaks correspond to, on the one hand, an asymmetric stretching of the OBO one, and on the other hand, to a CC stretching localized on the two phenyl rings. For the emission, the three main vibrational modes contributing to the overall shape appear at 663, 1294 and 1698 cm^{-1} . These modes again correspond to stretching of the rings and at the OBO moiety. For **Obo.11**, we can distinguish two important vibrational GS modes at 834 and 1703 cm^{-1} accounting for the emission band shape. These modes correspond to the stretching centered on OBO unit and on the naphthalene, respectively.

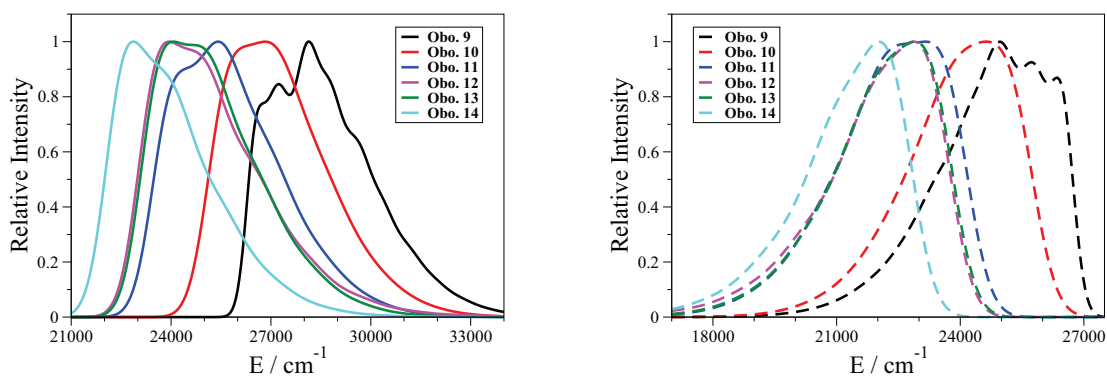


Figure 5.3: Absorption (left) and emission (right) band shapes of **Obo.9**, **Obo.10**, **Obo.11**, **Obo.12**, **Obo.13**, **Obo.14** computed with M06-2X. The experimental spectra can be found in Ref. 285.

Figure 5.5 provides the vibronic spectra of **Obo.17** and **Obo.19** with a direct comparison with measured spectra. For both absorption and emission bands, it is clear that theory provides an overall accurate reproduction of the experimental topologies, as the relative positions of all the peaks/shoulders are well restored, but for the shift of the 0-0 band discussed previously. Indeed, the experimental spectra of **Obo.17** (**Obo.19**) presents an absorption shoulder at ca. 400 (500) nm and an emission shoulder at ca. 455 (575) nm, respectively. These shoulders have a ca. half intensity compared to the main peaks. Using PCM-TD-M06-2X, the height of the shoulders are slightly overrated for **Obo.17** and underrated for **Obo.19**.

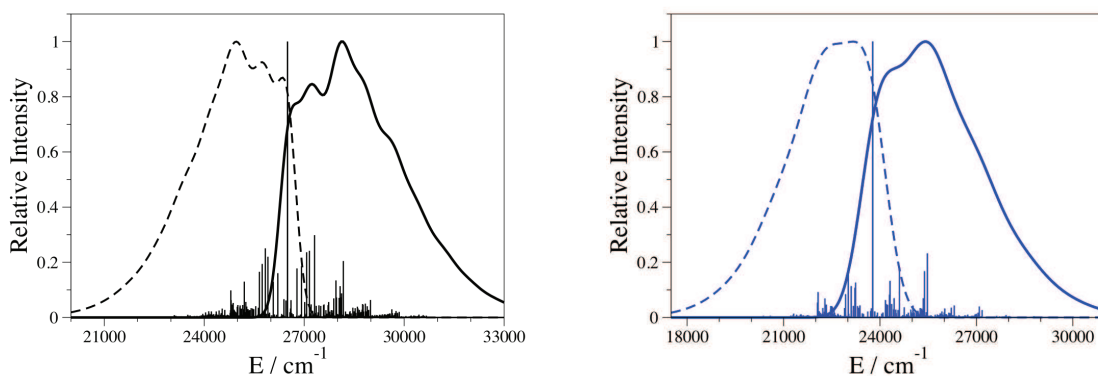


Figure 5.4: Absorption (full lines) and emission (dashed lines) spectra of **OBO.9** (left) and **OBO.11** (right) computed with M06-2X. The experimental spectra can be found in Ref. 285.

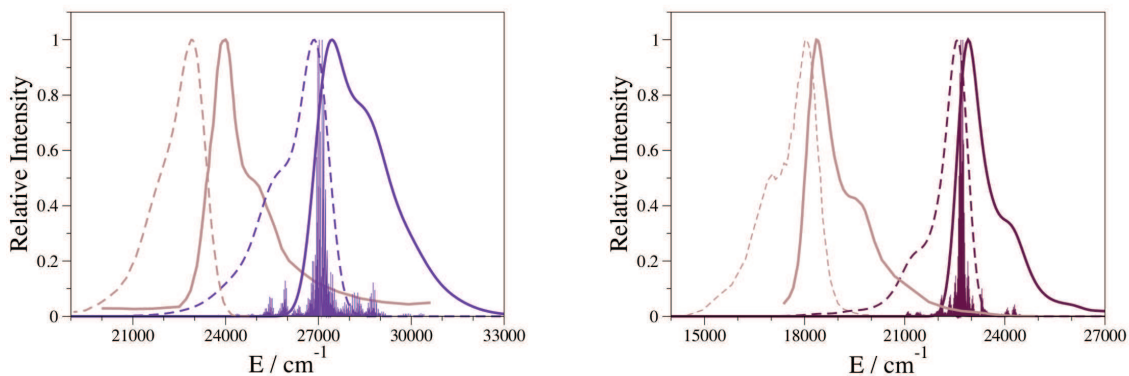


Figure 5.5: Theoretical (violet, indigo) and experimental (brown) spectra for absorption (full lines) and emission (dashed lines) of **Obo.17** (left) and **Obo.19** (right) computed with M06-2X. The experimental spectra are adapted with permission from Inorg. Chem 2006, 45, 8205-8210. Copyright 2006 American Chemical Society and from Dyes and Pigments, 92, K. Zyabrev and M. Dekhtyar and Y. Vlasenko and A. Chernega and Y. Slominskii and A. Tolmachev, New 2,2-difluoro-1,3,2(2H)oxazaborines and merocyanines derived from them, 749-757, Copyright (2011), with permission from Elsevier.

5.3.3 Double BF₂ complexes

So far, we have only used OBO dyes presenting one BF₂-chelating moiety. To the best of our knowledge, only Yamashita and coworkers,^{266,267} have synthesized (three) OBO dyes with two BF₂-chelating moieties around a tetracene, a perylene or an octafluorotetracene central core (see Figure 5.6). The 0-0 energies obtained with different solvent models and the M06-2X hybrid functional are listed in Table D.6 in Appendix D, whereas Figures 5.7 and 5.8 provide vibronic spectra of these three compounds. These dyes absorb and emit at rather long wavelengths compared to other OBO structures. The absorption bands are located between 420-470 (520-575) nm and the emission maxima take place in the 490-520 (520-570) nm region in theory (experiment), illustrating once more that the transition energies are overestimated by theory, although the trends when going from one system to another are reasonably restored by TD-DFT.

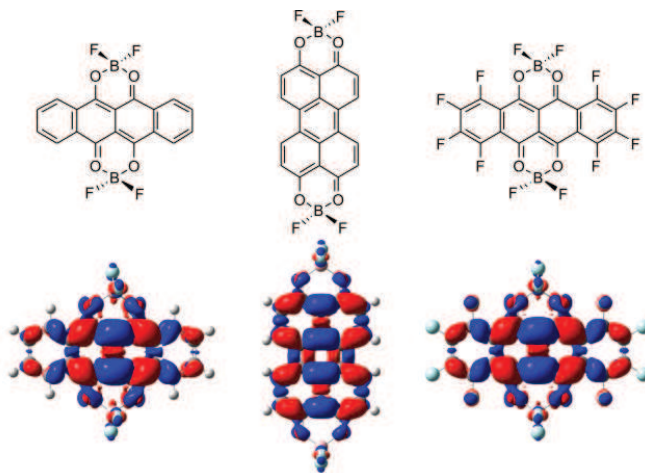


Figure 5.6: Representation of double BF₂ complexes based on: tetracene (left, **Obo.23**), perylene (middle, **Obo.24**) and octafluorotetracene (right, **Obo.25**) fused cores.

The calculated Stokes shifts of both **Obo.23** and **Obo.24** dyes are very small (6 and 4 nm, respectively with cLR), whereas the corresponding experimental values attain 6 nm for (**Obo.23**) and 3 nm for (**Obo.24**). These values are in fact comparable to the values measured for 6,11-dihydroxy-5,12-naphthacenedione (DHND) (10 nm)

and tetracene (4 nm), indicating that the **Obo.23** and **Obo.24** rigid chromophores are not significantly affected by the presence of the BF_2 groups. This is consistent with the reorganization of the electronic density (see Figure 5.6), that clearly corresponds to symmetric $\pi \rightarrow \pi^*$ transitions centered on the hydrocarbon cores. For **Obo.23** and **Obo.24**, we can distinguish a few key vibrational modes for both absorption and emission curves (see Figure 5.7). We note that the bands shapes of these two dyes are slightly red-shifted relative to DHND or tetracene moieties, but do conserve the same topology. For the absorption (emission) of **Obo.23**, the second maximum mainly implies one vibrational mode located at 1532 (1392) cm^{-1} (see stick spectra). These modes correspond to the stretching of the two central rings and of the full molecule, respectively.

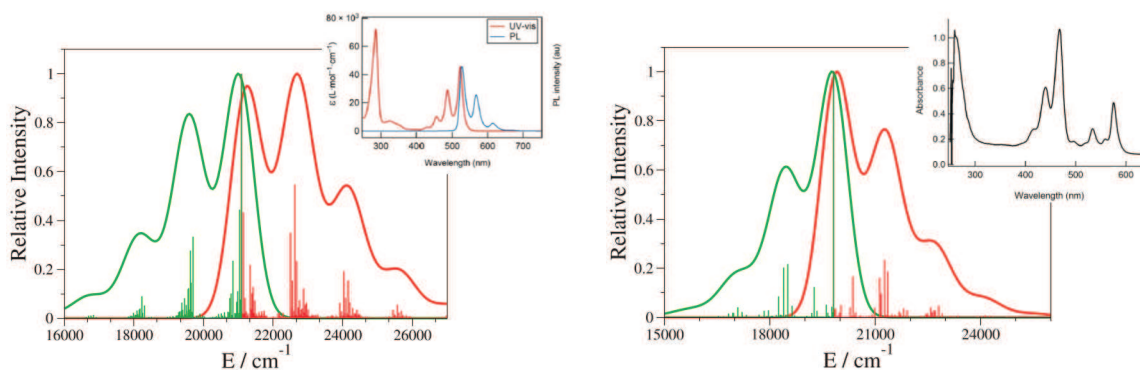


Figure 5.7: Convolved and stick spectra of the absorption (red) and emission (green) of **Obo.23** (left) and **Obo.24** (right). The experimental absorption and emission spectra for **Obo.23** and the experimental absorption spectra for **Obo.24** (the insets) are both reproduced from *Org. Lett.* 2009, **11**, 149-152 Ref. 266 with permission. Copyright 2009 American Chemical Society.

The octafluorotetracene compound, **Obo.25**, is characterized by a larger electron affinity than the two other structures due to the enhancement of its quadrupolar nature by fluorination (see Figure 5.6). When going from **Obo.23** to **Obo.25**, the replacement of the hydrogen atoms by fluorine atoms induces a red-shift. We compute a modest bathochromic shift of $+23$ ($+31$) nm for the emission which slightly underrates the experimental reference (see Figure 5.8).

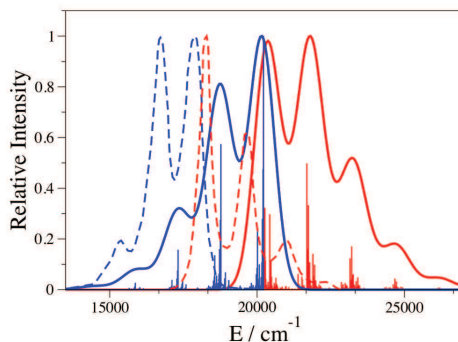
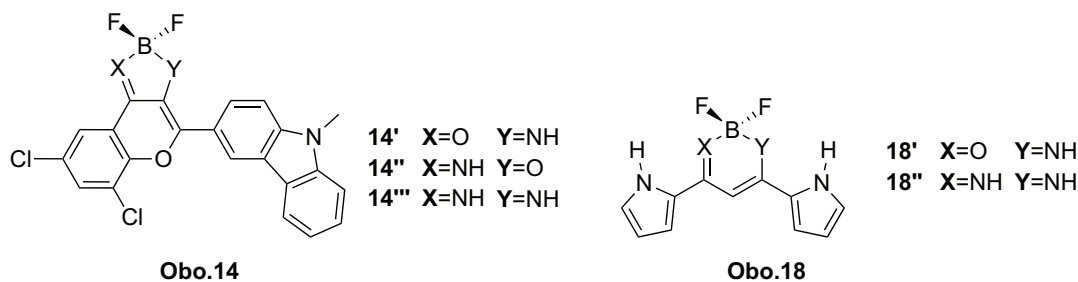


Figure 5.8: Experimental (dashed lines) and theoretical spectra (full lines) for absorption (red) and emission (blue) of **Obo.25**. The experimental spectra are adapted with permission from *Org. Lett.* 2009, **11**, 4326-4329. Copyright 2009 American Chemical Society.

5.3.4 Further discussions

To connect with our studies of BODIPY, aza-BODIPY and boranil dyes we have designed new fluorophores that are based on **Obo.14** and **Obo.18** (see Scheme 5.2) and assessed the impact of replacing the OBO sequence by OBN and NBN sequences.



Scheme 5.2: Representation of new chromophores.

The 0-0 energies obtained in dichloromethane can be found in Table 5.3. Vibrationally resolved absorption and emission bands for **Obo.14** and **Obo.14'** are also displayed in Appendix D. The simulated spectra of **Obo.18**, **Obo.18'** and **Obo.18''** (Figure 5.9) show successive displacements of both absorption and emission bands to smaller wavelengths. Indeed, going from **Obo.18** to **Obo.18'**, that is replacing

OBO by OBN induces modest hypsochromic shifts for both absorption -15 (-25) nm, and emission -7 (-17) nm, with cLR (*LR*). Interestingly, **Obo.18''** that presents the NBN sequence is shifted hypsochromically by -31 (-46) nm compared to **Obo.18**, so that the variations are not additive when changing one or two oxygen atoms. We underline that **Obo.18''** presents a large Stokes shifts of 35 nm compared to the other structures. On the contrary, **Obo.14'''**, with the NBN sequence, undergoes a shift to longer wavelengths compared to **Obo.14**. The AFCP energies indeed decrease in the order: **Obo.14''** > **Obo.14** > **Obo.14'''** > **Obo.14'**, indicating that NBN-bidentate ligand might also induce bathochromic shift in some cases. It might look counter intuitive that the transition energies of the two NBO structures are not in between their OBO and NBN counterparts. However, as can be seen in Figure 5.4, the **X** and **Y** atoms undergo contrasted changes of density upon photon absorption, so that the symmetric architectures (OBO and NBN) logically yield to intermediate values of transition energies. Of course, placing the nitrogen on the donor side (and the oxygen atom on the accepting side) favors the decrease of the AFCP energy.

Table 5.3: Theoretical PCM-TDDFT-M06-2X estimates of the experimental 0-0 energies for the dyes shown in Scheme 5.2 and Figure 5.10. All values are in eV.

Molecules	Eq.1.16 ($X=eq$)	Eq.1.17 ($Y=cLR, X=eq$)	Eq.1.19 ($Y=cLR, X=neq$)	Eq.1.17 ($Y=SS, X=eq$)	Eq.1.19 ($Y=SS, X=neq$)
Obo.14'	2.436	2.594	2.607	2.587	2.650
Obo.14''	2.737	2.863	2.881	2.795	2.955
Obo.14'''	2.538	2.669	2.680	2.672	2.748
Obo.18'	3.096	3.380	3.386	3.339	3.359
Obo.18''	3.252	3.503	3.504	3.493	3.501
Obo.26	2.746	2.627	2.650	2.162	2.351
Obo.27	2.648	2.947	2.949	2.854	2.880
Obo.28	2.344	2.636	2.639	2.610	2.635
Obo.29	2.339	2.616	2.622	2.482	2.508
Obo.30	2.138	2.322	2.328	2.117	2.173

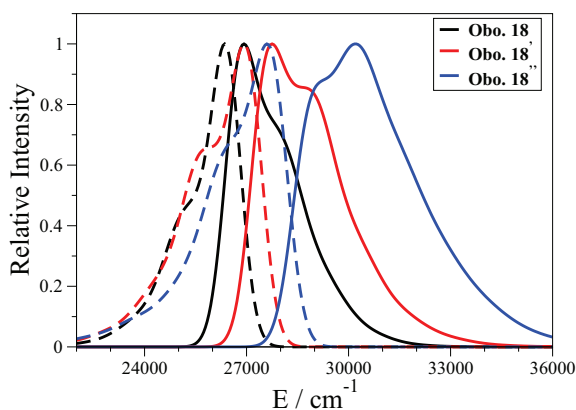


Figure 5.9: Absorption (full lines) and emission (dashed lines) spectra computed for **Obo.18**, **Obo.18'** and **Obo.18''**.

In the same vein, we have designed new chromophores using both electron donors and acceptors aiming to maximize the CT character of OBO dyes, or at least to shift the absorption maximum towards longer wavelengths. Figure 5.10 shows the density difference plots for five new chromophores, whereas the CT data are listed in Table 5.4. Starting with the three first dyes presenting identical donor (NMe_2) and acceptor (CN) groups, one notices that the strongest CT character is obtained with **Ovo.26** (see Table 5.4). Adding one or two thiophene rings in the central linker, does not imply a larger CT, as the excited state starts to become a $\pi \rightarrow \pi^*$ state localized on the central unit and, less and less implies the terminal groups. This phenomenon was already noticed for other families of push-pull systems.²⁹¹ Indeed, for **Obo.28** with two thiophenes (see top of Figure 5.10), the dimethylamino group does not play any role in the optical transition. The corresponding CT distance for **Obo.27** and

Table 5.4: CT parameters for the dyes in 5.9.

Dye	d^{CT}	q^{CT}	μ^{CT}	μ^{GS}	μ^{ES}
Obo.26	3.35	0.73	7.69	16.04	23.73
Obo.27	1.30	0.45	2.50	9.50	12.00
Obo.28	1.17	0.47	2.02	6.15	8.17
Obo.29	3.44	0.64	0.78	9.87	10.63
Obo.30	1.39	0.40	0.95	5.40	6.35

Obo.28 are 1.30 and 1.17 Å, respectively, that is much smaller than in **Obo.26** (3.35 Å).

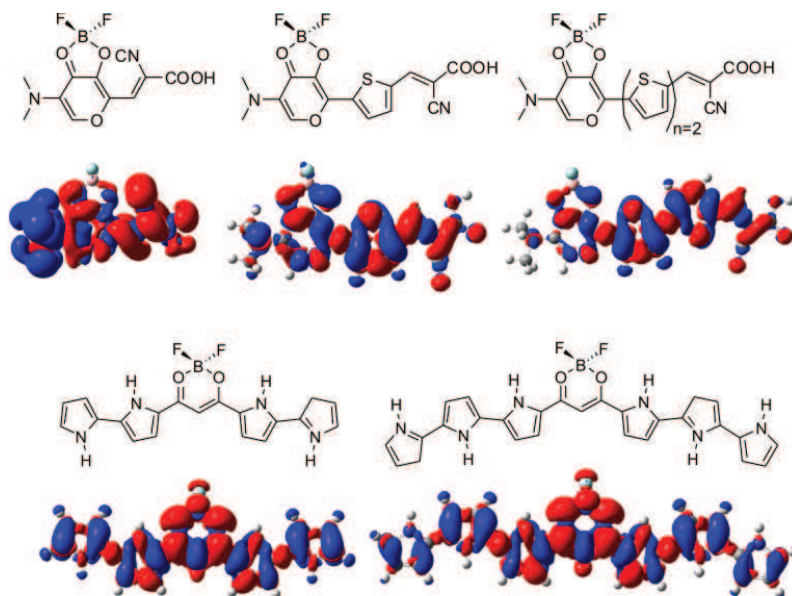


Figure 5.10: PCM-TD-M06-2X/6-31G(d) density difference plots for new chromophores: **Obo.26**, **Obo.27** and **Obo.28** (top, from left to right), **Obo.29** and **Obo.30** (bottom). The selected contour threshold is 0.0004 a.u.

Aiming to induce large bathochromic shift with OBO dyes, we have used an alternative strategy, by keeping the central OBO unit constant but expanding the side chains. This leads to **Obo.29** and **Obo.30** that are based on **Obo.18** (see bottom of Figure 5.10). Figures 5.1 and 5.10 demonstrate that **Obo.18**, **Obo.29** and **Obo.30** possess almost the same excited state topologies with a CT going from pyrrole groups to the OBO center. With cLR (*LR*) approach, the 0-0 energies are 3.297 (2.945), 2.622 (2.339) and 2.328 (2.138) eV, for **Obo.18**, **Obo.29** and **Obo.30**, respectively. This corresponds to successive decreases of -0.675 (-0.606) and -0.294 (-0.201) eV and hence, if one aims designing NIR absorbers, this strategy is much more effective than expanding the linker between one acceptor and one donor groups.

5.4 Conclusions

In this analysis of OBO dyes, we have first focused on assessing the adequacy of three environmental PCM models: LR, cLR and SS using both equilibrium and non-equilibrium limits. It turns out that the SS-PCM approach is not efficient to simulate the spectral properties of OBO chromophores since it yields the least consistent data. On the contrary, the difference between LR and cLR is rather small in terms of correlation with experiment (R^2 discrepancy not exceeding 0.025). However, it is worth to note that the LR–cLR difference is large in terms of absolute values. Part of the error can also be related to the difficulty of finding an exchange-correlation functional that reproduces the optical spectra of cyanine like molecules with TD-DFT. With the chosen protocol, we could not only reproduce the experimental trends for 0-0 energies (with a R^2 of ca. 0.95), but also obtain vibrationally-resolved absorption and emission band shapes, comparing favorably with experiment for most tested compounds. In addition, we found that 1) replacing the OBO sequence by NBO or NBN might produce both bathochromic and hypsochromic shifts; 2) increasing the length of the π -conjugation linker between a push and a pull group does not systematically induce a stronger CT character; 3) extending the π -path around a central OBO unit acting as an acceptor is the fastest track to red shifted absorption and emission.

CONCLUSION- PART I

In the first part of this thesis, we have devoted our efforts to define an efficient protocol to obtain the optical signatures of a large panel of fluoroborate complexes (aza-BODIPY, BODIPY, boranil and dioxaborine). As mentioned in the Introduction, these dyes can be viewed as *cis*-constrained cyanines and several also present a significant charger-transfer character. These two characters make the prediction of their optical properties a difficult challenge for TD-DFT. In order to reach our goal and to allow a meaningful comparison with the experiment, various parameters have been assessed. Indeed, we have used several atomic basis sets and a wide panel of global and range separated hybrids funtionals. It was shown that M06-2X is an adequate functional to investigate both the excited-state energies and structures of these fluoroborate. It provides a good consistency with the experiment for BODIPY, boranil and dioxaborine dyes and is well suited to model the variation of the 0-0 energies induced by side group, modifications of the skeleton, stiffening or extension of the π -path. Note that for the aza-BODIPY dyes, the BMK functional yields the best determination (0.98), but we stress that M06-2X results were also very satisfying ($R^2=0.95$). To assess the importance of solvent effects, PCM approach with LR, cLR and SS models for excited-states is the natural method of the choice. It turned out that there is a significant interplay between the selected solvation model and functional. We also underline that for the above-mentioned fluoroborates, the absorption, emission and 0-0 energies obtained with these variants of the PCM model significantly differ (variations of ca. 0.3 eV between LR and cLR/SS). For aza-BODIPY and BODIPY dyes, we have demonstrated that the SS model yields consistent chemical trends.

However, for the two other considered families, boranil and dioxaborine, both LR and cLR models clearly outperform the SS model. Indeed, for these two families we have found also that the combination of the SS-PCM scheme to a functional incorporating a low amount of exact exchange can yield unphysical values for molecules presenting a large increase of their dipole moments upon excitation. At this stage, we can conclude that the SS model is not the most adequate for the fluorophores considered in this thesis. Nevertheless, we underline that the developed protocol was successfully applied to provide: 1) the band shapes and the spectral signatures of dyes presenting significant vibronic coupling; 2) solvatochromic effects; 3) the CT nature for different states; 4) new structures with red-shifted absorption and emission bands.

Up to now, we have used TD-DFT with widely available approaches to model the optical signatures of all selected dyes. One of the most important advantages of this method that it can be coupled with environmental models, PCM in our thesis. However, the selected solvent model for the excited-state calculations has a dramatic impact on the obtained results. It should be mentioned that in the previous Chapters, which we have used cLR or SS to correct the total excited-state energies, the corresponding geometries being optimized at the LR level, the only implemented approach in commercial quantum chemistry packages. This blend cannot be considered as satisfying as it is clearly inconsistent for this class of molecules, as cLR/SS correction on the energy are far from negligible. This point encouraged us to perform the first cLR excited-state geometry optimizations for model compounds, allowing to obtain “full” cLR results. In the first Chapter of the second part, we provide a consistent approach for both cyanine derivatives as well as aza-BODIPY, BODIPY, boranil and dioxaborine derivatives, in order to assess the impact of our “solvent geometric error”.

As mentioned in the Method Chapter, to calculate the 0-0 energies and bands shapes, we need to compute the Zero point Vibrational Energies of the ground and excited-states and these tasks are, in practice, only doable with TD-DFT. However, computed the transition energies, that have up to now been systematically obtained with PCM-TD-DFT method can be determined with other approaches. Indeed, TD-DFT overshoots the transition energies of cyanines and several studies showed that the second order perturbation correction to single excitation configuration interaction, CIS(D),^{292,293} is more reliable to describe cyanine excited-states.²⁹⁴ CIS(D)

approach introduces dynamic electron correlation via double substitutions and it can be thought of as the excited-state analogue of Moller-Plesset theory (MP2) for the ground states. In the last Chapter of this thesis, we have investigated a large number of aza-BODIPY and BODIPY dyes using a combined CIS(D)/SOS-CIS(D) and TD-DFT approach, aiming to reduce the systematic overestimation of experimental energies.

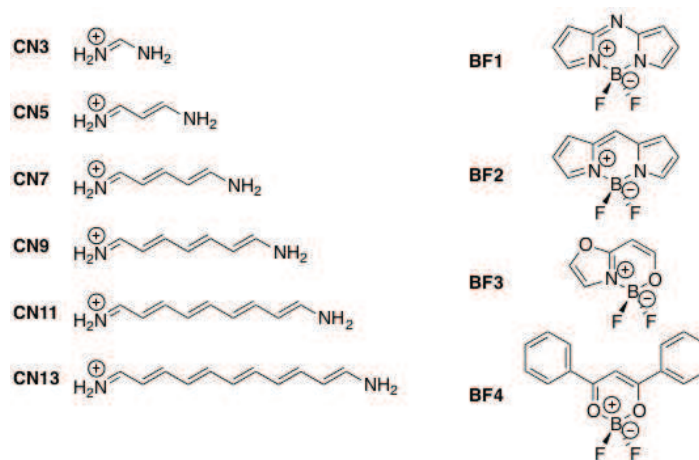
Part II

CHAPTER 6

EXCITED-STATES GEOMETRIES WITH CORRECTED LINEAR-RESPONSE MODEL

Since 2006 one can combine the calculation of TD-DFT gradients with PCM,²⁹⁵ but only within the LR approach and this procedure was used in the previous Chapters. More precisely, to determine the fluorescence wavelengths and hence the 0-0 energies of solvated dyes, we have used LR-PCM to determine the excited-state structures and, next, performed single point vertical cLR/SS-PCM calculations on these geometries. Whilst this procedure is apparently valid, it may only hold if the effects that are not included in the LR approach are captured by the vertical transition energy and only marginally affect the geometry of the emissive state. This is probably reasonable when the LR description is qualitatively correct, but we have explored several series of organic dyes (aza-BODIPY, BODIPY, boranil and dioxaborines) for which large difference between the LR and cLR/SS vertical transition energies have been found. This, in turns, indicates a possible significant modification of the excited-state potential energy surfaces. In this Chapter, we model excited-states using the cLR approach, not only to compute transition energies (as in previous Chapters), but also to optimize the geometrical parameters in a fully consistent approach. Our goal is therefore to appraise the validity of the LR-PCM approach for optimizing excited-state ge-

ometries and to unravel to a possible source of errors in our previous Chapters. As these cLR/LR differences are also large for cyanine derivatives, we have included both model streptocyanines and realistic cores representative of aza-BODIPY, BODIPY, boranil and dioxaborine derivatives (see Scheme 6.1) in this Chapter.



Scheme 6.1: Representation of the model streptocyanines (**CN_x**) and fluoroborates (**BF_x**) derivatives investigated herein.

6.1 Computational Details

All calculations have been performed with the latest version of Gaussian09 program²⁹⁶ that was modified to allow cLR optimization of the excited-state geometries.²⁹⁷ We have applied an improved energy convergence threshold (at least 10^{-10} a.u.), a tight geometry optimization criterion (10^{-5} a.u. on the residual root mean square force)²⁹⁸ and a high-level DFT integration grid (so-called *ultrafine* grid) in order to ensure the numerical stability of the presented data. Default parameters have been used for the PCM cavity and we have considered dichloromethane (DCM) as medium, as this solvent is commonly used for both cyanine and BODIPY derivatives. TD-DFT optimizations in gas phase have been performed with the analytical gradients implemented in Gaussian09, and the same holds for the LR-PCM excited-state calculations. For the **BF_x** compounds, it was checked that the obtained structures correspond to true minima of the potential energy surface by numerically differentiating the LR-PCM-TD-DFT forces. cLR optimizations have been performed through a numerical

eigenvalue-following algorithm²⁹⁹ starting from the optimal LR structures. However, to ensure a correct optimization, we had, on the one hand, to slightly modify the program to obtain the storage of the cLR energy in the adequate vector, and, on the other hand, to use a non-standard route as input. The validity of the computed numerical forces has been tested.³⁰⁰ The geometry calculations were performed with the M06-2X/6-31G(d) approach. Of course, the geometry optimizations have been performed in the equilibrium PCM limit whereas the reported emission wavelengths are computed in the non-equilibrium PCM limit, except for the LR model for which non-equilibrium emission values are ill-defined. This approach for cLR optimization has recently been checked with small system (cyanide, butadiene, diketoopyrrolopyrrole, the H-shaped chromophore of indigo, 2,1,3-benzothiadiazole, thieno[2,3-b]thiophene and two aza-compounds). We will not discuss the results obtained with these dyes as this is outside the scope of this thesis. We redirect the interested reader to Ref. 297 for more details.

6.2 Quasi-Linear Cyanines

We have first considered the prototypical cyanine derivatives, **CN_x**, that have been extensively investigated with a wide panel of theoretical methods,^{67,68,294,301–304} though the majority of these works have been focused on gas phase absorption energies. We have imposed the C_{2v} point group during all calculations. We are well aware that these cyanine dyes present a twisted excited-state geometry,⁶⁷ and that C_{2v} structures constitute true minima of the potential energy surface only for the ground-state, but this specificity is not relevant as most industrially relevant cyanine dyes, e.g. BOD-IPY, are constrained and cannot undergo significant twist in the excited-state. For the shortest and longest chain considered, the cLR (LR) vertical absorption energies are 7.482 (7.330) eV and 2.602 (2.297) eV, respectively. This confirms that the cLR corrections are non negligible for this class of molecules and that they tend to increase the transition energies computed with LR.

The main results obtained for emission are collected in Table 6.1. If one considers a given geometry and investigates the evolution of the fluorescence energies ω_{fluo} , as a function of the environmental model selected, one notices a strong positive solvatochromism, that is a large decrease of the emission energies compared to gas phase when LR is used. For the longest chain investigated, the LR correction exceeds

0.5 eV, which is a very large change for quite compact molecules. However, much smaller solvatochromic effects are predicted by cLR. Indeed, the gas and cLR values are extremely close for each geometries, which hints that the LR solvatochromic effects are too large. We underline that this LR–cLR discrepancy is not related to (non-)equilibrium effects, as the cLR equilibrium values are very close to their non-equilibrium counterparts (typical variations smaller than 0.01 eV).

Table 6.1: Relative cLR energies (ΔE , in eV) and cLR fluorescence transition energies (ω_{fluo} , in eV) obtained for the **CN x** dyes considering three different optimal C_{2v} geometries. Calculations at the cLR-PCM(DCM)-M06-2X/6-311+G(2d,p)//PCM(DCM)-M06-2X/6-31G(d) level considering equilibrium (ΔE , LR ω_{fluo}) or non-equilibrium (cLR ω_{fluo}) limits of the PCM model. For ΔE , the optimized cLR structure is used as reference.

Compound	Gas geometry				LR geometry				cLR geometry		
	ΔE	ω_{fluo}			ΔE	ω_{fluo}			ω_{fluo}		
		Gas	LR	cLR		Gas	LR	cLR	Gas	LR	cLR
CN3	+0.001	6.082	5.799	6.047	+0.002	6.147	5.861	6.112	6.098	5.815	6.063
CN5	+0.000	4.734	4.267	4.720	+0.001	4.756	4.287	4.742	4.746	4.297	4.732
CN7	+0.000	3.855	3.300	3.853	+0.001	3.860	3.305	3.858	3.862	3.308	3.860
CN9	+0.001	3.262	2.668	3.265	+0.001	3.256	2.660	3.258	3.264	2.670	3.267
CN11	+0.002	2.843	2.232	2.843	+0.001	2.837	2.226	2.839	2.845	2.236	2.847
CN13	+0.003	2.528	1.916	2.525	+0.001	2.519	1.906	2.519	2.526	1.915	2.525

If one now turns towards the geometrical effects, we note that the LR–cLR structural variations are very small and this is noticeable not only from the total energy differences (ΔE), but also from the cLR ω_{fluo} computed on different structures. For the latter, the variations are of the order of 0.05 eV for **CN3** and tend to decrease with the length of the conjugated path to attain ca. 0.01 eV for the longest chain considered. The differences between the solvated and gas-phase geometries are also very small, but the ω_{fluo} computed on the cLR excited-state structure is not systematically bracketed by its LR and gas counterparts, contrary to what was found in several small chromophores.²⁹⁷ In Figure 6.1 we present the excited-state geometrical parameters obtained for the longest chain, and, although no general cLR–LR trend can be found (e.g., no systematic increase or decrease) it is clear that the variations of bond lengths and valence angles when varying the environmental model are mostly trifling.

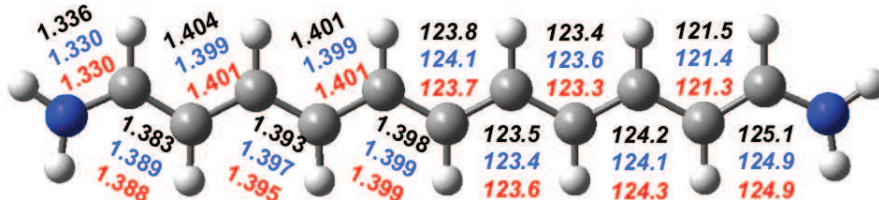


Figure 6.1: Excited-state geometrical parameters obtained for **CN13**. Left: bond lengths in Å, right: valence angles (*italics*) in degrees. The black, blue and red values correspond to gas, LR and cLR results.

In short, the large LR–cLR differences noted for cyanines can be attributed to a pure electronic effect, LR yielding accurate geometries, similar to the one obtained through both gas phase of cLR optimizations.

6.3 Fluoroborates

Let us now move towards the more realistic fluoroborate compounds. The TD-DFT optimizations in gas phase reveal that **BF1**, **BF2** and **BF4** belong to the C_s point group, the plane of symmetry including the central BF_2 unit, whereas, **BF3** is a C_1 molecule. In Figure 6.2, we provide top and bottom views of the ES geometries of

BF1. Clearly, both gas and cLR optimal structures are slightly bent with fluorine atoms located asymmetrically with respect to the π -conjugated skeleton, whereas the LR structure is a pseudo- C_{2v} molecule with fluorine atoms located almost perfectly symmetrically. In other words, the LR model yields larger structural variations with respect to gas phase than its cLR counterpart. The effect is similar for **BF2**, but in that case LR still yields a slightly bent structure. For **BF3**, the three geometries are qualitatively similar. The same holds for **BF4** for which all approaches foresee a nearly coplanar π -conjugated skeleton with a strongly asymmetric BF_2 group. The energetic data are collected in Table 6.2, and the difference of total cLR energies are almost unaffected by the selected geometry (variations of ca. 0.01 eV), but for the gas-phase structure of **BF4** that yields a +0.023 eV difference. For the two first dyes, the emission energies computed on cLR and gas phase geometries are rather close, while using LR structures yields larger fluorescence energies. This last outcome also holds for **BF3** for which the computed ω_{fluo} on the cLR structure is bracketed by its gas and LR counterparts. On the contrary, for **BF4**, gas and LR structures are similar and cLR provides larger emission energies. If one compares the cLR ω_{fluo} computed on LR and cLR geometries, the cLR structural effects are -0.063 eV, -0.031 eV, -0.128 eV and +0.061 for **BF1**, **BF2**, **BF3** and **BF4**, respectively. These values are, as expected, smaller than the “energetic” cLR corrections that amount to +0.379 eV, +0.310 eV, +0.234 eV and +0.216 eV,³⁰⁵ respectively, but are not completely negligible, especially for the asymmetric **BF3**. It is also noteworthy that the “geometric” cLR effect differs significantly for the four **BFx** dyes, though they all belong to the same class of molecules, hinting that the relative values of the transition energies are affected by a cLR optimization, not only the absolute values.



Figure 6.2: Top and bottom views of the optimal excited-state structures of **BF1** obtained in gas phase (left), with LR (center) and cLR (right) schemes.

Table 6.2: Relative cLR energies (ΔE , in eV) and cLR fluorescence transition energies (ω_{fluo} , in eV) obtained for the **BFx** dyes. See caption of Table 6.1 for more details.

ω_{fluo} Compound	Gas geometry				LR geometry				cLR geometry		
	ΔE	Gas	LR	cLR	ΔE	Gas	LR	cLR	Gas	LR	cLR
BF1	+0.006	2.637	2.277	2.618	+0.013	2.702	2.313	2.682	2.639	2.278	2.619
BF2	+0.007	2.894	2.593	2.907	+0.013	2.962	2.632	2.942	2.899	2.597	2.911
BF3	+0.013	3.776	3.536	3.747	+0.008	3.985	3.721	3.955	3.858	3.610	3.827
BF4	+0.023	3.519	3.236	3.423	+0.002	3.504	3.199	3.415	3.523	3.224	3.476

BF2 and **BF4** have been synthesized and their emission spectra measured in dichloromethane. The emission energies are 512 nm¹⁹⁶ and 396 nm,²⁸³ respectively. We notice that our cLR//cLR vertical emission energies attain 425 nm and 357 nm, respectively, that is remain strongly underrated compared to experiment. Indeed, the computed values are quite far from the measurements and we attribute this effect to the cyanine nature of the systems.

6.4 Conclusions

Using a new computational approach allowing to perform optimization of the excited-state geometries with a corrected Linear-Response environmental model, we have investigated the structures and fluorescence energies of a series of cyanine derivatives. For increasingly long model cyanine chains, we found that the gas, LR and cLR excited-state structures are extremely similar though the solvatochromic effects given by LR and cLR approaches are vastly different for fluorescence (and absorption) energies. For fluoroborates, LR has a tendency to yield excited-state structures that are significantly more planar than their gas phase counterpart whereas cLR geometries are rather twisted consistently with the gas phase prediction. This consequently affects the computed emission energies that are larger when one used LR structures (average difference of ca. +0.07 eV difference with respect to the cLR geometries for the four fluorophores cases). These cLR geometrical corrections generally present the correct sign to bring the theoretical values closer to their experimental counterpart for the particularly challenging cyanines, but remain too small to account, by themselves, for the difficulty to model cyanines/fluoroborates with TD-DFT. Let us now turn towards the electronic part of the problem by combing TD-DFT with alternative approaches for computing transitions energies.

CHAPTER 7

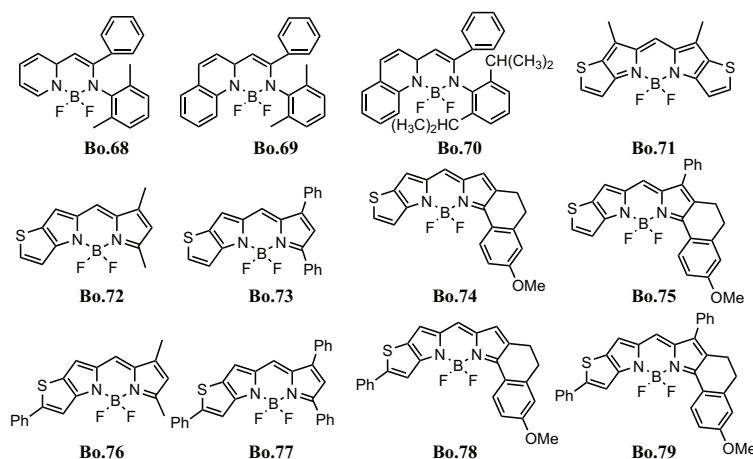
CONNECTING TD-DFT VERTICAL ENERGIES WITH SOS-CIS(D)

The simulation of the electronically excited state (ES) properties of both aza-BODIPY and BODIPY, that can be viewed as *cis*-constrained cyanines, could not be considered as completely satisfactory in Chapters 2 and 3 due to the well-documented *cyanine-problem*. Indeed, TD-DFT successfully restores several key features: 1) the band shapes of dyes presenting significant vibronic coupling; 2) the solvatochromic effects; 3) the relative charge transfer (CT) character of different states; 4) the impact of auxochromes on the evolution of the experimental 0-0 energies,^{94,95} but a serious drawback remained: the TD-DFT transition energies are overestimated. The mean signed error (MSE) is very large for BODIPY dyes (see Chapter 3). An apparent deadlock is reached, as on the one hand TD-DFT is not very accurate for these dyes, and, on the other hand theoretical schemes efficient for cyanines (e.g., CC3 or GW-BSE) do not allow analytic ES optimization,^{67,306} and their use to obtain the 0-0 energies of *real-life* BODIPY is impossible due to their computational requirements. For this reason, the present Chapter proposes the use of an alternative approach combining TD-DFT and Configuration Interaction Singles with a double correction, CIS(D), approaches for determining structures and transition energies, respectively. CIS(D), developed by Head-Gordon and coworkers,^{292,293} is one of the most adequate method to describe the transition energies in organic and inorganic molecules.^{91,292,293,307}

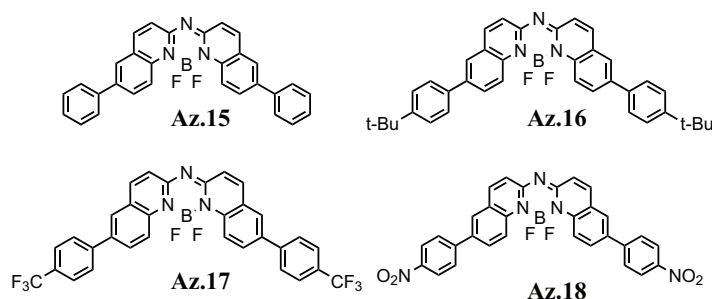
Comparisons of the performances of CIS, CIS(D) and TD-DFT vertical excitation energies have already been published.^{294,302,308,309} It was shown that CIS(D) generally outperforms both CIS and TD-DFT, though the extend of the CIS(D)–TD-DFT differences is strongly system-dependent. Interestingly, Grimme *et al.* and Moore *et al.* found that CIS(D) is an effective approach for model cyanines.^{294,302} We also note that, the spin-scaled approaches derived from CIS(D) were found to be, at least, as powerful as the original scheme to describe the excited states.^{310–312} For instance, TD-DFT, CIS(D) and Scaled-Component-Spin (SCS)-CIS(D) methods have been used to calculate gas phase ES energies of 32 valence states presenting $\pi \rightarrow \pi^*$ or $n \rightarrow \pi^*$ character and it was found that both CIS(D) and SCS-CIS(D) are more accurate than TD-DFT.^{307,313} The average deviation going from ca. 0.3 eV with TD-DFT to ca. 0.2 eV with CIS(D) and SCS-CIS(D). More recently, Goerigk *et al.*, found that both SCS-CIS(D) and Scaled-Opposite-Spin (SOS)-CIS(D) yield similar results, again superior to the TD-DFT method for 12 molecules including two charged species.⁵⁸ The spin-scaled approaches was also be applied with the second order of Coupled-Cluster (CC2)³¹⁴ by Winter and coworkers who performed a benchmark of the 0-0 energies of 66 aromatic organic molecules in gas phase using CC2, SCS-CC2 and SOS-CC2 and concluded that SCS-CC2 is the most accurate approach.³¹⁵ A disadvantage of CIS(D) and its variants, however is that they are, in practice, much less efficient than TD-DFT to determine the ES vibrational structures and geometries. This explains why, in Ref. 58 TD-DFT structural and vibrational data have been used to convert experimental 0-0 energies into vertical absorption values allowing the straightforward use of CIS(D). The aim of the present Chapter, in a similar line, is to assess the performance of both CIS(D) and SOS-CIS(D) methods to simulate the 0-0 energies for two recently synthesized series of BODIPY and aza-BODIPY dyes (see Schemes 7.1 and 7.2). Our goal is to reduce the systematic overestimation of experimental 0-0 energies obtained with TD-DFT by adding corrections obtained with CIS(D) and SOS-CIS(D) approaches for the vertical absorption and emission, respectively.

7.1 Computational Details

DFT, TD-DFT and CIS(D) calculations were carried out with the latest version of the Gaussian 09 program package,³¹⁶ applying both a tighten self-consistent field convergence criterion ($10^{-9} - 10^{-10}$ a.u.) and an improved optimization threshold



Scheme 7.1: Representation of the BODIPY dyes investigated in this Chapter. The measured longest wavelength of absorption (λ_{abs}), emission wavelength (λ_{emi}) and solvents used, as well as the experimental references can be found in Table E.1 in Appendix E.



Scheme 7.2: Representation of the aza-BODIPY dyes investigated in this Chapter. Experimental data and references can be found in Table E.2 in Appendix E.

(10^{-5} a.u. on average forces). The same DFT integration grid, the so-called *ultrafine* pruned (99,590) grid, was used for both the ground and excited states. Consistently with the results of Chapters 2 and 3, our DFT and TD-DFT calculations have been performed with the M06-2X hybrid exchange-correlation functional.¹¹⁶ As previously: 1) the geometrical and vibrational parameters have been determined with 6-31G(d); 2) the transition energies have been corrected with a much larger atomic basis set, 6-311+G(2d,p); 3) the SS-PCM^{99,102} solvation model in its non-equilibrium (neq) limit is applied.^{94,95} In short, we have followed the same approach as in the earlier Chapters. The SOS-MP2 and SOS-CIS(D) energies were determined with the *Q-Chem* package using the 6-31G(d) basis set and applying the Resolution of the Identity (RI) scheme,

with a double- ζ auxiliary basis set.³¹⁷

7.2 Protocol

The results of TD-DFT calculations were corrected with transition energies obtained with CIS(D) and SOS-CIS(D) methods. To simulate the AFCP energies using TD-DFT approach, we have applied the defined proposed strategy (see Chapter 1). For the CIS(D) and SOS-CIS(D) calculations, we have used the optimized geometries of the GS and ES obtained by PCM-DFT and PCM-TD-DFT approaches and performed single-point calculations in gas phase with the 6-31G(d) atomic basis set, SBS. The adiabatic energies are expressed as, [W= MP2 or SOS-MP2, Z= CIS(D) or SOS-CIS(D)]

$$E_{\text{SBS}}^{\text{adia}}(Z) = E_{\text{SBS}}^{\text{ES}}(Z) - E_{\text{SBS}}^{\text{GS}}(W) \quad (7.1)$$

In order to obtain the AFCP energies, we use

$$E_{\text{BE}}^{\text{AFCP}}(Z, \text{SS}, \text{neq}) = E_{\text{BE}}^{\text{AFCP}}(\text{TD}, \text{SS}, \text{neq}) + E_{\text{SBS}}^{\text{adia}}(Z) - E_{\text{SBS}}^{\text{adia}}(\text{TD}, \text{gas}) \quad (7.2)$$

where the TD-DFT adiabatic energies in the gas phase are simply,

$$E_{\text{SBS}}^{\text{adia}}(\text{TD}, \text{gas}) = E_{\text{SBS}}^{\text{ES}}(\text{TD}, \text{gas}) - E_{\text{SBS}}^{\text{GS}}(\text{gas}) \quad (7.3)$$

and the $E_{\text{BE}}^{\text{AFCP}}(\text{TD}, \text{SS}, \text{neq})$ are determined through Eq. 1.19. In short, in Eq. (7.2), structural, vibrational, basis set and solvation effects are determined with TD-DFT whereas vertical transition energies are computed with CIS(D) or SOS-CIS(D).

7.3 Results and discussion

7.3.1 BODIPY dyes

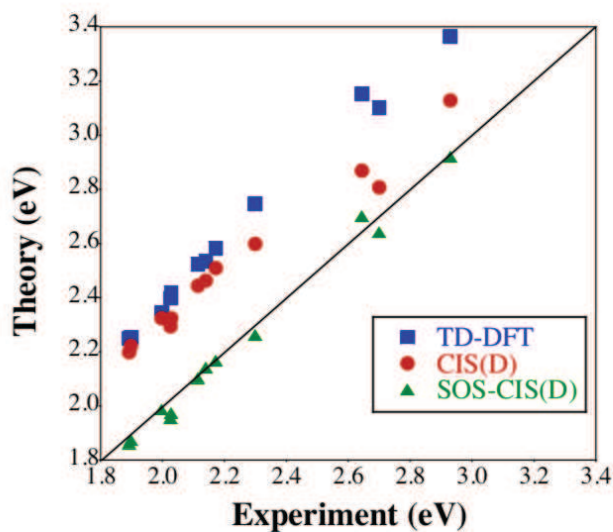
7.3.1.1 0-0 energies

In order to determine the most efficient approach to compute the AFCP energies of the BODIPY dyes presented in Scheme 7.1, we compare TD-DFT [$E_{\text{BE}}^{\text{AFCP}}(\text{TD}, \text{SS}, \text{neq})$, Eq. (1.19)], CIS(D) [$E_{\text{BE}}^{\text{AFCP}}(\text{CIS(D)}, \text{SS}, \text{neq})$, Eq. (7.2)] and SOS-CIS(D) [$E_{\text{BE}}^{\text{AFCP}}(\text{SOS} - \text{CIS(D)}, \text{SS}, \text{neq})$, Eq. (7.2)] figures. The result of a

statistical analysis for these 12 molecules is collected in Table 7.1: mean signed error (MSE), mean absolute error (MAE), standard deviation (SD), linear determination coefficient (R^2) as well as the maximal positive and negative deviations [Max(+) and Max(-)] whereas a graphical comparison between the theoretical and experimental energies is given in Figure 7.1. The *raw* data obtained with TD-DFT-M06-2X, CIS(D) and SOS-CIS(D) are provided in Appendix E. The results in Table 7.1 show a significant difference between the three selected approaches. First, while TD-DFT yields the maximal value of linear determination coefficient (0.992) with a relatively small SD (0.046 eV), this success is at the price of large MSE and MAE (0.403 eV), indicating that the experimental values are systematically overestimated, a result in agreement with the BODIPY study of Chapter 3. It is worth noting that such error significantly exceeds the typical TD-DFT inaccuracy.⁶² As mentioned before, our goal is to decrease the error between experimental and theoretical energies while conserving the high quality correlation obtained with TD-DFT. Going from TD-DFT to CIS(D) reduces the MSE and MAE by 0.124 eV but the R^2 (0.979) is slightly deteriorated compared to TD-DFT. We also note that CIS(D) provides the largest SD (0.069 eV). Interestingly, SOS-CIS(D) and TD-DFT provide very similar correlations. Indeed, for the SD (R^2), we obtain 0.046 eV (0.992) and 0.034 eV (0.991), for TD-DFT and SOS-CIS(D), respectively. The difference of R^2 obtained with these two methods is therefore completely negligible (0.001). More importantly, we underline that SOS-CIS(D) not only gives a small negative MSE (-0.020 eV), indicating that the experimental values are on average slightly underestimated but also yields a tiny MAE. Indeed, adding the SOS-CIS(D) corrections drastically reduces the MAE by more than one order of magnitude (0.403 eV to 0.030 eV). This is in the line of the work of Grimme and coworkers,³⁰⁷ but the improvement is much more significant here. In conclusion, the SOS-CIS(D) method clearly outperforms both TD-DFT and CIS(D) and appears as a nearly perfect approach to obtain the 0-0 energies of the BODIPY shown in Scheme 7.1, as can be seen in Figure 7.1.

Table 7.1: Statistical analysis for dyes shown in Scheme 7.1 obtained with PCM-TDDFT, CIS(D) and SOS-CIS(D) approaches. All values are given in eV but R^2 .

Method	MSE	MAE	SD	R^2	Max(+)	Max(-)
$E_{\text{BE}}^{\text{AFCP}}(\text{TD, SS, neq})$	0.403	0.403	0.046	0.992	0.510	0.348
$E_{\text{BE}}^{\text{AFCP}}(\text{CIS(D), SS, neq})$	0.279	0.279	0.069	0.979	0.339	0.108
$E_{\text{BE}}^{\text{AFCP}}(\text{SOS} - \text{CIS(D), SS, neq})$	-0.020	0.030	0.034	0.991	0.057	-0.072


 Figure 7.1: Comparison between TD-DFT, CIS(D), SOS-CIS(D) and E^{AFCP} experimental for the BODIPY dyes shown in Scheme 7.1.

To check that the exceptional performance of SOS-CIS(D), obtained with *only* 12 BODIPY dyes, is not a *lucky* outcome, it is necessary to increase the chemical diversity of the set of derivatives considered. In that framework, we computed with SOS-CIS(D) the AFCP energies of 35 structurally diverse BODIPY, extracted from a previous TD-DFT investigation (**Bo.1** to **Bo.35** in Chapter 3).⁹⁵ Table 7.2 lists the statistical data obtained for this larger set of compounds (raw data can be found in Appendix E). It is obvious that TD-DFT yields small SD and large R^2 but systematically overshoots the experimental 0-0 energies by a value close to 0.4 eV. This confirms that

TD-DFT approach is only *chemically accurate* for the ES energies of BODIPY dyes. On the contrary, SOS-CIS(D) yields a MAE smaller than 0.1 eV and the difference of R^2 between the two approaches is again negligible (0.004). Figure 7.2 confirms the improvement brought by SOS-CIS(D). For the records, we have determined the MAE for the full set of 47 BODIPY dyes and we obtained 0.382 eV (TD-DFT) and 0.079 eV [SOS-CIS(D)]. We conclude that the mixed SOS-CIS(D)//TD-DFT approach, that combines TD-DFT structural and vibrational data to SOS-CIS(D) vertical energies is extremely efficient for BODIPY dyes: it allows to attain both absolute and relative accuracies for large molecules, a feat beyond the reach of the methods taken separately.

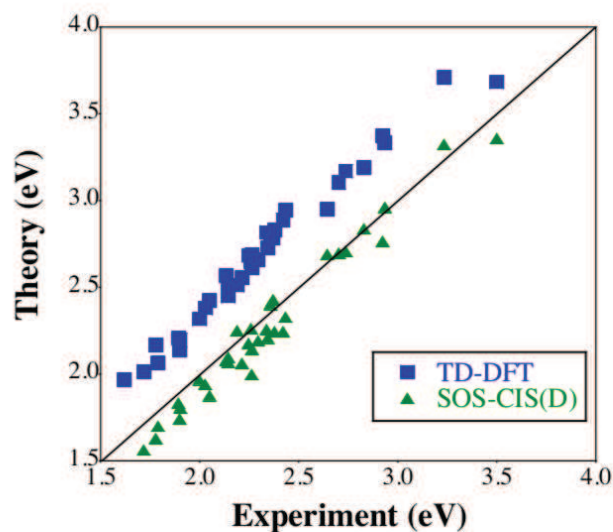


Figure 7.2: Comparison between TD-DFT, SOS-CIS(D) and E^{AFCP} experimental for the 35 BODIPY dyes investigated in Chapter 3.

Table 7.2: Statistical analysis for the 35 BODIPY dyes investigated in Chapter 3 obtained with PCM-TDDFT and SOS-CIS(D) approaches. All values are given in eV but R^2 .

Method	MSE	MAE	SD	R^2	Max(+)	Max(-)
$E_{\text{BE}}^{\text{AFCP}}(\text{TD}, \text{SS}, \text{neq})$	0.375	0.375	0.073	0.974	0.513	0.185
$E_{\text{BE}}^{\text{AFCP}}(\text{SOS} - \text{CIS(D)}, \text{SS}, \text{neq})$	-0.076	0.095	0.083	0.970	0.091	-0.264

7.3.1.2 Impact of the Auxochromes

Let us now turn towards a more chemical analysis. Figure 7.3 shows the density difference plots computed for four BODIPY dyes presenting the same core, namely **Bo.76**, **Bo.77**, **Bo.78** and **Bo.79** (see Scheme 7.1). In order to provide a more complete characterization of the ES of these compounds, we have determined the CT parameters through Le Bahers' model,^{152,153} and the results are listed in Table 7.3: the CT distance (d^{CT}), the transferred charge (q^{CT}) and the CT dipole moment (μ^{CT}). With the SOS-CIS(D) scheme, replacing the side methyl group (**Bo.76**) by a phenyl ring (**Bo.77**) induces a bathochromic shift of +39 nm (absorption) and +48 nm (emission), auxochromic effects matching well the corresponding experimental values of +40 nm and +43 nm, respectively. Interestingly, going from **Bo.76** to **Bo.77** induces a decrease of the CT distance from 1.81 to 1.28 Å (see Table 7.3). Although, one could consider that the phenyl substituent acts as a secondary weak electron donor (in blue in Figure 7.3), this indicates that the observed bathochromic shift is not related to an enhanced CT. Replacing the methyl group (**Bo.76**) by a strong anisol donor group and stiffening the dye (**Bo.78**) induces large bathochromic shifts of +94 nm and +63 nm for absorption and emission, respectively (experimental values: +74 nm and +74 nm, respectively). We again note that the CT distance and dipole decrease when going from **Bo.76** to **Bo.78**, so that the evolution of optical signatures of these compounds cannot be simply explained on the basis of the chemically-intuitive CT parameter.

7.3.1.3 Vibronic spectra

The simulated vibrationally-resolved spectra of **Bo.72**, **Bo.73**, **Bo.74** and **Bo.75** obtained with TD-DFT considering TD-DFT or SOS-CIS(D) 0-0 energies are displayed in the left and right panels of Figure 7.4. Of course, one only notices a redshift of all

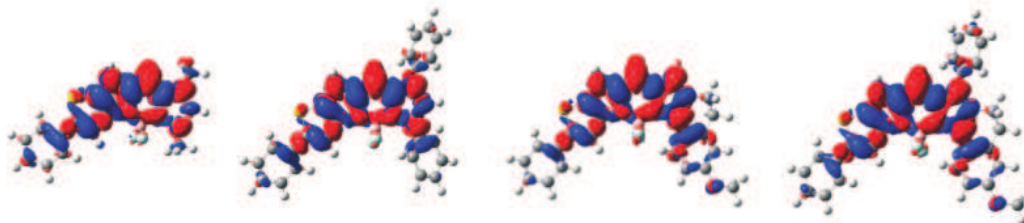


Figure 7.3: PCM-TD-M06-2X/6-31G(d) density difference plots (from left to right) for **Bo.76**, **Bo.77**, **Bo.78** and **Bo.79** BODIPY dyes. The blue (red) zones indicate density decrease (increase) upon transition. The selected contour threshold is 0.0004 a.u.

Table 7.3: The CT distance (d^{CT} in Å), transferred charge (q^{CT} in e), CT dipole (in Debye) for the molecules shown in Figure 7.3.

Dye	d^{CT}	q^{CT}	μ^{CT}
Bo.76	1.81	0.40	3.38
Bo.77	1.28	0.38	2.35
Bo.78	1.10	0.40	2.14
Bo.79	1.43	0.41	2.88

the spectra with the latter scheme, as the same vibrational structures are used in the two calculations. Compared to experiment,³¹⁸ the overall position of the bands is, as expected, much more accurate with SOS-CIS(D), and the successive redshifts in the **Bo.72** \rightarrow **Bo.75** series are also well restored.

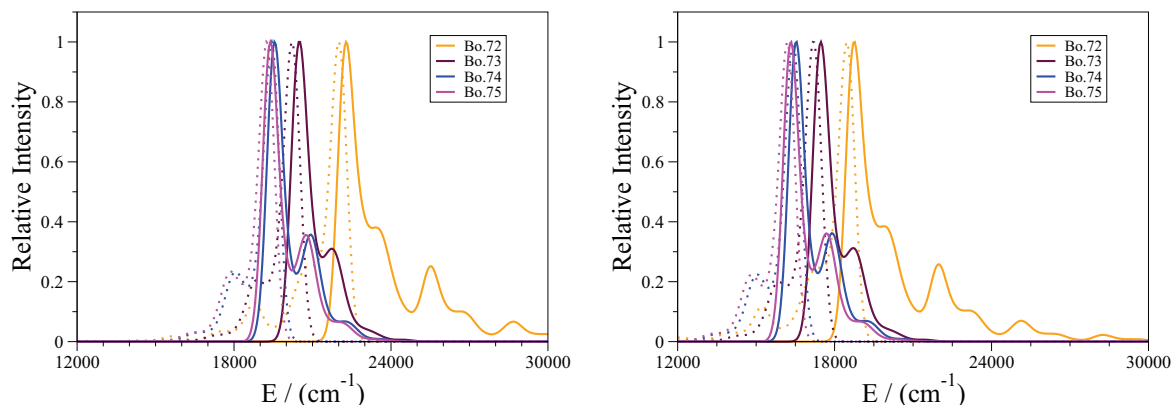


Figure 7.4: Absorption (full lines) and emission (dashed lines) TD-DFT (left) and SOS-CIS(D) (right) spectra for **Bo.72**, **Bo.73**, **Bo.74** and **Bo.75** dyes. Note that the vibrational structures are obtained through TD-DFT in both cases (see text).

It is also clear that theory reproduces the main features of the absorption and emission bands, with the presence of shoulders that are less intense for emission than for absorption.³¹⁸ In our calculations, the intensity of these shoulders is nevertheless slightly overestimated compared to experiment. To unravel the origin of these specific band shapes, we have examined the stick spectra (see Figure 7.5), but no specific vibrational mode particularly stands out as responsible for the presence of shoulders.

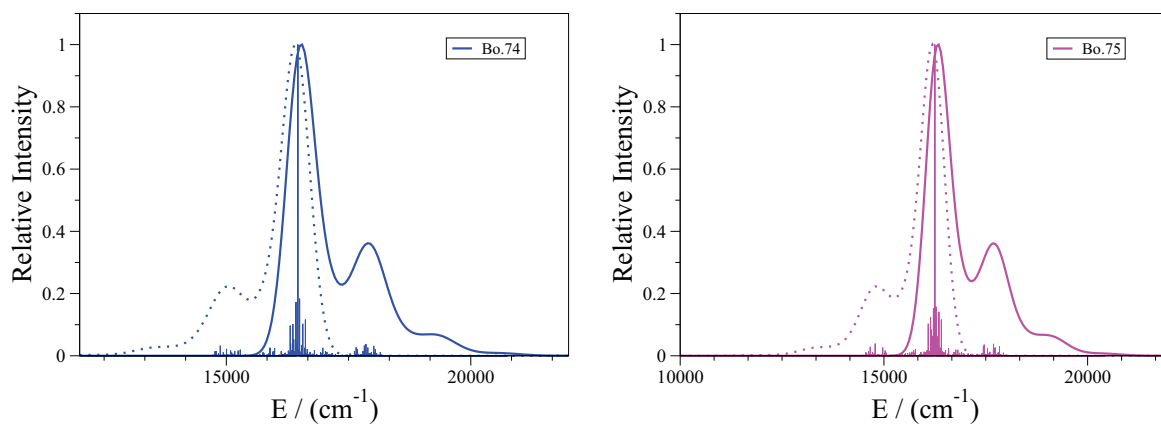


Figure 7.5: Absorption (full lines) and emission (dashed lines) of **Bo.74** (left) and **Bo.75** (right) together with the stick spectra. See caption of Figure 7.4 for more details.

7.3.2 Aza-BODIPY dyes

Recently, Wang and coworkers have synthesized a series of aza-BODIPY dyes presenting very extended π -delocalization.³¹⁹ Our aim is to observe if the new SOS-CIS(D)//TD-DFT protocol is also efficient for aza-BODIPY. The statical analysis for the four dyes of Scheme 7.2 is given in Table 7.4, whereas the 0-0 energies obtained with TD-DFT-M06-2X, CIS(D) and SOS-CIS(D) are available in Appendix E. We have not reported SD and R^2 in Table 7.4, as they would be insignificant for such a small set of molecules. For the three selected approaches, the computed 0-0 energies systematically exceed their experimental counterparts. In the case of TD-DFT, the deviation is as large as 0.4 eV, whereas the two perturbative approaches provide again more accurate results. Indeed, the range of deviations is 0.185–0.137 eV for CIS(D) and 0.077–0.037 eV for SOS-CIS(D). Therefore, the TD-DFT’s MSE and MAE are reduced by almost one order of magnitude when SOS-CIS(D) corrections are included, confirming the success of the proposed "mixed" protocol.

Table 7.4: Statistical analysis for dyes shown in Scheme 7.2 obtained with PCM-TDDFT, CIS(D) and SOS-CIS(D) approaches. All values are given in eV.

Method	MSE	MAE	Max(+)	Max(-)
E_{BE}^{AFCP} (TD, SS, neq)	0.425	0.425	0.457	0.407
E_{BE}^{AFCP} (CIS(D), SS, neq)	0.161	0.161	0.185	0.137
E_{BE}^{AFCP} (SOS – CIS(D), SS, neq)	0.056	0.056	0.077	0.037

Figure 7.6 shows the M06-2X density difference plots computed for the four aza-BODIPY dyes. Adding a ter-butyl (t-Bu) electron donor at both extremities (going from **Az.15** to **Az.16**) induces very small bathochromic shifts (+3 nm for the absorption and +4 nm for the emission). These computed values perfectly match experiment (+3 nm and +3 nm, respectively), and are also consistent with the similar topologies of the density difference plots shown in Figure 7.6. Indeed, the t-Bu groups do not tune the geometry of the core of the molecule nor play any direct role in the optical transition. The ES are only localized on the aza-BODIPY core and on the lateral phenyl rings. **Az.15** and **Az.16** also present similar CT parameters (see Table 7.5). Changing the t-Bu groups (**Az.16**) by electron withdrawing unit: CF_3 (**Az.17**) and NO_2 (**Az.18**), could be expected to yield much more significant effects. However, this is not the case as even the strong nitro groups participate only marginally in the ES

(see Figure 7.6). This is consistent with the very small auxochromic effects measured in Ref. 319 and reproduced by SOS-CIS(D).

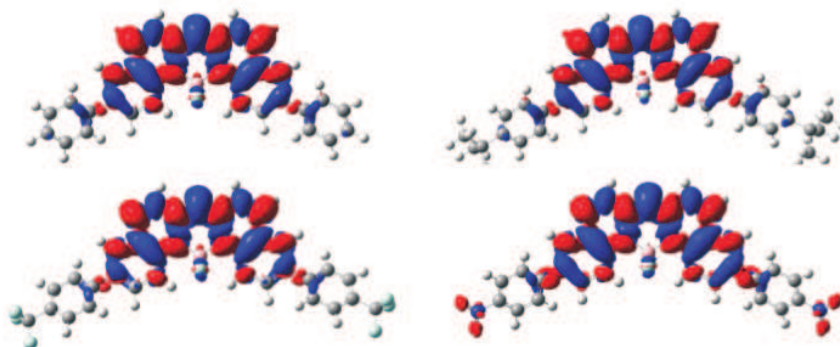


Figure 7.6: PCM-TD-M06-2X/6-31G(d) density difference plots for **Az.15** (top left), **Az.16** (top right) and **Az.17** (bottom left) and **Az.18** (bottom right). See the caption of Figure 7.3 for more details.

Table 7.5: CT parameters for the four aza-BODIPY dyes. See the caption of Table 7.3 for more details.

Dye	d^{CT}	q^{CT}	μ^{CT}
Az.15	0.40	0.50	0.97
Az.16	0.50	0.50	1.21
Az.17	0.28	0.49	0.64
Az.18	0.07	0.50	0.17

Eventually, we report theoretical absorption and emission band shapes calculated for the aza-BODIPY dyes of Scheme 7.2 in Figure 7.7. The four dyes present notable vibronic structures and here again theory very nicely reproduces the experimental band topologies. The stick spectra of **Az.15** is also given in the right panel of Figure 7.7, while the other stick spectra are available in Appendix E. For **Az.15**, we can distinguish major vibrational contributions explaining the emergence of the second band. These modes present an energy of 1467 and 1470 cm^{-1} for the GS (hence the emission spectrum) and the ES (hence the absorption spectrum), respectively. These

vibrational modes can be characterized as CC and CN stretching in the aza-BODIPY core, but they do not involve the BF_2 moiety nor the side phenyl rings.

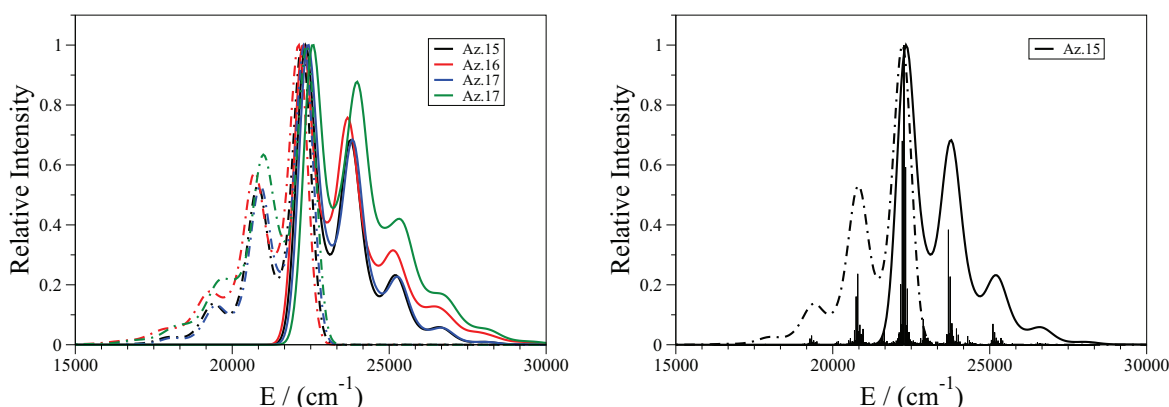


Figure 7.7: Absorption (full lines) and emission (dashed lines) of **Az.15**, **Az.16**, **Az.17** and **Az.18** dyes (left) and stick spectra for **Az.15** (right). See caption of Figure 7.4 for more details.

7.4 Conclusions

We have simulated the spectra of more than fifty fluoroborate derivatives of the (aza-)BODIPY family, using, as previously, structural relaxation, solvent and vibrational effects computed at the TD-DFT level but obtaining the transition energies with the (SOS)-CIS(D) approach. Such a blend approach allowed us to obtain, excited-state properties that are accurate, consistent and directly comparable to the experimental measurements for this key class of compounds. Such a success could not be attained by considering the methods separately. The mean absolute deviations on the 0-0 energies provided by TD-DFT are indeed cut by a factor of ca. 5 when adding SOS-CIS(D) corrections (it is now below 0.1 eV), while, in the same time, the very large theory/experiment correlation coefficients typical of TD-DFT are preserved. The SOS-CIS(D)//TD-DFT protocol presented in this Chapter is computationally efficient and can be straightforwardly applied to large set of real-life dyes, and it will be particularly interesting to circumvent the *cyanine-problem* of TD-DFT.

CONCLUSION- PART II

In the second part of this thesis, building from the *pros* and *cons* of the approach used in the first part, we have pursued our efforts in two principal directions. As mentioned in part I, the selected solvent model for the excited-states calculations has a dramatic impact on the obtained results: the transition energies obtained with cLR-PCM or SS-PCM being significantly different (typically ca. 0.2-0.3 eV larger) from their LR counterparts for fluoroborates. For this reason, we have computed, for the first time, the structures and fluorescence energies of cyanines derivatives as well as of aza-BODIPY, BODIPY, boranil and dioxaborine model systems obtained from their excited-state geometries optimized with the corrected Linear-Response solvent model. To this end, we have used the latest version of Gaussian09 program and modified it to allow numerical cLR optimizations. It turns out that: i) for most molecules the impact of using cLR rather than LR during the geometry optimization of the ES structures is small; ii) for the model of the cyanine molecules, the differences between the solvated and gas-phase geometries are tiny (the variations of the bond lengths and valence angles are trifling when changing the environmental model); iii) for fluoroborates, larger LR-cLR differences of transition energies were found, for instance the correction exceeds 0.1 eV for the model boranil; iv) the cLR geometry correction for fluoroborates is on average small but often brings theory closer to experiment. In short, the cLR geometrical corrections that allows one to perform more consistent calculations, bring a small correction for BODIPY derivatives but the magnitude of this correction is insufficient to model cyanines/fluoroborates very accurately.

As our highly desired goal is to obtain excited-states 0-0 energies that are both accurate and consistent with the experimental measurements, in the second Chapter of Part II, we have combined (SOS)-CIS(D) and TD-DFT approaches to calculate the transition energies of both aza-BODIPY and BODIPY. In fact, we have determined the optimal geometries of both ground and excited states, as well as the vibrational and solvent effects with TD-DFT whereas the vertical transition energies, both absorption and fluorescence, have been computed with (SOS)-CIS(D). Interestingly, such combination is very efficient to determine the optical signatures of these classes of compounds. The mean signed/absolute errors obtained with the TD-DFT scheme for the 0-0 energies, that was reported to be very large (ca. 0.3 eV) in the first part, is efficiently and strongly reduced when the SOS-CIS(D) correction is added (residual error of 0.05 eV). In addition, we underline that the large linear determination coefficient between theoretical and experimental obtained with TD-DFT is conserved when the SOS-CIS(D) corrections are plugged in. Therefore, the SOS-CIS(D)//TD-DFT combination can certainly be viewed as an interesting choice for other sets of molecules presenting a cyanine nature. This blend delivers theoretical estimates of the 0-0 energies that are accurate, consistent and physically meaningful, at list for this family of fluoroborates.

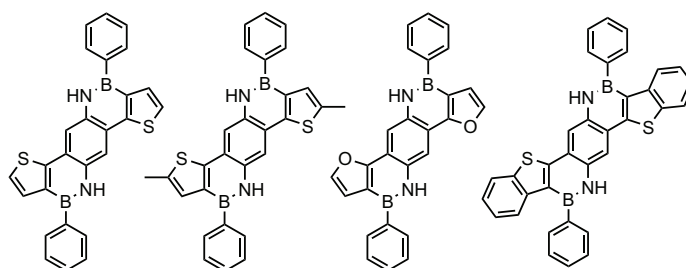
SUMMARY AND OUTLOOK

During this PhD, we have investigated the optical signatures of a large series of fluoroborates dyes belonging to the aza-BODIPY, BODIPY, boranil and dioxaborines families. The experimental success of these derivatives is due to their remarkable photo-physical properties, starting with large molar absorption coefficients, high fluorescence quantum yields, near-IR (NIR) emission, and going to the superior photostability in both solution and solid state. For this reason, in this thesis we have been interested to simulate their electronically excited-states with theoretical tools so to allow not only direct theory-experiment comparisons but also the efficient design of new dyes. The excited states of these dyes are presenting a cyanine nature, and in addition several dyes of this group also possess electronic transition with a significant charger-transfer character. This blend of nature makes any theoretical simulation a significant challenge. A specific effort was put to go beyond the vertical approximation by systematically computing vibronic contributions so to reach well-grounded comparisons with experiments. In the framework of TD-DFT calculations, the impact of several aspect has been assessed, including the selected atomic basis sets, the details of the continuum solvent model and the chosen exchange-correlation functional. For the latter aspect, M06-2X emerged as the most adequate functional to determine the 0-0 energies of aza-BODIPY, BODIPY, boranil and dioxaborines dyes. For all these four families, M06-2X yields (one of) the best linear determination coefficient (> 0.9). Regarding the atomic basis set efforts, we found that the geometrical and vibrational parameters can be determined with a relatively compact atomic basis set, that is 6-31G(d), whereas the transition energies need to be computed using a more extended

basis set, namely 6-311+G(2d,p). We found that including environment effects in our calculations is always crucial and we have applied three PCM variations, namely, the LR, cLR and SS models. We have obtained significant differences between the three selected solvation models when calculating the 0-0 energies. For both aza-BODIPY and BODIPY dyes, SS-PCM apparently yields accurate values, while, LR and cLR models are most effective for boranil and dioxaborines. Indeed, for these two latter classes of compounds, we have found that, for structures possessing a strong increase of their dipole moment upon absorption, the SS model might lead to unphysical values when combined to global hybrids incorporating a low amount of exact exchange. At this stage, we reached three important conclusions: i) PCM-TD-DFT provides yield very consistent 0-0 energies strong correlation with experiment); ii) the selected solvent model for the excited-state calculations plays an important role on the obtained results and especially, the LR approach gives significantly smaller transition energies than its cLR and SS counterparts; iii) despite the inclusion of both relaxation and vibrational effects, the transition energies are systematically overestimated with PCM-TD-DFT, irrespective of the selected PCM model a fact directly related to the cyanine nature of these compounds. These two latter points encouraged us to change and hopefully to improve our theoretical protocol. Related to the second conclusion, it is important to mention that in our works, we have used cLR or SS to correct the excited-state energies but the corresponding geometries were optimized at the LR level. This blend cannot be considered as satisfying: it can clearly become inconsistent for this class of molecules where LR and cLR energies are strongly different. For this reason, we have performed cLR excited-state geometry optimizations allowing to obtain “full” cLR results. Beyond generic conclusions, this method was found insufficient to solve the large errors obtained for cyanines/fluoroborates with the TD-DFT approach. Regarding the third conclusion, we have performed TD-DFT calculations for structures and vibrations and used (SOS)-CIS(D) for transition energies. This new computational protocol allowed us to reach accurate and consistent 0-0 energies directly comparable to the experiment for aza-BODOPY and BODIPY. The mean absolute deviations on the 0-0 energies obtained in this way is very small (below 0.1 eV) while the large correlation with experiment obtained with TD-DFT is maintained. In that sense, we have successfully solved the original goals of our PhD thesis.

Having an efficient protocol [SOS-CIS(D)//TD-DFT] at hand, as an intermedi-

ate perspective, we plan to investigate new series of molecules named *Ladder-Type BN-Embedded Hetroacenes* (see Scheme 7.3). These molecules, characterized by a rigid planar backbone and extended π -conjugation, exhibit high charge-carrier mobility, intense luminescence, and unique self-assembly behavior in both solution and surfaces.³²⁰ It would indeed be desirable to validate our "best shot" for a set of molecules not treated with theoretical models up to now.



Scheme 7.3: Representation of selected Ladder-Type BN-Embedded Hetroacenes dyes.

Secondly, dyes subject to excited-states intermolecular proton transfer (ESIPT) have received a widespread interest in recent years.^{321–323} Recently, in our group we have evaluated excited-state reaction paths and the optical properties of a series of hydroxyphenylbenzimidazole (HBI) derivatives. In this work, we have successfully determined the 0-0 energies and the vibrationally resolved spectra of the corresponding fluoroborate derivatives (boranil) but our recently developed protocol was not used for the "original" enol and keto isomers involved in the ESIPT process. Clearly testing our approach on ESIPT species that do not belong to the cyanine class but are nevertheless chemically similar would be very interesting. In the same line, a new series named *syn*- and *anti*-ladder-type anilido-pyridine boron difluorides (APBDs) were synthesized by stepwise incorporation of BODIPY into ladderized ligands,³²⁴ and such compounds could constitute a further test.

In this PhD, we have restricted our works to implicit solvent models using three variations of PCM approach. We have found that for the excited state the selected solvent model has a strong impact on the 0-0 energies. For this reason, we have performed cLR excited states geometry optimizations. However, the vibrational contributions were determined with the LR approach. It would be worth to further

modify our version of Gaussian09 program in order to allow the computation of both the relaxation and the vibrational effects with cLR-PCM approach.

In the same general framework of environmental effects, the dynamic of the dye, as well as the specific interactions with the solvent molecules can be very important. Recently in our group, we have used the molecular dynamics (MD) for two fluoroborates (aza-BODIPY and boranil).³²⁵ The inclusion of dynamical effects within an explicit solvation approach showed that the absorption spectra is not strongly influenced by the specific solute-solvent interactions for the tested cases. At this stage, an additional question arises: are the emission spectra strongly influenced by the solute-solvent interactions?

Finally, another interesting prospect has been recently reported with the synthesis of a new series of cyclometalated iridium(III) complexes incorporating a monostyryl/distyryl BODIPY ligand via an acetylide bond of 2,2'-bipyridine (bpy).³²⁶ These systems present a strong NIR absorption (644-729 nm) absorption, strong NIR emission (700-800 nm) bands and long-lived triplet excited-states. Previous work has examined the photo-physical properties of these transition metal complexes using DFT level but lack the important aspect of spin-orbital coupling.³²⁶ Such an information is essential in order to improve the properties of interacting with fluoroborates and constitute a further direction for developments.

LIST OF PUBLICATIONS

1. S. Chibani, B. Le Guennic, A. Charaf-Eddin, O. Maury, C. Andraud and D. Jacquemin
On the Computation of Adiabatic Energies in Aza-Boron-Dipyrromethene Dyes
J. Chem. Theory Comput. (FI=5.389), **8** (2012) 3303–3313.
2. S. Chibani, B. Le Guennic, A. Charaf-Eddin, A. D. Laurent and D. Jacquemin
Revisiting the Optical Signatures of BODIPY with Ab Initio Tools
Chem. Sci. (FI=8.601), **4** (2013) 1950–1963.
3. B. Le Guennic, S. Chibani, A. Charaf-Eddin, J. Massue, R. Ziessel, G. Ulrich and D. Jacquemin
The NBO Pattern in Luminescent Chromophores: Unravelling Excited-State Features with TD-DFT
Phys. Chem. Chem. Phys. (FI=4.189), **15** (2013) 7534–7540.
4. S. Chibani, A. Charaf-Eddin, B. Le Guennic and D. Jacquemin
Boranil and Related NBO Dyes: Insights From Theory
J. Chem. Theory Comput. (FI=5.310), **9** (2013) 3127–3135.
5. S. Chibani, A. Charaf-Eddin, B. Mennucci, B. Le Guennic and D. Jacquemin
Optical Signatures of OBO Fluorophores: a Theoretical Analysis

- J. Chem. Theory Comput. (FI=5.310), **10** (2014) 805–815.
6. S. Chibani, A. D. Laurent, A. Blondel, B. Mennucci and D. Jacquemin
Excited-State Geometries of Solvated Molecules: Going Beyond the Linear-Response Polarizable Continuum Model
J. Chem. Theory Comput. (FI=5.310), **10** (2014) 1848–1851.
7. J. Massue, K. Benelhadj, S. Chibani, B. Le Guennic, D. Jacquemin, P. Retailleau, G. Ulrich and R. Ziessel
Fluorescent 2-(2-Hydroxybenzofurane)benzoxazole (HBBO) Borate Complexes: Synthesis, Optical Properties and Theoretical Simulations
Tetrahedron Lett. (FI=2.391), **55** (2014) 4136–4140.
8. D. Jacquemin, S. Chibani, B. Le Guennic and B. Mennucci
Solvent Effects on Cyanine Derivatives: a PCM Investigation
J. Phys. Chem. A (FI=2.775), **118** (2014) 5343–5348.
9. S. Chibani, D. Jacquemin and A. D. Laurent
Modelling Solvent Effects on the Absorption and Emission Spectra of Constrained Cyanines with both Implicit and Explicit Models
Comput. Theor. Chem. (FI=1.368), *invited article*, **1040–1041** (2014) 321327.
10. P. Boulanger, S. Chibani, B. Le Guennic, I. Duchemin, X. Blase and D. Jacquemin
Combining the Bethe-Salpeter Formalism with Time-Dependent DFT Excited-State Forces to Describe Optical Signatures: NBO Fluoroborates as Working Examples
J. Chem. Theory Comput. (FI=5.310), **10** (2014) 4548–4556.
11. K. Benelhadj, J. Massue, P. Retailleau, S. Chibani, B. Le Guennic, D. Jacquemin, G. Ulrich and R. Ziessel
Solution- and Solid-State Luminescent Borate Complexes Based on a Substituted -Conjugated 2-(2-hydroxybenzofuran) Scaffold
Eur. J. Org. Chem. (FI=3.154), submitted.
12. S. Chibani, A. D. Laurent, B. Le Guennic and D. Jacquemin
Improving the Accuracy of Excited State Simulations of BODIPY and aza-BODIPY Dyes with a Joint SOS-CIS(D) and TD-DFT Approach
J. Chem. Theory Comput. (FI=5.310), **10** (2014) 4574–4582.

13. Y. Houari, S. Chibani, D. Jacquemin and A. D. Laurent
A TD-DFT Assessment of the Excited State Intramolecular Proton Transfer in HydroxyphenylBenzImidazole (HBI) Dyes
J. Phys. Chem. B (FI=3.377), submitted.
14. S. Chibani, S. Budzak, M. Medved, B. Mennucci and D. Jacquemin
Full cLR-PCM Calculations of the Solvatochromic Effects on Emission Energies
Phys. Chem. Chem. Phys. (FI=4.189), accepted.
15. S. Chibani, A. D. Laurent , B. Le Guennic and D. Jacquemin
Excited States of Ladder-Type π -conjugated Dyes with a Joint SOS-CIS(D) and PCM-TD-DFT Approach.
J. Phys. Chem. A (FI=2.775), submitted.

APPENDIX A

AZA-BORON-DIPYRROMETHENE DYES: AZA-BODIPY

Table A.1: Experimental λ_{abs} and λ_{fluo} energies for the dyes displayed in Scheme 2.1.

Dye	Solvent	$\lambda_{\text{abs}}(\text{nm})$	$\lambda_{\text{fluo}}(\text{nm})$	Ref.
Az.1	Acetonitrile	643	673	86
Az.2	Acetonitrile	710	732	86
Az.3	Acetonitrile	733	757	86
Az.4	Toluene	693	717	131
Az.5	Chloroform	799	823	130
Az.6	Toluene	728	746	133
Az.7	Dichloromethane	793	841	142
Az.8	Dichloromethane	715	748	142
Az.9	Chloroform	706	730	132
Az.10	Toluene	747	769	133
Az.11	Chloroform	723	734	132
Az.12	Chloroform	688	710	132
Az.13	Chloroform	708	732	132
Az.14	Chloroform	681	728	132

Table A.2: Computed solvent effects for the AZ.10 – AZ.14 (absorption energies), using a series of solvent models. All results obtained with the 6-31G(d) basis set.

Dye	Functional	$E^{\text{vert-a}}$					
		(LR,eq)	(cLR,eq)	(SS,eq)	(LR,neq)	(cLR,neq)	(SS,neq)
Az.1	B3LYP	1.874	2.187	2.178	2.081	2.189	2.183
	PBE0	1.904	2.227	2.220	2.117	2.229	2.224
	BMK	1.963	2.304	2.298	2.188	2.306	2.302
	M06-2X	1.938	2.284	2.279	2.168	2.286	2.282
	CAM-B3LYP	1.946	2.300	2.295	2.181	2.303	2.299
	ω B97X-D	1.950	2.307	2.302	2.187	2.309	2.306
Az.2	B3LYP	1.687	2.038	2.027	1.918	2.042	2.033
	PBE0	1.717	2.076	2.064	1.954	2.080	2.071
	BMK	1.752	2.122	2.109	1.997	2.126	2.116
	M06-2X	1.756	2.127	2.113	2.003	2.132	2.121
	CAM-B3LYP	1.760	2.138	2.126	2.012	2.142	2.133
	ω B97X-D	1.763	2.143	2.132	2.017	2.147	2.139
Az.3	B3LYP	1.584	1.923	1.908	1.806	1.924	1.913
	PBE0	1.623	1.972	1.959	1.852	1.974	1.963
	BMK	1.664	2.029	2.019	1.904	2.031	2.022
	M06-2X	1.676	2.051	2.035	1.920	2.048	2.038
	CAM-B3LYP	1.677	2.045	2.042	1.923	2.053	2.046
	ω B97X-D	1.681	2.048	2.050	1.931	2.062	2.054
Az.4	B3LYP	1.911	2.054	2.030	1.919	2.055	2.031
	PBE0	1.949	2.098	2.075	1.958	2.098	2.077
	BMK	1.974	2.185	2.168	2.036	2.185	2.169
	M06-2X	2.033	2.192	2.180	2.042	2.192	2.181
	CAM-B3LYP	2.039	2.202	2.191	2.048	2.202	2.191
	ω B97X-D	2.053	2.218	2.208	2.063	2.218	2.209
Az.5	B3LYP	1.575	1.764	1.657	1.667	1.777	1.691
	PBE0	1.611	1.809	1.700	1.707	1.822	1.734
	BMK	1.699	1.013	1.812	1.800	1.924	1.845
	M06-2X	1.732	1.953	1.864	1.835	1.963	1.894
	CAM-B3LYP	1.759	1.988	1.909	1.865	1.997	1.936
	ω B97X-D	1.789	2.023	1.954	1.896	2.031	1.978

Table A.3: Computed solvent effects for **Az.1** – **Az.5** (emission and adiabatic energies), using a series of solvent models. All results obtained with the 6-31G(d) basis set.

Dye	Functional	$E^{\text{vert-f}}$			E^{adia}	
		(LR,eq)	(SS,eq)	(SS,neq)	(LR,eq)	(SS,eq)
Az.1	B3LYP	1.662	1.968	1.967	1.767	2.073
	PBE0	1.694	2.014	2.013	1.798	2.118
	BMK	1.736	2.082	2.081	1.849	2.195
	M06-2X	1.718	2.067	2.066	1.829	2.178
	CAM-B3LYP	1.701	2.064	2.063	1.824	2.187
	ω B97X-D	1.697	2.064	2.063	1.821	2.187
Az.2	B3LYP	1.546	1.899	1.898	1.615	1.968
	PBE0	1.575	1.936	1.935	1.645	2.006
	BMK	1.590	1.966	1.965	1.669	2.044
	M06-2X	1.579	1.958	1.956	1.664	2.043
	CAM-B3LYP	1.559	1.948	1.946	1.658	2.047
	ω B97X-D	1.547	1.942	1.941	1.653	2.049
Az.3	B3LYP	1.435	1.766	1.764	1.509	1.840
	PBE0	1.472	1.814	1.813	1.547	1.890
	BMK	1.488	1.853	1.852	1.573	1.939
	M06-2X	1.489	1.861	1.860	1.582	1.955
	CAM-B3LYP	1.467	1.849	1.848	1.571	1.953
	ω B97X-D	1.458	1.848	1.847	1.570	1.960
Az.4	B3LYP	1.760	1.894	1.894	1.835	1.969
	PBE0	1.795	1.934	1.933	1.871	2.010
	BMK	1.843	1.992	1.992	1.933	2.082
	M06-2X	1.839	1.994	1.994	1.936	2.091
	CAM-B3LYP	1.828	1.989	1.989	1.933	2.094
	ω B97X-D	1.830	1.993	1.993	1.939	2.102
Az.5	B3LYP	1.485	1.594	1.585	1.529	1.638
	PBE0	1.514	1.635	1.627	1.562	1.683
	BMK	1.558	1.711	1.704	1.625	1.778
	M06-2X	1.557	1.729	1.723	1.640	1.811
	CAM-B3LYP	1.564	1.752	1.747	1.660	1.848
	ω B97X-D	1.570	1.767	1.762	1.677	1.874

Table A.4: Comparison between the (eq) adiabatic energies computed through Equation 1.13 with SBS and LBS. Δ is the absolute difference. All values are in eV.

Dye	Functional	Eq. 1.13 (LBS)	Eq. 1.13 (SBS)	Δ
Az.1	B3LYP	2.049	2.042	0.007
	PBE0	2.086	2.080	0.006
	BMK	2.169	2.162	0.007
	M06-2X	2.133	2.127	0.006
	CAM-B3LYP	2.149	2.143	0.006
	ω B97X-D	2.146	2.139	0.006
Az.2	B3LYP	1.924	1.920	0.004
	PBE0	1.956	1.953	0.003
	BMK	1.997	1.990	0.006
	M06-2X	1.975	1.968	0.006
	CAM-B3LYP	1.984	1.978	0.006
	ω B97X-D	1.984	1.976	0.008
Az.3	B3LYP	1.796	1.793	0.003
	PBE0	1.844	1.842	0.002
	BMK	1.901	1.895	0.006
	M06-2X	1.893	1.887	0.006
	CAM-B3LYP	1.894	1.888	0.005
	ω B97X-D	1.901	1.894	0.007
Az.4	B3LYP	1.946	1.944	0.002
	PBE0	1.982	1.980	0.002
	BMK	2.058	2.055	0.002
	M06-2X	2.049	2.048	0.001
	CAM-B3LYP	2.057	2.056	0.001
	ω B97X-D	2.060	2.059	0.002
Az.5	B3LYP	1.611	1.605	0.006
	PBE0	1.654	1.648	0.006
	BMK	1.759	1.750	0.009
	M06-2X	1.763	1.757	0.006
	CAM-B3LYP	1.800	1.794	0.006
	ω B97X-D	1.828	1.821	0.006
Az.6	B3LYP	1.923	1.921	0.002
	PBE0	1.953	1.952	0.002
	BMK	2.003	2.000	0.002
	M06-2X	1.990	1.989	0.002
	CAM-B3LYP	1.990	1.988	0.002
	ω B97X-D	1.982	1.980	0.002
Az.7	B3LYP	1.745	1.747	0.002
	PBE0	1.773	1.776	0.002
	BMK	1.813	1.812	0.001
	M06-2X	1.794	1.793	0.001
	CAM-B3LYP	1.795	1.794	0.001
	ω B97X-D	1.807	1.805	0.003

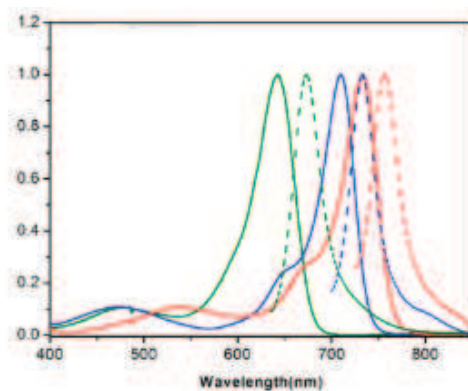


Figure A.1: Experimental vibronic spectra for dyes **Az.1**, **Az.2** and **Az.3**. The spectra is reprinted with permission from *J. Org. Chem.* **77**, 2012 669–673. Copyright 2012 American Chemical Society.

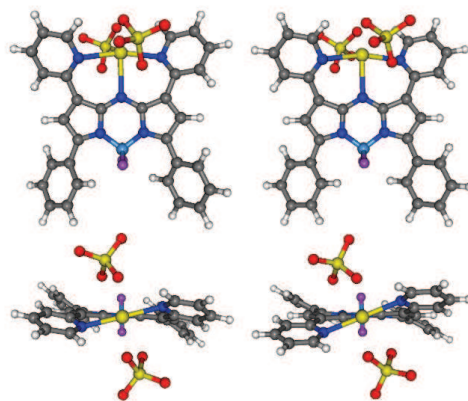


Figure A.2: Front and top view of the **Az.15(Hg²⁺)**-perchlorate complexes obtained at the PCM-BMK level of theory. The ground and excited-state minimal structures are found on the left and right hand sides, respectively.

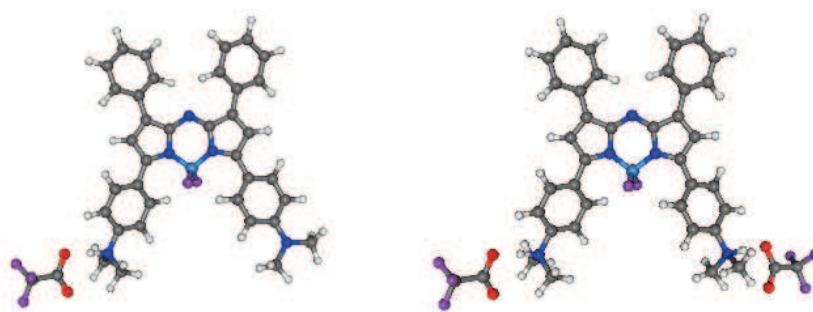


Figure A.3: PCM-BMK optimal ground-state structures for mono and di-protonated **Az.5** with TFA counterions.

APPENDIX B

BORON-DIPYRROMETHENE DYES: BODIPY

B.1 Experimental and theoretical data for the test and training sets.

Table B.1: Experimental wavelengths of absorption and fluorescence for the series of dyes in Scheme 3.1 (in main text). All values are in nm.

Dye	Solvent	λ_{abso}	λ_{fluo}	Ref.
Bo.1	Cyclohexane	504	515	169
Bo.2	Ethyl Acetate	406	444	82
Bo.3	Cyclohexane	526	532	166
Bo.4	Methanol	493	533	125, 162
Bo.5	Dichloromethane	516	570	170
Bo.6	Dichloromethane	527	587	170
Bo.7	Dichloromethane	519	542	180
Bo.8	Toluene	555	578	177
Bo.9	Methanol	564	593	163
Bo.10	Dichloromethane	641	643	179
Bo.11	Dichloromethane	542	562	173
Bo.12	Dichloromethane	612	629	173
Bo.13	Chloroform	579	583	171
Bo.14	Dichloromethane	415	430	168
Bo.15	Dichloromethane	454	464	168
Bo.16	<i>n</i> -Hexane	450	456	174
Bo.17	Toluene	646	666	177
Bo.18	Dichloromethane	711	733	178
Bo.19	Dichloromethane	403	480	176
Bo.20	Dichloromethane	466	604	176
Bo.21	Dichloromethane	427	520	176
Bo.22	Dichloromethane	474	583	176
Bo.23	Chloroform	758	774	75
Bo.24	Chloroform	692	703	75

Table B.2: E^{AFCP} determined with six different hybrid functionals using Equation 1.19 with SS. All values are in eV. Experimental values in Table B.1.

Dye	B3LYP	PBE0	BMK	M06-2X	CAM-B3LYP	ω B97X-D
Bo.1	2.859	2.947	2.988	2.947	2.975	2.984
Bo.2	3.209	3.312	2.889	3.375	3.406	3.431
Bo.3	2.692	2.739	2.757	2.729	2.755	2.741
Bo.4	2.651	2.793	2.906	2.890	2.907	2.906
Bo.5	2.764	2.816	2.852	2.830	2.862	2.869
Bo.6	2.405	2.454	2.532	2.499	2.543	2.566
Bo.7	2.679	2.769	2.877	2.818	2.842	2.861
Bo.8	2.287	2.361	2.419	2.514	2.539	2.557
Bo.9	2.299	2.350	2.403	2.451	2.470	2.528
Bo.10	2.068	2.114	2.209	2.197	2.201	2.234
Bo.11	2.553	2.625	2.683	2.685	2.689	2.697
Bo.12	2.198	2.252	2.337	2.319	2.322	2.267
Bo.13	2.544	2.585	2.604	2.568	2.575	2.574
Bo.14	3.053	3.147	3.293	3.336	3.323	3.330
Bo.15	2.844	2.929	3.085	3.107	3.120	3.139
Bo.16	2.671	2.809	3.070	3.171	3.214	3.249
Bo.17	2.100	2.145	2.207	2.209	2.233	2.242
Bo.18	1.888	1.937	1.994	2.015	2.011	2.027
Bo.19	2.659	2.819	3.128	3.191	3.145	3.172
Bo.20	1.669	1.845	2.498	2.798	2.875	2.871
Bo.21	2.458	2.588	2.883	2.953	2.913	2.947
Bo.22	1.825	2.075	2.631	2.785	2.758	2.801
Bo.23	1.722	1.787	1.926	1.970	1.963	1.991
Bo.24	1.988	2.054	2.164	2.168	2.194	2.223

Table B.3: Comparison between experimental and theoretical AFPC energies for the test set represented in Scheme 3.2 . All values are in eV and have been obtained with the M06-2X functional.

Dye	Solvent	Theory	Experiment	Ref.
Bo.25	Toluene	2.689	2.263	191
Bo.26	Cyclohexane	2.612	2.265	192
Bo.27	Cyclohexane	2.425	2.050	192
Bo.28	Dichloromethane	2.556	2.214	193
Bo.29	Dichloromethane	2.142	1.899	193
Bo.30	Dichloromethane	3.653	3.500	125
Bo.31	Ethanol	3.712	3.233	125
Bo.32	Toluene	2.661	2.295	194
Bo.33	Toluene	2.647	2.259	194
Bo.34	Dichloromethane	2.383	2.028	195
Bo.35	Dichloromethane	2.065	1.791	195

B.2 Additional simulation of spectral shapes.

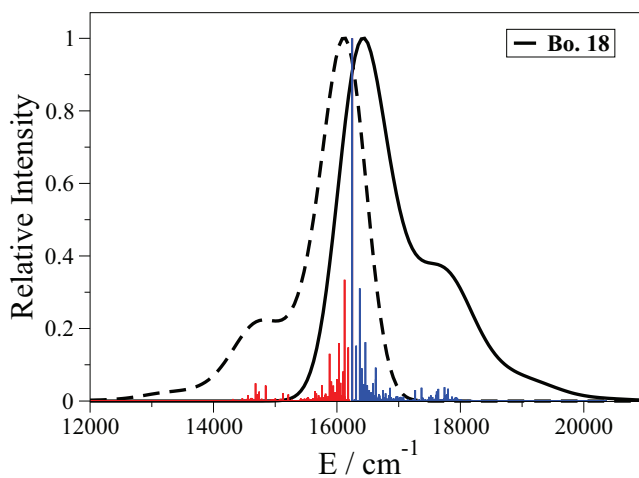


Figure B.1: Absorption (full) and emission (dashed) spectra of **Bo.18**. Experimental spectra might be found in Ref. 178.

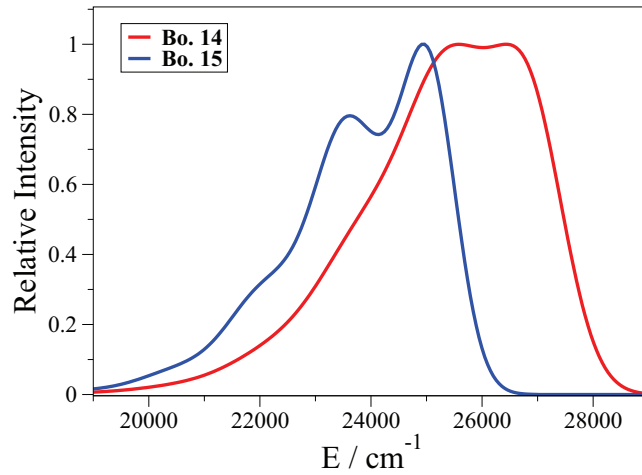


Figure B.2: Emission spectra of **Bo.14** and **Bo.15**. Experimental data can be found in Ref. 168

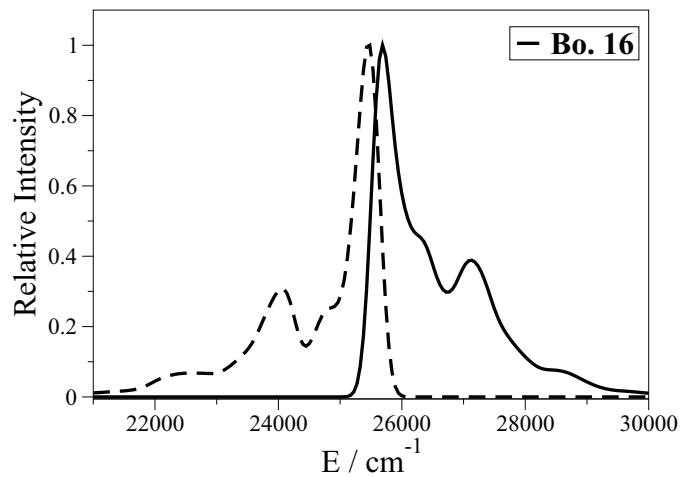


Figure B.3: Absorption (full) and emission (dashed) spectra of **Bo.16**. Experimental spectra might be found in Ref. 174.

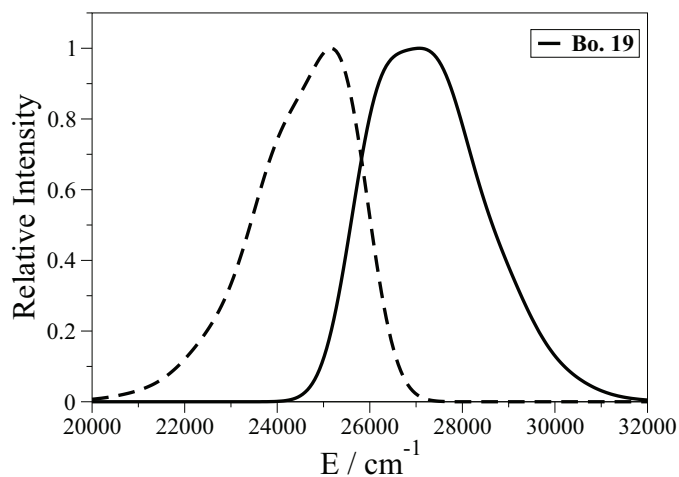


Figure B.4: Absorption (full) and emission (dashed) spectra of **Bo.19**. Experimental spectra might be found in Ref. 176.

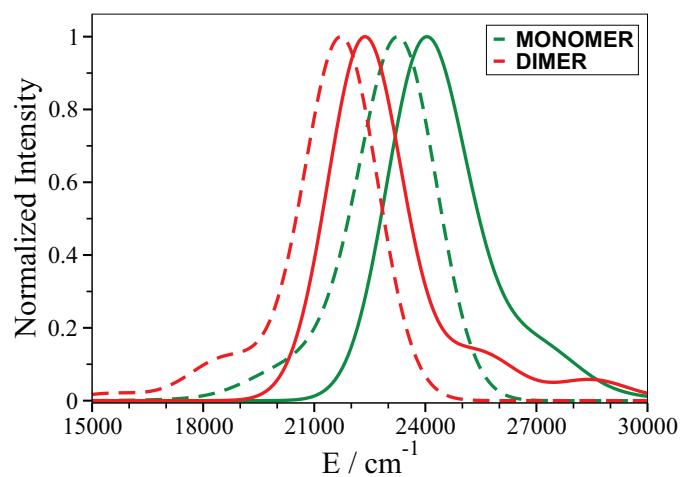


Figure B.5: Absorption (full) and emission (dashed) spectra of **Bo.36** and the corresponding monomer. Experimental spectra can be found in Ref.¹⁹⁸

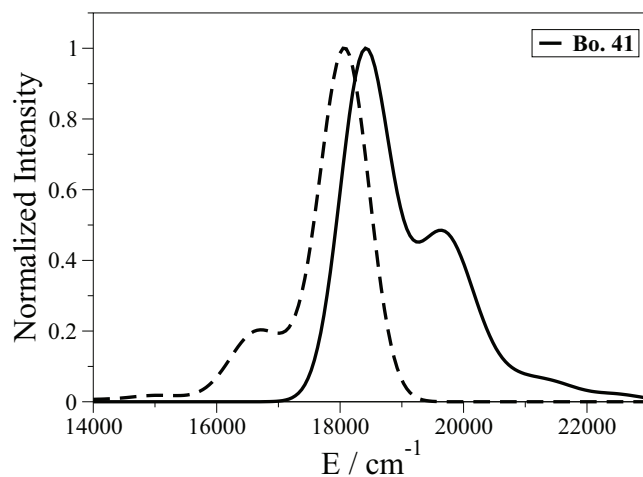


Figure B.6: Absorption (full) and emission (dashed) spectra of **Bo.41**. Experimental spectra might be found in Ref. 211.

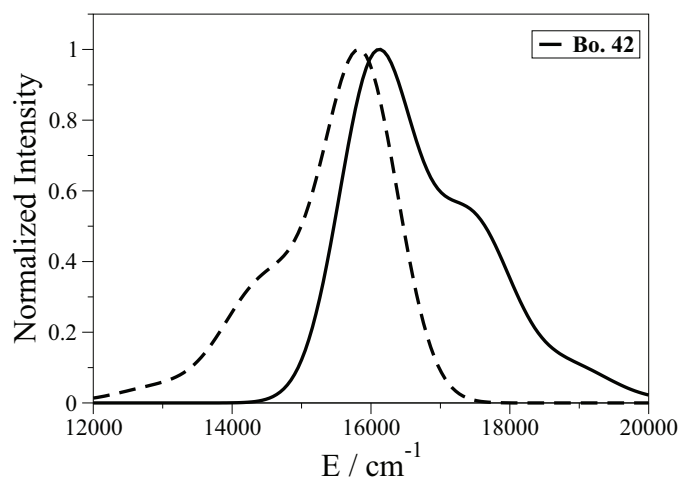


Figure B.7: Absorption (full) and emission (dashed) spectra of **Bo.42**. Experimental spectra might be found in Ref. 211.

B.3 Additional density difference plots.

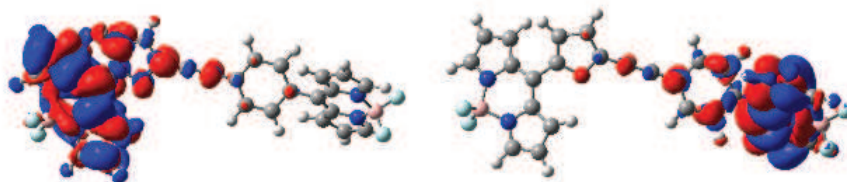


Figure B.8: Density difference plots for the first (left) and second (right) ES of **Bo.39**

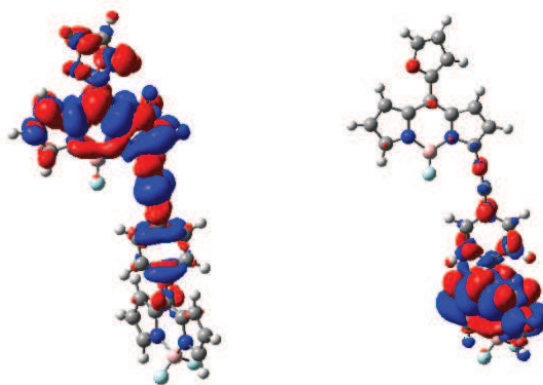


Figure B.9: Density difference plots for the first (left) and second (right) ES of **Bo.40**

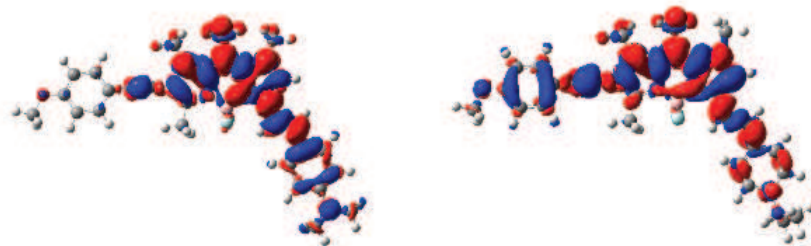


Figure B.10: Density difference plots for the neutral (left) and protonated (right) ES of **Bo.43**

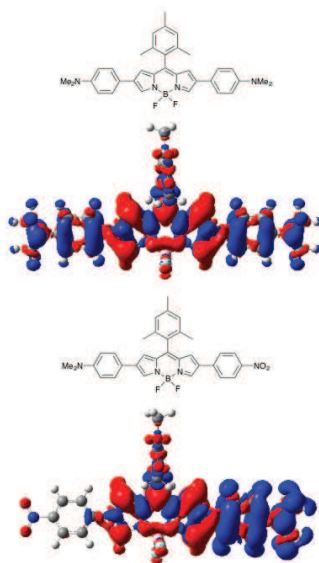


Figure B.11: Density difference plots for two non-emissive dyes proposed by Hayashi and coworkers.¹⁹⁹

B.4 Huang-Rhys graphs.

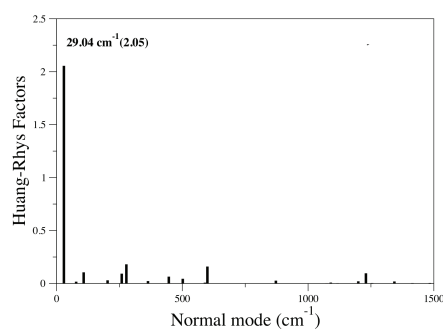


Figure B.12: Computed HR factors for **Bo.66**, the largest contributing mode is given.

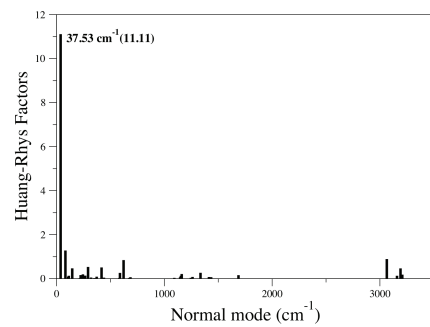


Figure B.13: Computed HR factors for **Bo.67**, the largest contributing mode is given.

B.5 List of transition energies.

Table B.4: List of 6-31G(d) transition energies (eV) computed with TD-DFT. Note that values in the main text and in Section B.1 for the AFCP energies are corrected for equilibrium/non-equilibrium difference, as well as for basis set effects.

BODIPY	Solvent	Functional	$E^{\text{abso}}(\text{SS, neq})$	$E^{\text{fluo}}(\text{SS, neq})$	$E^{\text{adia}}(\text{SS, eq})$	$\Delta E^{\text{ZPVE}}(\text{LR, eq})$
Bo.1	Cyclohexane	B3LYP	3.170	2.899	3.044	-0.138
		PBE0	3.230	3.003	3.124	-0.120
		BMK	3.225	3.058	3.147	-0.107
		M06-2X	3.182	3.027	3.110	-0.091
		CAM-B3LYP	3.205	3.063	3.137	-0.090
		ω B97X-D	3.206	3.070	3.140	-0.083
Bo.2	EthylEthanoate	B3LYP	3.540	3.206	3.380	-0.106
		PBE0	3.642	3.296	3.484	-0.102
		BMK	3.732	3.100	3.301	-0.092
		M06-2X	3.747	3.314	3.544	-0.090
		CAM-B3LYP	3.747	3.363	3.565	-0.084
		ω B97X-D	3.760	3.364	3.576	-0.077
Bo.3	Cyclohexane	B3LYP	2.923	2.813	2.872	-0.111
		PBE0	2.972	2.851	2.915	-0.105
		BMK	2.993	2.872	2.932	-0.123
		M06-2X	2.976	2.797	2.888	-0.093
		CAM-B3LYP	2.995	2.814	2.905	-0.083

Table B.4 – continued from previous page

BODIPY	Solvent	Functional	$E^{\text{abs}}(\text{SS, neq})$	$E^{\text{flu}}(\text{SS, neq})$	$E^{\text{adia}}(\text{SS, eq})$	$\Delta E^{\text{ZPVE}}(\text{LR, eq})$
Bo.4	Methanol	ω B97X-D	2.997	2.809	2.906	-0.103
		B3LYP	2.942	2.738	2.836	-0.119
		PBE0	3.053	2.853	2.957	-0.111
		BMK	3.114	2.917	3.019	-0.061
		M06-2X	3.113	2.904	3.014	-0.080
		CAM-B3LYP	3.137	2.927	3.039	-0.087
Bo.5	Dichloromethane	ω B97X-D	3.130	2.894	3.023	-0.080
		B3LYP	2.994	2.858	2.921	-0.089
		PBE0	3.039	2.908	2.968	-0.083
		BMK	3.070	2.949	3.005	-0.085
		M06-2X	3.029	2.918	2.969	-0.061
		CAM-B3LYP	3.058	2.951	3.000	-0.063
Bo.6	Dichloromethane	ω B97X-D	3.068	2.962	3.012	-0.063
		B3LYP	2.611	2.430	2.525	-0.070
		PBE0	2.667	2.488	2.582	-0.070
		BMK	2.733	2.532	2.635	-0.051
		M06-2X	2.742	2.541	2.630	-0.060
		CAM-B3LYP	2.775	2.568	2.676	-0.057
Bo.7	Dichloromethane	ω B97X-D	2.798	2.582	2.696	-0.054
		B3LYP	2.939	2.717	2.811	-0.092
		PBE0	3.012	2.818	2.907	-0.088
		BMK	3.062	2.876	2.963	-0.051

Table B.4 – continued from previous page

BODIPY	Solvent	Functional	$E^{\text{abso}}(\text{SS, neq})$	$E^{\text{fluo}}(\text{SS, neq})$	$E^{\text{adia}}(\text{SS, eq})$	$\Delta E^{\text{ZPVE}}(\text{LR, eq})$
Bo.8	Toluene	M06-2X	3.052	2.882	2.954	-0.072
		CAM-B3LYP	3.065	2.886	2.964	-0.067
		ω B97X-D	3.082	2.909	2.983	-0.058
		B3LYP	2.585	2.215	2.416	-0.093
		PBE0	2.683	2.293	2.499	-0.089
		BMK	2.739	2.389	2.590	-0.148
		M06-2X	2.743	2.474	2.636	-0.066
Bo.9	Methanol	CAM-B3LYP	2.774	2.485	2.661	-0.076
		ω B97X-D	2.780	2.533	2.683	-0.075
		B3LYP	2.494	2.281	2.390	-0.066
		PBE0	2.550	2.338	2.447	-0.065
		BMK	2.618	2.391	2.510	-0.093
		M06-2X	2.635	2.416	2.526	-0.036
		CAM-B3LYP	2.661	2.423	2.546	-0.045
Bo.10	Dichloromethane	ω B97X-D	2.710	2.445	2.572	-0.017
		B3LYP	2.247	2.083	2.167	-0.058
		PBE0	2.297	2.130	2.215	-0.058
		BMK	2.345	2.168	2.260	-0.018
		M06-2X	2.361	2.185	2.276	-0.031
		CAM-B3LYP	2.374	2.181	2.284	-0.041
		ω B97X-D	2.389	2.197	2.301	-0.024
Bo.11	Dichloromethane	B3LYP	2.787	2.661	2.721	-0.088

Table B.4 – continued from previous page

BODIPY	Solvent	Functional	$E^{\text{abs}}(\text{SS, neq})$	$E^{\text{flu}}(\text{SS, neq})$	$E^{\text{adia}}(\text{SS, eq})$	$\Delta E^{\text{ZPVE}}(\text{LR, eq})$		
Bo.12	Dichloromethane	PBE0	2.849	2.722	2.783	-0.083		
		BMK	2.895	2.749	2.821	-0.076		
		M06-2X	2.908	2.740	2.821	-0.067		
		CAM-B3LYP	2.913	2.742	2.826	-0.066		
		ω B97X-D	2.914	2.740	2.826	-0.063		
		B3LYP	2.381	2.262	2.325	-0.072		
		PBE0	2.434	2.312	2.378	-0.070		
		BMK	2.494	2.356	2.431	-0.050		
		M06-2X	2.509	2.368	2.443	-0.063		
		CAM-B3LYP	2.512	2.356	2.440	-0.058		
Bo.13	Chloroform	ω B97X-D	2.621	2.358	2.386	-0.069		
		B3LYP	2.744	2.678	2.716	-0.108		
		PBE0	2.782	2.713	2.752	-0.103		
		BMK	2.783	2.703	2.748	-0.095		
		M06-2X	2.754	2.675	2.718	-0.086		
		CAM-B3LYP	2.761	2.678	2.725	-0.083		
		ω B97X-D	2.756	2.669	2.718	-0.076		
		Bo.14	Dichloromethane	B3LYP	3.396	3.018	3.209	-0.097
				PBE0	3.492	3.099	3.295	-0.093
				BMK	3.672	3.203	3.430	-0.085
M06-2X	3.728			3.223	3.466	-0.081		
CAM-B3LYP	3.721			3.227	3.464	-0.081		

Table B.4 – continued from previous page

BODIPY	Solvent	Functional	$E^{\text{abso}}(\text{SS, neq})$	$E^{\text{fluo}}(\text{SS, neq})$	$E^{\text{adia}}(\text{SS, eq})$	$\Delta E^{\text{ZPVE}}(\text{LR, eq})$
Bo.15	Dichloromethane	ω B97X-D	3.724	3.235	3.467	-0.085
		B3LYP	3.110	2.827	2.972	-0.092
		PBE0	3.198	2.904	3.054	-0.089
		BMK	3.369	3.011	3.190	-0.078
		M06-2X	3.426	3.032	3.225	-0.080
Bo.16	<i>n</i> -hexane	CAM-B3LYP	3.431	3.050	3.236	-0.075
		ω B97X-D	3.437	3.060	3.243	-0.069
		B3LYP	3.250	2.415	2.820	-0.103
		PBE0	3.358	2.597	2.967	-0.105
		BMK	3.515	2.961	3.245	-0.119
Bo.17	Toluene	M06-2X	3.535	3.252	3.394	-0.142
		CAM-B3LYP	3.558	3.349	3.452	-0.153
		ω B97X-D	3.569	3.365	3.466	-0.139
		B3LYP	2.275	2.149	2.218	-0.079
		PBE0	2.325	2.199	2.267	-0.078
Bo.18	Dichloromethane	BMK	2.372	2.237	2.310	-0.076
		M06-2X	2.388	2.258	2.329	-0.066
		CAM-B3LYP	2.406	2.268	2.343	-0.063
		ω B97X-D	2.418	2.277	2.354	-0.065
		B3LYP	2.052	1.933	1.994	-0.071
Bo.18	Dichloromethane	PBE0	2.102	1.975	2.040	-0.069
		BMK	2.168	2.019	2.096	-0.074

Table B.4 – continued from previous page

BODIPY	Solvent	Functional	$E^{\text{abs}}(\text{SS, neq})$	$E^{\text{flu}}(\text{SS, neq})$	$E^{\text{adia}}(\text{SS, eq})$	$\Delta E^{\text{ZPVE}}(\text{LR, eq})$
Bo.19	Dichloromethane	M06-2X	2.187	2.023	2.107	-0.053
		CAM-B3LYP	2.182	2.010	2.099	-0.052
		ω B97X-D	2.190	2.008	2.103	-0.042
		B3LYP	3.164	2.469	2.752	-0.089
		PBE0	3.293	2.669	2.926	-0.090
		BMK	3.528	3.004	3.239	-0.079
		M06-2X	3.611	3.070	3.321	-0.085
Bo.20	Dichloromethane	CAM-B3LYP	3.560	3.049	3.283	-0.083
		ω B97X-D	3.575	3.051	3.291	-0.073
		B3LYP	2.238	1.294	1.668	-0.065
		PBE0	2.409	1.489	1.835	-0.069
		BMK	2.856	2.257	2.499	-0.076
		M06-2X	3.041	2.609	2.824	-0.064
		CAM-B3LYP	3.083	2.685	2.892	-0.060
Bo.21	Dichloromethane	ω B97X-D	3.186	2.731	2.940	-0.057
		B3LYP	2.997	2.228	2.572	-0.100
		PBE0	3.111	2.368	2.708	-0.100
		BMK	3.324	2.759	3.018	-0.113
		M06-2X	3.407	2.750	3.068	-0.080
		CAM-B3LYP	3.365	2.762	3.041	-0.085
		ω B97X-D	3.378	2.778	3.055	-0.080
Bo.22	Dichloromethane	B3LYP	2.348	1.470	1.801	-0.072

Table B.4 – continued from previous page

BODIPY	Solvent	Functional	$E^{\text{abso}}(\text{SS, neq})$	$E^{\text{fluo}}(\text{SS, neq})$	$E^{\text{adia}}(\text{SS, eq})$	$\Delta E^{\text{ZPVE}}(\text{LR, eq})$
		PBE0	2.523	1.747	2.043	-0.072
		BMK	2.909	2.424	2.646	-0.074
		M06-2X	3.058	2.595	2.820	-0.041
		CAM-B3LYP	3.079	2.615	2.834	-0.065
		ω B97X-D	3.148	2.646	2.872	-0.050

Table B.5: List of transition energies computed with TD-DFT. Only the lowest-lying excited-state reported. nc indicates that the excited-state calculation failed to converge to a meaningful states. See caption of Table B.4 for more details.

BODIPY	Form	Solvent	Functional	$E^{\text{abso}}(\text{SS, neq})$	$E^{\text{fluo}}(\text{SS, neq})$	$E^{\text{adia}}(\text{SS, eq})$	$\Delta E^{\text{ZPVE}}(\text{LR, eq})$
Bo.23		Chloroform	B3LYP	1.888	1.792	1.842	-0.073
			PBE0	1.959	1.851	1.906	-0.072
			BMK	2.096	1.953	2.028	-0.056
			M06-2X	2.159	1.979	2.069	-0.052
			CAM-B3LYP	2.160	1.972	2.068	-0.054
			ω B97X-D	2.204	2.008	2.109	-0.069
Bo.24		Chloroform	B3LYP	2.152	2.096	2.126	-0.094
			PBE0	2.211	2.151	2.183	-0.085
			BMK	2.307	2.228	2.269	-0.067
			M06-2X	2.332	2.232	2.284	-0.069
			CAM-B3LYP	2.350	2.245	2.298	-0.058
			ω B97X-D	2.382	2.275	2.329	-0.061
Bo.25		Toluene	B3LYP	2.896	2.155	2.607	-0.110
			PBE0	2.970	2.257	2.699	-0.104
			BMK	3.009	2.530	2.818	-0.089
			M06-2X	3.001	2.514	2.822	-0.092
			CAM-B3LYP	3.026	2.600	2.859	-0.082

Table B.5 – continued from previous page

BODIPY	Form	Solvent	Functional	$E^{\text{abso}}(\text{SS, neq})$	$E^{\text{fluo}}(\text{SS, neq})$	$E^{\text{adia}}(\text{SS, eq})$	$\Delta E^{\text{ZPVE}}(\text{LR, eq})$
			ω B97X-D	3.044	2.599	2.879	-0.082
Bo.26		Cyclohexane	B3LYP	2.676	nc	nc	nc
			PBE0	2.743	2.243	2.472	-0.074
			BMK	2.844	2.524	2.673	-0.068
			M06-2X	2.878	2.604	2.734	-0.080
			CAM-B3LYP	2.908	2.631	2.760	-0.059
			ω B97X-D	2.931	2.667	2.789	-0.052
Bo.27		Cyclohexane	B3LYP	2.424	2.231	2.321	-0.079
			PBE0	2.479	2.303	2.384	-0.070
			BMK	2.545	2.397	2.470	-0.066
			M06-2X	2.562	2.436	2.499	-0.047
			CAM-B3LYP	2.599	2.471	2.534	-0.046
			ω B97X-D	2.615	2.492	2.552	-0.023
Bo.28		Dichloromethane	M06-2X	2.792	2.642	2.710	-0.084
Bo.29		Dichloromethane	M06-2X	2.371	2.206	2.282	-0.069
Bo.30		Dichloromethane	M06-2X	4.349	3.495	3.902	-0.125
Bo.31		Ethanol	M06-2X	4.242	3.421	3.820	-0.112
Bo.32		Toluene	M06-2X	2.867	2.606	2.735	-0.064
Bo.33		Toluene	M06-2X	2.806	2.649	2.733	-0.058
Bo.34		Dichloromethane	M06-2X	2.598	2.416	2.515	-0.063
Bo.35		Dichloromethane	M06-2X	2.279	2.060	2.175	-0.056
Bo.36	Monomer	Dichloromethane	M06-2X	3.099	2.959	3.037	-0.068

Table B.5 – continued from previous page

BODIPY	Form	Solvent	Functional	$E^{\text{abs}}(\text{SS, neq})$	$E^{\text{flu}}(\text{SS, neq})$	$E^{\text{adia}}(\text{SS, eq})$	$\Delta E^{\text{ZPVE}}(\text{LR, eq})$
	Dimer		M06-2X	2.893	2.754	2.826	-0.085
Bo.37	Monomer	Dichloromethane	M06-2X	3.146	3.013	3.077	-0.072
	Dimer		M06-2X	2.709	2.488	2.603	-0.062
Bo.38	Monomer	Toluene	M06-2X	2.485	2.283	2.382	-0.084
	Dimer		M06-2X	2.170	1.803	1.996	-0.095
Bo.39		Toluene	M06-2X	2.963	2.424	2.749	-0.077
Bo.40		Toluene	M06-2X	2.637	2.387	2.525	-0.066

Table B.6: List of transition energies computed with TD-DFT. Only the lowest-lying excited-state reported. nc indicates that the excited-state calculation failed to converge to a meaningful states. See caption of Table B.4 for more details.

BODIPY	Form	Solvent	$E^{\text{abso}}(\text{SS, neq})$	$E^{\text{fluo}}(\text{SS, neq})$	$E^{\text{adia}}(\text{SS, eq})$	$\Delta E^{\text{ZPVE}}(\text{LR, eq})$
Bo.41	Neutral	Chloroform	2.457	2.275	2.372	-0.065
	Diprotonated		2.414	2.154	2.286	-0.081
Bo.42	Neutral	Chloroform	2.159	1.930	2.051	-0.046
	Diprotonated		2.476	2.260	2.372	-0.047
Bo.43	Neutral	Dioxan	2.438	2.245	2.348	-0.080
	Protonated		2.567	2.237	2.398	-0.082
Bo.44	Neutral	Water	2.682	2.460	2.579	-0.063
	Protonated		2.737	2.571	2.681	-0.063
	Deprotonated		2.615	2.352	2.475	-0.041
Bo.45	Neutral	Tetrahydrofuran	2.458	2.199	2.343	-0.038
	Protonated		2.744	2.559	2.672	-0.068
	Deprotonated (S1)		2.461	0.282	0.922	-0.060
	Deprotonated (S2)		2.461	2.216	2.487	-0.088
Bo.46		Acetontrile	3.062	2.958	3.008	-0.091
Bo.47	Free	Acetontrile	2.682	2.460	2.588	-0.047
	With $\text{CN}^-/\text{NH}_4^+$		2.633	2.279	2.458	-0.046
Bo.48	C=S	Chloroform	2.822	2.538	2.667	-0.057

Table B.6 – continued from previous page

BODIPY	Form	Solvent	$E^{\text{abso}}(\text{SS, neq})$	$E^{\text{fluo}}(\text{SS, neq})$	$E^{\text{adia}}(\text{SS, eq})$	$\Delta E^{\text{ZPVE}}(\text{LR, eq})$
	C=O		2.935	2.754	2.839	-0.065
Bo.49	Dithiane	Tetrahydrofuran	3.022	2.817	2.908	-0.074
	Carbonyl		3.128	2.922	3.013	-0.062
Bo.50	Sulfur	Dichloromethane	2.839	2.684	2.740	-0.057
	Sulfoxyde		3.078	2.812	2.933	-0.069
Bo.51	wo biphenyl	Dichloromethane	3.146	3.013	3.077	-0.073
Bo.51	w biphenyl	Dichloromethane	2.698	2.482	2.577	-0.051
Bo.52		Dichloromethane	2.368	2.268	2.317	-0.054
Bo.53		Toluene	3.063	2.915	2.993	-0.082
Bo.54		Toluene	2.899	2.797	2.847	-0.087
Bo.55		Toluene	2.843	2.684	2.765	-0.076
Bo.56		Toluene	2.519	2.398	2.461	-0.059
Bo.57		Chloroform	2.487	2.245	2.366	-0.044
Bo.58		Chloroform	2.485	2.241	2.363	-0.041
Bo.59		Dichloromethane	3.064	2.887	2.969	-0.072
Bo.60		Dichloromethane	2.967	2.753	2.844	-0.053
Bo.61		Dichloromethane	2.797	2.598	2.692	-0.053
Bo.62		Chloroform	2.604	2.504	2.560	-0.095
Bo.63		Chloroform	2.431	2.310	2.379	-0.071
Bo.64		Chloroform	2.340	2.208	2.280	-0.061
Bo.65		Chloroform	2.179	2.038	2.115	-0.057
Bo.66		Tetrahydrofuran	3.197	3.054	3.127	-0.082

Table B.6 – continued from previous page

BODIPY	Form	Solvent	$E^{\text{abs}}(\text{SS}, \text{neq})$	$E^{\text{fluo}}(\text{SS}, \text{neq})$	$E^{\text{adia}}(\text{SS}, \text{eq})$	$\Delta E^{\text{ZPVE}}(\text{LR}, \text{eq})$
Bo.67		Tetrahydrofuran	3.129	2.691	2.955	-0.065

APPENDIX C

BORANIL AND RELATED NBO DYES

Table C.1: Experimental λ_{abs} , λ_{fluo} and 0-0 energies for dyes shown in Schemes 4.1 and 4.2.

Dye	Solvent	$\lambda_{\text{abs}}(\text{nm})$	$\lambda_{\text{fluo}}(\text{nm})$	0-0	Ref.
Bor.1	Dichloromethane	427	588	2.505	12
Bor.2	Dichloromethane	468	544	2.463	12
Bor.3	Toluene	349	401	3.322	19
Bor.4	Toluene	375	422	3.122	19
Bor.5	Toluene	385	395	3.180	19
Bor.6	Dichloromethane	405	528	2.705	20
Bor.7	Dichloromethane	414	468	2.822	20
Bor.8	Toluene	372	471	2.983	16
Bor.9	Toluene	396	445	2.959	16
Bor.10	Toluene	427	474	2.760	16
Bor.11	Toluene	504	514	2.436	16
Bor.12	Toluene	403	539	2.688	16
Bor.13	Toluene	409	492	2.776	16
Bor.14	Toluene	443	506	2.625	16
Bor.15	Toluene	428	506	2.674	16
Bor.16	Toluene	362	417	3.199	19
Bor.17	Toluene	342	385	3.423	19
Bor.18	Toluene	342	387	3.414	19
Bor.19	Toluene	365	425	3.157	19
Bor.20	Toluene	371	439	3.083	19
Bor.21	Acetonitrile	499	535	2.401	249
Bor.22	Acetonitrile	504	537	2.384	249
Bor.23	Acetonitrile	509	538	2.370	249
Bor.24	Dichloromethane	413	430	2.943	248

Table C.2: Theoretical best estimates of the experimental 0-0 energies for the ten first dyes. All values are in eV and have been obtained from Equation 1.16 in the equilibrium limit (LR,eq).

Dyes	B3LYP	PBE0	M06	BMK	M06-2X	CAM-B3LYP	ω B97X-D	ω B97
Bor.1	2.254	2.368	2.432	2.616	2.720	2.744	2.770	2.975
Bor.2	2.291	2.385	2.410	2.523	2.576	2.639	2.653	2.838
Bor.3	3.267	3.390	3.359	3.576	3.637	3.607	3.613	3.772
Bor.4	3.013	3.125	3.077	3.307	3.357	3.351	3.372	3.552
Bor.5	3.223	3.337	3.305	3.532	3.502	3.533	3.548	3.688
Bor.6	2.524	2.618	2.610	2.861	2.854	2.928	2.980	3.194
Bor.7	2.657	2.751	2.743	2.981	2.965	3.033	3.080	3.237
Bor.8	2.816	2.922	2.897	3.132	3.189	3.206	3.250	3.437
Bor.9	2.981	3.067	2.849	3.244	3.223	3.286	3.296	3.466
Bor.10	2.394	2.727	2.736	3.057	3.076	3.128	3.189	3.339

Table C.3: Theoretical best estimates of the experimental 0-0 energies for the ten first dyes. All values are in eV and have been obtained from Equation 1.16 in the non-equilibrium limit (LR,neq).

Dyes	B3LYP	PBE0	M06	BMK	M06-2X	CAM-B3LYP	ω B97X-D	ω B97
Bor.1	2.280	2.404	2.475	2.683	2.795	2.822	2.851	3.072
Bor.2	2.110	2.463	2.491	2.609	2.668	2.731	2.747	2.944
Bor.3	3.271	3.394	3.363	3.581	3.643	3.612	3.618	3.777
Bor.4	3.019	3.131	3.083	3.292	3.362	3.356	3.380	3.557
Bor.5	3.230	3.345	3.313	3.539	3.510	3.541	3.557	3.696
Bor.6	2.724	2.819	2.849	3.081	3.079	3.063	3.128	3.327
Bor.7	2.785	2.880	2.840	3.124	3.071	3.163	3.212	3.376
Bor.8	2.823	2.929	2.903	3.139	3.196	3.213	3.256	3.443
Bor.9	2.989	3.075	3.036	3.251	3.231	3.294	3.303	3.473
Bor.10	2.387	2.731	2.743	3.064	3.084	3.135	3.196	3.347

Table C.4: Theoretical best estimates of the experimental 0-0 energies for the ten first dyes. All values are in eV and have been obtained from Equation 1.17 in the equilibrium limit (SS,eq).

Dyes	B3LYP	PBE0	M06	BMK	M06-2X	CAM-B3LYP	ω B97X-D	ω B97
Bor.1	1.128	1.405	1.633	2.229	2.506	2.574	2.642	2.949
Bor.2	2.219	2.384	2.430	2.579	2.663	2.733	2.740	2.956
Bor.3	3.272	3.415	3.385	3.647	3.721	3.689	3.696	3.868
Bor.4	3.073	3.194	3.140	3.389	3.443	3.435	3.456	3.643
Bor.5	3.313	3.437	3.418	3.647	3.619	3.656	3.670	3.810
Bor.6	2.526	2.641	2.636	2.914	2.928	2.975	3.026	3.282
Bor.7	2.824	2.960	2.909	3.251	3.233	3.298	3.342	3.501
Bor.8	2.821	2.954	2.929	3.204	3.280	3.283	3.339	3.545
Bor.9	3.104	3.195	1.926	3.385	3.365	3.426	3.435	3.609
Bor.10	0.901	1.660	1.692	2.993	3.167	3.225	3.304	3.468

Table C.5: Theoretical best estimates of the experimental 0-0 energies for the first ten dyes. All values are in eV and have been obtained from Equation 1.17 in the non-equilibrium limit (SS,neq).

Dyes	B3LYP	PBE0	M06	BMK	M06-2X	CAM-B3LYP	ω B97X-D	ω B97
Bor.1	1.067	1.349	1.579	2.207	2.487	2.558	2.629	2.941
Bor.2	0.480	2.314	2.409	2.562	2.649	2.721	2.728	2.947
Bor.3	3.271	3.415	3.384	3.647	3.720	3.689	3.696	3.868
Bor.4	3.073	3.194	3.140	3.369	3.443	3.435	3.458	3.643
Bor.5	3.312	3.437	3.417	3.647	3.619	3.656	3.671	3.810
Bor.6	2.535	2.665	2.700	2.975	2.993	2.956	3.023	3.282
Bor.7	2.806	2.949	2.862	3.254	3.200	3.295	3.342	3.507
Bor.8	2.819	2.953	2.927	3.202	3.280	3.283	3.338	3.545
Bor.9	3.104	3.195	3.145	3.384	3.365	3.426	3.434	3.609
Bor.10	0.806	1.645	1.681	2.988	3.166	3.225	3.302	3.468

Table C.6: Theoretical best estimates of the experimental AFCP energies, AFCP (SS,neq), for the ten first dyes. All values are in eV and have been obtained from Equation 1.19

Dyes	B3LYP	PBE0	M06	BMK	M06-2X	CAM-B3LYP	ω B97X-D	ω B97
Bor.1	1.492	1.780	2.016	2.399	2.598	2.653	2.707	2.978
Bor.2	2.540	2.812	2.814	2.605	2.693	2.758	2.767	2.986
Bor.3	3.274	3.417	3.387	3.649	3.722	3.691	3.697	3.869
Bor.4	3.075	3.195	3.141	3.390	3.444	3.435	3.457	3.643
Bor.5	3.316	3.439	3.419	3.649	3.620	3.657	3.671	3.810
Bor.6	2.701	2.822	2.827	3.106	3.023	3.133	3.098	3.280
Bor.7	3.292	3.239	2.917	3.277	3.253	3.313	3.356	3.518
Bor.8	2.832	2.966	2.941	3.213	3.282	3.284	3.339	3.546
Bor.9	3.105	3.196	1.919	3.385	3.365	3.427	3.435	3.610
Bor.10	0.914	1.678	1.712	3.020	3.172	3.231	3.306	3.469

Table C.7: Dipole moment of the ground and excited states for Bor.10. All values are in Debye.

Functional	Toluene			Acetonitrile		
	μ^{GS}	μ^{ES}	$\Delta\mu$	μ^{GS}	μ^{ES}	$\Delta\mu$
B3LYP	13.7	32.3	18.6	16.5	40.5	24.0
PBE0	14.0	29.6	15.6	16.2	37.0	20.8
M06	14.0	28.2	14.2	16.1	30.6	20.1
BMK	14.2	24.6	10.4	16.5	30.6	14.1
M06-2X	13.4	20.2	6.8	15.4	24.1	8.7
CAM-B3LYP	13.4	19.7	6.3	15.4	23.7	8.3
ω B97X-D	13.3	18.4	5.1	15.2	21.8	6.6
ω B97	12.7	16.8	4.1	14.5	19.3	4.8

Table C.8: Statistical analysis for the nine first dyes (that is **Bor.10** removed from the statistics) in Scheme 4.1 obtained from comparison between experimental and theoretical 0-0 energies. MSE, MAE and SD are in eV.

Functional	Method	MSE	MAE	SD	R^2
B3LYP	Eq.1.16 ($X=eq$)	-0.115	0.129	0.099	0.966
	Eq.1.16 ($X=neq$)	-0.092	0.114	0.134	0.929
	Eq.1.17 ($Y=SS, X=eq$)	-0.198	0.260	0.462	0.720
	Eq.1.17 ($Y=SS, X=neq$)	-0.399	0.461	0.763	0.797
	Eq.1.19 ($Y=SS, X=neq$)	-0.048	0.232	0.403	0.572
PBE0	Eq.1.16 ($X=eq$)	-0.011	0.085	0.101	0.972
	Eq.1.16 ($X=neq$)	0.042	0.077	0.086	0.951
	Eq.1.17 ($Y=SS, X=eq$)	-0.053	0.230	0.411	0.747
	Eq.1.17 ($Y=SS, X=neq$)	-0.066	0.240	0.429	0.752
	Eq.1.19 ($Y=SS, X=neq$)	0.090	0.254	0.336	0.596
M06	Eq.1.16 ($X=eq$)	-0.042	0.078	0.076	0.967
	Eq.1.16 ($X=neq$)	0.032	0.065	0.076	0.941
	Eq.1.17 ($Y=SS, X=eq$)	-0.184	0.274	0.447	0.551
	Eq.1.17 ($Y=SS, X=neq$)	-0.055	0.176	0.341	0.772
	Eq.1.19 ($Y=SS, X=neq$)	-0.076	0.274	0.430	0.348
BMK	Eq.1.16 ($X=eq$)	0.190	0.190	0.091	0.978
	Eq.1.16 ($X=neq$)	0.249	0.249	0.089	0.933
	Eq.1.17 ($Y=SS, X=eq$)	0.234	0.304	0.227	0.878
	Eq.1.17 ($Y=SS, X=neq$)	0.243	0.309	0.235	0.865
	Eq.1.19 ($Y=SS, X=neq$)	0.290	0.314	0.185	0.875
M06-2X	Eq.1.16 ($X=eq$)	0.218	0.218	0.074	0.985
	Eq.1.16 ($X=neq$)	0.277	0.277	0.057	0.969
	Eq.1.17 ($Y=SS, X=eq$)	0.300	0.300	0.141	0.954
	Eq.1.17 ($Y=SS, X=neq$)	0.299	0.304	0.142	0.954
	Eq.1.19 ($Y=SS, X=neq$)	0.326	0.326	0.112	0.960
CAM-B3LYP	Eq.1.16 ($X=eq$)	0.252	0.252	0.058	0.982
	Eq.1.16 ($X=neq$)	0.304	0.304	0.051	0.971
	Eq.1.17 ($Y=SS, X=eq$)	0.334	0.334	0.132	0.927
	Eq.1.17 ($Y=SS, X=neq$)	0.329	0.329	0.138	0.927
	Eq.1.19 ($Y=SS, X=neq$)	0.366	0.366	0.113	0.921
ω B97X-D	Eq.1.16 ($X=eq$)	0.278	0.278	0.051	0.985
	Eq.1.16 ($X=neq$)	0.332	0.332	0.058	0.962
	Eq.1.17 ($Y=SS, X=eq$)	0.365	0.365	0.120	0.933
	Eq.1.17 ($Y=SS, X=neq$)	0.362	0.362	0.124	0.932
	Eq.1.19 ($Y=SS, X=neq$)	0.385	0.385	0.103	0.933
ω B97	Eq.1.16 ($X=eq$)	0.455	0.455	0.044	0.983
	Eq.1.16 ($X=neq$)	0.512	0.512	0.061	0.964
	Eq.1.17 ($Y=SS, X=eq$)	0.567	0.567	0.077	0.956
	Eq.1.17 ($Y=SS, X=neq$)	0.566	0.566	0.080	0.954
	Eq.1.19 ($Y=SS, X=neq$)	0.576	0.576	0.071	0.956

Table C.9: Theoretical estimates of the experimental 0-0 energies for all tested dyes with the M06-2X functional. All values are in eV.

Dyes	Equation 1.16		Equation 1.17(SS)		Equation 1.19(SS)
	0-0 (LR,eq)	0-0 (LR,neq)	0-0 (SS,eq)	0-0 (SS,neq)	AFCP (SS,neq)
Bor.1	2.720	2.795	2.506	2.487	2.598
Bor.2	2.576	2.668	2.663	2.649	2.693
Bor.3	3.637	3.643	3.721	3.720	3.722
Bor.4	3.357	3.362	3.443	3.443	3.444
Bor.5	3.502	3.510	3.619	3.619	3.620
Bor.6	2.854	3.079	2.928	2.993	3.023
Bor.7	2.965	3.071	3.233	3.200	3.253
Bor.8	3.189	3.196	3.280	3.280	3.282
Bor.9	3.365	3.231	3.365	3.365	3.365
Bor.10	3.167	3.084	3.167	3.166	3.172
Bor.11	2.683	2.692	2.841	2.841	2.841
Bor.12	2.945	2.949	3.014	3.014	3.015
Bor.13	3.054	3.059	3.158	3.158	3.158
Bor.14	3.378	3.378	2.590	2.589	2.587
Bor.15	2.859	2.866	2.989	2.989	2.989
Bor.16	3.473	3.476	3.487	3.486	3.489
Bor.17	3.710	3.717	3.838	3.838	3.839
Bor.18	3.691	3.698	3.804	3.804	3.805
Bor.19	3.426	3.429	3.421	3.421	3.423
Bor.20	3.351	3.354	3.315	3.315	3.319
Bor.21	2.551	2.724	2.767	2.764	2.789
Bor.22	2.522	2.693	2.725	2.722	2.747
Bor.23	2.515	2.681	2.709	2.706	2.732
Bor.24	3.174	3.316	3.392	3.383	3.417
Bor.25	2.595	2.670	2.218	2.210	2.350

Table C.10: Adiabatic and zero-point vibrational energies obtained with the (LR,eq) approach. All values are in eV.

Dyes		B3LYP	PBE0	M06	BMK	M06-2X	CAM-B3LYP	ω B97X-D	ω B97
Bor.1	$E^{\text{adia}}(\text{LR, eq})$	2.330	2.446	2.499	2.705	2.791	2.814	2.838	3.047
	$\Delta E^{\text{ZPVE}}(\text{LR, eq})$	-0.077	-0.077	-0.067	-0.089	-0.071	-0.071	-0.068	-0.072
Bor.2	$E^{\text{adia}}(\text{LR, eq})$	2.402	2.486	2.522	2.643	2.672	2.719	2.748	2.901
	$\Delta E^{\text{ZPVE}}(\text{LR, eq})$	-0.111	-0.101	-0.111	-0.119	-0.096	-0.080	-0.095	-0.063
Bor.3	$E^{\text{adia}}(\text{LR, eq})$	3.379	3.501	3.468	3.684	3.742	3.709	3.717	3.866
	$\Delta E^{\text{ZPVE}}(\text{LR, eq})$	-0.112	-0.111	-0.109	-0.108	-0.105	-0.103	-0.104	-0.094
Bor.4	$E^{\text{adia}}(\text{LR, eq})$	3.117	3.228	3.178	3.402	3.455	3.449	3.469	3.646
	$\Delta E^{\text{ZPVE}}(\text{LR, eq})$	-0.104	-0.103	-0.101	-0.095	-0.098	-0.098	-0.097	-0.094
Bor.5	$E^{\text{adia}}(\text{LR, eq})$	3.347	3.453	3.436	3.595	3.601	3.634	3.656	3.777
	$\Delta E^{\text{ZPVE}}(\text{LR, eq})$	-0.124	-0.116	-0.130	-0.063	-0.099	-0.101	-0.108	-0.089
Bor.6	$E^{\text{adia}}(\text{LR, eq})$	2.620	2.710	2.690	2.909	2.948	3.013	3.070	3.271
	$\Delta E^{\text{ZPVE}}(\text{LR, eq})$	-0.095	-0.092	-0.080	-0.048	-0.094	-0.084	-0.091	-0.077
Bor.7	$E^{\text{adia}}(\text{LR, eq})$	2.759	2.846	2.822	3.008	3.037	3.115	3.171	3.313
	$\Delta E^{\text{ZPVE}}(\text{LR, eq})$	-0.102	-0.095	-0.080	-0.027	-0.071	-0.082	-0.091	-0.076
Bor.8	$E^{\text{adia}}(\text{LR, eq})$	2.895	3.003	2.957	3.197	3.278	3.282	3.332	3.525
	$\Delta E^{\text{ZPVE}}(\text{LR, eq})$	-0.079	-0.080	-0.060	-0.065	-0.088	-0.076	-0.082	-0.087
Bor.9	$E^{\text{adia}}(\text{LR, eq})$	3.084	3.167	2.956	3.310	3.317	3.381	3.417	3.548
	$\Delta E^{\text{ZPVE}}(\text{LR, eq})$	-0.103	-0.100	-0.107	-0.066	-0.094	-0.095	-0.122	-0.082
Bor.10	$E^{\text{adia}}(\text{LR, eq})$	2.466	2.813	2.846	3.081	3.168	3.213	3.271	3.413
	$\Delta E^{\text{ZPVE}}(\text{LR, eq})$	-0.072	-0.086	-0.110	-0.024	-0.092	-0.086	-0.082	-0.074

Table C.11: Adiabatic and zero-point vibrational energies obtained with the (LR,eq) approach using the M06-2X functional. All values are in eV.

Dyes	$E_{6-311+G(2d,p)}^{\text{adia}}(\text{LR, eq})$	$\Delta E^{\text{ZPVE}}(\text{LR, eq})$
Bor.11	2.756	-0.074
Bor.12	3.038	-0.093
Bor.13	3.181	-0.127
Bor.14	3.471	-0.093
Bor.15	2.954	-0.094
Bor.16	3.564	-0.092
Bor.17	3.822	-0.111
Bor.18	3.807	-0.115
Bor.19	3.516	-0.090
Bor.20	3.444	-0.092
Bor.21	2.629	-0.077
Bor.22	2.595	-0.073
Bor.23	2.593	-0.078
Bor.24	3.236	-0.062
Bor.25	2.648	-0.052

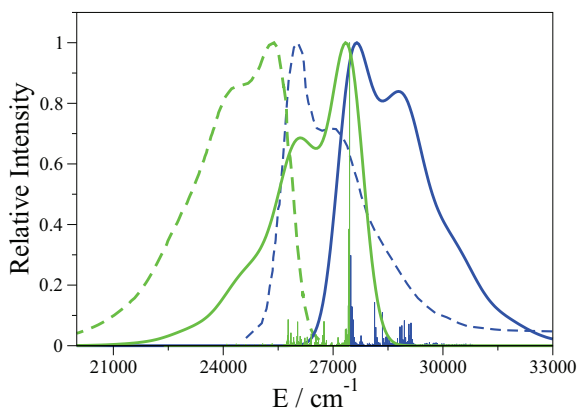


Figure C.1: Comparison between M06-2X (full lines) and experimental (dashed lines) spectra for **Bor.5**. The experimental spectra was taken from Ref. 19.

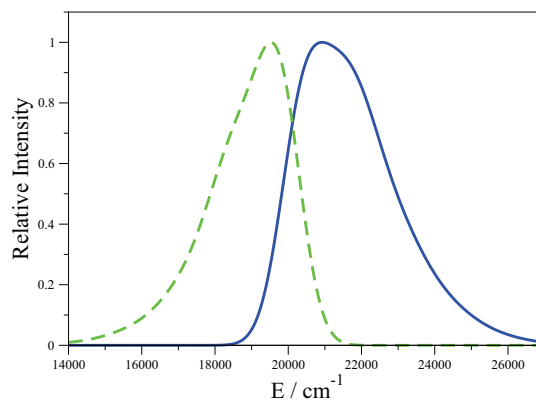


Figure C.2: Absorption (full) and emission spectra (dashed) of **Bor.2** computed with M06-2X. The experimental spectra can be found in Ref. 12.

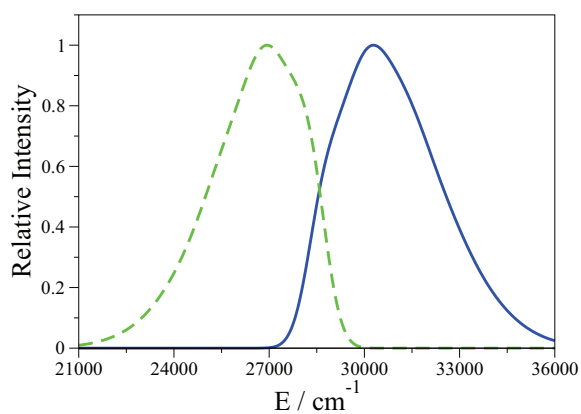


Figure C.3: Absorption (full) and emission spectra (dashed) of **Bor.3** computed with M06-2X. The experimental spectra can be found in Ref. 19.

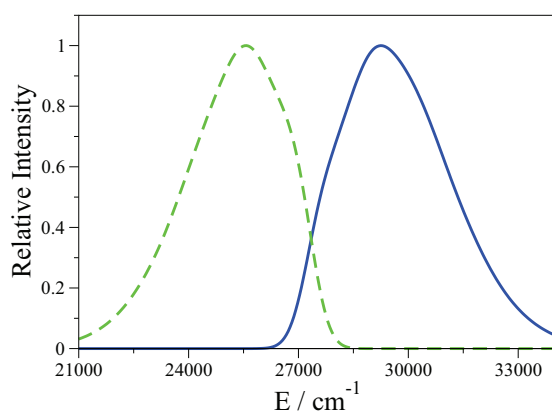


Figure C.4: Absorption (full) and emission spectra (dashed) of **Bor.16** computed with M06-2X. The experimental spectra can be found in Ref. 19.

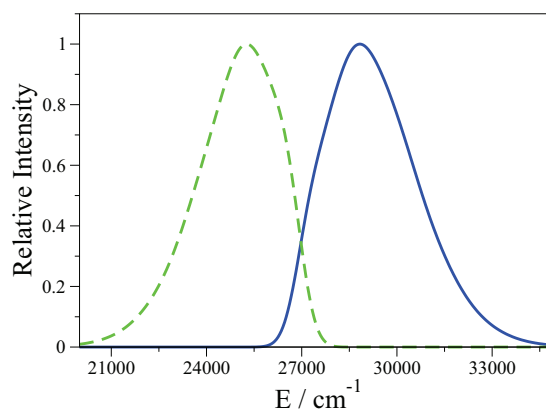


Figure C.5: Absorption (full) and emission spectra (dashed) of **19** computed with M06-2X. The experimental spectra can be found in Ref. 19.

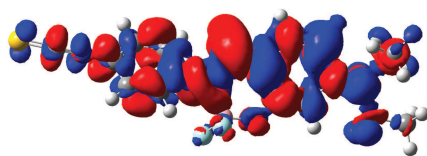


Figure C.6: Density difference plot for **Bor.7**

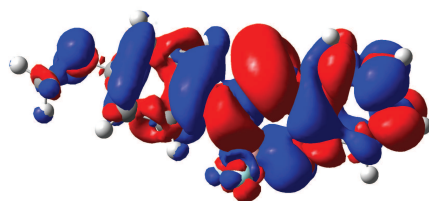


Figure C.7: Density difference plot for **Bor.8**

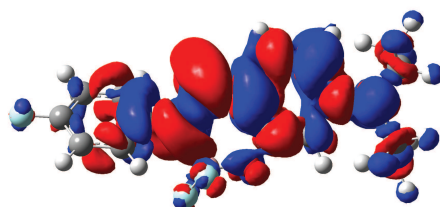


Figure C.8: Density difference plot for **Bor.9**

APPENDIX D

DIOXABORINE DYES

Table D.1: Experimental λ_{abs} , λ_{emi} and 0 – 0 energies for the dyes displayed in Scheme 5.1.

Dye	Solvent	$\lambda_{\text{abs}}(\text{nm})$	$\lambda_{\text{emi}}(\text{nm})$	0-0 (eV)	Ref.
Obo.1	Dichloromethane	345	394	3.370	283
Obo.2	Dichloromethane	380	396	3.197	283
Obo.3	Dichloromethane	398	490	2.823	283
Obo.4	Dichloromethane	360	393	3.299	283
Obo.5	Dichloromethane	397	433	2.993	283
Obo.6	Dichloromethane	415	460	2.841	283
Obo.7	Dichloromethane	411	437	2.927	283
Obo.8	Dichloromethane	380	462	2.973	283
Obo.9	Dichloromethane	398	437	2.976	285
Obo.10	Dichloromethane	426	459	2.806	285
Obo.11	Dichloromethane	443	515	2.603	285
Obo.12	Dichloromethane	467	537	2.482	285
Obo.13	Dichloromethane	463	526	2.517	285
Obo.14	Dichloromethane	491	574	2.343	285
Obo.15	Chloroform	336	455	3.207	261
Obo.16	Tetrahydrofuran	397	491	2.824	272
Obo.17	Dichloromethane	421	436	2.824	260
Obo.18	Dichloromethane	432	451	2.810	271
Obo.19	Dichloromethane	545	559	2.246	279
Obo.20	Dichloromethane	435	450	2.803	271
Obo.21	Dichloromethane	488	538	2.423	281
Obo.22	Dichloromethane	505	554	2.347	281

Table D.2: Theoretical best estimates of the experimental 0-0 energies for the dyes shown in Scheme 5.1. All values are in eV and have been obtained with the PCM-TDDFT-B3LYP and PCM-TDDFT-M06-2X approaches.

	Eq.1.16 ($X=eq$)		Eq.1.17 ($Y=SS, X=eq$)		Eq.1.19 ($Y=SS, X=neq$)	
Dyes	B3LYP	M06-2X	B3LYP	M06-2X	B3LYP	M06-2X
Obo.1	3.491	3.702	3.736	3.935	3.749	3.941
Obo.2	3.055	3.321	3.274	3.524	3.281	3.529
Obo.3	2.594	3.117	1.463	2.750	1.661	2.989
Obo.4	3.259	3.502	3.261	3.670	3.309	3.719
Obo.5	2.860	3.182	2.665	3.309	2.744	3.348
Obo.6	2.652	3.055	1.669	3.133	1.878	3.438
Obo.7	2.800	3.096	2.931	3.235	2.948	3.253
Obo.8	2.773	3.197	1.921	2.848	2.075	3.022
Obo.9	2.765	3.062	3.036	3.345	3.055	3.367
Obo.10	2.626	2.923	2.838	3.171	2.882	3.220
Obo.11	2.368	2.760	2.155	2.863	2.280	3.001
Obo.12	2.326	2.725	1.588	2.828	1.754	2.952
Obo.13	2.360	2.704	1.889	2.845	2.074	2.946
Obo.14	2.176	2.619	1.395	2.678	1.542	2.798
Obo.15	3.002	3.335	2.836	3.334	2.874	3.352
Obo.16	2.709	3.099	2.434	2.977	2.484	3.018
Obo.17	2.834	3.027	3.126	3.297	3.130	3.304
Obo.18	2.766	2.945	3.073	3.223	3.076	3.231
Obo.19	2.358	2.443	2.622	2.764	2.625	2.767
Obo.20	2.246	2.946	2.559	3.231	2.562	3.238
Obo.21	2.223	2.538	2.393	2.675	2.413	2.704
Obo.22	2.189	2.472	2.365	2.625	2.383	2.648

Table D.3: Theoretical PCM-TDDFT-M06-2X estimates of the experimental 0-0 energies for the dyes shown in Scheme 5.1. All values are in eV.

Molecules	Eq.1.16 (eq)	Eq.1.17 (cLR,eq)	Eq.1.19 (cLR,neq)	Eq.1.17 (SS,eq)	Eq.1.19 (SS,neq)
Obo.1	3.702	3.956	3.957	3.935	3.941
Obo.2	3.321	3.572	3.573	3.524	3.529
Obo.3	3.117	3.295	3.294	2.750	2.989
Obo.4	3.502	3.768	3.777	3.670	3.719
Obo.5	3.182	3.426	3.430	3.309	3.348
Obo.6	3.055	3.296	3.299	3.133	3.438
Obo.7	3.096	3.351	3.354	3.235	3.253
Obo.8	3.297	3.315	3.316	2.848	3.022
Obo.9	3.062	3.285	3.291	3.345	3.367
Obo.10	2.923	3.149	3.160	3.171	3.220
Obo.11	2.760	2.948	2.961	2.863	3.001
Obo.12	2.725	2.909	2.926	2.828	2.952
Obo.13	2.704	2.904	2.918	2.845	2.946
Obo.14	2.619	2.778	2.797	2.678	2.798
Obo.15	3.335	3.400	3.401	3.334	3.352
Obo.16	3.099	3.140	3.140	2.977	3.018
Obo.17	3.027	3.355	3.357	3.297	3.304
Obo.18	2.945	3.294	3.297	3.223	3.231
Obo.19	2.443	2.816	2.816	2.764	2.767
Obo.20	2.946	3.230	3.176	3.231	3.238
Obo.21	2.538	2.819	2.825	2.675	2.704
Obo.22	2.472	2.746	2.751	2.625	2.648

Table D.4: Theoretical estimates of the experimental 0-0 energies for the dyes shown in Scheme 5.1 with the PCM-TDA-M06-2X approach. All values are in eV.

Molecules	Eq.1.16 (eq)	Eq.1.17 (cLR,eq)	Eq.1.19 (cLR,neq)	Eq.1.17 (SS,eq)	Eq.1.19 (SS,neq)
Obo.1	4.152	4.488	4.491	4.473	4.489
Obo.2	3.445	3.764	3.766	3.712	3.720
Obo.3	3.229	3.443	3.441	2.820	3.061
Obo.4	3.659	3.996	4.006	3.904	3.952
Obo.5	3.298	3.601	3.606	3.486	3.526
Obo.6	3.158	3.448	3.451	3.186	3.489
Obo.7	3.097	3.512	3.517	3.290	3.310
Obo.8	3.437	3.447	3.450	2.946	3.124
Obo.9	3.252	3.558	3.564	3.613	3.636
Obo.10	3.089	3.390	3.402	3.403	3.454
Obo.11	2.897	3.129	3.142	3.007	3.154
Obo.12	2.852	3.081	3.099	2.961	3.102
Obo.13	2.835	3.084	3.099	2.994	3.111
Obo.14	2.744	2.942	2.962	2.808	2.942
Obo.15	3.521	3.613	3.614	3.532	3.554
Obo.16	3.272	3.341	3.340	3.163	3.206
Obo.17	3.161	3.578	3.581	3.530	3.536
Obo.18	3.068	3.507	3.510	3.452	3.458
Obo.19	2.571	3.036	3.037	2.995	2.997
Obo.20	3.070	3.238	3.241	3.460	3.466
Obo.22	2.570	2.899	2.905	2.779	2.805

Table D.5: Statistical analysis for the dyes shown in Scheme 5.1 obtained with the PCM-TDA-M06-2X approach.

Functional	Method	MSE	MAE	SD	R^2	Max(+)	Max(-)
M06-2X	Eq.1.16 ($X=eq$)	0.388	0.338	0.125	0.896	0.782	0.170
	Eq.1.17 ($Y=cLR, X=eq$)	0.610	0.610	0.146	0.849	1.118	0.406
	Eq.1.19 ($Y=cLR, X=neq$)	0.616	0.616	0.146	0.846	1.121	0.406
	Eq.1.17 ($Y=SS, X=eq$)	0.487	0.490	0.242	0.670	1.103	0.027
	Eq.1.19 ($Y=SS, X=neq$)	0.562	0.562	0.201	0.725	1.119	0.150

Table D.6: Theoretical PCM-TDDFT-M06-2X estimates of the experimental 0-0 energies for the dyes shown in Figure 5.6. All values are in eV.

Molecules	$E^{0-0}(\text{Exp})$	Eq.1.16 (eq)	Eq.1.17 (cLR,eq)	Eq.1.19 (cLR,neq)	Eq.1.17 (SS,eq)	Eq.1.19 (SS,neq)
Obo.23	2.357	2.396	2.615	2.615	2.641	2.643
Obo.24	2.151	2.334	2.457	2.458	2.489	2.492
Obo.25	2.230	2.280	2.507	2.507	2.527	2.528

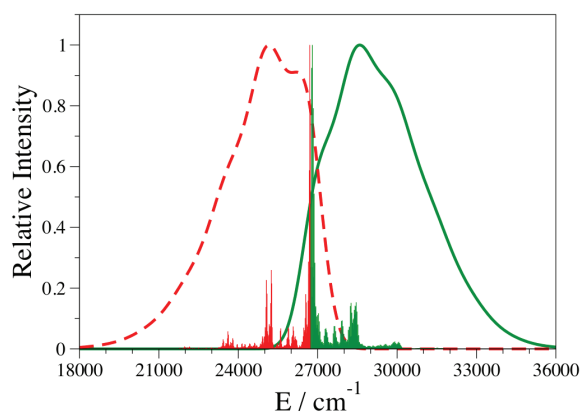


Figure D.1: Absorption (green) and emission spectra (red) of **Obo.8** computed with M06-2X. The experimental spectra can be found in Ref. 283.

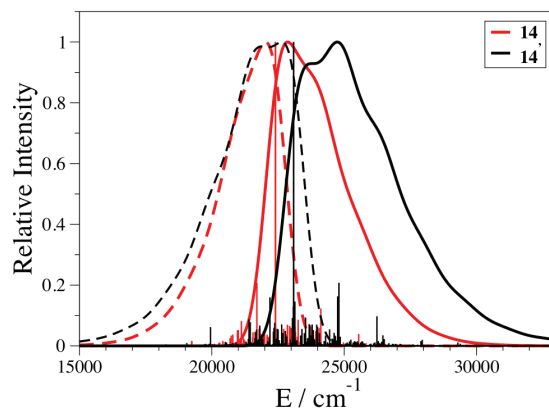


Figure D.5: Absorption (full lines) and emission (dashed lines) spectra for **Obo.14** and **Obo.14'** chromophores.

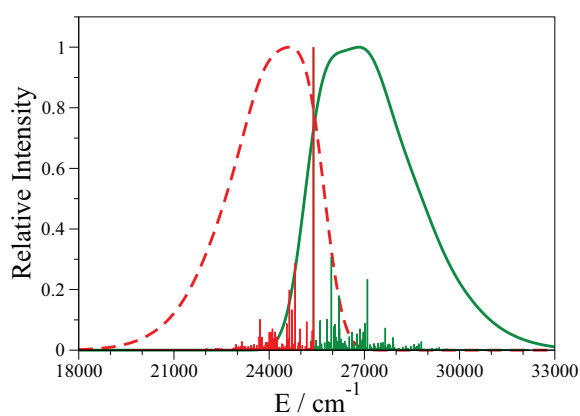


Figure D.2: Absorption (green) and emission spectra (red) of **Obo.10** computed with M06-2X. The experimental spectra can be found in Ref. 285.

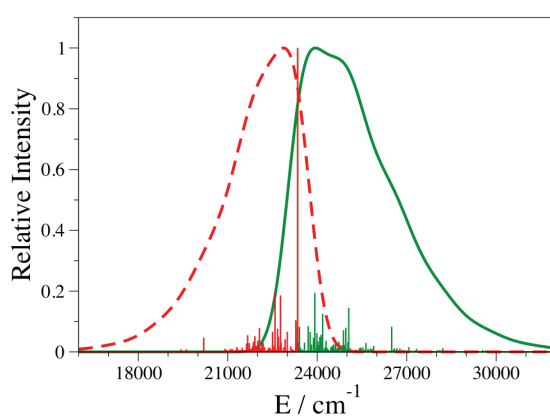


Figure D.3: Absorption (green) and emission spectra (red) of **Obo.12** computed with M06-2X. The experimental spectra can be found in Ref. 285.

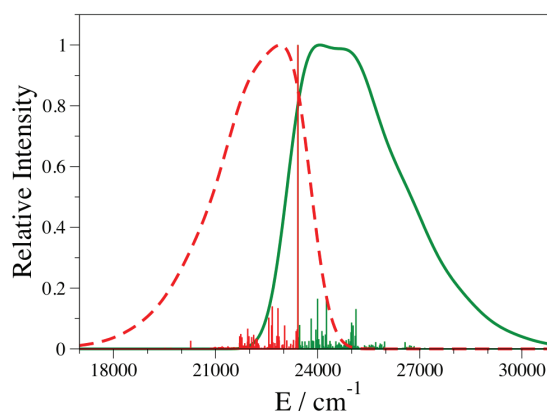


Figure D.4: Absorption (green) and emission spectra (red) of **Obo.13** computed with M06-2X. The experimental spectra can be found in Ref. 285.

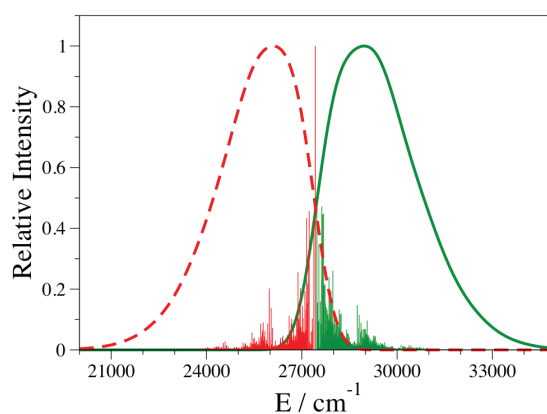


Figure D.6: Absorption (green) and emission spectra (red) of **Obo.15** computed with M06-2X. The measured spectra can be found in the original publication.²⁶¹

APPENDIX E

CONNECTING TD-DFT VERTICAL ENERGIES WITH SOS-CIS(D)

Table E.1: Experimental λ_{abs} , λ_{emi} and 0 – 0 energies for BODIPY dyes displayed in Scheme 7.1.

Molecules	Solvent	λ_{abs} (nm)	λ_{emi} (nm)	0-0(eV)	Ref.
Bo.68	Dichloromethane	397	453	2.930	327
Bo.69	Dichloromethane	447	493	2.644	327
Bo.70	Dichloromethane	447	472	2.700	327
Bo.71	Tetrahydrofuran	562	580	2.172	328
Bo.72	Chloroform	532	547	2.299	318
Bo.73	Chloroform	570	604	2.114	318
Bo.74	Chloroform	605	618	2.028	318
Bo.75	Chloroform	606	618	2.026	318
Bo.76	Chloroform	571	588	2.140	318
Bo.77	Chloroform	611	631	1.997	318
Bo.78	Chloroform	645	662	1.898	318
Bo.79	Chloroform	647	664	1.892	318

Table E.2: Experimental λ_{abs} , λ_{emi} and 0 – 0 energies for aza-BODIPY dyes displayed in Scheme 7.2.

Molecules	Solvent	$\lambda_{\text{abs}}(\text{nm})$	$\lambda_{\text{emi}}(\text{nm})$	0-0 (eV)	Ref.
Az.15	Dichloromethane	453	453	2.737	319
Az.16	Dichloromethane	456	456	2.719	319
Az.17	Dichloromethane	451	460	2.722	319
Az.18	Dichloromethane	455	460	2.710	319

Table E.3: Theoretical PCM-TDDFT-M06-2X, CIS(D) and SOS-CIS(D) estimates of the experimental 0-0 energies for the dyes shown in Scheme 7.1. All values are in eV.

Molecules	$E_{\text{BE}}^{\text{AFCP}}(\text{TD, SS, neq})$	$E_{\text{BE}}^{\text{AFCP}}(\text{CIS(D), SS, neq})$	$E_{\text{BE}}^{\text{AFCP}}(\text{SOS} - \text{CIS(D), SS, neq})$
Bo.68	3.364	3.129	2.921
Bo.69	3.154	2.869	2.702
Bo.70	3.102	2.808	2.642
Bo.71	2.583	2.510	2.168
Bo.72	2.748	2.599	2.263
Bo.73	2.524	2.445	2.103
Bo.74	2.419	2.325	1.975
Bo.75	2.398	2.295	1.955
Bo.76	2.534	2.464	2.142
Bo.77	2.345	2.325	1.987
Bo.78	2.255	2.222	1.876
Bo.79	2.249	2.199	1.862

Table E.4: Theoretical PCM-TDDFT-M06-2X, CIS(D) and SOS-CIS(D) estimates of the experimental 0-0 energies for the dyes shown in Scheme 7.2. All values are in eV.

Molecules	$E_{\text{BE}}^{\text{AFCP}}(\text{TD, SS, neq})$	$E_{\text{BE}}^{\text{AFCP}}(\text{CIS(D), SS, neq})$	$E_{\text{BE}}^{\text{AFCP}}(\text{SOS} - \text{CIS(D), SS, neq})$
Az.15	3.157	2.882	2.777
Az.16	3.126	2.856	2.756
Az.17	3.179	2.907	2.799
Az.18	3.125	2.888	2.782

E.1 Vibronic shapes

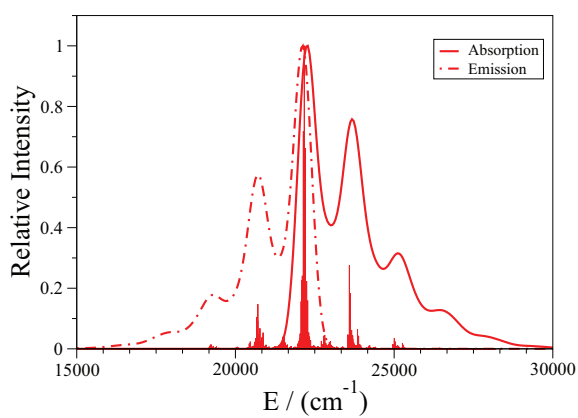


Figure E.1: Absorption (full lines) and emission (dashed lines) of **Az.16** computed with TD-DFT, SOS-CIS(D) being used for 0-0 energies. The experimental spectra can be found in Ref. 319.

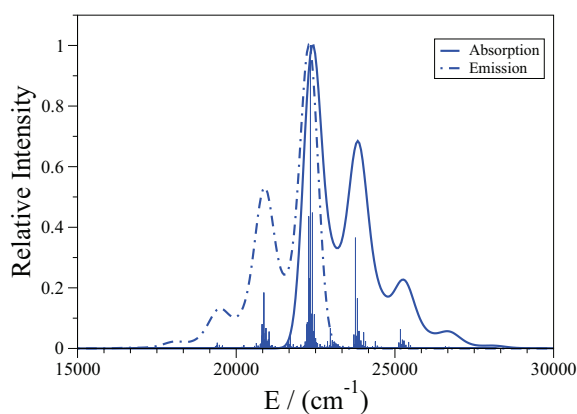


Figure E.2: Absorption (full lines) and emission (dashed lines) of **Az.17** computed with TD-DFT, SOS-CIS(D) being used for 0-0 energies. The experimental spectra can be found in Ref. 319.

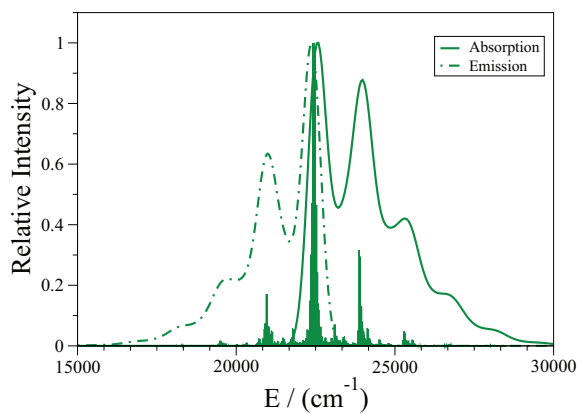


Figure E.3: Absorption (full lines) and emission (dashed lines) of **Az.18** computed with TD-DFT, SOS-CIS(D) being used for 0-0 energies. The experimental spectra can be found in Ref. 319.

BIBLIOGRAPHY

- [1] J. V. Frangioni. In vivo near-infrared fluorescence imaging. *Curr. Opin. Chem. Biol.*, 7:626–634, 2003.
- [2] O. Humbach, H. Fabian, U. Grzesik, U. Haken, and W. Heitmann. Analysis of oh absorption bands in synthetic silica. *J. Non-Cryst. Solids*, 203:19–26, 1996.
- [3] M. T. Harrison, S. V. Kershaw, M. G. Burt, A. L. Rogach, A. Kornowski, A. Eychmüller, and H. Weller. Colloidal nanocrystals for telecommunications. complete coverage of the low-loss fiber windows by mercury telluride quantum dots. *Pure Appl. Chem.*, 72:295–307, 2000.
- [4] X. Wang and M. Weck. Poly(styrene)-supported alq3 and bph2q. *Macromolecules*, 38:7219–7224, 2005.
- [5] Y. Cui and S. Wang. Diboron and triboron compounds based on linear and star-shaped conjugated ligands with 8-hydroxyquinolate functionality: Impact of intermolecular interaction and boron coordination on luminescence. *J. Org. Chem.*, 71:6485–6496, 2006.
- [6] Y. Qin, I. Kiburu, S. Shah, and F. Jakle. Synthesis and characterization of organoboron quinolate polymers with tunable luminescence properties. *Macromolecules*, 39:9041–9048, 2006.

- [7] Y. Qin, I. Kiburu, S. Shah, and F. Jakle. Luminescence tuning of organoboron quinolates through substituent variation at the 5-position of the quinolato moiety. *Org. Lett.*, 8:5227–5230, 2006.
- [8] Y. Nagata and Y. Chujo. Main-chain-type organoboron quinolate polymers: Synthesis and photoluminescence properties. *Macromolecules*, 40:6–8, 2007.
- [9] P. F. Kaiser, J. M. White, and C. A. Hutton. Enantioselective preparation of a stable boronate complex stereogenic only at boron. *J. Am. Chem. Soc.*, 130:16450–16451, 2008.
- [10] Y. Nagata, H. Otaka, and Y. Chujo. Synthesis of new main-chain-type organoboron quinolate polymer linked on quinolate ligand. *Macromolecules*, 41:737–740, 2008.
- [11] J. Feng, B. Liang, D. Wang, L. Xue, and X. Li. Novel fluorescent dyes with fused perylene tetracarboxylic diimide and bodipy analogue structures. *Org. Lett.*, 10:4437–4440, 2008.
- [12] Y. Zhou, Y. Xiao, S. Chi, and X. Qian. Isomeric boron-fluorine complexes with donor-acceptor architecture: Strong solid/liquid fluorescence and large stokes shift. *Org. Lett.*, 10:633–636, 2008.
- [13] S. Bakalova, F. Mendicuti, O. Castano, and J. Kaneti. Design and photophysical properties of a new molecule with a n–b–n linked chromophore. *Chem. Phys. Lett.*, 478:206–210, 2009.
- [14] Y. Tokoro, A. Nagai, and Y. Chujo. Synthesis of p-conjugated polymers containing organoboron benzo[h]quinolate in the main chain. *Macromolecules*, 43:6229–6233, 2010.
- [15] Y. Zhou, J. Kim, M. Kim, W. Son, S. Han, H. Kim, S. Han, Y. Kim, C. Lee, S. Kim, D. Kim, J. Kim, and J. Yoon. Novel bi-nuclear boron complex with pyrene ligand: Red-light emitting as well as electron transporting material in organic light-emitting diodes. *Org. Lett.*, 12:1272–1275, 2010.
- [16] D. Frath, S. Azizi, G. Ulrich, P. Retailleau, and R. Ziessel. Facile synthesis of highly fluorescent boranil complexes. *Org. Lett.*, 13:3414–3417, 2011.

- [17] X. Yang and M. Xia. Difluoro[2-(quinolin-2-yl)phenolato]- borane. *Acta Cryst. E*, 67:o1049, 2011.
- [18] R. Ma, Q. Yao, X. Yang, and M. Xia. Synthesis, characterization and photoluminescence properties of strong fluorescent bf_2 complexes bearing (2-quinolin-2-yl)phenol ligands. *J. Fluor. Chem.*, 137:93–98, 2012.
- [19] J. Massue, D. Frath, G. Ulrich, P. Retailleau, and R. Ziessel. Synthesis of luminescent 2-(20-hydroxyphenyl)benzoxazole (hbo) borate complexes. *Org. Lett.*, 14:230–233, 2012.
- [20] D. Frath, S. Azizi, G. Ulrich, and R. Ziessel. Chemistry on boranils: An entry to functionalized fluorescent dyes. *Org. Lett.*, 14:4774–4777, 2012.
- [21] A. D’Aléo, D. Gachet, V. Heresanu, M. Giorgi, and F. Frédéric. Efficient nir-light emission from solid-state complexes of boron difluoride with 2-hydroxychalcone derivatives. *Chem. Eur. J.*, 18:12764–12772, 2012.
- [22] S. Hattori, K. Ohkubo, Y. Urano, H. Sunahara, T. Nagano, Y. Wada, N. V. Tkachenko, H. Lemmetyinen, and S. Fukuzumi. Charge separation in a nonfluorescent donor-acceptor dyad derived from boron dipyrromethene dye, leading to photocurrent generation. *J. Phys. Chem. B*, 109:15368–15375, 2005.
- [23] S. Erten-Ela, M. D. Yilmaz, B. Icli, Y. Dede, S. Icli, and E. U. Akkaya. A panchromatic boradiazaindacene (bodipy) sensitizer for dye-sensitized solar cells. *Org. Lett.*, 10:3299–3302, 2008.
- [24] J. C. Forgie, P. J. Skabara, I. Stibor, F. Vilela, and Z. Vobecka. New redox stable low band gap conjugated polymer based on an edot-bodipy-edot repeat unit. *Chem. Mater.*, 21:1784–1786, 2009.
- [25] T. Rousseau, A. Cravino, T. Bura, G. Ulrich, R. Ziessel, and J. Roncali. Bodipy derivatives as donor materials for bulk heterojunction solar cells. *Chem. Commun.*, pages 1673–1675, 2009.
- [26] T. Rousseau, A. Cravino, T. Bura, G. Ulrich, R. Ziessel, and J. Roncali. Multi-donor molecular bulk heterojunction solar cells: improving conversion efficiency by synergistic dye combinations. *J. Mater. Chem.*, 19:2298–2300, 2009.

- [27] S. Kolemen, Y. Cakmak, S. Erten-Ela, Y. Altay, J. Brendel, M. Thelakkat, and E. U. Akkaya. Solid-state dye-sensitized solar cells using red and near-ir absorbing bodipy sensitizers. *Org. Lett.*, 12:3812–3815, 2010.
- [28] C. Y. Lee and J. T. Hupp. Dye sensitized solar cells: Tio2 sensitization with a bodipy-porphyrin antenna system. *Langmuir*, 26:3760–3765, 2010.
- [29] T. Bura, N. Leclerc, S. Fall, P. Leveque, T. Heiser, P. Retailleau, S. Rihn, A. Mirloup, and R. Ziessel. High-performance solution-processed solar cells and ambipolar behavior in organic field-effect transistors with thienyl-bodipy scaffoldings. *J. Am. Chem. Soc.*, 134:17404–17407, 2012.
- [30] M. T. Whited, P. I. Djurovich, S. T. Roberts, A. C. Durrell, C. W. Schlenker, S. E. Bradforth, and M. E. Thompson. Singlet and triplet excitation management in a bichromophoric near-infrared-phosphorescent bodipy-benzoporphyrin platinum complex. *J. Am. Chem. Soc.*, 133:88–96, 2011.
- [31] J. Lehl, J. F. Nierengarten, A. Harriman, T. Bura, and R. Ziessel. Artificial light-harvesting arrays: Electronic energy migration and trapping on a sphere and between spheres. *J. Am. Chem. Soc.*, 134:988–998, 2012.
- [32] K. Flavin, K. Lawrence, J. Bartelmess, M. Tasiar, C. Navio, C. Bittencourt, D. F. O’Shea, D. M. Guldi, and S. Giordani. Synthesis and characterization of boron azadipyrromethene single-wall carbon nanotube electron donoracceptor conjugates. *ACS Nano*, 5:1198–1206, 2011.
- [33] A. Florian, M. J. Mayoral, V. Stepanenko, and G. Fernandez. Alternated stacks of nonpolar oligo(p-phenyleneethynylene)-bodipy systems. *Chem. Eur. J.*, 18:14957–14961, 2012.
- [34] Q. Zheng, G. Xu, and P. N. Prasad. Conformationally restricted dipyrromethene boron difluoride (bodipy) dyes: Highly fluorescent, multicolored probes for cellular imaging. *Chem. Eur. J.*, 14:5812–5819, 2008.
- [35] P. Didier, G. Ulrich, Y. Mély, and R. Ziessel. Improved push-pull-push e-bodipy fluorophores for two-photon cell-imaging. *Org. Biomol. Chem.*, 7:3639–3642, 2009.

- [36] P. A. Bouit, K. Kamada, P. Feneyrou, G. Berginc, L. Toupet, O. Maury, and C. Andraud. Two-photon absorption-related properties of functionalized bodipy dyes in the infrared range up to telecommunication wavelengths. *Adv. Mater.*, 21:1151–1154, 2009.
- [37] P. Zhao, R. Li, H. Wang, F. Jian, and H. Guo. Experimental and theoretical comparative studies on two 2-pyrazoline derivatives. *Spectrochim. Acta A*, 74:87–93, 2009.
- [38] J. Murtagh, D. O. Frimannsson, and D. F. O’Shea. Azide conjugatable and ph responsive near-infrared fluorescent imaging probes. *Org. Lett.*, 11:5386–5389, 2009.
- [39] A. Coskun, M.D. Yilmaz, and E. U. Akkaya. Bis(2-pyridyl)-substituted boratriazaindacene as an nir-emitting chemosensor for hg(ii). *Org. Lett.*, 9:607–609, 2007.
- [40] J. Han, A. Loudet, R. Barhoumi, R. C. Burghardt, and K. Burgess. A ratio-metric ph reporter for imaging protein-dye conjugates in living cells. *J. Am. Chem. Soc.*, 131:1642–1643, 2009.
- [41] W. J. Shi, J. Y. Liu, and D. K. P. Ng. A highly selective colorimetric and fluorescent probe for cu²⁺ and hg²⁺ ions based on a distyryl bodipy with two bis(1,2,3-triazole)amino receptors. *Chem. Asian J.*, 7:196–200, 2012.
- [42] J. Killoran, L. Allen, J. F. Gallagher, W. M. Gallagher, and D. F. O’Shea. Synthesis of BF₂ chelates of tetraarylazadipyromethenes and evidence for their photodynamic therapeutic behaviour. *Chem. Comm.*, pages 1862–1863, 2002.
- [43] S. Atilgan, Z. Ekmekci, A. L. Dogan, D. Guc, and E. U. Akkaya. Water soluble distyryl-boradiazaindacenes as efficient photosensitizers for photodynamic therapy. *Chem. Commun.*, pages 4398–4400, 2006.
- [44] A. T. Byrne, A. E. O’Connor, M. Hall, J. Murtagh, K. O’Neill, K. M. Curran, K. Mongrain, J. A. Rousseau, R. Lecomte, S. McGee, J. J. Callanan, D. F. O’Shea, and W. M. Gallagher. Vascular-targeted photodynamic therapy with bf₂-chelated tetraaryl-azadipyromethene agents: a multi-modality molecular

- imaging approach to therapeutic assessment. *Br. J. Cancer.*, 101:1565–1573, 2009.
- [45] S. Erbas, A. Gorgulu, M. Kocakusakogullari, and E. U. Akkaya. Non-covalent functionalized swnts as delivery agents for novel bodipy-based potential pdt sensitizers. *Chem. Commun.*, pages 4956–4958, 2009.
- [46] S. Ozlem and E. U. Akkaya. Thinking outside the silicon box: Molecular and logic as an additional layer of selectivity in singlet oxygen generation for photodynamic therapy. *J. Am. Chem. Soc.*, 131:48–49, 2009.
- [47] N. Adarsh, R. R. Avirah, and D. Ramaiah. Tuning photosensitized singlet oxygen generation efficiency of novel aza-bodipy dyes. *Org. Lett.*, 12:5720–5723, 2010.
- [48] E. Runge and E. K. U. Gross. Density-functional theory for time-dependent systems. *Phys. Rev. Lett.*, 52:997–1000, 1984.
- [49] D. P. Chong and M. E. Casida, editors. *Time-Dependent Density-Functional Response Theory for Molecules*, volume 1 of *Recent Advances in Density Functional Methods*, pages 155–192. World Scientific, Singapore, 1995.
- [50] R. Bauernschmitt, R. Ahlrichs, F. H. Hennrich, and M. M. Kappes. Experiment versus time dependent density functional theory prediction of fullerene electronic absorption. *J. Am. Chem. Soc.*, 120:5052–5059, 1998.
- [51] S. Hirata, M. Head-Gordon, and R. J. Bartlett. Configuration interaction singles, time-dependent hartree-fock, and time-dependent density functional theory for the electronic excited states of extended systems. *J. Chem. Phys.*, 111:10774–10786, 1999.
- [52] C. Adamo and V. Barone. A tddft study of the electronic spectrum of s-tetrazine in the gas-phase and in aqueous solution. *Chem. Phys. Lett.*, 330:152–160, 2000.
- [53] M. Cossi and V. Barone. Time-dependent density functional theory for molecules in liquid solutions. *J. Chem. Phys.*, 115:4708–4717, 2001.
- [54] A. Dreuw and M. Head-Gordon. Single-reference ab initio methods for the calculation of excited states of large molecules. *Chem. Rev.*, 105:4009–4037, 2005.

- [55] V. Barone and A. Polimeno. Integrated computational strategies for uv/vis spectra of large molecules in solution. *Chem. Soc. Rev.*, 36:1724–1731, 2007.
- [56] R. Fortrie and H. Chermette. Vibronic quasi-free rotation effects in biphenyl-like molecules. td-dft study of bifluorene. *J. Chem. Theory Comput.*, 3:852–859, 2007.
- [57] F. Santoro, V. Barone, and R. Improta. Can td-dft calculations accurately describe the excited states behavior of stacked nucleobases? the cytosine dimer as a test case. *J. Comput. Chem.*, 29:957–964, 2008.
- [58] L. Goerigk and S. Grimme. Assessment of td-dft methods and of various spin scaled cis_nd and cc2 versions for the treatment of low-lying valence excitations of large organic dyes. *J. Chem. Phys.*, 132:184103, 2010.
- [59] A. Monari, X. Assfeld, M. Beley, and P. C. Gros. Theoretical study of new ruthenium-based dyes for dye-sensitized solar cells. *J. Phys. Chem. A*, 115:3596–3603, 2011.
- [60] D. Jacquemin, B. Mennucci, and C. Adamo. Excited-state calculations with td-dft: from benchmarks to simulations in complex environments. *Phys. Chem. Chem. Phys.*, 13:16987–16998, 2011.
- [61] A. Charaf-Eddin, A. Planchat, B. Mennucci, C. Adamo, and D. Jacquemin. Choosing a functional for computing absorption and fluorescence band shapes with td-dft. *J. Chem. Theory Comput.*, 9:2749–2760, 2013.
- [62] A. D. Laurent and D. Jacquemin. Td-dft benchmarks: A review. *Int. J. Quantum Chem.*, 113:2019–2039, 2013.
- [63] D. J. Tozer. Relationship between long-range charge-transfer excitation energy error and integer discontinuity in kohn-sham theory. *J. Chem. Phys.*, 119:12697–12699, 2003.
- [64] A. Dreuw and M. Head-Gordon. Failure of time-dependent density functional theory for long-range charge-transfer excited states: the zincbacteriochlorin-bacteriochlorin and bacteriochlorophyll-spheroidene complexes. *J. Am. Chem. Soc.*, 126:4007–4016, 2004.

- [65] M. J. G. Peach, P. Benfield, T. Helgaker, and D. J. Tozer. Excitation energies in density functional theory: an evaluation and a diagnostic test. *J. Chem. Phys.*, 128:044118, 2008.
- [66] D. Jacquemin, E. A. Perpète, G. Scalmani, M. J. Frisch, R. Kobayashi, and C. Adamo. An assessment of the efficiency of long-range corrected functionals for some properties of large compounds. *J. Chem. Phys.*, 126:144105, 2007.
- [67] R. Send, O. Valsson, and C. Filippi. Electronic excitations of simple cyanine dyes: Reconciling density functional and wave function methods. *J. Chem. Theory Comput.*, 7:444–455, 2011.
- [68] D. Jacquemin, Y. Zhao, R. Valero, C. Adamo, I. Ciofini, and D. G. Truhlar. Verdict: Time-dependent density functional theory “not guilty” of large errors for cyanines. *J. Chem. Theory Comput.*, 8:1255–1259, 2012.
- [69] A. D. Quartarolo, N. Russo, and E. Sicilia. Structures and electronic absorption spectra of a recently synthesised class of photodynamic therapy agents. *Chem. Eur. J.*, 12:6797–6803, 2006.
- [70] J. Yoshino, A. Furuta, T. Kambe, H. Itoi, N. Kano, T. Kawashima, Y. Ito, and M. Asashima. Intensely fluorescent azobenzenes: Synthesis, crystal structures, effects of substituents, and application to fluorescent vital stain. *Chem. Eur. J.*, 16:5026–5035, 2010.
- [71] T. Lazarides, T. M. McCormick, K. C. Wilson, S. Lee, D. W. McCamant, and R. Eisenberg. Sensitizing the sensitizer: The synthesis and photophysical study of bodipy-pt(ii)(diimine)(dithiolate) conjugates. *J. Am. Chem. Soc.*, 133:350–364, 2011.
- [72] Q. Bellier, S. Pegaz, C. Aronica, B. Le Guennic, C. Andraud, and O. Maury. Near-Infrared Nitrofluorene Substituted Aza-Boron-dipyrromethenes Dyes. *Org. Lett.*, 13:22–25, 2011.
- [73] H. Guo, Y. Jing, X. Yuan, S. Ji, J. Zhao, X. Lib, and Y. Kan. Highly selective fluorescent off–on thiol probes based on dyads of bodipy and potent intramolecular electron sink 2,4-dinitrobenzenesulfonyl subunits. *Org. Biomol. Chem.*, 9:3844–3853, 2011.

- [74] S. G. Awuah, J. Polreis, V. Biradar, and Y. You. Singlet oxygen generation by novel nir bodipy dyes. *Org. Lett.*, 13:3884–3887, 2011.
- [75] M. Nakamura, T. Tahara, K. Takahashi, T. Nagata, H. Uoyama, D. Kuzuhara, S. Mori, T. Okujima, H. Yamada, and H. Uno. -fused bis-bodipy as a candidate for nir dye. *Org. Biomol. Chem.*, 10:6840–6849, 2012.
- [76] L. Gai, H. Lu, B. Zou, G. Lai, Z. Shen, and Z. Li. Synthesis and spectroscopic properties of bodipy dimers with effective solid-state emission. *RSC Adv.*, 2:8840–8846, 2012.
- [77] B. Le Guennic, O. Maury, and D. Jacquemin. Aza-boron-dipyrromethene dyes: Td-dft benchmarks spectral analysis and design of original near-ir structures. *Phys. Chem. Chem. Phys.*, 14:157–164, 2012.
- [78] T. K. Khan, M. S. Shaikh, and M. Ravikanth. Synthesis and photophysical properties of covalently linked boron dipyrromethene dyads. *Dyes Pigm.*, 94:66–73, 2012.
- [79] Y. Ni, W. Zeng, K. W. Huang, and J. Wu. Benzene-fused bodipys: synthesis and the impact of fusion mode. *Chem. Commun.*, 49:1217–1219, 2013.
- [80] J. B. Prieto, F. L. Arbeloa, V. M. Martnez, T. A. Lopez, and I. Lopez Arbeloa. Structural and spectroscopic characteristics of pyrromethene 567 laser dye. a theoretical approach. *Phys. Chem. Chem. Phys.*, 6:4247–4253, 2004.
- [81] T. Chaudhuria, S. Mulab, S. Chattopadhyay, and M. Banerjee. Photophysical properties of the 8-phenyl analogue of pm567: A theoretical rationalization. *Spectrochim. Acta A*, 75:739–744, 2010.
- [82] J. Banuelos, V. Martin, C. F. A. Gomez-Duran, I. J. A. Cordoba, E. Pena-Cabrera, I. Garcia-Moreno, A. Costela, M. E. Perez-Ojeda, T. Arbeloa, and I. L. Arbeloa. New 8-amino-bodipy derivatives: Surpassing laser dyes at blue-edge wavelengths. *Chem. Eur. J.*, 17:7261–7270, 2011.
- [83] A. Stromeck-Faderl, D. Pentlehner, U. Kensy, and B. Dick. High-resolution electronic spectroscopy of the bodipy chromophore in supersonic beam and superfluid helium droplets. *ChemPhysChem*, 12:1969–1980, 2011.

- [84] C. A. Osorio-Martínez, A. Urías-Benavides, C.F.A. Gómez-Durañ, J. Bañuelos, I. Esnal, I.L. Arbeloa, and E. Peña-Cabrera. 8-aminobodipys: Cyanines or hemicyanines? the effect of the coplanarity of the amino group on their optical properties. *J. Org. Chem.*, 77:5434–5438, 2012.
- [85] K.K. Jagtap, D.K. Maity, A.K. Ray, K. Dasgupta, and S.K. Ghosh. High efficiency dye laser with low fluorescence yield pyrromethene dyes: experimental and theoretical studies. *Appl. Phys. B*, 103:917–924, 2011.
- [86] X. Zhang, H. Yu, and Y. Xiao. Replacing phenyl ring with thiophene: An approach to longer wavelength aza-dipyrromethene boron difluoride (aza-bodipy) dyes. *J. Org. Chem.*, 77:669–673, 2012.
- [87] N. Boens, V. Leen, W. Dehaen, L. Wang, K. Robeyns, W. Qin, X. Tang, D. Beljonne, C. Tonnele, J. M. Paredes, M. J. Ruedas-Rama, A. Orte, L. Crovetto, E. M. Talavera, and J. M. Alvarez-Pez. Visible absorption and fluorescence spectroscopy of conformationally constrained, annulated bodipy dyes. *J. Phys. Chem. A*, 116:9621–9631, 2012.
- [88] Y. Chen, J. zhao, H. Guo, and L. Xiz. Geometry relaxation-induced large stokes shift in red-emitting borondipyrromethenes (bodipy) and applications in fluorescent thiol probes. *J. Org. Chem.*, 77:2192–2206, 2012.
- [89] M. J. Calhorda, C. H. Suresh, P. T. Gomes, R. E. Di Paolo, and A. L. Macanita. Photophysical properties of iminopyrrolyl boron complexes: A dft interpretation. *Dalton Trans.*, 41:13210–13217, 2012.
- [90] J. L. Jin, H. B. Li, Y. Geng, Y. Wu, Y. A. duan, and Z. M. Su. Theoretical insight into the origin of large stokes shift and photophysical properties of anilido-pyridine boron difluoride dyes. *ChemPhysChem*, 13:3714–3722, 2012.
- [91] L. Goerigk, J. Moellmann, and S. Grimme. Computation of accurate excitation energies for large organic molecules with double-hybrid density functionals. *Phys. Chem. Chem. Phys.*, 11:4611–4620, 2009.
- [92] R. Send, M. Kühn, and F. Furche. Assessing excited state methods by adiabatic excitation energies. *J. Chem. Theory Comput.*, 7:2376–2386, 2011.

- [93] D. Jacquemin, A. Planchat, C. Adamo, and B. Mennucci. A td-dft assessment of functionals for optical 0-0 transitions in solvated dyes. *J. Chem. Theory Comput.*, 8:2359–2372, 2012.
- [94] S. Chibani, B. Le Guennic, A. Charaf-Eddin, O. Maury, C. Andraud, and D. Jacquemin. On the computation of adiabatic energies in aza-boron-dipyrromethene dyes. *J. Chem. Theory Comput.*, 8:3303–3313, 2012.
- [95] S. Chibani, B. Le Guennic, A. Charaf-Eddin, A. D. Laurent, and D. Jacquemin. Revisiting the optical signatures of bodipy with ab initio tools. *Chem. Sci.*, 4:1950–1963, 2013.
- [96] S. Chibani, A. Charaf-Eddin, B. Le Guennic, and D. Jacquemin. Boranil and related nbo dyes: Insights from theory. *J. Chem. Theory Comput.*, 9:3127–3135, 2013.
- [97] V. Barone, J. Bloino, M. Biczysko, and F. Santoro. Fully integrated approach to compute vibrationally resolved optical spectra: From small molecules to macrosystems. *J. Chem. Theory Comput.*, 5:540–554, 2009.
- [98] D. Jacquemin and C. Adamo. Basis set and functional effects on excited-state properties: Three bicyclic chromogens as working examples. *Int. J. Quantum Chem.*, 112:2135–2141, 2012.
- [99] J. Tomasi, B. Mennucci, and R. Cammi. Quantum mechanical continuum solvation models. *Chem. Rev.*, 105:2999–3094, 2005.
- [100] R. Cammi and B. Mennucci. The linear response theory for the polarizable continuum model. *J. Chem. Phys.*, 110:9877–9886, 1999.
- [101] M. Caricato, B. Mennucci, J. Tomasi, F. Ingrosso, R. Cammi, S. Corni, and G. Scalmani. Formation and relaxation of excited states in solution: A new time dependent polarizable continuum model based on time dependent density functional theory. *J. Chem. Phys.*, 124:124520, 2006.
- [102] R. Improta, G. Scalmani, M. J. Frisch, and V. Barone. Toward effective and reliable fluorescence energies in solution by a new state specific polarizable continuum model time dependent density functional theory approach. *J. Chem. Phys.*, 127:074504, 2007.

- [103] S. Fabrizio, I. Roberto, L. Alessandro, B. Julien, and B. Vincenzo. Effective method to compute franck-condon integrals for optical spectra of large molecules in solution. *J. Chem. Phys.*, 126:084509, 2007.
- [104] S. Fabrizio, I. Roberto, L. Alessandro, B. Julien, and B. Vincenzo. Effective method to compute vibrationally resolved optical spectra of large molecules at finite temperature in the gas phase and in solution. *J. Chem. Phys.*, 126:184102, 2007.
- [105] F. Santoro, A. Lami, R. Improta, J. Bloino, and V. Barone. Effective method for the computation of optical spectra of large molecules at finite temperature including the duschinsky and herzberg-teller effect: The qx band of porphyrin as a case study. *J. Chem. Phys.*, 128:224311, 2008.
- [106] B. Valeur. *Molecular Fluorescence: Principles and Applications*. Wiley-VCH, Weinheim, 2002.
- [107] F. J. Avila Ferrer, J. Cerezo, E. Stendardo, R. Improta, and F. Santoro. Insights for an accurate comparison of computational data to experimental absorption and emission spectra: Beyond the vertical transition approximation. *J. Chem. Theory Comput.*, 9:2072–2082, 2013.
- [108] W. Kohn and L. J. Sham. Self-consistent equations including exchange and correlation effects. *Phys. Rev.*, 140:A1133–A1138, 1965.
- [109] J. P. Perdew, K. Burke, and M. Ernzerhof. Generalized gradient approximation made simple. *Phys. Rev. Lett.*, 77:3865, 1996.
- [110] A. D. Becke. Density-functional thermochemistry. 3. the role of exact exchange. *J. Chem. Phys.*, 98:5648–5652, 1993.
- [111] P. J. Stephens, F. J. Devlin, C. F. Chabalowski, and M. J. Frisch. Ab initio calculation of vibrational absorption and circular dichroism spectra using density functional force fields. *J. Phys. Chem.*, 98:11623–11627, 1994.
- [112] M. Ernzerhof and G. E. Scuseria. Assessment of the perdew-burke-ernzerhof exchange-correlation functional. *J. Chem. Phys.*, 110:5029–5036, 1999.

- [113] C. Adamo and V. Barone. Toward reliable density functional methods without adjustable parameters: the pbe0 model. *J. Chem. Phys.*, 110:6158–6170, 1999.
- [114] C. Adamo, G. E. Scuseria, and V. Barone. Accurate excitation energies from time-dependent density functional theory: Assessing the pbe0 model. *J. Chem. Phys.*, 111:2889–2899, 1999.
- [115] D. Jacquemin, E. A. Perpète, G. E. Scuseria, I. Ciofini, and C. Adamo. Td-dft performance for the visible absorption spectra of organic dyes: conventional versus long-range hybrids. *J. Chem. Theory Comput.*, 4:123–135, 2008.
- [116] Y. Zhao and D. G. Truhlar. The m06 suite of density functionals for main group thermochemistry, thermochemical kinetics, noncovalent interactions, excited states, and transition elements: two new functionals and systematic testing of four m06-class functionals and 12 other functionals. *Theor. Chem. Acc.*, 120:215–241, 2008.
- [117] A. D. Boese and J. M. L. Martin. Development of density functionals for thermochemical kinetics. *J. Chem. Phys.*, 121:3405–3416, 2004.
- [118] D. Jacquemin, E. A. Perpète, I. Ciofini, C. Adamo, R. Valero, Y. Zhao, and D. G. Truhlar. On the performances of the m06 family of density functionals for electronic excitation energies. *J. Chem. Theory Comput.*, 6:2071–2085, 2010.
- [119] T. Yanai, D. P. Tew, and N. C. Handy. A new hybrid exchange-correlation functional using the coulomb-attenuating method (cam-b3lyp). *Chem. Phys. Lett.*, 393:51–56, 2004.
- [120] J. D. Chai and M. Head-Gordon. Systematic optimization of long-range corrected hybrid density functionals. *J. Chem. Phys.*, 128:084106, 2008.
- [121] J. D. Chai and M. Head-Gordon. Long-range corrected hybrid density functionals with damped atom–atom dispersion corrections. *Phys. Chem. Chem. Phys.*, 10:6615–6620, 2008.
- [122] N. Mardirossian, J. A. Parkhill, and M. Head-Gordon. Benchmark results for empirical post-gga functionals: Difficult exchange problems and independent tests. *Phys. Chem. Chem. Phys.*, 13:19325–19337, 2011.

- [123] D. Jacquemin, E. A. Perpète, I. Ciofini, and C. Adamo. Assessment of the ω b97 family for excited-state calculations. *Theor. Chem. Acc.*, 128:127–136, 2011.
- [124] M. Isegawa, R. Peverati, and D. G. Truhlar. Performance of recent and high-performance approximate density functionals for time-dependent density functional theory calculations of valence and rydberg electronic transition energies. *J. Chem. Phys.*, 137:244104, 2012.
- [125] A. Loudet and K. Burgess. Bodipy dyes and their derivatives: Syntheses and spectroscopic properties. *Chem. Rev.*, 107:4891–4932, 2007.
- [126] G. Ulrich, R. Ziessel, and A. Harriman. The chemistry of fluorescent bodipy dyes: Versatility unsurpassed. *Angew. Chem. Int. Ed.*, 47:1184–1201, 2008.
- [127] A. Loudet, R. Bandichhor, L. Wu, and K. Burgess. Functionalized bf₂ chelated azadipyrrromethene dyes. *Tetrahedron*, 64:3642–3654, 2008.
- [128] D. Zhao, G. Li, D. Wu, X. Qin, P. Neuhaus, Y. Cheng, S. Yang, Z. Lu, X. Pu, C. Long, and J. You. Regiospecific n-heteroarylation of amidine for full-color-tunable boron difluoride dyes with mechanochromic luminescence. *Angew. Chem. Int. Ed.*, 52:1–6, 2013.
- [129] K. Rurack, M. Kollmannsberger, and J. Daub. Molecular switching in the near infrared (nir) with a functionalized borondipyrrromethene dye. *Angew. Chem. Int. Ed.*, 40:385–387, 2001.
- [130] S. O. McDonnell and D. F. O’Shea. Near-infrared sensing properties of dimethylamino-substituted bf₂azadipyrrromethenes. *Org. Lett.*, 8(16):3493–3496, 2006.
- [131] A. Loudet, R. Bandichhor, L. Wu, and K. Burgess. Functionalized bf₂ chelated azadipyrrromethene dyes. *Tetrahedron*, 64:3642 – 3654, 2008.
- [132] W. L. Zhao and E. M. Carreira. Conformationally restricted aza-bodipy: Highly fluorescent stable near-infrared-absorbing dye. *Chem. Eur. J.*, 12:7254–7263, 2006.
- [133] A. Loudet, R. Bandichhor, K. Burgess, A. Palma, S. O. McDonnell, M. J. Hall, and D. F. O’Shea. B,o-chelated azadipyrrromethenes as near-ir probes. *Org. Lett.*, 10:4771–4774, 2008.

- [134] V.F. Donyagina, S. Shimizu, N. Kobayashi, and E. A. Lukyanets. Synthesis of n,n-difluoroboryl complexes of 3,3'-diarylazadiisoindolymethenes. *Tetrahedron Lett.*, 48:6152–6154, 2008.
- [135] K. Umezawa, A. Nakamura, H. Makino, D. Citterio, and K. Suzuki. Bright, color-tunable fluorescent dyes in the visible-near-infrared region. *J. Am. Chem. Soc.*, 130:1550–1551, 2008.
- [136] Y. Kubo, Y. Minowa, T. Shoda, and K. Takeshita. Synthesis of a new type of dibenzopyrromethene boron complex with near-infrared absorption property. *Tetrahedron Lett.*, 51:1600–1602, 2010.
- [137] Y. W. Wang, A. B. Descalzo, Z. Shen, X. Z. You, and K. Rurack. Dihydronaphthalene-fused boron-dipyrrromethene (bodipy) dyes: Insight into the electronic and conformational tuning modes of bodipy fluorophores. *Chem. Eur. J.*, 16:2887–2903, 2010.
- [138] A. Burghart, H. J. Kim, M. B. Welch, L. H. Thoresen, J. Reibenspies, K. Burgess, F. Bergstrom, and L. B. A. Johansson. 3,5-diaryl-4,4-difluoro-4-bora-3a,4a-diaza-s-indacene (bodipy) dyes: synthesis, spectroscopic, electrochemical, and structural properties. *J. Org. Chem.*, 64:7813–7819, 1999.
- [139] K. Rurack, M. Kollmannsberger, and J. Daub. A highly efficient sensor molecule emitting in the near infrared (nir): 3,5-distyryl-8-(p-dimethylaminophenyl)difluoroboradiaza-s-indacene. *New. J. Chem.*, 25:289–292, 2001.
- [140] L. Bonardi, G. Ulrich, and R. Ziessel. Tailoring the properties of borondipyrrromethene dyes with acetylenic functions at the 2,6,8 and 4-b substitution positions. *Org. Lett.*, 10:2183–2186, 2008.
- [141] S. Goeb and R. Ziessel. Convenient synthesis of green diisoindolodithienylpyrromethene?dialkynyl borane dyes. *Org. Lett.*, 9:737–740, 2007.
- [142] R. Gresser, M. Hummert, H. Hartmann, K. Leo, and M. Riede. Synthesis and characterization of near-infrared absorbing benzannulated aza-bodipy dyes. *Chem. Eur. J.*, 17:2939–2947, 2011.

- [143] R. Gresser, H. Hartmann, M. Wrackmeyer, K. Leo, and M. Riede. Synthesis of thiophene-substituted aza-bodipys and their optical and electrochemical properties. *Tetrahedron*, 67:7148–7155, 2011.
- [144] Q. Bellier, F. Dalier, E. Jeanneau, O. Maury, and C. Andraud. Thiophene-substituted aza-bodipy as a strategic synthon for the design of near-infrared dyes. *New J. Chem.*, 36:768–773, 2012.
- [145] P.-A. Bouit, K. Kamada, P. Feneyrou, G. Berginc, L. Toupet, O. Maury, and C. Andraud. Two-photon absorption-related properties of functionalized bodipy dyes in the infrared range up to telecommunication wavelengths. *Adv. Mater.*, 21:1151–1154, 2009.
- [146] L. Gao, W. Senevirathna, and G. Sauvé. Azadipyrromethene-based conjugated oligomers with near-ir absorption and high electron affinity. *Org. Lett.*, 13:5354–5357, 2011.
- [147] L. Jiao, Y. Wu, S. Wang, X. Hu, P. Zhang, C. Yu, K. Cong, Q. Meng, E. Hao, and M. G. H. Vicente. Accessing near-infrared-absorbing bf2-azadipyrromethenes via a pushpull effect. *J. Org. Chem.*, 79:1830–1835, 2014.
- [148] To the best of our knowledge, this recent investigation by Zhang and coworkers,⁸⁶ where theoretical (gas-phase) fluorescence wavelengths are presented for three dyes is the only work where Aza-BODIPY excited-state geometries have been determined. However, the authors did not compute the vibrational spectra of the excited-state, and hence, had no access to the 0-0 energies nor the vibronic couplings.
- [149] It was checked that the cLR correction tends to decrease the computed transition energies compared to the zero-order (solvent free) response, that is, cLR correction goes in the good direction.
- [150] SS Calculations fail to properly converge, making calculations on an equal footing impossible.
- [151] Value computed in gas phase with counterpoise, CP, corrections for BSSE effects (gas phase model was used because PCM-CP corrections are not implemented in the Gaussian09).

- [152] T. Le Bahers, C. Adamo, and I. Ciofini. A qualitative index of spatial extent in charge-transfer excitations. *J. Chem. Theory Comput.*, 7:2498–2506, 2011.
- [153] D. Jacquemin, T. Le Bahers, C. Adamo, and I. Ciofini. What is the best atomic charge model to describe through-space charge-transfer excitations? *Phys. Chem. Chem. Phys.*, 14:5383–5388, 2012. Code available at Université de Nantes, <http://www.sciences.univ-nantes.fr/CEISAM/erc/marches/>.
- [154] B3LYP: 1.975 eV **15(a)** and 2.150 eV **15(Hg²⁺)**; BMK: 2.082 eV **15(a)** and 2.238 eV **15(Hg²⁺)**.
- [155] Using the ZPVE correction obtained on the *naked* dye, **15(Hg²⁺)**.
- [156] G. Ulrich, R. Ziessel, and A. Harriman. The chemistry of fluorescent bodipy dyes: Versatility unsurpassed. *Angew. Chem. Int. Ed.*, 47:1184–1201, 2008.
- [157] A. B. Nepomnyashchii and A. J. Bard. Electrochromy and electrogenerated chemiluminescence of bodipy dyes. *Acc. Chem. Res.*, 45:1844–1853, 2012.
- [158] S. Niu, G. Ulrich, P. Retailleau, J. Harrowfield, and R. Ziessel. New insights into the solubilization of bodipy dyes. *Tetrahedron Lett.*, 50:3840–3844, 2009.
- [159] S. L. Niu, G. Ulrich, R. Ziessel, A. Kiss, P. Renard, and A. Romieu. Water-soluble bodipy derivatives. *Org. Lett.*, 11:2049–2052, 2009.
- [160] T. Bura and R. Ziessel. Water-soluble phosphonate-substituted bodipy derivatives with tunable emission channels. *Org. Lett.*, 13:3072–3075, 2011.
- [161] J. Fan, X. Liu, M. Hu, H. Zhu, F. Song, and X. Peng. Development of an oxidative dehydrogenation-based fluorescent probe for cu²⁺ and its biological imaging in living cells. *Anal. Chim. Acta*, 735:107–113, 2012.
- [162] T. G. Pavlopoulos, J. H. Boyer, M. Shah, K. Thangaraj, and M. L. Soong. Laser action from 2,6,8-position trisubstituted 1,3,5,7-tetramethylpyrromethene-bf₂ complexes: part 1. *Appl. Opt.*, 29:3885–3886, 1990.
- [163] B. P. Wittmershaus, J. J. Skibicki, J. B. McLafferty, Y. Zhang, and S. Swan. Spectral properties of single bodipy dyes in polystyrene microspheres and in solutions. *J. Fluores.*, 11:119–128, 2001.

- [164] M. Galletta, S. Campagna, M. Quesada, G. Ulrichb, and R. Ziessel. The elusive phosphorescence of pyrromethene–bf₂ dyes revealed in new multicomponent species containing ru(ii)–terpyridine subunits. *Chem. Commun.*, pages 4222–4224, 2005.
- [165] C. Goze, G. Ulrich, L. J. Mallon, B. D. Allen, A. Harriman, and R. Ziessel. Synthesis and photophysical properties of borondipyrromethene dyes bearing aryl substituents at the boron center. *J. Am. Chem. Soc.*, 128:10231–10239, 2006.
- [166] M. Liras, P. J. Bañuelos, M. Pintado-Sierra, I. García-Moreno, Á. Costela, L. Infantes, R. Sastre, and F. Amat-Guerri. Synthesis, photophysical properties, and laser behavior of 3-amino and 3-acetamido bodipy dyes. *Org. Lett.*, 9:4183–4186, 2007.
- [167] C. Tahtaoui, C. Thomas, F. Rohmer, P. Klotz, G. Duportail, Y. Mély, D. Bonnet, and M. Hibert. Convenient method to access new 4,4-dialkoxyand 4,4-diaryloxy-diaza-s-indacene dyes: Synthesis and spectroscopic evaluation. *J. Org. Chem.*, 72:269–272, 2007.
- [168] Y. Zhou, Y. Xiao, D. Li, M. Fu, and X. Qian. Novel fluorescent fluorineboron complexes: Synthesis, crystal structure, photoluminescence, and electrochemistry properties. *J. Org. Chem.*, 73:1571–1574, 2008.
- [169] I. J. Arroyo, R. Hu, G. Merino, B. Z. Tang, and E. Pena-Cabrera. The smallest and one of the brightest. efficient preparation and optical description of the parent borondipyrromethene system. *J. Org. Chem.*, 74:5719–5722, 2009.
- [170] S. Rihn, P. Retailleau, N. Bugsaliewicz, A. De Nicola, and R. Ziessel. Versatile synthetic methods for the engineering of thiophene-substituted bodipy dyes. *Tetrahedron Lett.*, 50:7008 – 7013, 2009.
- [171] K. Umezawa, A. Matsui, Y. Nakamura, D. Citterio, and K. Suzuki. Bright, color-tunable fluorescent dyes in the vis/nir region: Establishment of new “tailor-made” multicolor fluorophores based on borondipyrromethene. *Chem. Eur. J.*, 15:1096–1106, 2009.

- [172] A. Haefele, C. Zedde, P. Retailleau, G. Ulrich, and R. Ziessel. Boron asymmetry in a bodipy derivative. *Org. Lett.*, 12:1672–1675, 2010.
- [173] L. Jiao, C. Yu, M. Liu, Y. Wu, K. Cong, T. Meng, Y. Wang, and E. Hao. Synthesis and functionalization of asymmetrical benzo-fused bodipy dyes. *J. Org. Chem.*, 75:6035–6038, 2010.
- [174] Y. Kubota, T. Tsuzuki, K. Funabiki, M. Ebihara, and M. Matsui. Synthesis and fluorescence properties of a pyridomethenebf₂ complex. *Org. Lett.*, 12:4010–4013, 2010.
- [175] J.-H. Olivier, A. Haefele, P. Retailleau, G. Ulrich, and R. Ziessel. Borondipyrromethene dyes with pentane-2,4-dione anchors. *Org. Lett.*, 12:408–411, 2010.
- [176] Y. Kubota, H. Hara, S. Tanaka, K. Funabiki, and M. Matsui. Synthesis and fluorescence properties of novel pyrazine–boron complexes bearing a -iminoketone ligand. *Org. Lett.*, 13:6544–6547, 2011.
- [177] V. Leen, D. Miscoria, S. Yin, A. Filarowski, J. M. Ngongo, M. van der Auweraer, N. Boens, and W. Dehaen. 1,7-disubstituted boron dipyrromethene (bodipy) dyes: Synthesis and spectroscopic properties. *J. Org. Chem.*, 76:8168–8176, 2011.
- [178] Y. Tomimori, T. Okujima, T. Yano, S. Mori, N. Ono, H. Yamada, and H. Uno. Synthesis of π -expanded o-chelated boronedipyrromethene as an nir dye. *Tetrahedron*, 67:3187–3193, 2011.
- [179] G. Ulrich, S. Goeb, A. De Nicola, P. Retailleau, and R. Ziessel. Chemistry at boron: Synthesis and properties of red to near-ir fluorescent dyes based on boron-substituted diisoindolomethene frameworks. *J. Org. Chem.*, 76:4489–4505, 2011.
- [180] C. Yu, L. Jiao, H. Yin, J. Zhou, W. Pang, Y. Wu, Z. Wang, and E. Yang, G. and Hao. -/-formylated boron–dipyririn (bodipy) dyes: Regioselective syntheses and photophysical properties. *Eur. J. Org. Chem.*, 2011:5460–5468, 2011.
- [181] Y. Cakmak, S. Kolemen, S. Duman, Y. Dede, Y. Dolen, B. Kilic, Z. Kostereli, L. T. Yildirim, A. L. Dogan, D. Guc, and E. U. Akkaya. Designing excited

- states: Theory-guided access to efficient photosensitizers for photodynamic action. *Angew. Chem. Int. Ed.*, 50:11937–11941, 2011.
- [182] T. Kowada, S. Yamaguchi, and K. Ohe. Highly fluorescent bodipy dyes modulated with spirofluorene moieties. *Org. Lett.*, 12:296–299, 2010.
- [183] Y. Hayashi, N. Obata, M. Tamaru, S. Yamaguchi, Y. Matsuo, A. Saeki, S. Seki, Y. Kureishi, S. Saito, S. Yamaguchi, and H. Shinokubo. Facile synthesis of biphenyl-fused bodipy and its property. *Org. Lett.*, 14:866–869, 2012.
- [184] T. K. Khan, S. K. Jana, M. Rajeswara Rao, M. S. Shaikh, and M. Ravikanth. Synthesis and electronic properties of meso-furyl boron dipyrromethenes. *Inorg. Chim. Act.*, 383:257–266, 2012.
- [185] R. Hu, C. F. A. Gómez-Durán, J. W. Y. Lam, J. L. Belmonte-Vázquez, C. Deng, S. Chen, R. Ye, E. Peña-Cabrera, Y. Zhong, K. S. Wong, and Ben Z. Tang. Synthesis, solvatochromism, aggregation-induced emission and cell imaging of tetraphenylethene-containing bodipy derivatives with large stokes shift. *Chem. Commun.*, 48:10099–10101, 2012.
- [186] B. C. Popere, A. M. Della Pelle, A. Poe, G. Balaji, and S. Thayumanavan. Predictably tuning the frontier molecular orbital energy levels of panchromatic low band gap bodipy-based conjugated polymers. *Chem. Sci.*, 3:3093–3102, 2012.
- [187] A. C. Benniston, S. Clift, J. Hagon, H. Lemmetyinen, N. V. Tkachenko, W. Clegg, and R. W. Harrington. Effect on charge transfer and charge recombination by insertion of a naphthalene-based bridge in molecular dyads based on borondipyrromethene (bodipy). *ChemPhysChem*, 13:3672–3681, 2012.
- [188] C. A. Swamy P, P. Mukherjee, and P. Thilafae. Dual emissive borane–bodipy dyads: molecular conformation control over electronic properties and fluorescence response towards fluoride ions. *Chem. Commun.*, 2013:993–995, 2013.
- [189] I. Esnal, J. Banuelos, I. Lopez Arbeloa, A. Costela, I. Garcia-Moreno, M. Garzon, A. R. Agarrabeitia, and M. J. Ortis. Nitro and amino bodipys: crucial substituents to modulate their photonic behavior. *RSC Adv.*, 3:1547–1556, 2013.

- [190] A. Wakamiya, T. Murakami, and S. Yamaguchi. Benzene-fused bodipy and fully-fused bodipy dimer: impacts of the ring-fusing at the b bond in the bodipy skeleton. *Chem. Sci.*, 4:1002–1007, 2013.
- [191] T. K. Khan and M. Ravikanth. 3-(pyridine-4-thione)bodipy as a chemodosimeter for detection of hg(ii) ions. *Dyes Pigm.*, 95:89–95, 2012.
- [192] T. Rohand, M. Baruah, W. Qin, N. Boens, and W. Dehaen. Functionalisation of fluorescent bodipy dyes by nucleophilic substitution. *Chem. Commun.*, pages 266–268, 2006.
- [193] T. Uppal, X. Hu, F. R. Fronczek, S. Maschek, P. Bobadova-Parvanova, and M. G. H. Vicente. Synthesis, computational modeling and properties of benzo-appended bodipys. *Chem. Eur. J.*, 18:3893–3905, 2012.
- [194] V. Leen, T. Leemans, N. Boens, and W. Dehaen. 2- and 3-monohalogenated bodipy dyes and their functionalized analogues: Synthesis and spectroscopy. *Eur. J. Org. Chem.*, pages 4386–4396, 2011.
- [195] C. Yu, Y. Xu, L. Jiao, J. Zhou, Z. Wang, and E. Hao. Isoindole-bodipy dyes as red to near-infrared fluorophores. *Chem. Eur. J.*, 18:6437–6442, 2012.
- [196] A. Schmitt, B. Hinkeldey, M. Wild, and G. Jung. Synthesis of the core compound of the bodipy dye class: 4,4'-bora-(3a,4a)-diazas-indacene. *J. Fluores.*, 19:755–758, 2009.
- [197] I. J. Arroyo, R. Hu, B. Z. Tang, F. I. Lopez, and E. Pena-Cabrera. 8-alkenylborondipyrromethene dyes. general synthesis, optical properties, and preliminary study of their reactivity. *Tetrahedron*, 67:7244–7250, 2011.
- [198] S. Rihn, M. Erdem, A. D. Nicola, P. Retailleau, and R. Ziessel. Phenylodine(iii) bis(trifluoroacetate) (pifa)-promoted synthesis of bodipy dimers displaying unusual redox properties. *Phenylodine(III) Bis(trifluoroacetate) (PIFA)-Promoted Synthesis of Bodipy Dimers Displaying Unusual Redox Properties*, 13:1916–1919, 2011.
- [199] Y. Hayashi, S. Yamaguchi, W. Young Cha, D. Kim, and H. Shinokubo. Synthesis of directly connected bodipy oligomers through suzuki-miyaura coupling. *Org. Lett.*, 13:2992–2995, 2011.

- [200] A. Poirel, A. De Nicola, P. Retailleau, and Z. Ziessel. Oxidative coupling of 1,7,8-unsubstituted bodipys: Synthesis and electrochemical and spectroscopic properties. *J. Org. Chem.*, 77:7512–7525, 2012.
- [201] G. Ulrich and R. Ziessel. Convenient and efficient synthesis of functionalized oligopyridine ligands bearing accessory pyrromethene-bf₂ fluorophores. *J. Org. Chem.*, 69:2070–2083, 2004.
- [202] A. Harriman, J. P. Rostron, Michele Cesario, Gilles Ulrich, and Raymond Ziessel. Electron transfer in self-assembled orthogonal structures. *J. Phys. Chem. A*, 110:7994–8002, 2006.
- [203] A. Haefele, G. Ulrich, P. Retailleau, and R. Ziessel. Synthesis of multi-branched dipyrromethene dyes with soluble diethynylphenyl links. *Tetrahedron Lett.*, 49:3716–3721, 2008.
- [204] X. Zhang, Y. Xiao, and X. Qian. Highly efficient energy transfer in the light harvesting system composed of three kinds of boron-dipyrromethene derivatives. *Org. Lett.*, 10:29–32, 2008.
- [205] G. Barin, M. D. Yilmaz, and E. U. Akkaya. Boradiazaindacene (bodipy)-based building blocks for the construction of energy transfer cassettes. *Tetrahedron Lett.*, 50:1738–1740, 2009.
- [206] A. Harriman, L. J. Mallon, K. J. Elliot, A. Haefele, G. Ulrich, and R. Ziessel. A. harriman and l. j. mallon and k. j. elliot and a. haefele and g. ulrich and r. ziessel. *J. Am. Chem. Soc.*, 131:13375–13386, 2009.
- [207] S. Mula, G. Ulrich, and R. Ziessel. Dual bodipy fluorophores linked by polyethyleneglycol spacers. *Tetrahedron Lett.*, 50:6383–6388, 2009.
- [208] S. Diring, F. Puntoriero, F. Nastasi, S. Campagna, and R. Ziessel. Star-shaped multichromophoric arrays from bodipy dyes grafted on truxene core. *J. Am. Chem. Soc.*, 131:6108–6110, 2009.
- [209] T. Bura, P. Retailleau, and R. Ziessel. Efficient synthesis of panchromatic dyes for energy concentration. *Angew. Chem. Int. Ed.*, 49:6659–6663, 2010.

- [210] A. Coskun, E. Deniz, and E. U. Akkaya. Effective pet and ict switching of boradiazaindacene emission: A unimolecular, emission-mode, molecular half-subtractor with reconfigurable logic gates. *Org. Lett.*, 7:5187–5189, 2005.
- [211] E. Deniz, G. C. Isbasar, O. A. Bozdemir, L. T. Yildirim, A. Siemiarzuck, and E. U. Akkaya. Bidirection switching of near ir emitting boradiazaindacene fluorophores. *Org. Lett.*, 10:3401–3403, 2008.
- [212] N. Boens, W. Qin, M. Baruah, W. M. De Borggraeve, A. Filarowski, N. Smidom, M. Ameloot, L. Crovetto, E. M. Talavera, and J. M. Alvarez-Pez. Rational design, synthesis, and spectroscopic and photophysical properties of a visible-light-excitable, ratiometric, fluorescent near-neutral ph indicator based on bodipy. *Chem. Eur. J*, 17:10924–10934, 2011.
- [213] S. Niu, G. Ulrich, P. Retailleau, and R. Ziessel. Regioselective synthesis of 5-monostyryl and 2-teracyanobutadiene bodipy dyes. *Org. Lett.*, 13:4996–4999, 2011.
- [214] Q. Li, Y. Yue, Y. Guo, and S. Shao. Fluoride anions triggered “off-on” fluorescent sensor for hydrogen sulfate anions based on a bodipy scaffold that works as a molecular keypad lock. *Sens. Actua. B*, 173:797–801, 2012.
- [215] Z. Yin, A. Y. Tam, K. Wong, C. Tao, B. Li, C. Poon, L. Wua, and V. Yam. Functionalized bodipy with various sensory units - a versatile colorimetric and luminescent probe for ph and ions. *Dalton Trans.*, 41:11340–11350, 2012.
- [216] G. Ulrich, R. Ziessel, and A. Haefele. A general synthetic route to 3,5-substituted boron dipyrromethenes: Applications and properties. *J. Org. Chem.*, 77:4298–4311, 2012.
- [217] Determined from vertical absorption calculations at the PCM(SS,neq) level. The anionic form does not significantly emit experimentally so that one cannot determine a meaningful experimental AFCP reference.
- [218] A. Coskun and E. U. Akkaya. Difluorobora-s-diazaindacene dyes as highly selective dosimetric reagents for fluoride anions. *Tetrahedron Lett.*, 45:4947–4949, 2004.

- [219] Z. Ekmekci, M. Deniz Yilmaz, and Engin U. Akkaya. A monostryrylboradiazaindacene (bodipy) derivative as colorimetric and fluorescence probe for cyanide ions. *Org. Lett.*, 10:461–464, 2008.
- [220] M. Pamuk and F. Algi. Synthesis of a novel on/off fluorescent cadmium(ii) probe. *Tetrahedron Lett.*, 53:7010–7012, 2012.
- [221] S. Yin, W. Yuan, J. Huang, D. Xie, B. Liu, K. Jiang, and H. Qiu. A bodipy derivative as a colorimetric, near-infrared and turn-on chemosensor for cu²⁺. *Spectrochim. Acta A.*, 96:82–88, 2012.
- [222] X. Zhang, Y. Xu, P. Guo, and X. Qian. A dual channel chemodosimeter for hg²⁺ and ag⁺ using a 1, 3-dithiane modified bodipy. *New J. Chem.*, 36:1621–1625, 2012.
- [223] R. Guliyev, S. Ozturk, E. Sahin, and E. U. Akkaya. Expanded bodipy dyes: Anion sensing using a bodipy analog with an additional difluoroboron bridge. *Org. Lett.*, 14:1528–1531, 2012.
- [224] C. Zhao, X. Wang, J. Cao, P. Feng, J. Zhang, Y. Zhang, Y. Yang, and Z. Yang. Bodipy-based sulfoxide: Synthesis, photophysical characterization and response to benzenethiols. *Dyes Pigm.*, 96:328–332, 2013.
- [225] S. Madhu, S. Kumar Basu, S. Jadhav, and M. Ravikanth. 3,5-diformylborondipyrromethene for selective detection of cyanide anion. *Analyst*, 138:299–306, 2013.
- [226] B. Wang, P. Li, F. Yu, P. Song, X. Sun, S. Yang, Z. Lou, and K. Han. A reversible fluorescence probe based on se-bodipy for the redox cycle between hclo oxidative stress and h₂s repair in living cells. *Chem. Commun.*, 49:1014–1016, 2013.
- [227] The state-specific calculation with the copper structure did not converged to physically meaningful results, showing the limits of our approach in the present case.
- [228] To reduce the computational load, we use NH₄⁺ instead of tetrabutylammonium as in the experiment.

- [229] L. Wu and K. Burgess. A new synthesis of symmetric boraindacene (bodipy) dyes. *Chem. Commun.*, pages 4933–4935, 2008.
- [230] V. P. Yakubovskiy, M. P. Shandura, and Y. P. Kovtun. Boradipyrrromethenecyanines derived from conformationally restricted nuclei. *Dyes Pigm.*, 87:17–21, 2010.
- [231] J. F. Araneda, W. E. Piers, B. Heyne, M. Parvez, and R. McDonald. High Stokes shift anilido-pyridine boron difluoride dyes. *Angew. Chem. Int. Ed.*, 50:12214–12217, 2011.
- [232] X. D. Jiang, R. Gao, Y. Yue, G. T. Sun, and W. Zhao. A new bodipy dye bearing 3,4,4a-trihydroxanthene moieties. *Org. Biomol. Chem.*, 10:6861–6865, 2012.
- [233] X. D. Jiang, H. Zhang, Y. Zhang, and W. Zhao. Development of non-symmetric thiophene-fused bodipys. *Tetrahedron*, 68:9795–9801, 2012.
- [234] A. Poirel, A. De Nicola, and R. Ziessel. Oligothiophenyl-bodipys: Red and near-infrared emitters. *Org. Lett.*, 14:5696–5699, 2012.
- [235] C. Ikeda, T. Maruyama, and T. Nabeshima. Convenient and highly efficient synthesis of boron-dipyrins bearing an arylboronate center. *Tetrahedron Lett.*, 50:3349–3351, 2009.
- [236] M. P. Shandura, V. P. Yakubovskiy, and Y. P. Kovtun. 3,5-bis(acetaldehyde) substituted bodipy. *Org. Biomol. Chem.*, 11:835–841, 2013.
- [237] O. Buyukcakir, O. A. Bozdemir, S. Kolemen, S. Erbas, and E. U. Akkaya. Tetraarylbodipy dyes: Convenient synthesis and characterization of elusive near IR fluorophores. *Org. Lett.*, 11:4644–4647, 2009.
- [238] T. Bura, P. Retailleau, G. Ulrich, and R. Ziessel. Highly substituted bodipy dyes with spectroscopic features sensitive to the environment. *J. Org. Chem.*, 76:1109–1117, 2011.
- [239] S. Niu, G. Ulrich, P. Retailleau, and R. Ziessel. Bodipy-bridged push-pull chromophores: optical and electrochemical properties. *Tetrahedron Lett.*, 52:4848–4853, 2011.

- [240] W. Shi, P. Lo A. Singh, I. Ledoux-Rak, and Dennis K.P. Ng. Synthesis and second-order nonlinear optical properties of push-pull bodipy derivatives. *Tetrahedron*, 68:8712–8718, 2012.
- [241] M. Andrzejak and M. T. Pawlikowski. Vibronic effects in the 1(1)b(u)(1(1)b(2)) excited singlet states of oligothiophenes. fluorescence study of the 1(1)a(g)(1(1)a(1)) \rightarrow 1(1)b(u)(1(1)b(2)) transition in terms of dft, tddft, and casscf methods. *J. Phys. Chem. A*, 112:13737–13744, 2008.
- [242] Roel S. S., Carmen R. D., Cristina C. F., Reyes M. O., Victor H., Juan T. L. N., and Alan A. Optical absorption and emission properties of end-capped oligothiophenoacenes: A joint theoretical and experimental study. *Org. Elec.*, 11:1701–1712, 2010.
- [243] Q. Wu, Q. Peng, Y. Niu, X. Gao, and Z. Shuai. Theoretical insights into the aggregation-induced emission by hydrogen bonding: A qm/mm study. *J. Phys. Chem. A*, 116:3881–3888, 2012.
- [244] J. Er, M. Tang, C. Chia, M. Vendrell H. Liew, and Y. Chang. Megastokes bodipy-triazoles as environmentally sensitive turn-on fluorescent dyes. *Chem. Sci.*, 4:2168–2176, 2013.
- [245] J. Massue, D. Frath, P. Retailleau, G. Ulrich, and R. Ziessel. Synthesis of luminescent ethynyl-extended regioisomers of borate complexes based on 2-(2'-hydroxyphenyl)benzoxazole (hbo). *Chem. Eur. J.*, 19:5375–5386, 2013.
- [246] J. Massue, P. Retailleau, G. Ulrich, and R. Ziessel. Synthesis of luminescent bph2-coordinated 2-(2-hydroxyphenyl)benzoxazole (hbo). *New J. Chem.*, 37:1224–1230, 2013.
- [247] More precisely, they have used the PBE0 hybrid functional and the 6-311+G(2d,p) atomic basis set.
- [248] M. Santra, H. Moon, M. Park, T. lee, Y. K. Kim, and K. H. Ahn. Dramatic substituent effects on the photoluminescence of boron complexes of 2-(benzothiazol-2-yl)phenols. *Chem. Eur. J.*, 18:9886–9893, 2012.

- [249] R. S. Singh, M. Yadav, R. K. Gupta, R. Pandey, and D. S. Pandey. Luminescent n,o-chelated chroman-bf₂ complexes: structural variants of bodipy. *Dalton Trans.*, 42:1696–1707, 2013.
- [250] S. Chibani, B. Le Guennic, A. Charaf-Eddin, A. D. Laurent, and D. Jacquemin. Revisiting the optical signatures of bodipy with ab initio tools. *Chem. Sci.*, 4:1950–1963, 2013.
- [251] P. J. Stephens, F. J. Devlin, C. F. Chabalowski, and M. J. Frisch. Ab initio calculation of vibrational absorption and circular dichroism spectra using density functional force fields. *J. Phys. Chem.*, 98:11623–11627, 1994.
- [252] D. Jacquemin, V. Wathelet, E. A. Perpète, and C. Adamo. Extensive tddft benchmark: Singlet-excited states of organic molecules. *J. Chem. Theory Comput.*, 5:2420–2435, 2009.
- [253] Y. L. Chow, C. I. Johansson, Y. Zhang, R. Gautron, L. Yang, A. Rassat, and S. Yang. Spectroscopic and electrochemical properties of 1,3-diketoneboron derivatives. *J. Phys. Org. Chem.*, 9:7–16, 1996.
- [254] A. G. Mirochnik, B. V. Bukvetskii, E. V. Gukhman, P. A. Zhikhareva, and V. E. Karasev. Crystal structure and excimer fluorescence of dibenzoylmethanato-boron difluoride. *Russ. Chem. Bull.*, 50:1612–1615, 2001.
- [255] V. A. Reutov, E. V. Gukhman, and E. E. Kafitulova. Boron difluoride β -diketonates: Iii. boron difluoride 3-organylpenta-2,4-dionates. *Russ. J. Gen. Chem.*, 73:1441–1444, 2003.
- [256] C. Risko, E. Zojer, P. Brocorens, S. R. Marder, and J. L. Brédas. Bis-aryl substituted dioxaborines as electron-transport materials: a comparative density functional theory investigation with oxadiazoles and siloles. *Chem. Phys.*, 313:151–157, 2005.
- [257] H. Maeda and Y. Kusunose. Dipyrrolyldiketone difluoroboron complexes: novel anion sensors with c-h...x- interactions. *Chem. Eur. J.*, 11:5661–5666, 2005.
- [258] K. V. Zybrev, A. Y. Ilchenko, Y. L. Slominskii, N. N. Romanov, and A. I. Tolmachev. Polymethine dyes derived from 2,2-difluoro-3,1,2-(2h)-

- oxaaxoniaboratines with polymethylene bridge groups in the chromophore. *Dyes Pigm.*, 71:199–206, 2006.
- [259] C. Fujimoto, Y. Kusunose, and H. Maeda. Ch...anion interaction in bf₂ complexes of c₃-bridged oligopyrroles. *J. Org. Chem.*, 71:2389–2394, 2006.
- [260] H. Maeda and Y. Ito. Bf₂ complex of fluorinated dipyrrolyldiketone: a new class of efficient receptor for acetate anions. *Inorg. Chem.*, 45:8205–8210, 2006.
- [261] E. V. Fedorenko, A. G. Mirochnik, V. E. Karasev, and B. V. Bukvetskii. The structure and luminescence of isomeric boron difluoride acetylnaphtholates. *Russ. J. Gen. Chem.*, 80:2192–2195, 2006.
- [262] G. Zhang, J. Chen, S. J. Payne, S. E. Kooi, J. N. Demas, and C. L. Fraser. Multi-emissive difluoroboron dibenzoylmethane polylactide exhibiting intense fluorescence and oxygen-sensitive room-temperature phosphorescence. *J. Am. Chem. Soc.*, 129:8942–8943, 2007.
- [263] F. P. Macedo C. Gwengo, S. V. Lindeman, M. D. Smith, and J. R. Gardinier. β -diketonate, β -ketoiminate, and β -diiminate complexes of difluoroboron. *Eur. J. Inorg. Chem.*, 20:3200–3211, 2008.
- [264] K. Zyabrev, A. Doroshenko, E. Mikitenko, Y. Slominskii, and A. Tolmachev. Design, synthesis, and spectral luminescent properties of a novel polycarbocyanine series based on the 2,2-difluoro-1,3,2-dioxaborine nucleus. *Eur. J. Org. Chem.*, pages 1550–1558, 2008.
- [265] C. Ran, X. Xu, S. B. Raymond, B. J. Ferrara, K. Neal, B. J. Bacsikai, Z. Medarova, and A. Moore. Design, synthesis, and testing of difluoroboron-derivatized curcumins as near-infrared probes for in vivo detection of amyloid- β deposits. *J. Am. Chem. Soc.*, 131:15257–15261, 2009.
- [266] K. Ono, H. Yamaguchi, K. Taga, K. Saito, J. Nishida, and Y. Yamashita. Synthesis and properties of bf₂ complexes to dihydroxydiones of tetracene and perylene: novel electron acceptors showing n-type semiconducting behavior. *Org. Lett.*, 11:149–152, 2009.
- [267] K. Ono, J. Hashizume, H. Yamaguchi, M. Tomura, J. Nishida, and Y. Yamashita. Synthesis, crystal structure, and electron-accepting property of the

- bf2 complex of a dihydroxydione with a perfluorotetracene skeleton. *Org. Lett.*, 11:4326–4329, 2009.
- [268] F. R. Kersey, G. Zhang, G. M. Palmer, M. W. Dewhirst, and C. L. Fraser. Stereocomplexed poly(lactic acid)-poly(ethylene glycol) nanoparticles with dual-emissive boron dyes for tumor accumulation. *ACS Nano*, 4:4989–4996, 2010.
- [269] G. Zhang, J. Lu, and C. L. Fraser. Mechanochromic luminescence quenching: force-enhanced singlet-to-triplet intersystem crossing for iodide-substituted difluoroboron-dibenzoylmethane-dodecane in the solid state. *Inorg. Chem.*, 49:10747–10749, 2010.
- [270] H. Maeda, Y. Bando, Y. Haketa, Y. Honsho, S. Seki, H. Nakajima, and N. Tohnai. Electronic and optical properties in the solid-state molecular assemblies of anion-responsive pyrrole-based π -conjugated systems. *Chem. Eur. J.*, 16:10994–11002, 2010.
- [271] H. Maeda, M. Takayama, K. Kobayashic, and H. Shinmori. Modification at a boron unit: tuning electronic and optical properties of π -conjugated acyclic anion receptors. *Org. Biomol. Chem.*, 8:4308–4315, 2010.
- [272] E. V. Fedorenko, I. B. L'vov, V. I. Vovna, D. Kh. Shlyk, and A. G. Mirochnik. Effect of hydration on the luminescence properties of 2,2-difluoro-4-methylnaphto[2,1-e]-1,3,2-dioxaborine. quantum chemical modeling and experiment. *Russ. Chem. Bull*, 59:1041–1046, 2010.
- [273] T. Liu, A. D. Chien, J. Lu, G. Zhang, and C. L. Fraser. Arene effects on difluoroboron β -diketonate mechanochromic luminescence. *J. Mater. Chem.*, 21:8401–8408, 2011.
- [274] A. O. Gerasov, K. V. Zyabrev, M. P. Shandura, and Y. P. Kovtun. The structural criteria of hydrolytic stability in series of dioxaborine polymethine dyes. *Dyes Pigm.*, 89:76–85, 2011.
- [275] G. Zhang, J. P. Singer, S. E. Kooi, R. E. Evans, E. L. Thomas, and C. L. Fraser. Reversible solid-state mechanochromic fluorescence from a boron lipid dye. *J. Mater. Chem.*, 21:8295–8299, 2011.

- [276] H. Maeda, K. Kitaguchi, and Y. Haketa. Anion-responsive covalently linked and metal-bridged oligomers. *Chem. Commun.*, 47:9342–9344, 2011.
- [277] N. D. Nguyen, G. Zhang, J. Lu, A. E. Shermana, and C. L. Fraser. Alkyl chain length effects on solid-state difluoroboron β -diketonate mechanochromic luminescence. *J. Mater. Chem.*, 21:8409–8415, 2011.
- [278] Y. Haketa, S. Sakamoto, K. Chigusa, T. Nakanishi, and H. Maeda. Synthesis, crystal structures, and supramolecular assemblies of pyrrole-based anion receptors bearing modified pyrrole β -substituents. *J. Org. chem.*, 76:5177–5184, 2011.
- [279] K. Zyabrev, M. Dekhtyar, Y. Vlasenko, A. Chernega, Y. Slominskii, and A. Tolmachev. New 2,2-difluoro-1,3,2(2h)oxazaborines and merocyanines derived from them. *Dyes Pigm.*, 92:749–757, 2011.
- [280] V. I. Vovna, M. V. Kazachek, and I. B. L'vov. Excited states and absorption spectra of β -diketonate complexes of boron difluoride with aromatic substituents. *Opt. Spectro.*, 112:497–505, 2012.
- [281] A. Felouat, A. D'Aléo, and F. Fages. Synthesis and photophysical properties of difluoroboron complexes of curcuminoid derivatives bearing different terminal aromatic units and a meso-aryl ring. *J. Org. Chem.*, 78:4446–4455, 2013.
- [282] C. Glotzbach, U. Kauscher, J. Voskuhl, N. S. Kehr, M. C. A. Stuart, R. Frohloch, H. J. Galla, B. J. Ravoo, K. Nagura, S. Saito, S. Yamaguchi, and E. U. Wurthwein. Fluorescent modular boron systems based on nnn- and ono-tridentate ligands: Self-assembly and cell imaging. *J. Org. Chem.*, 78:4410–4418, 2013.
- [283] S. Xu, R. E. Evans, T. Liu, G. Zhang, J. N. Demas, C. O. Trindle, and C. L. Fraser. Aromatic difluoroboron β -diketonate complexes: effects of π -conjugation and media on optical properties. *Inorg. Chem.*, 52:3597–3610, 2013.
- [284] S. Chambon, A. D'Aléo, C. Baffert, G. Wantza, and F. Fages. Solution-processed bulk heterojunction solar cells based on bf₂-hydroxychalcone complexes. *Chem. Comm.*, 49:3555–3557, 2013.

- [285] A. D'Aléo and F. Fages. Boron difluoride complexes of 3-hydroxyflavone derivatives: efficient bioinspired dyes for solution and solid-state emission. *Photochem. Photobiol. Sci.*, 12:500–510, 2013.
- [286] H. Maeda, W. Hane, Y. Bando, Y. Terashima, Y. Haketa, H. Shibaguchi, T. Kawai, M. Naito, K. Takaishi, M. Uchiyama, and A. Muranaka. Chirality induction by formation of assembled structures based on anion-responsive π -conjugated molecules. *Chem. Eur. J.*, 19:16263–16271, 2013.
- [287] More precisely, they have used the B3LYP hybrid functional and apolarized double-zeta atomic basis set.
- [288] They have used the B3LYP hybrid functional and the 6-31G(d) atomic basis set.
- [289] V. Weijo, B. Mennucci, and L. Frediani. Toward a general formulation of dispersion effects for solvation continuum models. *J. Chem. Theory Comput.*, 6(11):3358–3364, 2010.
- [290] Aleksandr V. Marenich, Christopher J. Cramer, and Donald G. Truhlar. Uniform treatment of solute–solvent dispersion in the ground and excited electronic states of the solute based on a solvation model with state-specific polarizability. *J. Chem. Theory Comput.*, 9:3649–3659, 2013.
- [291] I. Ciofini, T. Le Bahers, C. Adamo, F. Odobel, and D. Jacquemin. Through-space charge transfer in rod-like molecules: Lessons from theory. *J. Phys. Chem. C*, 116:11946–11955, 2012.
- [292] M. Head-Gordon, R. J. Rico, M. Oumi, and T. J. Lee. A doubles correction to electronic excited-states from configuration-interaction in the space of single substitutions. *Chem. Phys. Lett.*, 219:21–29, 1994.
- [293] M. Head-Gordon, D. Maurice, and M. Oumi. A perturbative correction to restricted open-shell configuration-interaction with single substitutions for excited-states of radicals. *Chem. Phys. Lett.*, 246:114–121, 1995.
- [294] B. Moore II and J. Autschbach. Longest-wavelength electronic excitations of linear cyanines: The role of electron delocalization and of approximations in

- time- dependent density functional theory. *J. Chem. Theory Comput.*, 9:4991–5003, 2013.
- [295] G. Scalmani, M. J. Frisch, B. Mennucci, J. Tomasi, R. Cammi, and V. Barone. Geometries and properties of excited states in the gas phase and in solution: theory and application of a time-dependent density functional theory polarizable continuum model. *J. Chem. Phys.*, 124:094107, 2006.
- [296] M. J. Frisch, G. W. Trucks, H. B. Schlegel, G. E. Scuseria, M. A. Robb, J. R. Cheeseman, G. Scalmani, V. Barone, B. Mennucci, G. A. Petersson, H. Nakatsuji, M. Caricato, X. Li, H. P. Hratchian, A. F. Izmaylov, J. Bloino, G. Zheng, J. L. Sonnenberg, M. Hada, M. Ehara, K. Toyota, R. Fukuda, J. Hasegawa, M. Ishida, T. Nakajima, Y. Honda, O. Kitao, H. Nakai, T. Vreven, J. A. Montgomery, Jr., J. E. Peralta, F. Ogliaro, M. Bearpark, J. J. Heyd, E. Brothers, K. N. Kudin, V. N. Staroverov, R. Kobayashi, J. Normand, K. Raghavachari, A. Rendell, J. C. Burant, S. S. Iyengar, J. Tomasi, M. Cossi, N. Rega, J. M. Millam, M. Klene, J. E. Knox, J. B. Cross, V. Bakken, C. Adamo, J. Jaramillo, R. Gomperts, R. E. Stratmann, O. Yazyev, A. J. Austin, R. Cammi, C. Pomelli, J. W. Ochterski, R. L. Martin, K. Morokuma, V. G. Zakrzewski, G. A. Voth, P. Salvador, J. J. Dannenberg, S. Dapprich, A. D. Daniels, O. Farkas, J. B. Foresman, J. V. Ortiz, J. Cioslowski, and D. J. Fox. Gaussian 09 Revision C.01, 2009. Gaussian Inc. Wallingford CT.
- [297] S. Chibani, A. D. Laurent, A. Blondel, B. Mennucci, and D. Jacquemin. Excited-state geometries of solvated molecules: Going beyond the linear-response polarizable continuum model. *J. Chem. Theory Comput.*, 10:1848–1851, 2014.
- [298] For the large and quite floppy **BF₄**, standar optimizatio thersholds have been applied.
- [299] A. Banerjee, N. Adams, J. Simons, and R. Shepard. Search for stationary points on surfaces. *J. Phys. Chem.*, 89:52–57, 185.
- [300] We have used ethylene as test molecule. We have first checked that the computed forces actually corresponded to numerical derivatives of the cLR energies obtained "by hand". Next, we have performed a manual scan of the double bond

length with vertical cLR and confirmed that the minimal point was indeed the one reached at the end of the corresponding geometry optimization.

- [301] M. Schreiber, V. Bub, and M. P. Fulscher. The electronic spectra of symmetric cyanine dyes: A caspt2 study. *Phys. Chem. Chem. Phys.*, 3:3906–3912, 2001.
- [302] S. Grimme and F. Neese. Double-hybrid density functional theory for excited electronic states of molecules. *J. Chem. Phys.*, 127:154116, 2007.
- [303] D. Jacquemin. New cyanine dyes or not? theoretical insights for model chains. *J. Phys. Chem. A*, 115:2442–2445, 2011.
- [304] P. Boulanger, D. Jacquemin, I. Duchemin, and X. Blase. Fast and accurate electronic excitations in cyanines with the many-body bethesalpeter approach. *J. Chem. Theory Comput.*, 10:1212–1218, 2014.
- [305] These values are the cLR-LR fluorescence energy differences determined on optimal LR geometries.
- [306] P. Boulanger, D. Jacquemin, I. Duchemin, and X. Blase. Fast and accurate electronic excitations in cyanines with the many-body bethe salpeter approach. *J. Chem. Theory Comput.*, 10:1212–1218, 2014.
- [307] S. Grimme and E. I. Izgorodina. Calculation of 00 excitation energies of organic molecules by cis (d) quantum chemical methods. *Chem. Phys.*, 305:223–230, 2004.
- [308] M. Oumi, D. Maurice, and M. Head-Gordon. Ab initio calculations of the absorption spectrum of chalcone. *Spectrochim. Acta A*, 55:525–537, 1999.
- [309] T. J. Lee, S. Parthiban, and M. Head-Gordon. Accurate calculations on excited states: New theories applied to the -ox, -xo, and -xo2 (x=cl and br) chromophores and implications for stratospheric bromine chemistry. *Spectrochim. Acta A*, 55:561–574, 1999.
- [310] R. C. Lochan, Y. Shao, and M. Head-Gordon. Quartic-scaling analytical energy gradient of scaled opposite-spin second-order moller?plesset perturbation theory. *J. Chem. Theory Comput.*, 3:988–1003, 2007.

- [311] Y. M. Rhee and M. Head-Gordon. Scaled second-order perturbation corrections to configuration interaction singles: Efficient and reliable excitation energy methods. *J. Phys. Chem.*, 111:5314–5326, 2007.
- [312] Y. M. Rhee, D. Casanova, and M. Head-Gordon. Quartic-scaling analytical gradient of quasidegenerate scaled opposite spin second-order perturbation corrections to single excitation configuration interaction. *J. Chem. Theory Comput.*, 5:1224–1236, 2009.
- [313] All the excited states structures have been optimized with TD-DFT approach.
- [314] N. O. C. Winter and C. Hättig. Scaled opposite-spin cc2 for ground and excited states with fourth order scaling computational costs. *J. Chem. Phys.*, 134:184101, 2011.
- [315] N. O. C. Winter, N. K. Graf, S. Leutwyler, and C. Hättig. Benchmarks for 0–0 transitions of aromatic organic molecules: Dft/b3lyp, adc(2), cc2, sos-cc2 and scs-cc2 compared to high-resolution gas-phase data. *Phys. Chem. Chem. Phys.*, 15:6623–6630, 2013.
- [316] M. J. Frisch, G. W. Trucks, H. B. Schlegel, G. E. Scuseria, M. A. Robb, J. R. Cheeseman, G. Scalmani, V. Barone, B. Mennucci, G. A. Petersson, H. Nakatsuji, M. Caricato, X. Li, H. P. Hratchian, A. F. Izmaylov, J. Bloino, G. Zheng, J. L. Sonnenberg, M. Hada, M. Ehara, K. Toyota, R. Fukuda, J. Hasegawa, M. Ishida, T. Nakajima, Y. Honda, O. Kitao, H. Nakai, T. Vreven, J. A. Montgomery, Jr., J. E. Peralta, F. Ogliaro, M. Bearpark, J. J. Heyd, E. Brothers, K. N. Kudin, V. N. Staroverov, R. Kobayashi, J. Normand, K. Raghavachari, A. Rendell, J. C. Burant, S. S. Iyengar, J. Tomasi, M. Cossi, N. Rega, J. M. Millam, M. Klene, J. E. Knox, J. B. Cross, V. Bakken, C. Adamo, J. Jaramillo, R. Gomperts, R. E. Stratmann, O. Yazyev, A. J. Austin, R. Cammi, C. Pomelli, J. W. Ochterski, R. L. Martin, K. Morokuma, V. G. Zakrzewski, G. A. Voth, P. Salvador, J. J. Dannenberg, S. Dapprich, A. D. Daniels, Ö. Farkas, J. B. Foresman, J. V. Ortiz, J. Cioslowski, and D. J. Fox. Gaussian 09 Revision D.01, 2009. Gaussian Inc. Wallingford CT 2009.
- [317] Y. Shao, L. Fusti-Molnar, Y. Jung, J. Kussmann, C. Ochsenfeld, S. Brown, A. T. B. Gilbert, L. V. Slipchenko, S. V. Levchenko, D. P. O’Neill, R. A. Dis-

- tasio Jr, R. C. Lochan, T. Wang, G.J.O. Beran, N.A. Besley, J.M. Herbert, C.Y. Lin, T. Van Voorhis, S.H. Chien, A. Sodt, R.P. Steele, V.A. Rassolov, P. Maslen, P.P. Korambath, R.D. Adamson, B. Austin, J. Baker, E.F.C. Bird, H. Daschel, R.J. Doerksen, A. Dreuw, B.D. Dunietz, A.D. Dutoi, T.R. Furlani, S.R. Gwaltney, A. Heyden, S. Hirata, C.-P. Hsu, G.S. Kedziora, R.Z. Khalliulin, P. Klunziger, A.M. Lee, W.Z. Liang, I. Lotan, N. Nair, B. Peters, E.I. Proynov, P.A. Pieniazek, Y.M. Rhee, J. Ritchie, E. Rosta, C.D. Sherrill, A.C. Simmonett, J.E. Subotnik, H.L. Woodcock III, W. Zhang, A.T. Bell, A.K. Chakraborty, D.M. Chipman, F.J. Keil, A. Warshel, W.J. Hehre, H.F. Schaefer III, J. Kong, A.I. Krylov, P.M.W. Gill, and M. Head-Gordon. Advances in methods and algorithms in a modern quantum chemistry program package. *Phys. Chem. Chem. Phys.*, 8:3172–3191, 2006.
- [318] X. D. Jiang, H. Zhang, Y. Zhang, and W. Zhao. Development of non-symmetric thiophene-fused bodipys. *Tetrahedron*, 68:9795–9801, 2012.
- [319] D. Wang, R. Liu, C. Chen, S. Wang, J. Chang, C. Wu, and H. Zhu. Synthesis, photophysical and electrochemical properties of aza-boron-diquinomethene complexes. *Dyes Pigm.*, 99:240–249, 2013.
- [320] X. Wang, F. Zhang, J. Liu, R. Tang, Y. Fu, D. Wu, Q. Xu, X. Zhuang, G. He, and X. Feng. Ladder-type bn-embedded heteroacenes with blue emission. *Org. Lett.*, 15:5714–5717, 2013.
- [321] J. Lee, C. Hoon Kim, and T. Joo. Active role of proton in excited state intramolecular proton transfer reaction. *J. Phys. Chem. A*, 49:3976–3978, 2013.
- [322] M. Savarese, P. A. Netti, N. Rega, C. Adamo, and I. Ciofini. Junghwa lee , chul hoon kim , and taiha joo. *Phys. Chem. Chem. Phys.*, 16:8661–8666, 2014.
- [323] Y. Houari, A. Charaf-Eddin, A. D. Laurent, J. Massue, R. Ziessel, G. Ulrich, and D. Jacquemin. Modeling optical signatures and excited-state reactivities of substituted hydroxyphenylbenzoxazole (hbo) esipt dyes. *Phys. Chem. Chem. Phys.*, 16:1319–1321, 2014.
- [324] Q. Hao, S. Yu, S. Li, J. Chen, Y. Zeng, T. Yu, G. Yang, and Y. Li. Locked planarity: A strategy for tailoring ladder-type π -conjugated anilidopyridine boron difluorides. *J. Org. Chem.*, 79:459–464, 2014.

- [325] S. Chibani, D. Jacquemin, and A. D. Laurent. Modelling solvent effects on the absorption and emission spectra of constrained cyanines with both implicit and explicit qm/efp models. *Comput. Theor. Chem.*, 1041-1041:321–327, 2014.
- [326] P. Majumdar, X. Yuan, S. Li, B. Le Guennic, J. Ma, C. Zhang, D. Jacquemin, and J. Zhao. Cyclometalated ir(iii) complexes with styryl-bodipy ligands showing near ir absorption/emission: preparation, study of photophysical properties and application as photodynamic/luminescence imaging materials. *J. Mater. Chem. B*, 2:2838–2854, 2014.
- [327] M. Graser, H. Kopacka, K. Wurst, M. Ruetz, C. R. Kreutz, T. Muller, C. Hirtenlehner, U. Monkowius, G. Knor, and B. Bildstein. Efficient fluorophores based on pyridyl-enolato and enamido difluoroboron complexes: Simple alternatives to boron-dipyrromethene (bodipy) dyes. *Inorg. Chem. Acta*, 405:116–120, 2013.
- [328] K. Tanaka, H. Yamane, R. Yoshii, and Y. Chujo. Efficient light absorbers based on thiophene-fused boron dipyrromethene (bodipy) dyes. *Bioorg. Med Chem.*, 21:2715–2719, 2013.

Thèse de Doctorat

Siwar CHIBANI

TD-DFT Simulation of the Properties of the Excited States

Résumé

Au cours de cette thèse, nous avons défini un protocole de calcul quantique permettant des simulations qualitativement et quantitativement précises des spectres d'absorptions et d'émission de colorants appartenant aux familles des aza-BODIPY, BODIPY, boranils et dioxaborines. Ce protocole utilise la TD-DFT pour déterminer avec efficacité les paramètres structuraux et vibrationnels des états fondamentaux et excités, et l'approche SOS-CIS(D) pour calculer précisément les énergies d'absorption et de fluorescence à l'aide de calcul verticaux. Cette approche "hybride" permet de traiter un grand nombre de composés en un temps de calcul relativement faible, d'atteindre une précision de l'ordre de 0.1 eV ainsi qu'une cohérence avec les données expérimentales impressionnante ($R^2 > 0.95$). Plus précisément, nous avons montré que la fonctionnelle d'échange-corrélation M06-2X est la plus performante pour déterminer les énergies 0-0 et les topologies des bandes de ces molécules. En étudiant les effets de la base atomique, nous avons pu montrer que les structures et signatures vibrationnelles peuvent être calculées précisément avec une base compacte, 6-31G(d), tandis que les énergies totales requièrent l'utilisation d'une base plus étendue, 6-311+G(2d,p). Lors de cette thèse, plusieurs modèles de prise en compte des effets de solvant (LR, cLR et SS-PCM) ont été testés. Il en découle que SS-PCM est le modèle le plus adéquate pour les aza-BODIPY et les BODIPY tandis que les approches LR et cLR sont plus adaptées pour les boranils et les dioxaborines. Les modèles utilisés dans cette thèse ont été testés sur un grand nombre de composés en vue d'analyser les effets auxochromes, solvatochromes, acidochromes... en lien avec des données expérimentales récentes.

Mots clés

Energies 0-0, Spectre vibronique, Théorie de la Fonctionnelle de la densité Dépendante du Temps (TD-DFT), Calcul *Ab initio*.

Abstract

During this thesis, we have defined an efficient protocol to simulate qualitatively and quantitatively the absorption and emission spectra of aza-BODIPY, BODIPY, boranils and dioxaborines dyes. In this protocol, we have used the TD-DFT level to determine the structural parameters and vibrational effects for both ground and excited states, and we have calculated the vertical absorption and emission transition energies at the SOS-CIS(D) level. This "hybride" approach can be used for a large number of compounds in a relatively low computing time to achieve an accuracy of about 0.1 eV and an impressive consistency with the experimental data ($R^2 > 0.95$). Specifically, we have shown that the M06-2X exchange-correlation functional is the most efficient to determine the 0-0 energies and the topologies of the bands of these molecules. By studying the atomic basis set effects, we have found that the structures and vibrational signatures can be calculated precisely with a compact atomic basis set, 6-31G(d), while the total energies require the use of a larger atomic basis set, 6-311+G(2d,p). To Take into account the solvent effect, several PCM models (LR, cLR and SS-PCM) have been tested. SS-PCM approach is the most appropriate model for the aza-BODIPY and BODIPY while LR and cLR approaches are more suitable for boranils and dioxaborines. The models used in this thesis have been tested on a large number of compounds to analyze the auxochromic, solvatochromic, acidochromic effects... in connection with recent experimental data.

Key Words

0-0 energies, Vibronic spectra, Time-Dependent Density Functional Theory (TD-DFT), *Ab initio* calculation.